

OPTIMISATION OF DESIGN OF COMPOSITE STRUCTURES

Antonio Miravete

WOODHEAD PUBLISHING LIMITED

OPTIMISATION OF DESIGN OF COMPOSITE STRUCTURES

OPTIMISATION OF DESIGN OF COMPOSITE STRUCTURES

**Antonio Miravete
Department of Mechanical Engineering
University of Zaragoza**

**WOODHEAD PUBLISHING LIMITED
Cambridge England**

Published by Woodhead Publishing Limited, Abington Hall,
Abington, Cambridge CB21 6AH, England
www.woodheadpublishing.com

First published 1996

© Woodhead Publishing Ltd, 1996

Conditions of sale

All rights reserved. No part of this publication may be reproduced or transmitted in any form or by any means, electronic or mechanical, including photocopy, recording, or any information storage and retrieval system, without permission in writing from the publisher.

British Library Cataloguing in Publication Data

A catalogue record for this book is available from the British Library.

ISBN-13: 978-1-85573-208-7

ISBN-10: 1-85573-208-4

Printed by Victoire Press, Cambridge, England.

CONTENTS

Preface	vii
Symbols and notation	viii
1 Introduction and preliminaries	1
1.1 Introduction	1
1.2 Anisotropic constitutive relations	2
1.3 Laminate theories	7
1.4 Numerical methods of stress analysis	11
1.5 Failure criteria	13
1.6 Numerical methods for design optimisation	14
References	16
2 Design optimisation of constant thickness composite structures	19
2.1 Introduction	19
2.2 Special configurations: SMC and fabric composites	21
2.3 Homogenisation of laminated plates	29
2.4 The free-edge effect	31
2.5 Conclusions	34
References	35
3 Shells	39
3.1 Introduction	39
3.2 Spherical dome	39
3.3 Spherical vessel	46
3.4 Pipeline and submersible hull	51
3.5 Conclusions	55
References	56
4 Constant thickness plates	59
4.1 Introduction	59
4.2 Design optimisation of composite plates in bending	59
4.3 Design optimisation of composite plates in buckling	71
4.4 Conclusions	81
References	83
5 Constant thickness sandwiches	87
5.1 Introduction	87
5.2 Core materials	87
5.3 Optimum design of sandwich constructions	98
5.4 Buckling	105
5.5 Conclusions	113
References	114

6 Design optimisation of variable thickness composite structures	117
6.1 Introduction	117
6.2 Variable thickness laminate stress distribution	118
6.3 Conclusions	135
References	135
7 Variable thickness beams	137
7.1 Introduction	137
7.2 Behaviour of variable thickness composite beams	138
7.3 Optimisation of variable thickness composite beams	148
7.4 Conclusions	152
References	153
8 Variable thickness plates	155
8.1 Introduction	155
8.2 Model assumptions and method of analysis	155
8.3 Determination of elastic constants and strengths	158
8.4 Optimisation of laminated composite plates	160
8.5 Conclusions	181
References	182
9 Variable thickness sandwiches	185
9.1 Introduction	185
9.2 One-dimensional laminated composite panels	186
9.3 Two-dimensional laminated composite panels	188
9.4 Conclusions	198
References	199

PREFACE

Composite materials have been increasingly used during the last decades, to lighten structures in fields such as aeronautics and space. Two steps are essential to take advantage of these materials: design and optimisation.

Optimisation of composite structures is a recent issue, because both optimisation techniques and composite structures have been developed during the last few decades and therefore, the conjunction of them is even more recent. As using composite materials is an expensive but efficient way of getting minimum weight structures, it is logical to attempt to find out how to design properly optimised laminated composite plates with no reduction in their strength.

Since many kinds of ground and air vehicles have rectangular plates as a common structural element, an increasing demand for improved structural efficiency in such applications has resulted. Composite materials offer a number of advantages other than their high stiffness to density values: for example, it is possible to shape them by orientating the filaments in the various layers in order to optimise the desired structural behaviour.

Although there is much literature related to plate analysis, the most modern references lack adequate information which could allow a designer to tailor or synthesise an optimal design. There are two reasons for this: firstly, the difficulty of accurately assessing the level of strains and stresses in any point of a laminated composite plate and, secondly, the need to implement an optimisation procedure able to find the minimum weight structure.

Fortunately, the current development of numerical techniques and the existence of powerful computers provide a solution to the two problems mentioned above.

Recently, a number of books dealing with design on composite materials have been published. This is the first step for relating theory of composite materials to real life, the objective being to produce information that can be used for design purposes.

The aim of this book is to provide another step forward and to obtain rules, not only to design composite structures properly but to do this in an optimum way. Two software packages are included with the book for designing and optimising rectangular, constant and variable thickness composite plates.

The author wishes to express his gratitude to Steve W Tsai and Ran Y Kim, for their encouragement and support in the course of the work related to variable thickness structures.

The support of the Mechanics and Surface Interactions Branch (WRDC/MLBM), Non-metallic Material Division, Materials Laboratory, Wright Research and Development Center, Wright Patterson Air Force Base, Ohio, USA is also acknowledged.

Special thanks are due to Juan J Alba, María J Casamayor, Luis Castejón, Javier Fernández and Jesús Saldaña, who are all members of the Group of Composite Materials of the University of Zaragoza. Finally I wish to express my appreciation to Teresa Laborde who was in charge of editing text and graphics.

Antonio Miravete

Symbols and notation

a	Length of the plate; or nodal displacement vector
a'	Relative nodal displacement
a^e	Nodal displacement vector of the finite element e
B	Geometric matrix used in the finite element method; $B = L N$
b	Width of the plate
C_{ij}	Stiffness matrix in the generalized Hooke's law; in concentrated notation, $i,j=1,2,3,4,5,6$
c	Strain-displacement matrix, or core thickness in a sandwich panel
D	Matrix of elastic constants
E	Young modulus
e_{ij}	Strain energy of the j th layer of the element i
\tilde{e}_{ij}	Strain energy density of the j th layer of the element i
\tilde{e}'_{ij}	Strain energy density of the j th layer of the element i
e'_{ij}	Relative strain energy of the j th layer of the element i
F_{ij}, F_i	Strength parameters in stress formulation of the quadratic failure criterion
f^e	Nodal forces in the finite element e
G_{12}	In-plane shear modulus
h_0	Ply thickness
K	Stiffness matrix of the whole plate
K'	Relative stiffness matrix of the whole plate
K_B	Stiffness matrix of the whole plate due to bending stresses
K_S	Geometric matrix of the whole plate
k^e	Elemental stiffness matrix
l	Diagonal of a plate
l_i	Surface area of the element i
M	Applied bending moment
N	Shape function matrix
N_x	Applied compressive force in x -direction per unit width
$N_{x cr}$	Critical compressive force in x -direction per unit width

N_y	Applied compressive force in y-direction per unit width
$N_{y\ cr}$	Critical compressive force in y-direction per unit width
N_{xy}	Applied compressive force in xy- or 12-plane per unit width
$N_{xy\ cr}$	Critical compressive force in xy- or 12-plane per unit width
P	Applied transverse load
Q	Reduced stiffness matrix for plane stress
q^e	Distributed forces in the finite element e
Q_{yy}	Term of the reduced matrix for plane stress $Q_{yy} = E_y / (1 - \nu_{12}\nu_{21})$
r	Strength/stress ratio or strength ratio
S	Positive pure shear strength in the xy- or 12-plane of a ply
S'	Negative pure shear strength in the xy- or 12-plane of a ply
T	Transformation matrix
t	Total laminate thickness
t_1	Difference between the total laminate thickness (t) and the minor thickness of a tapered plate
t_{ij}	Thickness of the jth layer of the ith element
u	Deflection in the x-direction
V	Strain energy of a single plate element subjected to in-plane stresses
V_B	Strain energy of a single plate element due to plate bending
V_e	Volume of the finite element e
V_{ij}	Volume of the jth layer of the ith element
V_s	Strain energy of a single plate element due to in-plane stresses
v	Deflection in the y-direction
w	Deflection in the z-direction
X	Uniaxial tensile strength of a ply along the x-axis
X'	Uniaxial compressive strength of a ply along the x-axis
Y	Uniaxial tensile strength of a ply along the y-axis
Y'	Uniaxial compressive strength of a ply along the y-axis
Z	Uniaxial tensile strength of a ply along the z-axis
Z'	Uniaxial compressive strength of a ply along the z-axis
α_{ij}	Thickness of the jth layer of the ith element normalized to maximum thickness
γ_{ij}	Shear strain component
$\delta\epsilon$	Strain generated by a virtual displacement

δu	Displacement generated by a virtual displacement
δ^e	Vector of nodal deflections
δa^e	Virtual displacements in the finite element e
ε_i	Strain component
ε_i	Relative strain component
ε_0	Initial strains
θ	Angle between x-axis and fiber or principal axis of layer
Λ	Scaling parameter
λ	Lagrangian parameter; or coefficient used to formulate an eigenvalue problem
v	Number of cycle of iteration
ϕ	Angle of variation of thickness
ρ_{ij}	Mass density of the jth layer of the ith element
σ_i	Stress component
σ_i	Relative stress component
σ_0	Initial stresses
τ_{ij}	Shear stress component



One-dimensional thin plate



One-dimensional thick plate



One-dimensional sandwich plate



One-dimensional simply supported plate



One-dimensional clamped plate



One-dimensional cantilever plate



Two-dimensional thin plate



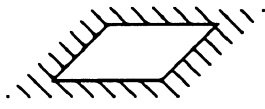
Two-dimensional thick plate



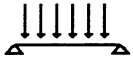
Two-dimensional sandwich plate



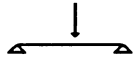
Two-dimensional simply supported plate



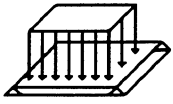
Two-dimensional clamped plate



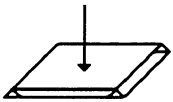
One-dimensional plate subjected to a uniform transverse load



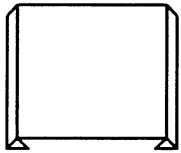
One-dimensional plate subjected to a point transverse load



Two-dimensional plate subjected to a uniform transverse load



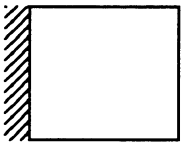
Two-dimensional plate subjected to a point transverse load



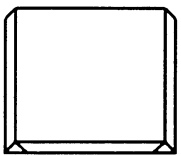
One-dimensional simply supported plate



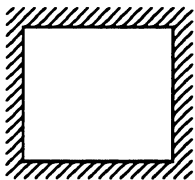
One-dimensional clamped plate



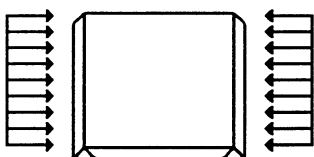
One-dimensional cantilever plate



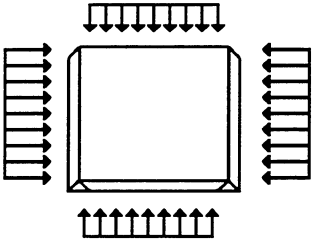
Two-dimensional simply supported plate



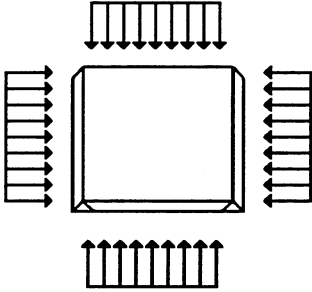
Two-dimensional simply supported plate



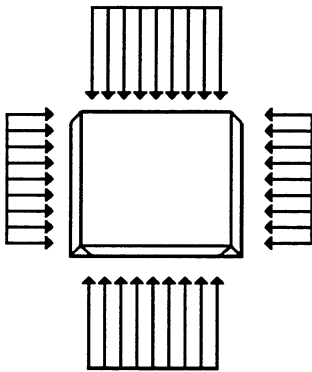
Two-dimensional plate subjected to a uniaxial uniform compression load



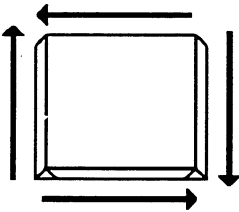
Two-dimensional plate subjected to a biaxial uniform compression load ($N_y=N_x/2$)



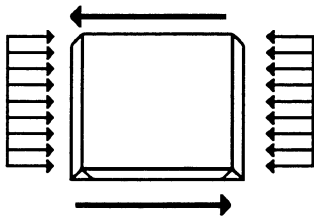
Two-dimensional plate subjected to a biaxial uniform compression load ($N_y=N_x$)



Two-dimensional plate subjected to a biaxial uniform compression load ($N_y=N_x*2$)



Two-dimensional plate subjected to a uniform in-plane shear load



Two-dimensional plate subjected to a uniaxial uniform compression and in-plane shear load

1 INTRODUCTION AND PRELIMINARIES

Designing with composite materials is complex because there are many variables to consider: orientation of fibres, number of plies, ply thickness, type of fibre, type of matrix, configuration, etc. Thus, the optimum design is not obvious and different cases must be considered.

The chapters of this book fall into three groups. Chapter 1 provides a general background on composite materials: anisotropic constitutive relations, laminated plates and shear theories to be applied to thin and thick laminates, respectively. Chapters 2 to 5 are concerned with constant thickness composite structures, and provide a survey of various design methodologies of shells, plates and sandwich constructions. Chapters 6 to 9 examine variable thickness composite structures, and consider beams, plates and sandwiches. The users' manuals of DAC and OPTI, two software packages for designing constant and variable thickness structures respectively, are presented separately.

First of all, constant thickness structures are studied. Shells, plates and sandwiches are analysed in terms of design optimisation, the weight being the optimisation criterion. Different applications are reviewed and a comparison with standard materials and optimum configurations is given for each case.

Secondly, variable thickness structures are studied. Beams, plates and sandwiches are analysed and a comparison with constant thickness structures and optimum configurations is given for each case.

1.1. Introduction

The aim of this chapter is to define the basis of the analyses described in this book. First, anisotropic constitutive relations are presented in order to obtain the stress-strain relations for composite materials.

Then, the formulation of two theories which are the most widely used in the field of composites design is described. These are the laminated plate theory and the first order shear theory.

The laminated plate theory is simple and easy to implement. The results obtained by means of this theory are accurate for thin plates (characteristic length/thickness > 10). Thus, this theory is very useful for this type of plate because several optimisation criteria for design may be easily obtained.

When working with thick plates (characteristic length/thickness < 10), the interlaminar effect cannot be neglected and thus, a shear theory must be used. For design optimisation purposes, the first order shear theory gives good results and therefore, that methodology will be used in this book. To obtain very accurate results, a higher order shear theory is more adequate.

A rational basis of structural engineering design must be based on the ability to predict the load and hence, the stress, likely to be encountered in practice. Therefore, a numerical method to carry out the stress analyses in an optimum way must be selected.

Failure criteria are needed for design optimisation and materials improvement. The most frequently used criteria are extensions of similar criteria for isotropic materials, which include those for maximum stress, maximum strain and quadratic. The choice of an appropriate failure criterion is made in this chapter.

Finally, the numerical methods applied in this text for optimisation purposes are described.

1.2 Anisotropic constitutive relations

Laminated composites are constructed from orthotropic plies containing collimated unidirectional fibres, woven cloth or chopped strand mattings. Generally, in a macroscopic sense, the lamina is assumed to behave as a homogeneous orthotropic material. The constitutive relation for a linear elastic orthotropic material in the fibre co-ordinate system, Fig. 1.1, is (1-3):

$$\begin{bmatrix} \epsilon_1 \\ \epsilon_2 \\ \epsilon_3 \\ \gamma_{23} \\ \gamma_{31} \\ \gamma_{12} \end{bmatrix} = \begin{bmatrix} S_{11} & S_{12} & S_{13} & 0 & 0 & 0 \\ S_{12} & S_{22} & S_{23} & 0 & 0 & 0 \\ S_{13} & S_{23} & S_{33} & 0 & 0 & 0 \\ 0 & 0 & 0 & S_{44} & 0 & 0 \\ 0 & 0 & 0 & 0 & S_{55} & 0 \\ 0 & 0 & 0 & 0 & 0 & S_{66} \end{bmatrix} \begin{bmatrix} \sigma_1 \\ \sigma_2 \\ \sigma_3 \\ \tau_{23} \\ \tau_{31} \\ \tau_{12} \end{bmatrix} \quad [1.1]$$

where the stress components (σ_j, τ_{ij}) are defined in Fig. 1.1 and S_{ij} are elements of the compliance matrix. The strain components (ϵ_j, γ_{ij}) are defined in a manner analogous to the stress components.

In a thin lamina a plane stress is commonly assumed by setting:

$$\sigma_3 = \tau_{31} = \tau_{13} = 0 \quad [1.2]$$

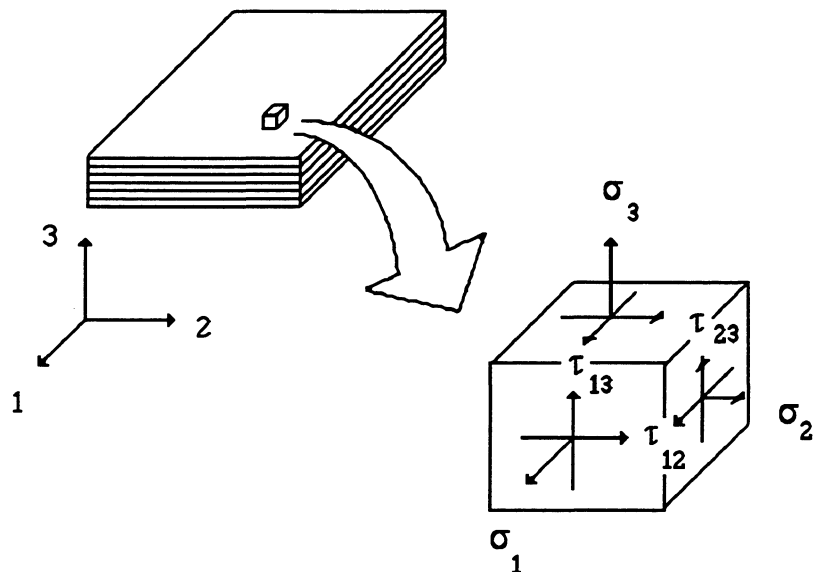


Figure 1.1 Definition of stress components and principal material directions for an orthotropic material.

For equation 1.1 this assumption leads to:

$$\begin{aligned}\varepsilon_3 &= S_{13}\sigma_1 + S_{23}\sigma_2 \\ \gamma_{23} &= \gamma_{31} = 0\end{aligned}\tag{1.3}$$

Thus, ε_3 is not an independent strain component and does not need to be included in the constitutive relationship for plane stress. Equation 1.1 becomes:

$$\begin{bmatrix} \varepsilon_1 \\ \varepsilon_2 \\ \gamma_{12} \end{bmatrix} = \begin{bmatrix} S_{11} & S_{12} & 0 \\ S_{12} & S_{22} & 0 \\ 0 & 0 & S_{66} \end{bmatrix} \begin{bmatrix} \sigma_1 \\ \sigma_2 \\ \tau_{12} \end{bmatrix}\tag{1.4}$$

S_{ij} may be related to the engineering constants as:

$$\begin{aligned}S_{11} &= 1/E_1, \quad S_{12} = -\nu_{12}/E_1 = -\nu_{21}/E_2 \\ S_{22} &= 1/E_2, \quad S_{66} = 1/G_{12}\end{aligned}\tag{1.5}$$

The relation in equation 1.4 may be inverted to obtain the stress components from the strain components:

$$\begin{bmatrix} \sigma_1 \\ \sigma_2 \\ \tau_{12} \end{bmatrix} = \begin{bmatrix} Q_{11} & Q_{12} & 0 \\ Q_{12} & Q_{22} & 0 \\ 0 & 0 & Q_{66} \end{bmatrix} \begin{bmatrix} \varepsilon_1 \\ \varepsilon_2 \\ \gamma_{12} \end{bmatrix}\tag{1.6}$$

where Q_{ij} are the reduced stiffnesses:

$$\begin{aligned}Q_{11} &= E_1 / (1 - \nu_{12}\nu_{21}) \\ Q_{12} &= \nu_{12}E_2 / (1 - \nu_{12}\nu_{21}) = \nu_{21}E_1 / (1 - \nu_{12}\nu_{21}) \\ Q_{22} &= E_2 / (1 - \nu_{12}\nu_{21}) \\ Q_{66} &= G_{12}\end{aligned}\tag{1.7}$$

For a lamina whose principal material axes are oriented at an angle with respect to the x - y system (see Fig. 1.2), the stresses and strains transform according to:

$$\begin{bmatrix} \sigma_1 \\ \sigma_2 \\ \tau_{12} \end{bmatrix} = [T] \begin{bmatrix} \sigma_x \\ \sigma_y \\ \tau_{xy} \end{bmatrix}\tag{1.8}$$

and

$$\begin{bmatrix} \epsilon_1 \\ \epsilon_2 \\ \gamma_{12}/2 \end{bmatrix} = [T] \begin{bmatrix} \epsilon_x \\ \epsilon_y \\ \gamma_{xy}/2 \end{bmatrix} \quad [1.9]$$

where the transformation matrix is:

$$[T] = \begin{bmatrix} m^2 & n^2 & 2mn \\ n^2 & m^2 & -2mn \\ -mn & mn & m^2-n^2 \end{bmatrix} \quad [1.10]$$

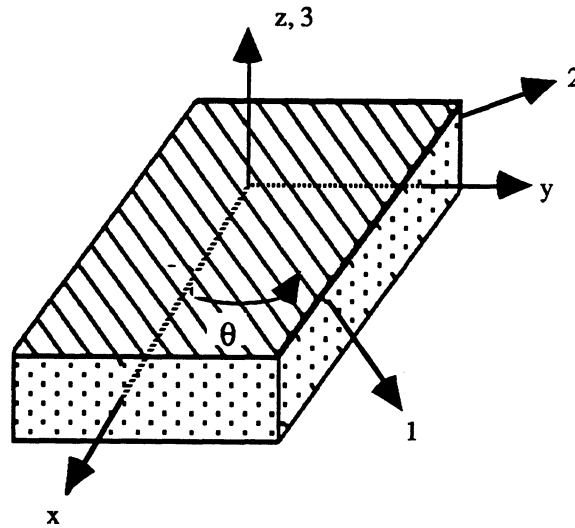


Figure 1.2 Positive rotation of principal material axes (1-2) from arbitrary x-y axes.

in which

$$m = \cos\theta$$

$$n = \sin\theta \quad [1.11]$$

From equations 1.8 and 1.9 it is possible to establish the stress-strain relation in any co-ordinate system. In this way the compliance relation becomes:

$$\begin{bmatrix} \epsilon_x \\ \epsilon_y \\ \gamma_{xy} \end{bmatrix} = \begin{bmatrix} \bar{s}_{11} & \bar{s}_{12} & \bar{s}_{16} \\ \bar{s}_{12} & \bar{s}_{22} & \bar{s}_{26} \\ \bar{s}_{16} & \bar{s}_{26} & \bar{s}_{66} \end{bmatrix} \begin{bmatrix} \sigma_x \\ \sigma_y \\ \tau_{xy} \end{bmatrix} \quad [1.12]$$

Similarly, the stiffness relation becomes:

$$\begin{bmatrix} \sigma_x \\ \sigma_y \\ \tau_{xy} \end{bmatrix} = \begin{bmatrix} \bar{Q}_{11} & \bar{Q}_{12} & \bar{Q}_{16} \\ \bar{Q}_{12} & \bar{Q}_{22} & \bar{Q}_{26} \\ \bar{Q}_{16} & \bar{Q}_{22} & \bar{Q}_{66} \end{bmatrix} \begin{bmatrix} \epsilon_x \\ \epsilon_y \\ \gamma_{xy} \end{bmatrix} \quad [1.13]$$

where the bars denote transformed properties obtained from:

$$\begin{aligned} \bar{S}_{11} &= m^4 S_{11} + m^2 n^2 (2S_{12} + S_{66}) + n^4 S_{22} \\ \bar{S}_{21} = \bar{S}_{12} &= m^2 n^2 (S_{11} + S_{22} - S_{66}) + S_{12} (m^4 + n^4) \\ \bar{S}_{22} &= n^4 S_{11} + m^2 n^2 (2S_{12} + S_{66}) + m^4 S_{22} \\ \bar{S}_{16} &= 2m^3 n (S_{11} - S_{12}) + 2mn^3 (S_{12} - S_{22}) - mn (m^2 - n^2) S_{66} \\ \bar{S}_{26} &= 2mn^3 (S_{11} - S_{12}) + 2m^3 n (S_{12} - S_{22}) + mn (m^2 - n^2) S_{66} \\ \bar{S}_{66} &= 4m^2 n^2 (S_{11} - S_{12}) - 4m^2 n^2 (S_{12} - S_{22}) + (m^2 - n^2)^2 S_{66} \end{aligned} \quad [1.14]$$

$$\begin{aligned} \bar{Q}_{11} &= m^4 Q_{11} + 2m^2 n^2 (Q_{12} + 2Q_{66}) + n^4 Q_{22} \\ \bar{Q}_{21} = \bar{Q}_{12} &= m^2 n^2 (Q_{11} + Q_{22} - 4Q_{66}) + (m^4 + n^4) Q_{12} \\ \bar{Q}_{22} &= n^4 Q_{11} + 2m^2 n^2 (Q_{12} + 2Q_{66}) + m^4 Q_{22} \\ \bar{Q}_{16} &= m^3 n (Q_{11} - Q_{12}) + mn^3 (Q_{12} - Q_{22}) - 2mn (m^2 - n^2) Q_{66} \\ \bar{Q}_{26} &= mn^3 (Q_{11} - Q_{12}) + m^3 n (Q_{12} - Q_{22}) + 2mn (m^2 - n^2) Q_{66} \\ \bar{Q}_{66} &= m^2 n^2 (Q_{11} + Q_{22} - 2Q_{12} - 2Q_{66}) + (m^4 + n^4) Q_{66} \end{aligned} \quad [1.15]$$

Hygrothermal strains. As fibrous composite materials are processed at elevated temperatures, thermal strains introduced during cool-down to room temperature may lead to residual stresses and changes in dimensions. Furthermore, matrices may be hygroscopic and tend to absorb moisture which may lead to swelling strains and stresses in the material. The constitutive relationship with temperature and swelling strains included takes the following form:

$$\begin{bmatrix} \sigma_x \\ \sigma_y \\ \tau_{xy} \end{bmatrix} = \begin{bmatrix} \bar{Q}_{11} & \bar{Q}_{12} & \bar{Q}_{16} \\ \bar{Q}_{12} & \bar{Q}_{22} & \bar{Q}_{26} \\ \bar{Q}_{16} & \bar{Q}_{22} & \bar{Q}_{66} \end{bmatrix} \begin{bmatrix} \epsilon_x \\ \epsilon_y \\ \gamma_{xy} \end{bmatrix} \quad [1.16]$$

$$\begin{bmatrix} \epsilon_x \\ \epsilon_y \\ \gamma_{xy} \end{bmatrix} = \begin{bmatrix} \bar{S}_{11} & \bar{S}_{12} & \bar{S}_{16} \\ \bar{S}_{12} & \bar{S}_{22} & \bar{S}_{16} \\ \bar{S}_{16} & \bar{S}_{26} & \bar{S}_{66} \end{bmatrix} \begin{bmatrix} \sigma_x \\ \sigma_y \\ \tau_{xy} \end{bmatrix} + \begin{bmatrix} \epsilon_x^T \\ \epsilon_y^T \\ \gamma_{xy}^T \end{bmatrix} + \begin{bmatrix} \epsilon_x^S \\ \epsilon_y^S \\ \gamma_{xy}^S \end{bmatrix}$$

where superscripts T and S denote temperature and swelling-induced strains, respectively.

Inversion of equation 1.16 gives:

$$\begin{bmatrix} \sigma_x \\ \sigma_y \\ \tau_{xy} \end{bmatrix} = \begin{bmatrix} \bar{Q}_{11} & \bar{Q}_{12} & \bar{Q}_{16} \\ \bar{Q}_{12} & \bar{Q}_{22} & \bar{Q}_{26} \\ \bar{Q}_{16} & \bar{Q}_{26} & \bar{Q}_{66} \end{bmatrix} \begin{bmatrix} \epsilon_x & -\epsilon_x^T & -\epsilon_x^S \\ \epsilon_y & -\epsilon_y^T & -\epsilon_{xy}^S \\ \gamma_{xy} & -\gamma_{xy}^T & -\gamma_{xy}^S \end{bmatrix} \quad [1.17]$$

The thermal and swelling strains may in many cases be expressed as linear functions of the temperature and the moisture concentration:

$$\begin{bmatrix} \epsilon_x^T \\ \epsilon_y^T \\ \gamma_{xy}^T \end{bmatrix} = \Delta T \begin{bmatrix} \alpha_x \\ \alpha_y \\ \alpha_{xy} \end{bmatrix} \quad [1.18]$$

$$\begin{bmatrix} \epsilon_x^S \\ \epsilon_y^S \\ \gamma_{xy}^S \end{bmatrix} = \Delta C \begin{bmatrix} \beta_x \\ \beta_y \\ \beta_{xy} \end{bmatrix} \quad [1.19]$$

where ΔT and ΔC are the temperature change and moisture concentration change from the reference state. As might be expected, transformations for expansional strains are similar to those for mechanical strains (equation 1.9).

Note that in the principal material co-ordinate system:

$$\alpha_{16} = \beta_{16} = 0 \quad [1.20]$$

as no shear strain is introduced in the principal co-ordinate system because of a change in temperature or moisture concentration.

In many cases, only the steady state temperature and moisture concentration in the composite is of interest. For this case, ΔT and ΔC are constants throughout the material. However, in a transient situation, the transfer of heat by

conduction or diffusion of water has to be considered. There is an obvious analogy between the two phenomena that was first recognised by Fick who developed a mathematical formalism for diffusion, similar to heat transfer.

1.3 Laminate theories

1.3.1 Laminated plates theory

The basic assumptions for the laminated plates theory¹⁻¹⁷ are:

- 1 The plate is constructed of an arbitrary number of layers of orthotropic sheets bonded together. However, the orthotropic axes of material symmetry of an individual layer need not coincide with the x-y axes of the plate.
- 2 The plate is thin, i.e., the thickness h is much smaller than the other physical dimensions.
- 3 The displacements u , v , and w are small compared with the plate thickness.
- 4 In-plane strains ϵ_x , ϵ_y and ϵ_{xy} are small compared with unity.
- 5 In order to include in-plane force effects, nonlinear terms in the equations of motion involving products of stresses and plate slopes are retained. All other nonlinear terms are neglected.
- 6 Transverse shear strains ϵ_{xz} and ϵ_{yz} are negligible.
- 7 Tangential displacements u and v are linear functions of the z co-ordinate.
- 8 The transverse normal strain ϵ_z is negligible.
- 9 Each ply obeys Hook's law.
- 10 The plate has constant thickness.
- 11 Rotary inertia terms are negligible.
- 12 There are no body forces.
- 13 Transverse shear stresses σ_{xz} and σ_{yz} vanish on the surfaces $z = \pm h/2$.

A laminate is made up of a number of plies with an arbitrary planar orientation (see Fig. 1.3). For the displacements of the cross-section of the laminate, it is assumed that a line, originally straight and perpendicular to the middle surface, remains so during deformation. This assumption leads to the vanishing of the out-of-plane shear strains:

$$\gamma_{xz} = \gamma_{yz} = 0 \quad [1.21]$$

where the laminate co-ordinate system ($x - y - z$) is indicated in Fig. 1.3.

Moreover, the strain ϵ_z in the thickness direction is neglected. Consequently, the laminate strains are reduced to ϵ_x , ϵ_y , and γ_{xy} , by the above assumptions, which constitute the Kirchhoff hypothesis for plates. Assuming that the cross-sections undergo only stretching and rotation leads to the following strain distribution,

$$\begin{bmatrix} \varepsilon_x \\ \varepsilon_y \\ \gamma_{xy} \end{bmatrix} = \begin{bmatrix} \varepsilon_x^0 \\ \varepsilon_y^0 \\ \gamma_{xy}^0 \end{bmatrix} + z \begin{bmatrix} K_x \\ K_y \\ K_{xy} \end{bmatrix} \quad [1.22]$$

where $(\varepsilon_x^0, \varepsilon_y^0, \gamma_{xy}^0)$ and (K_x, K_y, K_{xy}) are the mid-plane strains and curvatures, respectively, and z is the distance from the mid-plane.

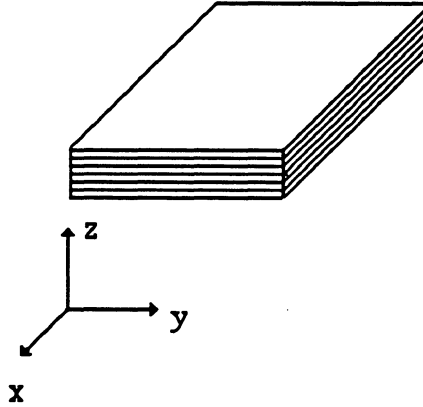


Figure 1.3 Laminate co-ordinate system.

The resultant forces and moments are obtained by integration of the stresses in each layer over the laminate thickness, h :

$$\begin{bmatrix} N_x \\ N_y \\ N_{xy} \end{bmatrix} = \int_{-h/2}^{h/2} \begin{bmatrix} \sigma_x \\ \sigma_y \\ \tau_{xy} \end{bmatrix}_k dz \quad [1.23]$$

$$\begin{bmatrix} M_x \\ M_y \\ M_{xy} \end{bmatrix} = \int_{-h/2}^{h/2} \begin{bmatrix} \sigma_x \\ \sigma_y \\ \tau_{xy} \end{bmatrix}_k z dz \quad [1.24]$$

where (N_x, N_y, N_{xy}) and (M_x, M_y, M_{xy}) are the force and moment resultants, respectively. The subscript k represents the k^{th} lamina in the laminate.

Combination of equations 1.17 to 1.19, 1.22 to 1.24 leads to:

$$\begin{bmatrix} N_x \\ N_y \\ N_{xy} \end{bmatrix} = \begin{bmatrix} A_{11} & A_{12} & A_{16} \\ A_{12} & A_{22} & A_{26} \\ A_{16} & A_{26} & A_{66} \end{bmatrix} \begin{bmatrix} \varepsilon_x^0 \\ \varepsilon_y^0 \\ \gamma_{xy}^0 \end{bmatrix} + \begin{bmatrix} B_{11} & B_{12} & B_{16} \\ B_{12} & B_{22} & B_{26} \\ B_{16} & B_{26} & B_{66} \end{bmatrix} \begin{bmatrix} K_x \\ K_y \\ K_{xy} \end{bmatrix} \quad [1.25]$$

$$\begin{bmatrix} M_x \\ M_y \\ M_{xy} \end{bmatrix} = \begin{bmatrix} B_{11} & B_{12} & B_{16} \\ B_{12} & B_{22} & B_{26} \\ B_{16} & B_{26} & B_{66} \end{bmatrix} \begin{bmatrix} \varepsilon_x^0 \\ \varepsilon_y^0 \\ \gamma_{xy}^0 \end{bmatrix} + \begin{bmatrix} D_{11} & D_{12} & D_{16} \\ D_{12} & D_{22} & D_{26} \\ D_{16} & D_{26} & D_{66} \end{bmatrix} \begin{bmatrix} K_x \\ K_y \\ K_{xy} \end{bmatrix} \quad [1.26]$$

A_{ij} , B_{ij} and D_{ij} are called extensional stiffnesses, coupling stiffnesses, and bending stiffnesses, respectively. They are calculated from:

$$\begin{aligned} A_{ij} &= \sum_{k=1}^N (\bar{Q}_{ij})_k (z_k - z_{k-1}) \\ B_{ij} &= \frac{1}{2} \sum_{k=1}^N (\bar{Q}_{ij})_k (z_k^2 - z_{k-1}^2) \\ D_{ij} &= \frac{1}{3} \sum_{k=1}^N (\bar{Q}_{ij})_k (z_k^3 - z_{k-1}^3) \end{aligned} \quad [1.27]$$

1.3.2 First order shear theory

For composites having a high ratio of in-plane Young's moduli to interlaminar shear moduli and ratios of in-plane dimensions to thickness less than ten, significant differences between the exact solutions and results from classical theory are observed. In particular, maximum plate deflections are shown to be considerably larger than predicted by classical laminated plate theory. As a result it is appropriate to develop a first order laminated plate theory which can be applied to moderately thick plates.

There are several references related to shear theories (18-27). In this section a shear theory (Whitney¹⁸) which includes the effects of transverse shear deformation and rotary inertia is considered. Solutions to the theory are also presented for the purpose of assessing the effect of transverse shear deformation on the behaviour of laminated plates. The approach presented is an extension of theories developed by Reissner and Mindlin for homogeneous, isotropic plates to laminates consisting of an arbitrary number of bonded anisotropic layers. Such an extension was originally due to Yang, Norris, and Stavsky with some later modification by Whitney and Pagano.

1.3.2.1 Constitutive equations

The basic assumptions for the shear deformation theory are:

- 1 The plate is constructed of an arbitrary number of layers of orthotropic sheets bonded together. However, the orthotropic axes of material symmetry of an individual layer need not coincide with the x-y axes of the plate.
- 2 The plate is thin, i.e., the thickness h is much smaller than the other physical dimensions.
- 3 The displacements u, v, and w are small compared with the plate thickness.
- 4 In-plane strains ϵ_x , ϵ_y and ϵ_{xy} are small compared with unity.
- 5 In order to include in-plane force effects, nonlinear terms in the equations of motion involving products of stresses and plate slopes are retained. All other nonlinear terms are ignored.
- 6 Tangential displacements u and v are linear functions of the z co-ordinate.
- 7 The transverse normal strain ϵ_z is negligible.
- 8 Each ply obeys Hook's law.
- 9 The plate has constant thickness.
- 10 There are no body forces.
- 11 Transverse shear stresses σ_{xz} and σ_{yz} vanish on the surfaces $z = \pm h/2$.

Thus the displacements are now assumed to be of the form:

$$\begin{aligned}
 u &= u^0(x,y,t) + z \psi_x(x,y,t) \\
 v &= v^0(x,y,t) + z \psi_y(x,y,t) \\
 w &= w(x,y,t)
 \end{aligned}
 \tag{1.28}$$

Using equation 1.28 in conjunction with the strain-displacement relations:

$$\begin{aligned}
 \epsilon_{11} &= \frac{\partial u_1}{\partial x_1} & \epsilon_{22} &= \frac{\partial u_2}{\partial x_2} & \epsilon_{33} &= \frac{\partial u_3}{\partial x_3} \\
 \epsilon_{23} &= \frac{\partial u_3}{\partial x_2} + \frac{\partial u_2}{\partial x_3} & \epsilon_{13} &= \frac{\partial u_3}{\partial x_1} + \frac{\partial u_1}{\partial x_3} & \epsilon_{12} &= \frac{\partial u_1}{\partial x_2} + \epsilon_{11} = \frac{\partial u_2}{\partial x_1}
 \end{aligned}
 \tag{1.29}$$

The following results are obtained:

$$\begin{aligned}
 \epsilon_x &= \epsilon_x^0 + z \kappa_x \\
 \epsilon_y &= \epsilon_y^0 + z \kappa_y \\
 \epsilon_{xy} &= \epsilon_{xy}^0 + z \kappa_{xy}
 \end{aligned}
 \tag{1.30}$$

where the mid plane strains are defined in the usual manner, by the equation:

$$\epsilon_x^0 = \frac{\partial u^0}{\partial x} \quad \epsilon_y^0 = \frac{\partial v^0}{\partial y} \quad \epsilon_{xy}^0 = \frac{\partial u^0}{\partial y} + \frac{\partial v^0}{\partial x}$$

and

$$\kappa_x = \frac{\partial \psi_x}{\partial x}, \quad \kappa_y = \frac{\partial \psi_y}{\partial y}, \quad \kappa_{xy} = \frac{\partial \psi_x}{\partial y} + \frac{\partial \psi_y}{\partial x} \quad [1.31]$$

In addition, the interlaminar shear strains are given by the relationships:

$$\begin{aligned} \varepsilon_{xz} &= \frac{\partial u}{\partial z} + \frac{\partial w}{\partial x} = \psi_x + \frac{\partial w}{\partial x} \\ \varepsilon_{yz} &= \frac{\partial v}{\partial z} + \frac{\partial w}{\partial y} = \psi_y + \frac{\partial w}{\partial y} \end{aligned} \quad [1.32]$$

Using equation 1.30 in conjunction with the assumption of plane stress within each ply, equation 1.22, and the definition of force and moment resultants, equations 1.23 and 1.24, a constitutive relation of exactly the same form as given by equations 1.25 and 1.26 can be obtained, i.e. in abbreviated notation:

$$\begin{bmatrix} N \\ M \end{bmatrix} = \begin{bmatrix} A & B \\ B & D \end{bmatrix} \begin{bmatrix} \varepsilon \\ \kappa \end{bmatrix} \quad [1.33]$$

where the stiffness terms A_{ij} , B_{ij} , and D_{ij} are defined by equation 1.27. Applying the definition of shear force resultants, we obtain an additional constitutive relation involving transverse shear. Following Reissner and Mindlin we introduce a parameter k in this constitutive relation for transverse shear. Thus we obtain:

$$\begin{bmatrix} Q_y \\ Q_x \end{bmatrix} = k \begin{bmatrix} A_{44} & A_{45} \\ A_{45} & A_{55} \end{bmatrix} \begin{bmatrix} \varepsilon_{yz} \\ \varepsilon_{xz} \end{bmatrix} \quad [1.34]$$

where ε_{yz} and ε_{xz} are defined in equation 1.32 and

$$A_{ij} = \int_{-h/2}^{h/2} C_{ij} dz \quad (i, j = 4, 5) \quad [1.35]$$

with the C_{ij} terms denoting anisotropic stiffnesses. Values associated with the factor k may be obtained in the literature.²⁸

1.4 Numerical methods of stress analysis

Although in a few cases boundary element methods have been used, the bulk of a considerable body of literature uses the finite element method.²⁹⁻³⁴ Thus, the analyses of the structures studied in this text have been carried out by means of the finite element method. By means of this technique, strains and stresses can be obtained in any point of the plate.

With the finite element method, the interior of the plate is idealised as an assembly of discrete elements over which the unknown displacements are represented approximately by linear, quadratic, etc, variations. Thus, the governing equation of internal equilibrium is satisfied approximately.

Let δa^e be a virtual displacement of the nodes. This displacement generates the following displacements inside the finite element:

$$\delta u = N \delta a^e \quad [1.36]$$

and the following strains inside the finite element:

$$\delta \varepsilon = B \delta a^e \quad [1.37]$$

The work done by the node forces is equal to the addition of the products of each component of force by the corresponding displacement

$$\delta a^{eT} q^e \quad [1.38]$$

Analogously, the internal work-normalised to volume-done by distributed stresses and forces is

$$\delta \varepsilon^T \sigma - \delta u^T \quad [1.39]$$

or

$$\delta a^T (B^T \sigma - N^T b) \quad [1.40]$$

The external work must be equal to the internal work integrated on the elemental volume. Therefore,

$$\delta a^{eT} q^e = \delta a^{eT} \left(\int_{v^e} B^T \sigma \, dv - \int_{v^e} N^T b \, dv \right) \quad [1.41]$$

This expression is valid for any virtual displacement. Thus,

$$q^e = \int_{v^e} B^T \sigma \, dv - \int_{v^e} N^T b \, dv \quad [1.42]$$

For a linear relationship between stresses and strains, the following expression can be obtained:

$$q^e = k^e a^e + f^e \quad [1.43]$$

where k^e is the elemental stiffness matrix:

$$k^e = \int_{v^e} B^T D B \, dv \quad [1.44]$$

and

$$f^e = - \int_{v^e} N^T b \, dv - \int_{v^e} B^T D \varepsilon_0 \, dv + \int_{v^e} B^T \sigma_0 \, dv \quad [1.45]$$

The force-displacement relation for the whole plate is given by:

$$[K] \{a\} = \{q\} \quad [1.46]$$

where $[K]$ is the stiffness matrix of the structure, $\{a\}$ is the displacement vector, and $\{q\}$ is the force vector.

The strain energy e_{ij} of the j^{th} layer of the i^{th} element is given by:

$$e_{ij} = \{a\}_i^t [k]_{ij} \{a\}_i \quad [1.47]$$

The element strains $\{\varepsilon\}_i$ in the i^{th} element are expressed by:

$$\{\varepsilon\}_i = [c] \{a\}_i \quad [1.48]$$

where $[c]$ is the strain-displacement matrix. The stresses $\{\sigma\}_{ij}$ in the j^{th} layer of the i^{th} element are given by:

$$\{\sigma\}_{ij} = [Q]_{ij} \{\varepsilon\}_i \quad [1.49]$$

where $[Q]_{ij}$ is the matrix of elastic constants of the j^{th} layer of the i^{th} element.

1.5 Failure criteria

For optimisation processes, the concept of the strength/stress ratio is extremely useful. Thus, the chosen failure criterion must have a unique strength/stress ratio for each combined state of stress and the corresponding state of strain. Owing to this, a quadratic criterion has been applied.

According to Tsai and Wu,³⁵ there exists a failure surface in the stress-space in the following scalar form:

$$F_{ij} \sigma_{ij} + F_i \sigma_i = 1 \quad i, j = 1, 2, 3, 4, 5, 6 \quad [1.50]$$

where the contracted notation is used; F_i and F_{ij} are strength tensors of the second and fourth rank, respectively.

One method of applying the strength criterion is to transform the stress components into the material-symmetry axes. The final expression will be composed by the following terms:

$$\begin{aligned} & F_1 \sigma_1' + F_2 (\sigma_2' + \sigma_3') + F_{11} \sigma_1'^2 \\ & + F_{22} (\sigma_2'^2 + \sigma_3'^2 + 2 \sigma_4'^2) + F_{66} (\sigma_5'^2 + \sigma_6'^2) \\ & + 2 F_{12} (\sigma_1' \sigma_2' + \sigma_1' \sigma_3') + 2 F_{23} (\sigma_2' \sigma_3' + \sigma_4'^2) = 1 \end{aligned} \quad [1.51]$$

where

$$F_1 = 1/X - 1/X' \quad [1.52]$$

$$F_{11} = 1/(X X') \quad [1.53]$$

$$F_2 = 1/Y - 1/Y' \quad [1.54]$$

$$F_{22} = 1/(Y Y') \quad [1.55]$$

$$F_{33} = 1/(Z Z') \quad [1.56]$$

$$F_{66} = 1/(S S') \quad [1.57]$$

The coupling or interaction terms can be calculated by means of the following formula:

$$F_{ij} = F_{ij}^* [F_{ii} F_{jj}]^{1/2} \quad i \neq j \quad [1.58]$$

and $F_{ij}^* = -0.5$ [1.59]

The strength/stress ratio r is the ratio between the maximum, ultimate or allowable strength, and the applied stress:

$$\{\sigma\}_{\max} = r \{\sigma\}_{\text{applied}} \quad [1.60]$$

Since each combination of stress components in equation 1.50 reaches its maximum when the left-hand side reaches unity, we can substitute equation 1.60 into:

$$F_{ij} \sigma_i \sigma_j + F_i \sigma_i = 1 \quad [1.61]$$

$$[F_{ij} \sigma_i \sigma_j] r^2 + [F_i \sigma_i] r - 1 = 0 \quad [1.62]$$

If we define

$$a = F_{ij} \sigma_i \sigma_j \quad [1.63]$$

$$b = F_i \sigma_i \quad [1.64]$$

Then, the strength/stress ratio r is the positive square root in the quadratic formula:

$$r = - (b / 2a) + [(b / 2a)^2 + 1/a]^{1/2} \quad [1.65]$$

1.6 Numerical methods for design optimisation

The recurrence relations proposed here for resizing the elements for variable thickness structures are based on the optimality criteria, which are not rigorous in the mathematical sense, but are found to give near optimum weight designs for large structures in an efficient way.

The optimality criterion for the generalised stiffness requirement can be stated as, "the optimum structure is the one in which the ratio of the average strain energy density to the mass density is the same in all the elements".³⁶ This criterion can be written as:

$$l = \lambda \bar{e}_{ij} / \rho_{ij} \quad i=1, \dots, m$$

$$j=1, \dots, m \quad [1.66]$$

where λ is the Lagrangian parameter, \bar{e}_{ij} is the strain energy density of the j th layer of the i th element, and ρ_{ij} is the mass density. The strain energy density is given by:

$$\bar{e}_{ij} = e_{ij} / V_{ij} \quad [1.67]$$

where V_{ij} is the volume of the element defined by:

$$V_{ij} = t_{ij} l_i \quad [1.68]$$

where t_{ij} is the thickness of the j th layer of the i th element and l_i is the surface area of the i th element. The design variable t_{ij} can be written as:

$$t_{ij} = \Lambda \alpha_{ij} \quad [1.69]$$

where α_{ij} is the relative thickness (normalised to the maximum thickness) of the j th layer of the i th element, and Λ is the scaling parameter. Introducing the scaling parameter in equation 1.46 gives:

$$\Lambda [K'] \{a\} = \{q\} \quad [1.70]$$

or

$$[K'] \{a'\} = \{q\} \quad [1.71]$$

where

$$\{a\} = \{a'\} / \Lambda \quad [1.72]$$

and $[K']$ is the stiffness matrix for the whole structure obtained by using the relative design vector α_{ij} . Introducing the scaling parameter into equations 1.47 to 1.49, the relations between the actual quantities and the relative quantities at element level can be expressed as:

$$[k]_{ij} = \Lambda [k']_{ij} \quad [1.73]$$

$$\{a\}_i = \{a'\}_i / \Lambda \quad [1.74]$$

$$\{\varepsilon\}_i = \{\varepsilon'\}_i / \Lambda \quad [1.75]$$

$$\{\sigma\}_{ij} = \{\sigma'\}_{ij} / \Lambda \quad [1.76]$$

where the prime quantities are the relative values.

Introducing equations 1.67, 1.73 and 1.74 into equation 1.66 gives: \bar{e}'_{ij}

$$1 = \lambda \bar{e}'_{ij} / (\Lambda^2 \rho_{ij}) \quad [1.77]$$

where

$$\bar{e}'_{ij} = \{r'\}_i^t [K']_{ij} \{r'\}_i / (\alpha_{ij} l_i) \quad [1.78]$$

Multiplying both sides of equation 1.77 by α_{ij}^2 and taking the square root gives:

$$\alpha_{ij} = B \alpha_{ij} (\bar{e}'_{ij} / \rho_{ij})^{1/2} \quad [1.79]$$

where B is a constant. Equation 1.79 can be rewritten in an iterative form as:

$$(\alpha_{ij})_{v+1} = B (\alpha_{ij})_v (\bar{\epsilon}'_{ij} / \rho_{ij})_v^{1/2} \quad [1.80]$$

where v and $v+1$ refer to the cycles of iteration.

In this procedure the resizing of an element is achieved by dividing the design variable by the minimum actual strength/stress ratio for that element:

$$(\alpha_{ij})_{v+1} = (\alpha_{ij})_v / (\tau)_{\min v} \quad [1.81]$$

Therefore, the election of the appropriate failure criterion is critical. If the strength/stress ratio defined by the failure criterion is unique for each combined state of stress and the corresponding state of strain, the application of equation 1.81 is efficient and simple. Otherwise, the application of the procedure becomes more complicated.

For constant thickness structures, sensitivity studies are usually applied to obtain optima configurations. Other optimisation procedures are also available.³⁷⁻⁵¹

References

- 1 Ashton J E, Halpin J C and Petit P H, Primer on Composite Materials: Analysis, Westport, Connecticut, Technomic, 1969.
- 2 Jones R M, Mechanics of Composite Materials, McGraw-Hill, New York, 1975.
- 3 Whitney J M, Daniel I M and Pipes R B, Experimental Mechanics of Fiber Reinforced Composite Materials, Prentice-Hall, Englewood Cliffs, New Jersey, 1984.
- 4 Stavsky Y, 'Thermoelasticity of heterogeneous allotropic plates', J Eng Mech Div, vol 89, no EM 2 1963, 89.
- 5 Halpin J C and Pagano N J, 'Consequences of Environmentally Induced Dilatation in Solids' in Recent Advances in Eng Sci, vol 5 (1970), p 3.
- 6 Whitney J M and Ashton J E, 'Effect of environment on the elastic response of layered composite plates', AIAA J, vol 9, no 9, 1970, 1708.
- 7 Ozisik M N, Heat Conduction, Wiley, New York, 1980.
- 8 Springer G S, (ed.) Environmental Effects on Composite Materials, Technomic, Westport, Connecticut, 1981.
- 9 Pipes R B, Vinson J R and Chou T W, 'On the hygrothermal response of laminated composite systems', J Comp Mat 1976, 10, 129.
- 10 Carlsson L A, 'Out-of-plane hygroinstability of multi-ply paperboard', Fibre Sci and Tech, 1981, 14, 201.
- 11 Timoshenko S P and Goodier J N, Theory of Elasticity, 3rd ed McGraw-Hill, New York, 1970.
- 12 Horgan C O, 'Some remarks on Saint-Venant's principle for transversely isotropic composites', J Elasticity, 1972, 2, 335.
- 13 Choi I and Horgan C O, 'Saint-Venant's Principle and End Effects in Anisotropic Elasticity', J App Mech, vol 44 (1977), p 424.
- 14 Horgan C O 'Saint-Venant's end effects in composites', J Comp Mat, 1982, 16, 411.

- 15 Carlsson L A , Sindelar P and Nilsson S, 'Decay of end effects in graphite/epoxy bolted joints', Comp. Sci. Tech. 1986, 26, 307.
- 16 Arridge R G C, Barham P I, Farell C J and Keller A , 'The importance of end effects in the measurement of moduli of highly anisotropic materials', J Mater Sci. 1976, 11, 788.
- 17 Carlsson L A , Pipes R B , 'Experimental characterisation of advanced composite materials', Prentice Hall, Inc New York, 1987.
- 18 Lo, K H, Christensen, R M, Wu, E M, 'A high order theory of plate deformation part I: Homogeneous plates', ASME, J Appl Mech. 1977, 44, 663.
- 19 Lo, K H, Christensen, R M, Wu, E M, 'A high order theory of plate deformation part II: Laminated plates', ASME, J Appl Mech. 1977, 44, 669.
- 20 Reissner, E, 'On transverse bending of plates, including the effects of transverse shear deformation', Int J Solids Struct. 1975, 11, 569.
- 21 Kant T, Owen D R J, Zienkiewicz O C, 'A refined higher order Co plate bending element', Comput Struct. 1982, 15, 77.
- 22 Reddy J N, 'A simple higher order theory for laminated composite plates', ASME J Appl Mech. 1984, 51, 745.
- 23 Pandya B N, Kant T, 'A refined higher-order generally orthotropic Co plate bending element', Comput Struct. 1988, 28, 119.
- 24 Lakshminarayana H V, Ramani T S, 'On improving the performance of a shear-flexible triangular laminated composite plate finite element' , Proc Int Conf Com Mat and Struct, Madras, 1988.
- 25 Prathap G, Somashekar BR, 'A field-consistent 8-noded laminated anisotropic plate element', Proc Int Conf Com Mat and Struct, Madras, 1988.
- 26 Tessler A, 'An improved higher-order theory for orthotropic plates', Proc RevMech Comp, Bal Harbour, Florida, 1988.
- 27 Miravete A, 'A Simple Finite Element Formulation for Three-Dimensional Laminated Composite Plates', Proc 5th Conf Comp Struct, Paisley, Scotland, 1989.
- 28 Withney J M, 'Shear correction factors of orthotropic laminates under static load', ASME J Appl. Mechanics, 1973, 40, 302-304.
- 29 Zienkiewicz O C, Taylor R L and Too J M, 'Reduced integration techniques in general analysis of plates and shells', Int J Num Meth Engng. 1971, 3, 275.
- 30 Pawsey S E, Clough R W, 'Improved numerical integration of thick shell finite elements', Int J Num Meth Engng. 1971, 3, 545.
- 31 Hughes T J R, Taylor R L and Kanoknukulchal W, 'A simple and efficient finite element for plate bending', Int J Num Meth Engng. Vol11, 1529, 1977
- 32 Pugh, E D L, Hinton, E and Zienkiewicz, O C, 'A study of quadrilateral plate bending with reduced integration', Int J Num Meth Engng. 1978, 12, 1059.
- 33 Lee S W and Pian T H, 'Improvement of plate and shell finite elements by mixed formulations', AIAA J. 1978, 16, 29.
- 34 Hughes T J R and Tezduyar T E, 'Finite Elements based upon Mindlin plate theory, with particular reference to the four-node bilinear.
- 35 Tsai S W and Wu E M, 'A general theory of strength for anisotropic materials', J Comp. Mat. 1971, 5, 58.

- 36 Khot N S, Venkayya V B and Berke L, 'Optimum design of structures with stress and displacement constraints', AIAA, 14, pp131-1322, 1976.
- 37 Donaldson S, 'Simplified weight saving techniques for composite panels', J Reinf Plastics and Composites, 1983.
- 38 Wurzel D P, 'On the optimal design of bidirectional composites', AFWAL-TR-83-4060, Air Force Materials Laboratory, 1983
- 39 Massard T N, 'Computer sizing of composite laminates for strength', J Reinf Plastics and composites, 1984, 3, 300.
- 40 Maksimovic S, 'Optimum design of composite structures', Proc 3rd Conf Comp Struct, Paisley, pp 148, 1985
- 41 Tsai S W, Composites design, (ed. Tsai, S W, Massard, T N, Susuki, I), 1985
- 42 Watkins R I, Morris A J, 'A multicriteria objective function optimization scheme for laminated composites for use in multilevel structural optimization schemes', Comp Meth in Eng 1987, 233.
- 43 Iyengar N G R, 'Optimal design of fiber reinforced composite plates', Proc Advances in Aerospace structures, Madras, pp 71, 1988.
- 44 Pedersen P, 'On Optimal orientation of Orthotropic Materials', (inpress).
- 45 Leissa A W, 'Buckling of laminated composite plates and shell panels', AFWAL-TR-85-3069, Airforce Materials Laboratory, 1985.
- 46 Muc A, 'Optimal fibre orientation for simply-supported, angle-ply plates under biaxial compression', Comp Struct, 1988, 9, 161.
- 47 Reissner E and Stavsky Y, ASME J Appl Mech 1961, 28, 83), 402.
- 48 Timoshenko S P and Woinowsky-Krieger S, 'Theory of plates and shells', McGraw- Hill, New York, 1959
- 49 Cook R D, Concepts and Applications of Finite Element Analysis, John Wiley, New York, 1981.
- 50 Reissner E, 'The effect of transverse shear deformation on the bending of elastic plates', ASME J Appl Mech 1945, 12, A69-A77.
- 51 Mindlin R D, 'Influence of rotatory inertia and shear deformation on flexural motions of isotropic elastic plates', ASME J Appl Mech.

2 DESIGN OPTIMISATION OF CONSTANT THICKNESS COMPOSITE STRUCTURES

2.1 Introduction

Unlike variable thickness composites where stress concentration effects in the area of change of thickness are critical, constant thickness composites design is related to the global behaviour of the structure, particularly stiffness and strength.

Firstly, stiffness and strength properties of some composite material systems are presented. Next, special configurations like SMC and fabric composites are analysed and micromechanical formulations given so as to obtain the ply stiffness and strength parameters as a function of fibre and matrix properties.

Also, a comparison study between a fabric and a [0/90] configuration is carried out in order to find out whether a fabric can be modelled as two unidirectional plies. The behaviour of balanced and unbalanced fabrics is studied. Balanced fabrics (same amount of fibres in the two principal directions of the fabric) have seen most use in industrial applications. Square plates subjected to transverse uniform load must be designed with balanced fabrics. However, non-square plates should not be designed with such a configuration; non-balanced fabrics must be used. The homogenisation of laminated plates is also analysed. When the number of repetitions is higher than ten, the laminate behaves as a homogeneous material and can be treated as an orthotropic non-laminated material.

Finally, the free edge effect is studied from the point of view of design optimisation. Different solutions are described for minimising the delamination process on laminated composite materials. Design optimisation of some constant thickness composite structures like shells, plates and sandwich constructions is analysed in Chapters 3 - 5.

Composite materials embrace a wide range of reinforcing fibres, such as boron, glass, carbon and aramid. Advanced composite materials are used mostly in the form of pre-impregnated sheets which consist of a number of aligned unidirectional rovings impregnated with an epoxy resin matrix. In this form a variety of structural materials can be made by stacking plies in different directions in much the same way as plywood. With these variations in ply orientation, stiffness and strength properties change and, as a consequence, a large number of laminate configurations need evaluation. Some stiffness and strength properties for advanced composite materials have been included in Table 2.1.¹ Studies on the effect of different laminate orientations and lay-ups have reduced somewhat the number of configurations that are likely to be used for structural members, and this has simplified the collection of design data. Glass fibre is a comparatively cheap fibre with a high specific strength (see Table 2.2)² and has seen extensive commercial utilisation in the form of chopped strand matting (Table 2.3)² and woven roving (WR) (Table 2.4).²

Table 2.1 Stiffness and strength properties of boron, carbon and aramid fibres composite materials.

Type	CFRP	BFRP	CFRP	KFRP	CFRTP	CFRP	CFRP	CCRP	CCRP
Fibre	T300	B(4)	AS	Kev 49	AS 4	H-IM6	T300	T300	T300
Matrix	N5208	N5505	3501	epoxy	PEEK	epoxy	F934	F934	F934
					APC2		4-mil	13-mil	7-mil
v/f (%)	70	50	66	60	66	66	60	60	60
ho, mm	0.125	0.125	0.125	0.125	0.125	0.125	0.100	0.325	0.175
Density	1.60	2.00	1.60	1.46	1.60	1.60	1.50	1.50	1.50
Ply stiffness (GPa)									
E_x	181.00	204.00	138.00	76.00	134.00	203.00	148.00	74.00	66.00
E_y	20.30	18.50	8.96	5.50	8.90	11.20	9.65	74.00	66.00
ν_x	0.28	0.23	0.30	0.24	0.28	0.32	0.30	0.05	0.04
E_s	7.17	5.59	7.10	2.30	5.10	8.40	4.55	4.55	4.10
Strength (MPa)									
X	1500	1260	1447	1400	2130	3500	1314	499	375
X'	1500	2500	1447	235	1100	1540	1220	352	279
Y	40	61	52	12	80	56	43	458	368
Y'	246	202	206	53	200	150	168	352	278
S	68	67	93	34	160	98	48	46	46

Table 2.2 Stiffness and strength properties of unidirectional fibre glass composite materials

Type	GFRP	GRFP	GFRP	GFRP	GFRP
Fibre	Unid-R-600	Unid-R-1200	Unid-E-1200	Unid-E-500	Unid-E-glass
Matrix	Epoxy	Epoxy	Vinylester	Polyester	Epoxy
v/f (%)	65.31	69.67	40.23	51.85	45.00
ho, mm	1.00	1.00	0.44	0.49	0.25
Density	2.082	2.141	1.674	1.926	1.800
Ply stiffness (GPa)					
E_x	57.100	60.830	31.161	39.296	38.60
E_y	15.067	19.865	7.452	10.289	8.27
ν_x	0.3020	0.2955	0.3397	0.3222	0.26
E_s	5.032	6.517	2.738	4.260	4.14
Strength (MPa)					
X	1300.0	1600.0	500.0	1000.0	1062.0
X'	1100.0	1400.0	500.0	900.0	610.0
Y	80.0	70.0	50.0	60.0	31.0
Y'	70.0	65.0	50.0	60.0	118.0
S	75.00	70.00	50.00	65.00	72.0

Table 2.3 Stiffness and strength properties of fibre glass fabrics composite materials

Type	GFRP	GFRP	GFRP	GFRP	GFRP	GFRP
Fibre	Fab-E-500A	Fab-E-500B	Fab-E-580	Fab-E-600	Fab-E-500C	Fab-E-500D
Matrix	Polyester	Polyester	Polyester	Polyester	Vinylester	Polyester
v/f (%)	27.41	31.58	40.91	40.91	48.51	31.58
ho, mm	0.70	0.61	0.55	0.56	0.40	0.61
Density	1.584	1.642	1.773	1.773	1.802	1.642
Ply stiffness (GPa)						
E_x	14.440	16.228	19.817	20.065	9.320	16.228
E_y	13.639	15.312	19.817	19.569	36.960	15.312
ν_x	0.1480	0.1415	0.1309	0.1326	0.0825	0.1415
E_s	2.070	2.260	2.781	2.781	3.347	2.260
Strength (MPa)						
X	196.0	400.0	185.0	185.0	350.0	200.0
X'	196.0	400.0	180.0	180.0	350.0	160.0
Y	180.0	380.0	180.0	180.0	320.0	200.0
Y'	180.0	380.0	175.0	175.0	320.0	160.0
S	45.00	40.00	45.00	45.00	45.00	50.00

Table 2.4 Stiffness and strength properties of chopped strand matting fibre glass composite materials.

Type	GFRP	GFRP	GFRP	GFRP
Fibre	CSM-E-600A	CSM-E-300	CSM-E-600B	CSM-Unifilo
Matrix	Polyester	Polyester	Vinylester	Vinylester
v/f (%)	16.51	23.53	37.72	35.94
ho, mm	1.40	0.49	0.61	0.48
Density	1.431	0.529	1.635	1.607
Ply stiffness (GPa)				
E_x	7.733	9.771	14.236	13.641
E_y	7.733	9.771	14.236	13.641
ν_x	0.3426	0.3354	0.3287	0.3292
E_s	2.880	3.659	5.357	5.131
Strength (MPa)				
X	100.0	140.0	160.0	180.0
X'	100.0	140.0	150.0	180.0
Y	100.0	140.0	160.0	180.0
Y'	100.0	140.0	160.0	180.0
S	30.00	30.00	30.00	30.00

2.2 Special configurations: SMC and fabric composites

2.2.1 Short fibre composites

Short fibre composites include sheet moulding composites (SMC) and whisker composites. Using laminated plate theory, we can derive:

- The Q-isotropic constants for randomly oriented fibres in the plate can be obtained using the plane stress constants mentioned before.

- The Q-isotropic strengths can be obtained using the $[\pi/3]$ Q-isotropic laminates subjected to uniaxial tensile and compressive stresses, and pure shear, together with the quadratic failure criterion.
- The strength is based on the last-ply-failure (LPF) on the assumption that the SMC strength reaches its ultimate at LPF. The Tresca and Mises criteria can be modified to predict the shear strength. Sensitivity of the fibre volume on the SMC strength will also be shown. The cost effectiveness in terms of fibre volume can then be predicted accordingly.

Tsai³ has modelled the SMC configuration by using the Q-isotropic constants (see Table 2.5):

Table 2.5 Modelling of SMC by means of the Q-isotropic constants

Type	CFRP	BFRP	CFRP	GFRP	KFRP	CFRTP	CFRP	CFRP	CCRP	CCRP
Fibre	T300	B(4)	AS	E-glass	Kev 49	AS 4	H-IM6	T300	T300	T300
Matrix	N5208	N5505	3501	epoxy	epoxy	PEEK	epoxy	F934	F934	F934
						APC2		4-mil	13-mil	7-mil
Linear combinations of [Q], GPa								tape	cloth	cloth
U1*	76.37	87.70	59.66	20.54	32.44	57.04	85.88	62.47	58.84	52.37
U4*	22.61	28.36	16.96	5.51	10.54	17.28	25.43	19.73	19.05	16.66
U5*	26.88	29.67	21.35	7.47	10.95	19.88	30.23	21.37	29.89	17.85
* invariant										
Q-isotropic constants										
E, GPa	69.68	78.53	54.84	18.96	29.02	51.81	78.35	56.24	52.67	47.0
nu	0.30	0.32	0.28	0.27	0.32	0.30	0.30	0.32	0.32	0.32
G, GPa	26.88	29.67	21.35	7.47	10.95	19.88	30.23	21.37	19.89	17.8

Q-isotropic constants are defined as follows:

$$E^{\text{iso}} = [1 - \nu^{\text{iso}2}]U_1, \nu^{\text{iso}} = \frac{U_4}{U_1}, G^{\text{iso}} = U_5 \quad [2.1]$$

The micromechanics formulas for SMC (E-glass/epoxy SMC) are given by the empirical model by Manera and Massot:

$$\bar{E} = \left[\frac{16}{45}E_f + 2E_m \right] = \nu_f + \frac{8}{9}E_m \quad [2.2]$$

$$\bar{G} = \left[\frac{2}{15}E_f + \frac{3}{4}E_m \right] = \nu_f + \frac{1}{3}E_m \quad [2.3]$$

$$\bar{\nu} = \frac{e}{2G} - 1 \quad [2.4]$$

This formula for isotropic media is not reliable because the ratio of E over G is close to one. Error is magnified when one is subtracted from this ratio. The strength is given by the following expression:

$$\bar{X} = 510\nu_f + 14 \quad [2.5]$$

2.2.2 Woven composites

Woven composites are intended to cover fabric, as well as structures made by filament winding and braiding. Since fibres must cross over, laminated plate theory that is applicable to discrete plies in a multidirectional laminate must be modified. The author is not aware of any simple theory that can predict the stiffness and strength of woven composites. The simplest way is to use a [0/90] laminate of the same ply material to model a balanced woven fabric. For unbalanced fabrics, the ratio between the 0 and 90 degree plies can match that between the warp and fill yarns. The difficulties in taking account of the fibre cross over arise from the loss of stiffness and strength along the fibres. When fibres are not straight their effective stiffness will reduce. Their tensile strength will reduce because of the additional bending stress and contact stress at cross over points. The compressive strength will also reduce because fibres are more prone to buckling. Another factor that causes difficulty is the fibre volume fraction, which is not likely to be as uniform as that for cross ply composites. Voids are also more likely to occur near the cross over points.

A comparison between the stiffness and strength of a [0/90] composite and those of a balanced fabric made from the same composite material has been shown by Tsai³ (Table 2.6). While the fibre volume fractions are only comparable, the use of cross ply to model fabric is accurate within 20% for glass and kevlar composites. However for graphite composites which have stiff fibres the model is not accurate. For the purpose of design, it is best to use the experimentally measured fabric data directly, replacing the ply data of a unidirectional composite. Further development of the model for the fibre cross over will include the degraded fibre stiffness and strength.

2.2.2.1 Comparison of [0/90] and woven fabric

The predictions of elastic constants of fabrics, filament-wound and braided structures can be made if it is possible to replace the woven composite by a multidirectional laminate consisting of the same fibre angles and ply group ratios. Only then can the micromechanics formulas for stiffness be applied to the plies without modification. In Table 2.6, three ply materials are compared to see how close [0/90] laminates can represent balanced woven fabrics of the same fibres and fibre volume fractions. Thus, under each of the three ply materials, the first column lists the engineering constants of the unidirectional ply. In the second column, the predicted effective laminate stiffness of a [0/90] cross-ply laminate are listed. The predicted values are indicated by an asterisk. These laminate stiffnesses can be compared with those measured from a balanced woven fabric or cloth, listed in the third column. The same bases of comparison apply to the other two ply materials. For the stiffnesses in the x- and y-directions, the [0/90] laminate is higher than those measured from the fabric. This is not unexpected when the fibres in the fabric are not straight, and is true for graphite and kevlar/epoxy composites. The laminate stiffness is 19 and 14% higher than the fabric stiffness, respectively. In the case of the glass/epoxy composite, the laminate stiffness is 18% less than the fabric stiffness. There was apparently a difference in the fibre volume fractions that may account for the lower laminate stiffness. The Poisson's ratio and shear moduli of the [0/90] laminates are close to those of the fabrics.

The predicted strengths of [0/90] are also compared with corresponding strengths measured from fabrics in the table below. With only one exception the compressive strength of glass-epoxy fabric, cross-ply laminates have higher strengths than the fabrics. This is not unexpected because the fibres in fabrics are bent. The fibres in contact will cause local stress concentrations that would reduce tensile strengths. Bent fibres reduce buckling strengths which, in turn, reduce compressive strengths.

Table 2.6 Comparison of [0/90] and woven fabrics for carbon, glass and aramid fibre composites

Type	Graphite/epoxy			E-glass/epoxy			kevlar 49/epoxy		
	CFRP	CCRP	CCRP	GFRP	GFRP	GCRP	KFRP	KFRP	KCRP
Fibre	T300	T300	T300	E-glass	E-glass	F161	kev 49	kev 49	kev 49
Matrix	F934	F934	F934	epoxy	epoxy	6581	epoxy	epoxy	N5209
	[0]	[0/90]		[0]	[0/90]		[0]	[0/90]	
	tape	laminata	cloth	tape	laminata	cloth	tape	laminata	cloth
Stiffness (GPa)									
Ex	148.00	79.2*	66.00	38.60	23.6*	29.6	76.00	41.0*	35.8
Ey	9.65	79.2*	66.00	8.27	23.6*	26.9	5.50	41.0*	35.8
v/x	0.30	0.04*	0.04	0.26	0.09*	0.12	0.34	0.05*	0.09
Es	4.55	4.6*	4.10	4.14	4.1*	6.24	2.30	2.3*	1.79
Strengths (MPa)									
X	1314	664	375	1062	545*	489	1400	704*	582
X'	1220	899	279	610	306*	390	235	165*	189
Y	43	664	368	31	545*	444	12	704*	582
Y'	168	899	278	118	306*	305	53	165*	189
S	48	49*	46	72	80*	133	34	34*	84

* Predicted values

2.2.2.2 Balanced and unbalanced fabrics

Though both balanced and unbalanced fabrics are available, most fabrics used in engineering applications are balanced. This configuration is recommended only in those cases, where values of stresses in 0° and 90° directions are very similar. If there is a significant difference between values of stresses in 0° and 90° directions, unbalanced fabrics must be used.

Let us consider a rectangular plate (thickness: t, length: a and width: b) subjected to transverse uniform load (q). By means of the theory described in Chapter 1, the deflection of the plate is given by the following expression:

$$f = k \cdot 10^{-2} q a^4 / (E_y t^3) \quad [2.6]$$

Figures 2.1 and 2.2 show the deflection (value of k) of a fibreglass/epoxy resin rectangular plate, simply supported and clamped along the four edges, respectively. In both cases, the maximum deflection is given by balanced configurations for non-square plates. The next deflection is given by lightly unbalanced configurations (60% of fibres in the transverse direction and 40% in the longitudinal direction) and so on.

The stiffest plate is composed of an unbalanced configuration (100% of fibres in the transverse direction): k = 0.18 and k = 0.9 for a plate with b > 2.5 a, and clamped and simply supported along the four edges, respectively. For a balanced configuration: k = 0.36 and k = 1.8 for a plate with b > 2.5 a, and clamped and simply supported along the four edges, respectively. Thus, a narrow plate (b > 2.5 a), composed of a balanced configuration presents a double deflection with respect to the optimum configuration (an unbalanced configuration, 100% fibres in the transverse direction).

For narrow plates, the deflection decreases linearly with the percentage of fibres in the transverse direction.

For square plates, there are slight differences between the five configurations represented in Fig. 2.1 and 2.2. The optimum one corresponds to a balanced configuration.

Another finding is the big difference between deflections of simply-supported and clamped plates. There is a factor of 5.

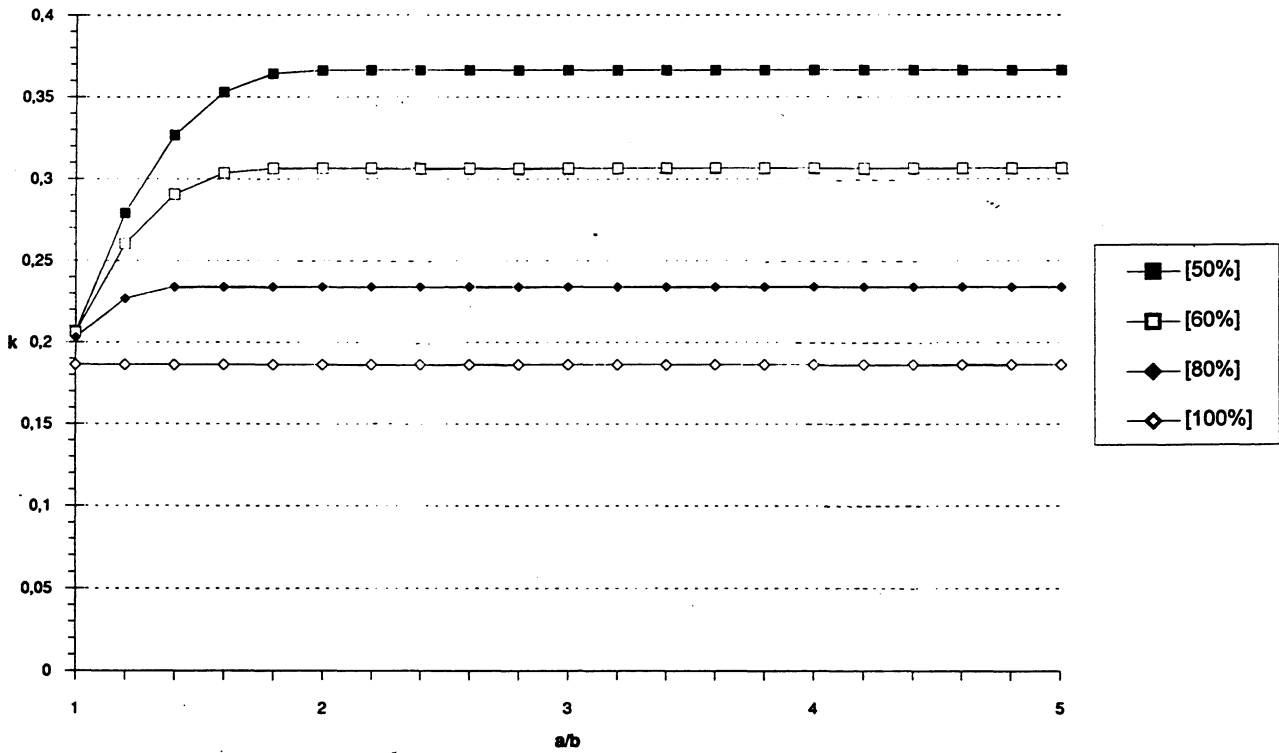


Figure 2.1 T300/5208, rectangular plate, all clamped edges, uniform load. $\{(0_p/90_q)_{20}\}_s$; $p + q = 5$.

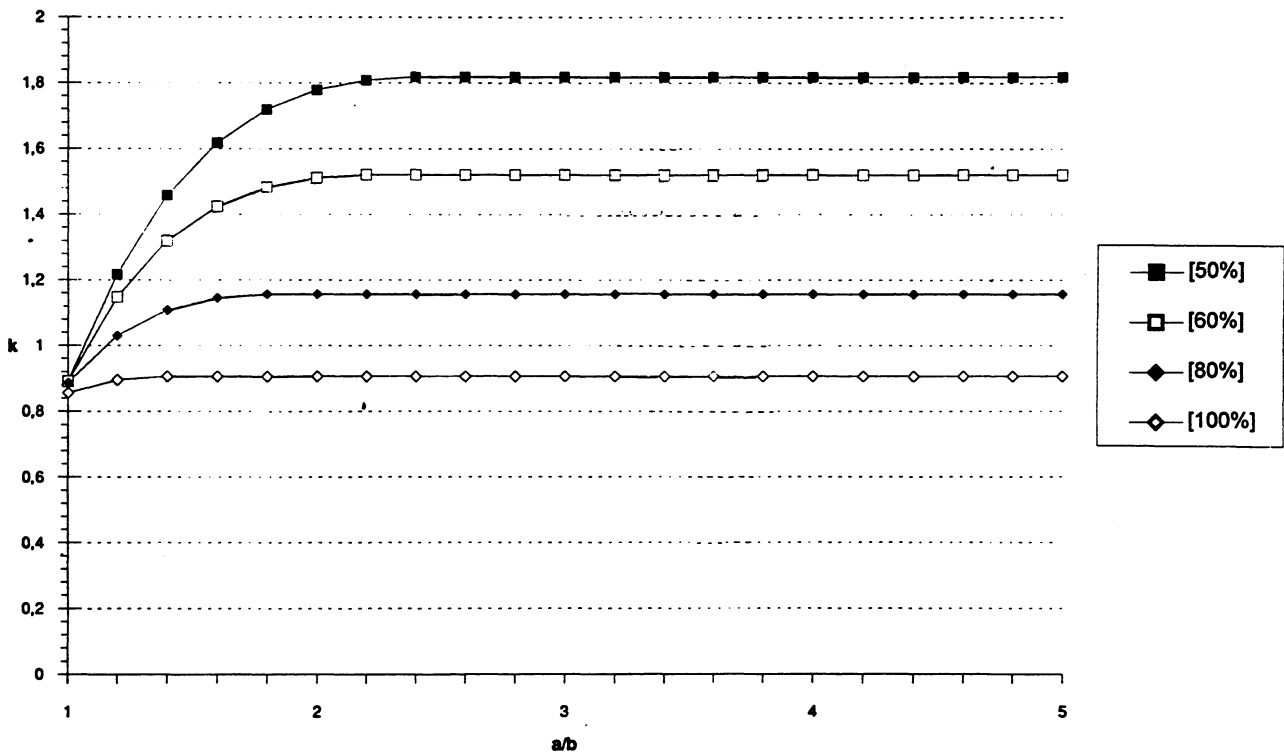


Figure 2.2 T300/5208, rectangular plate, all supported edges, uniform load- $\{(0_p/90_q)_{20}\}_s$; $p + q = 5$.

In both cases, the maximum deflection is given by balanced configurations for non-square plates. The next deflection is given by lightly unbalanced configurations (60% of fibres in the transverse direction and 40% in the longitudinal direction) and so on.

Similar conclusions are obtained for aramid fibre composite plates. The stiffest plate is composed of an unbalanced configuration (100% of fibres in the transverse direction): $k = 0.22$ and $k = 1.15$ for a plate with $b > 2.5 a$, and clamped and simply supported along the four edges, respectively (Fig. 2.3 and 2.4). For a balanced configuration: $k = 0.44$ and $k = 2.30$ for a plate with $b > 2.5 a$, and clamped and simply supported along the four edges, respectively.

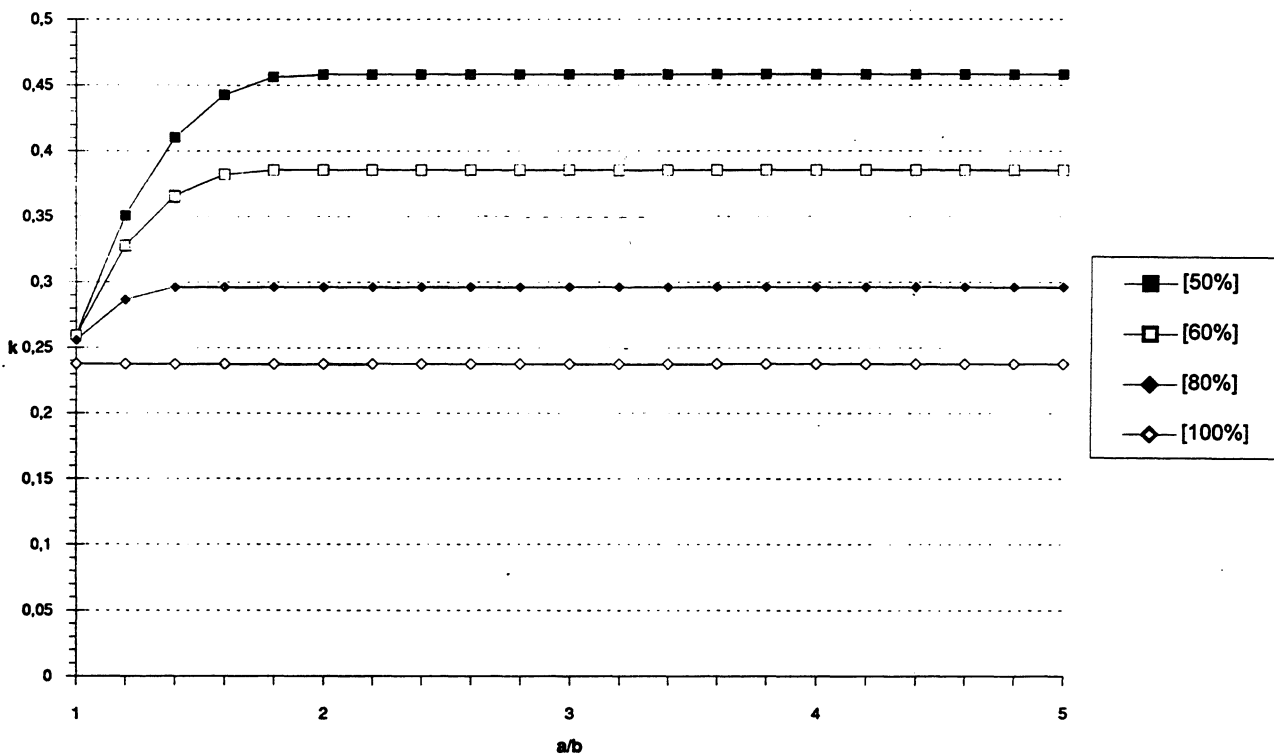


Figure 2.3 Kevlar, rectangular plate, all clamped edges, uniform load $\{(0_p/90_q)_{20}\}_s$; $p + q = 5$.

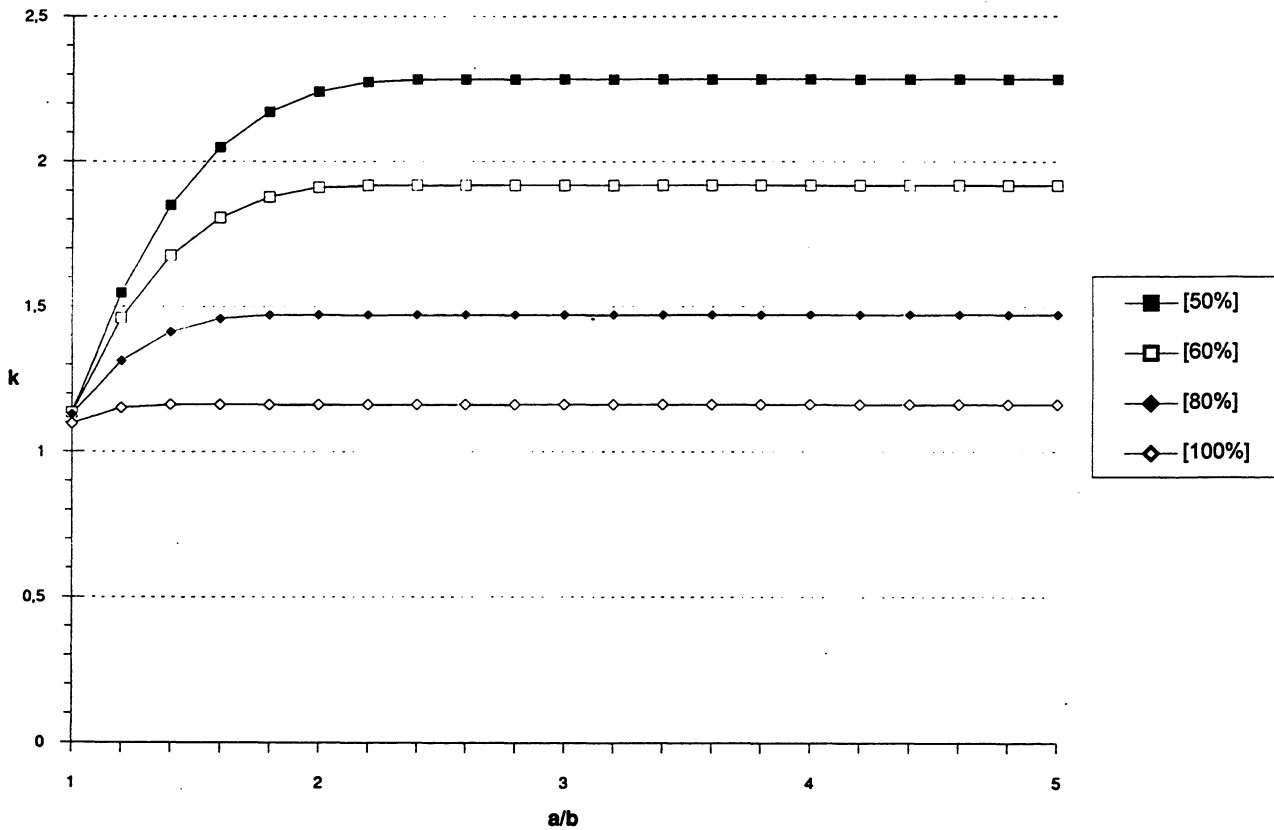


Figure 2.4. Kevlar, rectangular plate, all supported edges, uniform load- $\{(0_p/90_q)_{20}\}_s$; $p + q = 5$

Results for glass fibre composite plates follow the same trends as those observed for carbon and aramid fibres. As might be predicted, values reported for fibreglass are the least stiff of the three systems analysed. The stiffest plate is composed of an unbalanced configuration (100% of fibres in the transverse direction): $k = 0.68$ and $k = 3.2$ for a plate with $b > 2.5 a$, and clamped and simply supported along the four edges, respectively (Fig. 2.5 and 2.6). For a balanced configuration: $k = 1.15$ and $k = 5.7$ for a plate with $b > 2.5 a$, and clamped and simply supported along the four edges, respectively.

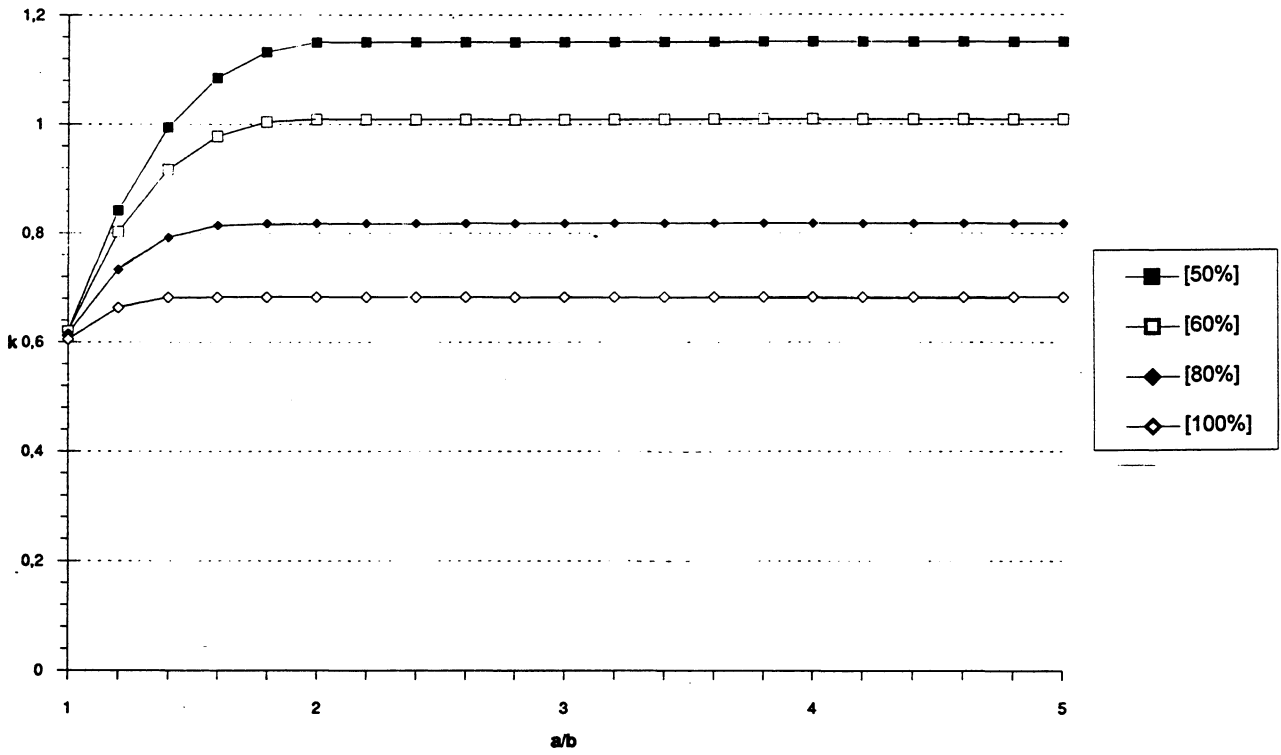


Figure 2.5 Scotchply, rectangular plate, all clamped edges, uniform load- $\{(0_p/90_q)_{20}\}_s$; $p + q = 5$.

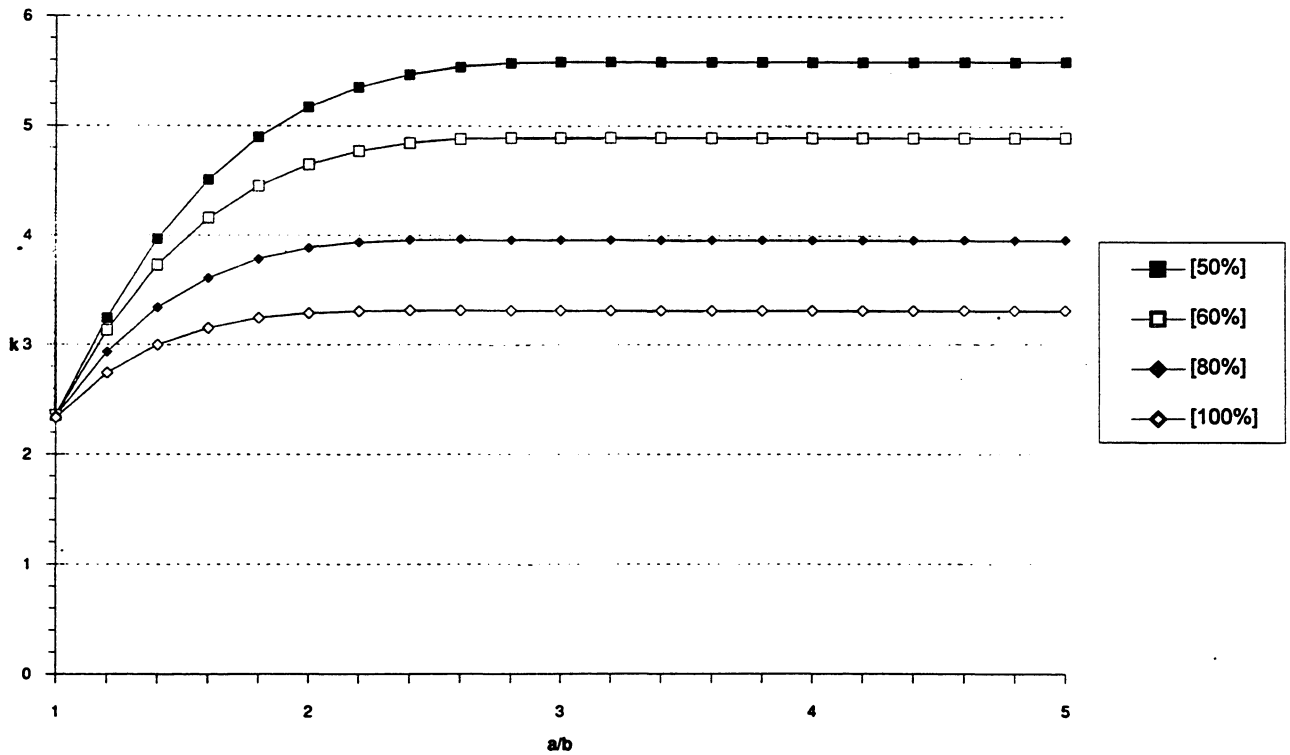


Figure 2.6 Scotchply, rectangular plate, all supported edges, uniform load- $\{(0_p/90_q)_{20}\}_s$; $p + q = 5$.

2.3 Homogenisation of laminated plates

It has been found through experience and demonstrated analytically that ply groups in a laminate should be dispersed or spliced as much as possible to improve laminate strength and toughness. In a finely dispersed laminate, all ply groupings have as few plies as possible. If we have a total of 16 plies each of 0° and 90° orientations, the most dispersed symmetric laminate will be [0/90] repeated eight times at the top half of the laminate, and [90/0] eight times at the bottom half, which is shown on the right in the matrix below. The least dispersed laminate will be eight [0] and eight [90] at the top, and eight [90] and eight [0] at the bottom.

The fewer plies in a ply group, the smaller the percentage of this ply group will be in a total laminate. When the ply group fails, the effect is more localised in a dispersed laminate than in a laminate having fewer but thicker ply groups. One way to build up a highly dispersed laminate is to use repeating sub-laminates, which is therefore one of the recommended design practices.

Let us consider the sublaminates [0/45/-45]. By means of the classical laminated theory described in Chapter 1, for one repetition, the normalised stiffness matrix $ABBD$ presents the following configuration (normalised stiffness matrix is not symmetric):¹

$$\begin{bmatrix} A & B \\ B & D \end{bmatrix} = \begin{bmatrix} 19.989 & 6.536 & .000 & -4.019 & 1.310 & -1.355 \\ 6.536 & 11.862 & .000 & 1.310 & 1.399 & -1.355 \\ .000 & .000 & 6.660 & -1.355 & -1.355 & -1.310 \\ -12.058 & 3.930 & 4.064 & 22.669 & 5.662 & -2.709 \\ 3.930 & 4.198 & 4.064 & 5.662 & 10.929 & -2.709 \\ 4.064 & 4.064 & 3.930 & -2.799 & -2.709 & 5.787 \end{bmatrix}$$

For two repetitions, the normalised stiffness matrix $ABBD$ of the laminate [0/45/-45]₂ is given by the following expression:

$$\begin{bmatrix} A & B \\ B & D \end{bmatrix} = \begin{bmatrix} 19.989 & 6.536 & 0.000 & -2.010 & 0.655 & -0.677 \\ 6.536 & 11.862 & 0.000 & 0.655 & 0.700 & -0.677 \\ 0.000 & 0.000 & 6.660 & -0.677 & -0.677 & 0.655 \\ -6.029 & 1.965 & -2.032 & 20.659 & 6.317 & -0.677 \\ 1.965 & 2.099 & -2.032 & 6.317 & 11.628 & -0.677 \\ -2.032 & -2.032 & 1.965 & -0.677 & -0.677 & 6.442 \end{bmatrix}$$

The normalised stiffness matrix $ABBD$ of the laminate [0/45/-45]₃ presents the following configuration:

$$\begin{bmatrix} A & B \\ B & D \end{bmatrix} = \begin{bmatrix} 19.989 & 6.536 & 0.000 & -1.340 & 0.437 & -0.452 \\ 6.536 & 11.862 & 0.000 & 0.437 & 0.466 & -0.452 \\ 0.000 & 0.000 & 6.660 & -0.452 & -0.452 & 0.437 \\ 4.019 & 1.310 & -1.355 & 20.287 & 6.439 & -0.301 \\ 1.310 & 1.399 & -1.355 & 6.439 & 11.758 & -0.301 \\ -1.355 & -1.355 & 1.310 & -0.301 & -0.301 & 0.563 \end{bmatrix}$$

For five repetitions, the normalised stiffness matrix $ABBD$ of the laminate $[0/45/-45]_5$ is given by the following expression:

$$\begin{bmatrix} A & B \\ B & D \end{bmatrix} = \begin{bmatrix} 19.989 & 6.536 & 0.000 & -0.804 & 0.262 & -0.271 \\ 6.536 & 11.862 & 0.000 & 0.262 & 0.280 & -0.271 \\ 0.000 & 0.000 & 6.660 & -0.271 & -0.271 & 0.262 \\ -2.412 & 0.786 & -0.813 & 20.097 & 6.501 & -0.108 \\ 0.786 & 0.840 & -0.813 & 6.501 & 11.824 & -0.108 \\ -0.813 & -0.813 & 0.786 & -0.108 & -0.108 & 6.625 \end{bmatrix}$$

The normalised stiffness matrix $ABBD$ of the laminate $[0/45/-45]_8$ presents the following configuration:

$$\begin{bmatrix} A & B \\ B & D \end{bmatrix} = \begin{bmatrix} 19.989 & 6.536 & 0.000 & -0.502 & 0.164 & -0.169 \\ 6.536 & 11.862 & 0.000 & 0.164 & 0.175 & -0.169 \\ 0.000 & 0.000 & 6.660 & -0.169 & -0.169 & 0.164 \\ -1.507 & 0.491 & -0.508 & 20.031 & 6.522 & -0.042 \\ 0.491 & 0.525 & -0.508 & 6.522 & 11.847 & -0.042 \\ -0.508 & -0.508 & 0.491 & -0.042 & -0.042 & 6.64 \end{bmatrix}$$

For fifteen repetitions, the normalised stiffness matrix $ABBD$ of the laminate $[0/45/-45]_{15}$ is given by the following expression:

$$\begin{bmatrix} A & B \\ B & D \end{bmatrix} = \begin{bmatrix} 19.989 & 6.536 & 0.000 & -0.268 & 0.087 & -0.090 \\ 6.536 & 11.862 & 0.000 & 0.087 & 0.093 & -0.090 \\ 0.000 & 0.000 & 6.660 & -0.090 & -0.090 & 0.087 \\ -0.804 & 0.262 & -0.271 & 20.001 & 6.532 & -0.012 \\ 0.262 & 0.280 & -0.271 & 6.532 & 11.858 & -0.012 \\ -0.271 & -0.271 & 0.262 & -0.012 & -0.012 & 6.656 \end{bmatrix}$$

For one sublaminar, since the laminate is non-symmetric, matrix B is not zero and since the laminate is balanced, this configuration is orthotropic in plane stress but anisotropic in bending. For the laminate $[0/45/45]_{15}$ all the elements

of matrices B and terms D_{13} y D_{23} are lower than 1. Thus, it has been shown that increasing the number of sublaminates, matrices B tend to zero and values D_{ij} tend to A_{ij} . In general, when the number of repetitions is higher than ten, the laminate behaves as a homogeneous material and can be treated as an orthotropic non-laminated material.

2.4 The free-edge effect

When a multi-directional laminate is subjected to tension, compression or bending loads, a delamination process occurs along the free edges of the structure. The resultant interlaminar stresses present significant values along a width approximately equal to the laminate thickness. Delamination along the straight free edge of composite laminates under an in-plane uniaxial load has been observed since the early 1970s. Since then a large amount of work has been reported on the free-edge problem in composite laminates, indicating that free-edge delamination is attributed to the existence of interlaminar stresses which are highly localised in the region of a free edge under in-plane loading.

It has been shown by Kim⁴ (in Pagano) that in addition to interlaminar tensile stress, other mechanisms such as transverse cracking and interlaminar shearing appear to be significant at the onset and growth of delamination. The $[0/90/\pm 45]_s$ laminate which has a compressive interlaminar normal stress does not show any delamination under static tension, but under fatigue tension shows considerable delamination at the interface between the $+45^\circ$ and -45° plies. The interlaminar shear stress at the $+45^\circ$ and -45° interface is not large enough to reach the interlaminar shear strength under static loading, but under fatigue loading, the shear stress becomes significant because of the high fatigue sensitivity of the epoxy matrix.

The next section covers several methods for the suppression of delamination by designing proper stacking sequences, reinforcing free edges, and toughening the matrix.

2.4.1 Optimum design for controlling delamination

In most cases the presence and growth of free-edge delamination significantly reduces the load-carrying capability and stiffness of composite laminates. Because of this adverse effect of delamination on the integrity of composite structures, a great deal of work has been reported in the literature. However, most of this work has been concerned with the aspects of stress analysis and prediction of delamination initiation and growth. Very little work has been reported on the aspect of controlling delamination.

Delamination can be alleviated by employing a tough material system and/or a change in laminate configuration. A number of different approaches are considered in the literature, including:

- A design of a proper stacking sequence of a laminate.^{4,5,6,7}
- Reinforcing the free-edge regions by stitching or wrapping.^{8,9,10}
- Using a tough resin or altering the mechanical properties of certain layers in the region of potential delamination by adding or replacing some layers with toughened materials, such as adhesive film, hybridisation, etc.^{11,12}

It has been shown by Tsai³ that for static loads, a spiral stacking sequence of Q-isotropic laminates reduces the delamination normal stress component considerably, see Fig. 2.7

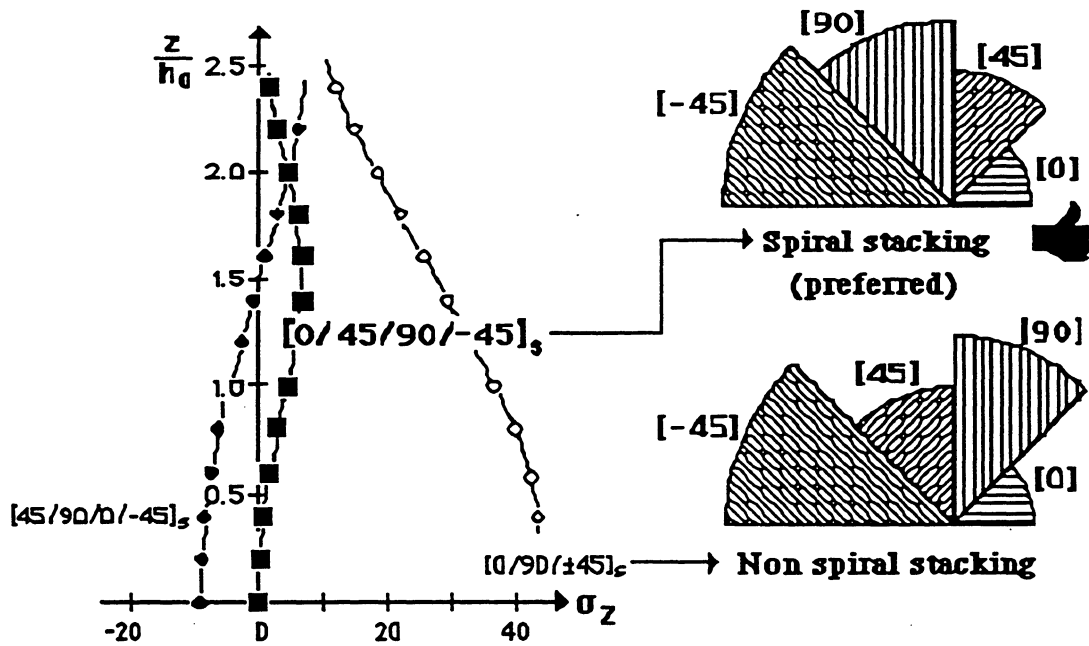


Figure 2.7 Effect of a spiral stacking sequence on delamination normal stress component.

According to Kim (Pagano)⁴ for fatigue loads, an appropriate stacking sequence for a given laminate can provide a considerable reduction in the interlaminar stresses. The effect of the interlaminar normal stress in the $[-45/0/90]_s$ laminate is intensified considerably with an interchange of the 90° and 0° layer positions. This increase of interlaminar normal stress triggers the delamination at a much lower stress level.

Let us consider a Q-isotropic laminate of $\pm 30^\circ$ and 90° plies. The stacking sequence of $[\pm 30/90]_s$ generates a tensile interlaminar normal stress at the free edge in the mid-plane under applied uniaxial tension and, thus, the laminate is delamination prone. If we change the stacking sequence to that of a $[90/\pm 30]_s$ laminate, then the free-edge normal stress becomes compressive, which does not cause delamination.

As another example, let us consider 16 plies of $[0/\pm 45/90]_{2s}$ and $[0_2/\pm 45_2/90_2]_s$. The maximum interlaminar normal stress at the mid-plane is much smaller in the dispersed plies than in the grouped plies. The former dispersed laminate $[0/\pm 45/90]_{2s}$ does not display any delamination until final failure under static loading. A laminate design with a proper stacking sequence can reduce the interlaminar tensile stress component in such a way that the probability of delamination will be greatly reduced or eliminated.

By means of homogeneous laminates, delamination can be reduced considerably. Free edge stress is inversely proportional to the repeating index r (see Fig. 2.8, Tsai³). The tendency to delaminate is drastically reduced if many repeated sub-laminates are used. The same tendency, i.e. higher r , will make LamRank (a software package by Tsai³ that ranks laminates in terms of in-plane strengths) applicable to designing for flexural loads. It is therefore necessary to use sub-laminates that are as thin as possible.

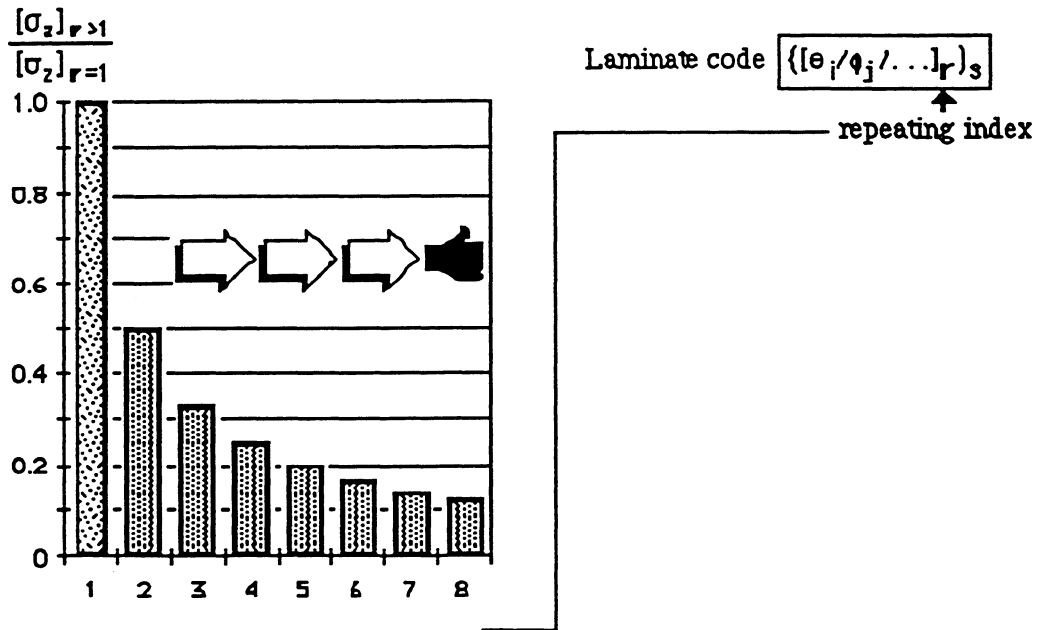


Figure 2.8 Effect of number of sublaminates on free edge stress.

It is possible to prevent or delay the free-edge delamination by suppressing the interlaminar stresses by means of free-edge reinforcement (Kim (Pagano)⁴). Figure 2.9 shows a specimen reinforced with fibre glass woven cloth using a structural adhesive. The reinforced specimen does not show any evidence of delamination at an applied axial tension of 552 MPa, whereas extensive delamination occurred in the unreinforced specimen subjected to an applied tension of 414 MPa. Delamination in this specimen was initiated at 365 MPa as indicated by acoustic emission. No delamination signature by acoustic emission is observed in the reinforced specimens until final failure. The delamination threshold strain is an average of four specimens and is determined by acoustic emission. The reinforced specimens of the first six laminates do not show any delamination until final failure, but the last three laminates, which are subjected to a larger value of σ_z , all delaminate prior to failure. The strength of the reinforced specimen increased by 140% compared with the unreinforced specimen. The large increase in strength suggested that the effect of delamination on static strength may be much more significant in matrix controlled failure modes than in fibre-controlled failure modes.

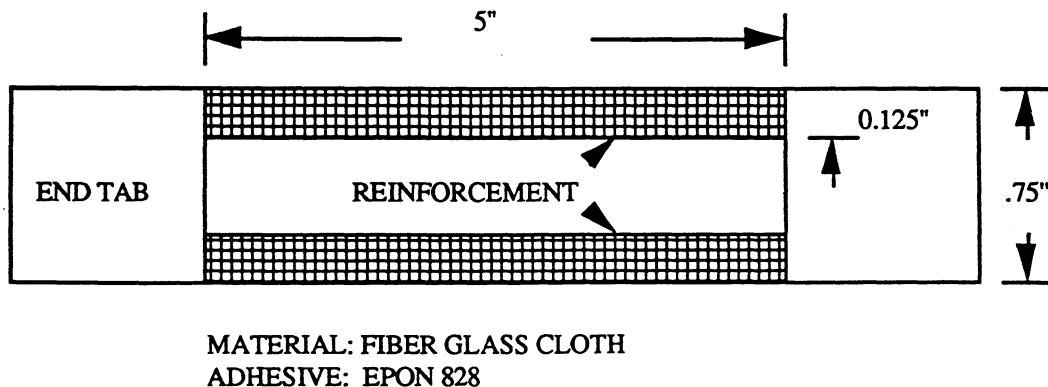


Figure 2.9 Minimisation of delamination effect by using a reinforcement.

Resistance to delamination can also be increased by employing a tough matrix such as thermoplastic. No delamination is observed in the $[\pm 30/90]_s$ laminate of PEEK/AS4 graphite composite, but as discussed earlier, this laminate with epoxy resin experiences extensive delamination. However, there will be some sacrifice in performance in other parameters, such as compressive strength and temperature capability. Other research work on the toughening of laminates that are prone to delamination introduce an interleaf or adhesive layer. Chen et al¹¹ performed finite element analysis of the free-edge problem for a specimen containing an adhesive layer at the mid-plane which is confined to 3.2 mm from the free edge. The adhesive strips reduce the interlaminar stresses and improve the delamination resistance. Soni and Kim¹² conducted analysis and experiment for a $[0/\pm 45/90]_s$ laminate containing a structural adhesive layer in the mid-plane where the critical interlaminar normal stress is present. The stress level at the onset of delamination is increased by approximately 40%.

It is conceivable to control free-edge delamination by novel design of stacking sequence in conjunction with the proper reinforcement of toughened interfaces without any significant sacrifice of other important performance parameters of advanced composite materials.

2.5 Conclusions

At the beginning of this chapter, stiffness and strength properties of some composite material systems were presented. Also, special configurations like SMC and fabrics were analysed. SMC laminates can be treated as unidirectional Q-isotropic configurations. It is important to note that fabric and $[0/90]$ unidirectional laminate give similar results in terms of stiffness and strength parameters (errors lower than 20%). Another conclusion arrived at is that balanced fabric is the optimum configuration for square plates subjected to transverse loads. In those cases, where the plate is rectangular but not square ($a \neq b$), balanced fabrics do not give good results. For very narrow plates ($b > 2.5 a$), the deflection obtained is twice the optimum one: unbalanced fabric. The homogenisation of laminated plates was also analysed. Homogeneous laminates are very interesting in terms of design. When the number of repetitions is higher than 10, the laminate behaves as a homogeneous material and can be treated as an orthotropic non-laminated material.

Finally, the free-edge effect has been analysed from the point of view of design optimisation. The following minimise the free-edge effect:

- A proper stacking sequence of the laminate.
- Reinforcing the free-edge regions by stitching or wrapping.
- Using a tough resin or altering the mechanical properties of certain layers in the region of potential delamination by adding or replacing some layers with toughened materials, such as adhesive film, hybridisation.

References 13-47 give further information about the free-edge effect.

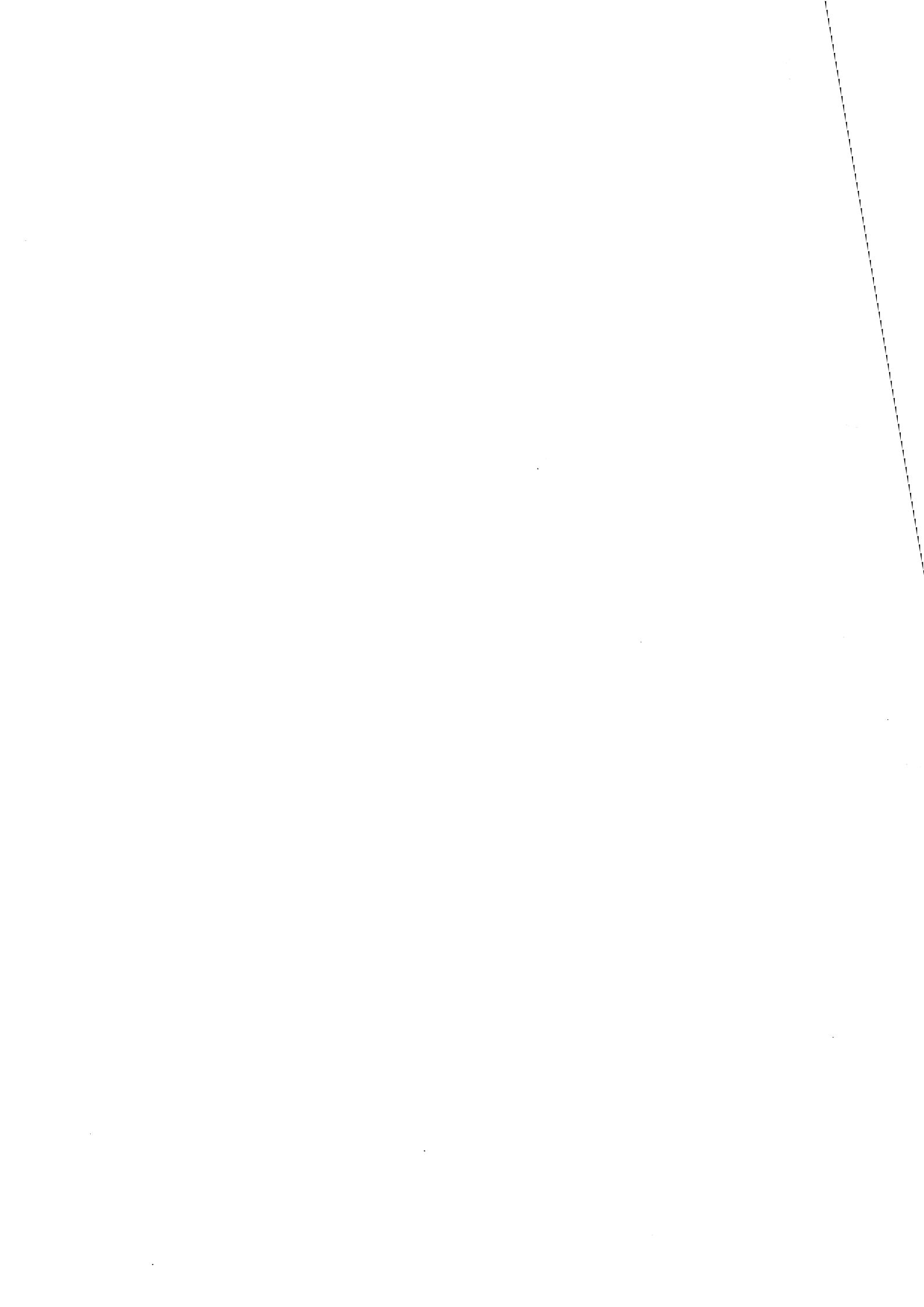
In the following chapters, shells, plates and sandwich constructions will be analysed.

References

1. Tsai S W, 'Composites Design', Think Composites, Dayton, OH, 1988.
2. Antequera P, Jiménez L and Miravete A, 'Los Materiales Compuestos de Fibra de Vidrio', Universidad de Zaragoza, 1992.
3. Tsai S W, 'Theory of Composites Design', Think Composites, Dayton, OH, 1992.
4. Pagano N J, Composite Materials Series, Volume 5: Interlaminar Response of Composite Materials, Elsevier Science Publishers, Amsterdam, The Netherlands, 1989.
5. Pagano N J and Pipes R B, The influence of stacking sequence on laminate strength, J Comp Mater 1971, 5, 50-57.
6. Pagano N J, Stress field in composite laminates, Int J Solids and Struct 1978, 14 385-400.
7. Lackman L M and Pagano N J, On the prevention of delamination of composite laminates, in: proc structures, structural dynamics and materials conference, Las Vegas, Nevada, April 1974, AIAA Paper 74.
8. Kim R Y, Prevention of free edge delamination, in: materials and processes - Continuing Innovations, 28th National SAMPE Symposium and Exhibition (1983).
9. Pipes R B and Daniel I M, Moire analysis of the interlaminar shear edge effect in laminated composites, J Compos Mater, 1971, 5, 255.
10. Howard W E , Gossard T Jr and Jones R M, Reinforcement of composite laminate free edges with Ushaped Caps, AIAA 86-0972 (1986).
11. Chen W S, Rogers C and Aker S, Improvement of edge delamination strength of composite laminates using adhesive layers, ASTM-STP-893 (1984) 266-285.
12. Soni S R and Kim R Y, Analysis of suppression of free edge delamination by introducing adhesive layer, ICCM-VI, eds. F L Matthews, N C R Buskell, J M Hodgkinson and J Morton, Elsevier Science Publishers, London, England, 1987, pp 5219-5230.
13. Pipes R B and Pagano N J , Interlaminar stresses in composite laminates under uniform axial extension, J Comp Mater, 1970, 4, 538-548.
14. Puppo A H and Evensen H A, Interlaminar shear in laminated composites under generalized plane stress, J Compos Mater, 1970, 4 204.
15. Whitney J M and Browning C E, 'Free-edge delamination of tensile coupons', J Comp Mater, 1973, 6 300-303.
16. Pagano N J and Pipes R B, 'Some observations on the interlaminar strength of composite laminates', Int J Mech Sci , 1973, 15, 679-688.
17. Pagano N J and Soni S R, 'Global-local laminate variational model', Int J Solids and Struct 19(3) (1983) 207
18. Sendeckyj G P, Maddux G E and Porter E, Damage Documentation in Composite by Stereo Radiography, ASTM-STP-775 (1982) 16.
19. Andrews R J, Moran T J and Crane R L, 'New capabilities for ultrasonic imaging of defects in fiber reinforced composites', 11th Ann Mini Symp Aerospace Science and Technology, ed Soni S R, Air Force Institute of Technology, WPAFB, OH, 1985, p 21.
20. Freeman S M, Damage Progression in Graphite-Epoxy by a Deplying Technique, AFWAL-TR-81-3157 (1981)
21. Kim R Y, private communication.

22. Harris A and Orringer O, Investigation of angle-ply delamination specimen for interlaminar strength test, J Compos Mater, 1978, 12 285.
23. O'Brien T K, 'Mixed-mode strain energy release rate effects on edge delamination of composites', NASA Technical Report 84592, 1983.
24. Rodini B T Jr and Eisenmann J R, 'An analytical and experimental investigation of edge delamination in composite laminates', in Proceedings of the 4th Conference on Fibrous Composites, eds. E M Lenoe, D W Oplinger and J J Burke. Plenum Press, New York, 1978, pp 441-457.
25. Kim R Y and Rosi S R, 'Experimental and analytical studies on the onset of delamination in laminated composites', J Compos Mater, 1984, 18.
26. Wang A S D and Crossman F W, 'Initiation and growth of transverse cracks and edge delamination in composite laminates, Part II, Experimental Correlation', J Compos Mater (supplement), 1980, 14, 71.
27. Reifsnider K L, Henneke II E G and Stinchcomb W W, Delamination in Q-Isotropic Graphite-Epoxy Laminates, ASTM-STP-617 (1977) 93-103.
28. Soni S R and Kim R Y, Delamination of composite laminates stimulated by interlaminar shear, ASTMSTP-839 (1986) 286-3307.
29. Stalnaker D O and Stinchcomb W W, Load history-edge damage studies in two Q-isotropic graphite epoxy laminates, ASTM-STP-674 (1979) 620-641.
30. Masters J E and Reifsnider K L, An Investigation of Cumulative Damage Development in Q-Isotropic Graphite/Epoxy Laminates ASTM-STP-775 (1982) 40.
31. Rybicki E F and Schmueser D W, 'Effect of stacking sequence and lay-up angle of free edge stresses around a hole in a laminated plate under tension, J Compos Mater, 1978, 12, 300-313.
32. Curtis P T, Effect of Edge Stresses on the Failure of (0,45,90) CFRP laminates, Royal Aircraft Establishment, TR 80054, 1980.
33. Kim R Y and Soni S R, 'Initiation of delamination of composite laminates, in Proceedings of the 1982 Joint Conference on Experimental Mechanics (Society for Experimental Stress Analysis, 1982) pp 244-251.
34. Tsai S W, Mechanics of Composite Materials, Part II - Theoretical Aspects, Technical Report AFMBL-TR66-149, Air Force Materials Laboratory, 1966.
35. Kim R Y and Soni S R, Suppression of free edge delamination by hybridization, ICCM-V, ed. W C Harrigan Jr, J Strife and A K Dhingra, Metallurgical Society, Inc, 1985 pp 1557-1572.
36. Withney J M and Nuismer R J, Stress fracture criteria for laminated composites containing stress concentrations, J Compos Mater, 1974, 8, 258-265.
37. Tsai S W and Wu E, A General Theory of Strength for Anisotropic Materials J Compos Mater 5 (1971) 58.
38. Tsai S W and Hahn H T, Introduction to Composite Materials, Technomic Publishing Co, Westport, CT, 1980, p 302.
39. Kim R Y and Soni S R, Failure of composite laminates due to combined interlaminar normal and shear stresses, in Composite 86: Recent Advances in Japan and the United States, ed. K Kawata, S Umekawa, Kobayashi Japan Society for Composite Materials, Tokyo, Japan, 1986, pp 341-350.
40. Pagano N J and Hahn H T, Evaluation of Composite Curing Stresses, ASTM-STP-617 (1977) 317.
41. Kim R Y, On the Off-axis and Angle-ply Strength of Composites, ASTM-STP-734 (1979) 91-108.
42. Rotem A and Hahn Z, 'Failure modes of angle ply laminates', J Compos Mater, 1975, 9, 191.

43. O'Brien T K, 'Characterization of delamination onset and growth in a composite laminate', in Damage in Composite Materials, ed. K L Reifsnider, ASTM-STP-775 (1982) 140-167.
44. Pipes R B, Kaminski B E and Pagano N J, Influence of the Free Edge upon the Strength of Angle-Ply Laminates, ASTM-STP-521 (1973) 218.
45. Whitcomb J D, Analysis of Instability-Related Growth of a Through-Width Delamination, NASA Technical Memorandum 86301, 1984.
46. Chai H, Babcock C D and Knauss W G, 'One-dimensional modelling of failure in laminated plates by delamination buckling', Int J Solids and Struct, 1981, 17, 1069-1083.
47. Donaldson S L, 'The effect of interlaminar fracture properties on the delamination buckling of composite laminates', Compos Sci and Technol, 1987, 28, 33, 34.



3 SHELLS

3.1 Introduction

Shell structures have come to fruition in the twentieth century. Although the Pantheon of Rome, built in AD 1 and the Mosque of Santa Sofia in Istanbul, built in AD 538 feature shell roofs spanning large distances, they are relatively thick in cross section. It was not until the 1920s that the thin shell roof emerged as a practical means for spanning large distances. This emergence was due to a multiplicity of factors: the ability to form and reinforce depths of composite materials, architectural imagination and the development of analytical tools to ensure the structural integrity of the completed design. Availability of high-strength composite materials, at about the same time, had a similar impact on structural form in aerospace and mechanical engineering design.

Another reason for designing shells with composite materials is that strength is the main parameter in this type of structure and specific strength is one of the most favourable properties of composite materials compared with conventional metallic materials. For instance, a conventional material used in shells is A-42 steel, whose strength is 260 MPa and weight is 8 kg/dm³. A common composite material, such as unidirectional fibre glass/polyester resin presents 500 MPa and 1.7 kg/dm³. Thus the specific strength ratio is about 9. Interesting developments in shell composite structures are given in refs 1-21.

In this chapter, four types of shell structure are analysed: a spherical dome subjected to uniform vertical load, a spherical vessel simply supported and subjected to the weight of an internal fluid, a pipeline subjected to internal pressure and finally, a submarine structure subjected to external pressure. The calculations of the shell structures described in this chapter have been carried out by means of the classical laminated theory reported in Chapter 1. The optimisation procedure used for the ranking of laminates is Lamrank by Tsai.¹

3.2 Spherical dome

In this section, a spherical dome subjected to a uniform vertical load is analysed, the objective being to evaluate in which cases it is worth using a composite material and when this is the case, to assess the weight saving of the composite structure and to obtain the optimal lay-up for each case. A representation of a spherical dome and the definition of variables are shown in Fig. 3.1.

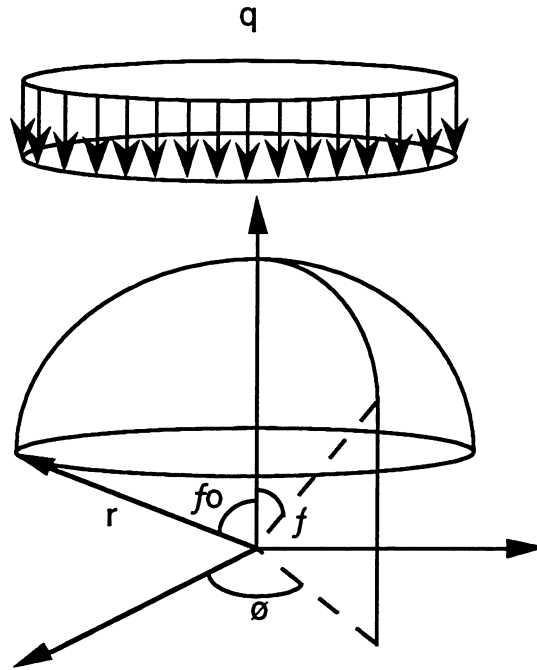


Figure 3.1 Representation of a spherical dome and definition of variables.

In-plane loads are given by the following expressions:

$$N_f = -\frac{r \cdot q}{1 + \cos f} \quad [3.1]$$

$$N_\theta = r \cdot q \cdot \left(\frac{1}{1 + \cos f} - \cos f \right) \quad [3.2]$$

$$(N_{f\theta} = 0) \quad [3.3]$$

N_f is always negative, because there is a compression along the meridian lines. This compression increases with the value of angle f .

$$N_f = -a q / 2 \text{ for } f = 0 \text{ and } N_f = -a q \text{ for } f = 90.$$

N_θ is also negative for values of $f < 51^\circ 50'$. N_θ equals zero for $f = 51^\circ 50'$ and is positive for values of f higher than $51^\circ 50'$. In other words, for values of f higher than this value, there is tension in the parallel direction.

$$\frac{1}{1 + \cos f} - \cos f = 0 \quad [3.4]$$

In-plane loads defined in equations 3.1 and 3.2 are represented in Fig. 3.2 for $r = 2 \text{ m}$, $f_0 = 90^\circ$ and $q = 1 \text{ MPa}$. The value of angle β varies from 225° to 315° , β being defined as:

$$\beta = \text{arctg} \left(\frac{N_f}{N_\theta} \right) \quad [3.5]$$

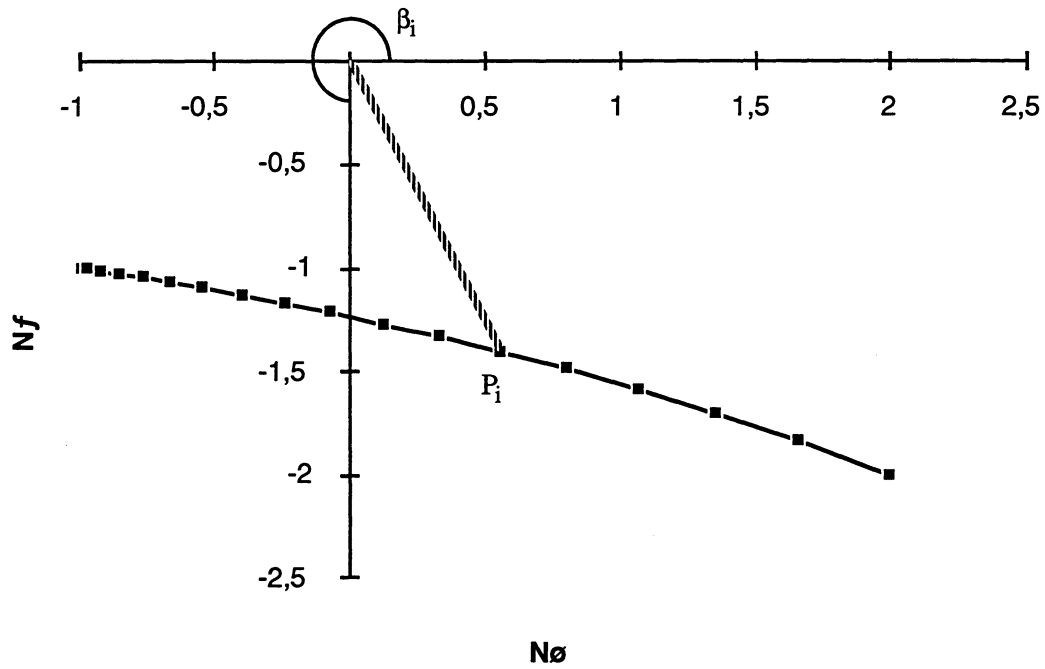


Figure 3.2. Representation of in-plane loads of a spherical dome.

The weight savings of some composite material systems in comparison with the standard material A 42 steel are shown in Fig. 3.3 - 3.6. These graphics can be easily modified to obtain the weight saving with respect to another isotropic material:

$$WS(i) = 100 \cdot \left\{ 1 - \left(1 - \frac{WS(A-42)}{100} \right) \cdot \frac{\sigma(i) \cdot \rho(A-42)}{\sigma(A-42) \cdot \rho(i)} \right\} \quad [3.6]$$

where:

WS(i): weight saving with respect to the isotropic material (i)

WS(A-42): weight saving with respect to A-42 steel

$\sigma(i)$: strength of the isotropic material (i)

$\sigma(A-42)$: strength of A-42 steel (260 MPa)

$r(i)$: density of the isotropic material (i)

$r(A-42)$: density of A-42 steel (8 Kg/dm³)

Figure 3.3 shows the weight saving of a general spherical dome made of unidirectional fibre glass/vinylester resin UNI-E1200 with respect to A-42 steel. The weight saving is a function of the angle f . An average weight saving can be obtained in terms of the angle f_0 (Table 3.1).

Table 3.1 Average weight saving for the UNI-E1200

f_0	AVERAGE WEIGHT SAVING
15°	45.2 %
30°	45.3 %
45°	55.1 %
60°	66.9 %
75°	67.9 %
90°	68.7 %

Thus, in terms of weight saving, the most favourable composite dome is the semispherical one. For angles f_0 lower than 90°, the weight saving does not reach the optimum value. The lower value of f_0 , the lower the weight saving.

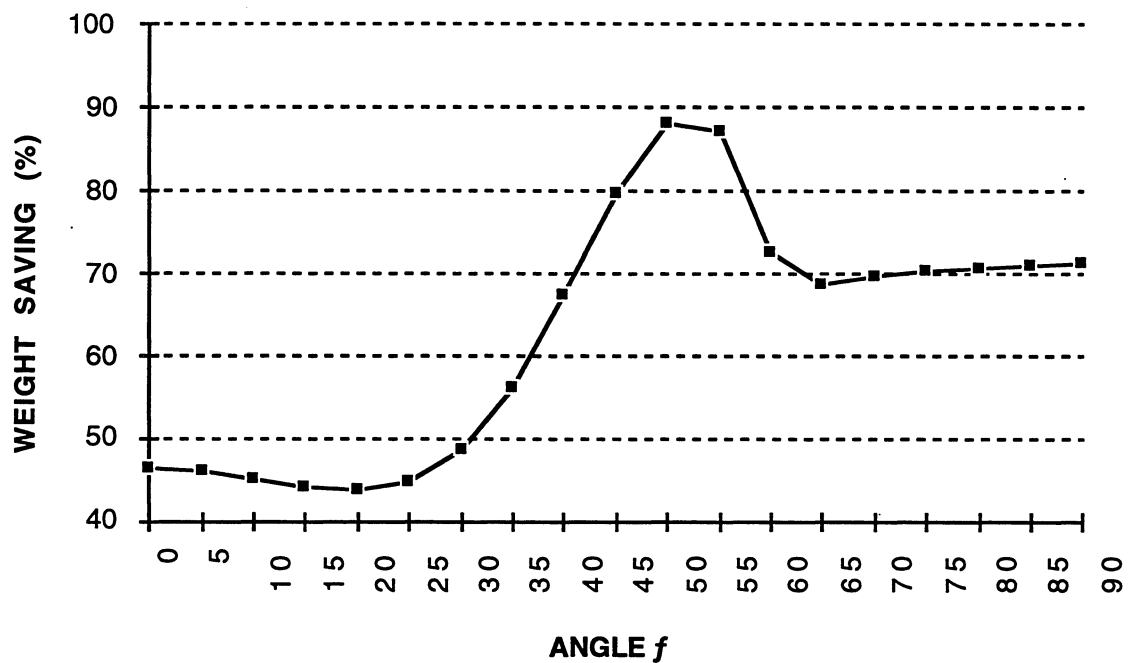


Figure 3.3 Weight saving of a fibre glass/vinylester UNI-E 1200 composite dome versus the angle f .

For a fabric fibre glass/polyester resin FAB-E-580, the weight saving of a general spherical dome with respect to A-42 steel is shown in Figure 3.4. The average weight saving is represented in terms of the angle f_0 (Table 3.2).

Table 3.2 Average weight saving for the FAB-E-580

f_0	AVERAGE WEIGHT SAVING
15°	66.4 %
30°	66.4 %
45°	66.4 %
60°	66.5 %
75°	66.6 %
90°	66.7 %

The most favourable composite dome is the semispherical one.

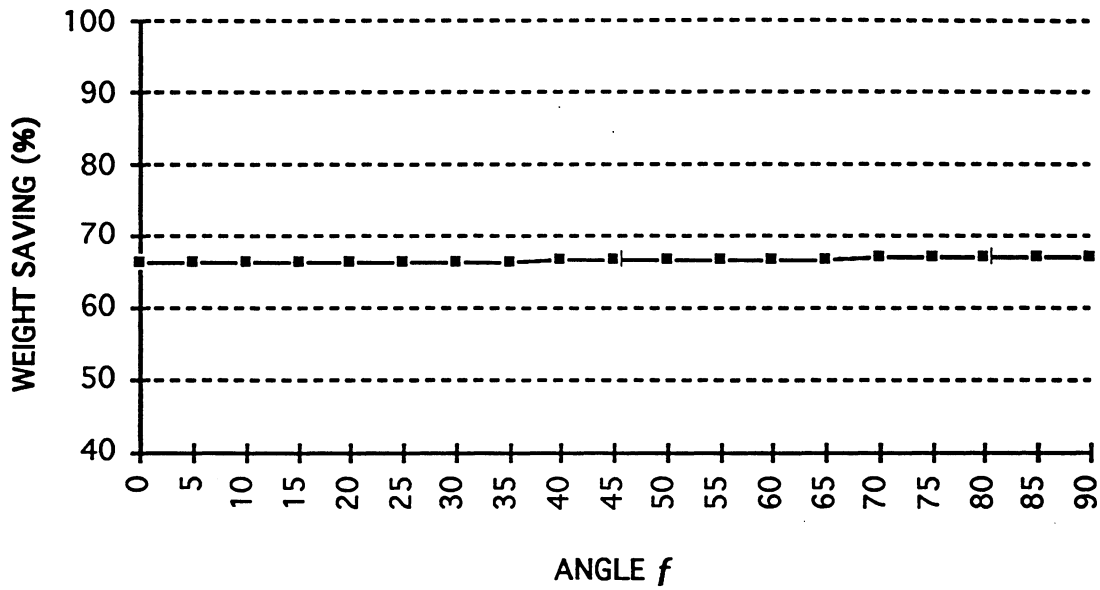


Figure 3.4 Weight saving of a fibre glass/polyester FAB-E-580 composite dome versus the angle f .

Figure 3.5 shows the weight saving of a general spherical dome made of unidirectional prepreg fibre glass/epoxy resin Scotchply with respect to A-42 steel. The average weight saving can be obtained in terms of the angle f_0 (Table 3.3).

Table 3.3 Average weight saving for the SCOTCHPLY

f_0	AVERAGE WEIGHT SAVING
15°	80.8 %
30°	81.3 %
45°	84.2 %
60°	85.9 %
75°	84.1 %
90°	82.1 %

Thus, in terms of weight saving, the most favourable composite domes are those with $f_0 = 60^\circ$. There are very slight differences between the values obtained for different angles. There is a considerable difference between the average weight saving obtained for this configuration and the other two.

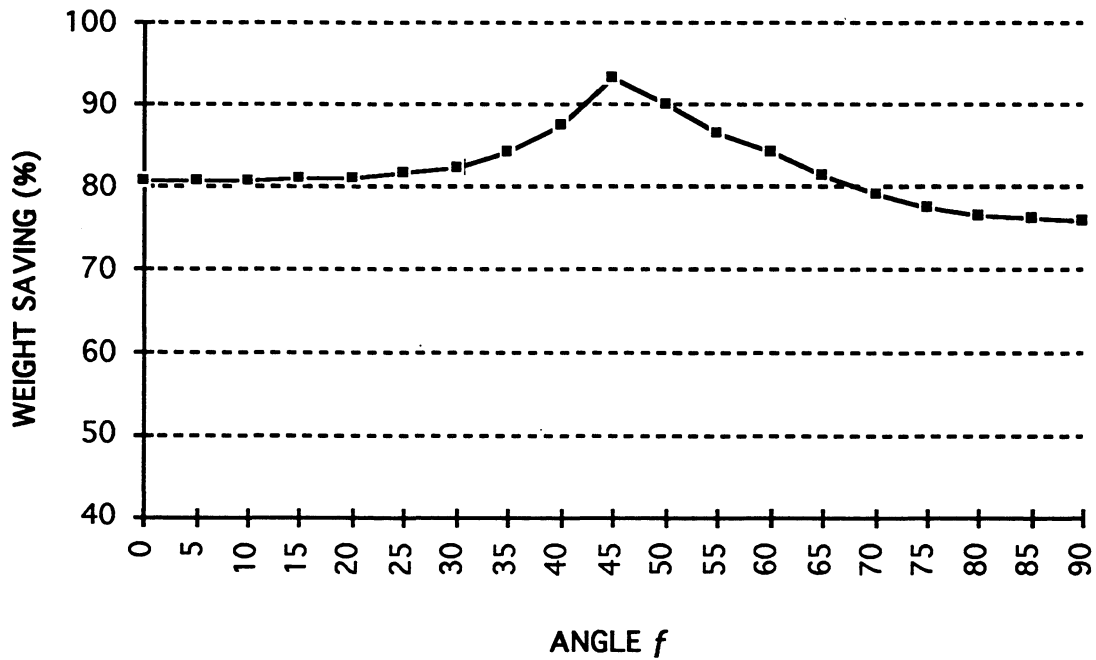


Figure 3.5 Weight saving of a fibre glass/epoxy prepreg Scotchply composite dome versus the angle f .

For a unidirectional carbon fibre/epoxy laminate (T300/N5208) the weight saving of a general spherical dome with respect to A 42 steel is shown in Figure 3.6. The average weight saving can be obtained in terms of the angle f_0 (Table 3.4).

Table 3.4 Average weight saving for the T300/N5208

f_0	AVERAGE WEIGHT SAVING
15°	97.1 %
30°	97.1 %
45°	97.4 %
60°	96.7 %
75°	95.4 %
90°	94.4 %

Thus, in terms of weight saving, the most favourable composite domes are those with $f_0 = 15^\circ$. There are very slight differences between the values obtained for different angles. There is a considerable difference between the average weight saving obtained for this configuration and the other two.

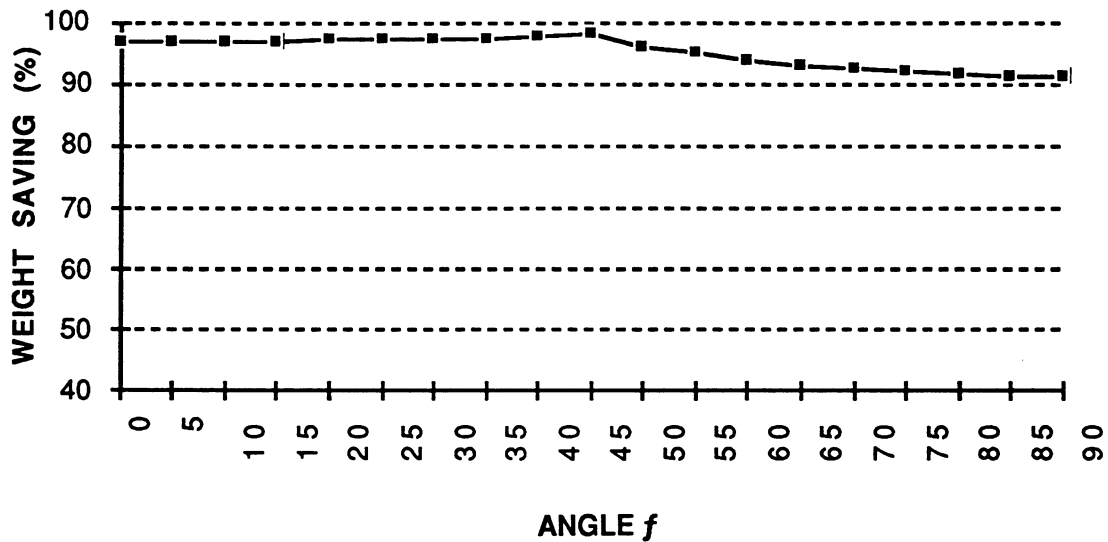


Figure 3.6 Weight saving of a unidirectional carbon fibre/epoxy resin T300/N520 composite dome versus the angle f .

It is interesting to note that the optimum value of the angle f_0 varies drastically from one material to another. In other words, a universal optimum angle f_0 for all composite material systems does not exist.

Table 3.5 shows the optimum sublaminates for different values of b and for the four material systems analysed above. The angle b is related to f :

$$f = 0^\circ \text{ -----} > b = 225^\circ$$

$$f = 90^\circ \text{ -----} > b = 315^\circ$$

The optimum sublaminates are defined for each parallel circle. A four-digit laminate code for the sublaminates is used. The digits in the code represent the number of plies in the sublaminates, and the order of ply angles selected. The first number represents the number of plies in the sublaminates in the parallel circle direction, the second number represents the number of plies in the sublaminates in the meridian circle direction, the third number represents the number of plies at 45° with respect to the parallel circle direction and the fourth number represents the number of plies at -45° with respect to the parallel circle direction. For a generalised $\pi/4$ laminate code [4211] means $[0_4/90_2/45/-45]$.

Table 3.5 Representation of optimum sublaminates for four composite materials

β	UNI-E-1200	TEJ-E-500	SCOTCH	T300-5208
225°	0055	0100	5500	5500
230°	4600	0100	0055	5500
235°	0433	0100	0433	4600
240°	0433	0100	0433	4600
245°	0622	0100	0433	3700
250°	0622	0100	0622	2800
255°	0100	0100	0100	2800
260°	0100	0100	0100	1900
265°	0100	0100	0100	1900
270°	0100	0100	0100	1900
275°	0100	0100	0100	1900
280°	0100	0100	2800	3700
285°	0811	0100	4600	4600
290°	1900	0100	5500	5500
295°	1900	0100	6400	5500
300°	2800	0100	7300	6400
305°	2800	0100	7300	6400
310°	3700	0100	8200	6400
315°	4600	0100	8200	6400

Once again, it is interesting to note that the optimum sublaminates vary drastically from one material to another. The following conclusions can be drawn:

- Optimum laminate with all the plies in meridian and parallel directions have been selected. Number of plies in meridian and parallel directions are related to the magnitude of N_r and N_θ in-plane loads respectively.
- Unidirectional material systems analysed here present an optimum weight saving for $f = 51^\circ 50'$, because the state of stress is unidirectional for this value. This maximum does not appear in the case of a fabric.
- Unidirectional configurations present bad results in a compression-compression state, with a weight saving of about 45% in the area of f ranged between 0° and 30° . Fabric configurations present better results, with a weight saving of around 67%.
- The optimum sublaminate for the fabric is $[0/90]$, i.e. all the fibres are oriented in the meridian and parallel directions.

3.3 Spherical vessel

In this section, a spherical vessel supported on a ring and subjected to the weight of an internal fluid is analysed, the objective being to evaluate in which cases it is worth using composite materials and when this is the case, to assess the weight saving of the composite structure and to obtain the optimum lay-up for each case. A representation of a spherical dome and the definition of variables are shown in Fig. 3.7.

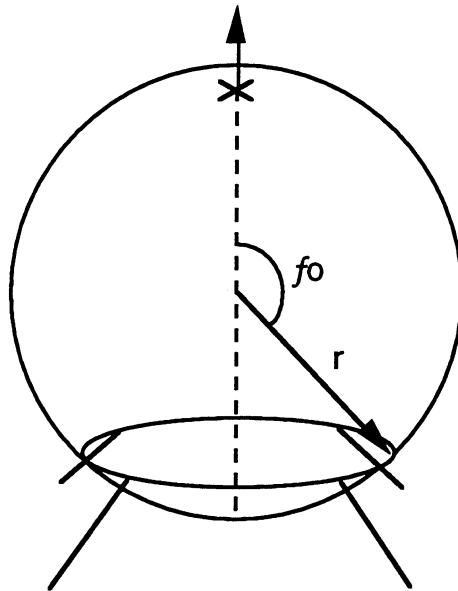


Figure 3.7 Representation of a spherical vessel and definition of variables.

Equations 3.7 - 3.9 give the in-plane loads for the part of the vessel over the support ring ($f < f_0$), along the meridian (N_f) and the parallel (N_θ):

$$N_f = \frac{\rho \cdot r^2}{6} \cdot \left(1 - \frac{2 \cdot \cos^2 f}{1 + \cos f} \right) \quad [3.7]$$

$$N_\theta = \frac{\rho \cdot r^2}{6} \cdot \left(5 - 6 \cdot \cos f + \frac{2 \cdot \cos^2 f}{1 + \cos f} \right) \quad [3.8]$$

$$N_{f\theta} = 0 \quad [3.9]$$

The resultant in the support ring presents a modulus equal to the weight of the internal fluid and its direction is vertical:

$$R = 4 \pi r^3 \rho / 3 \quad [3.10]$$

Equations 3.11 - 3.13 give the in-plane loads for the part of the vessel under the support ring ($f > f_0$), along the meridian (N_f) and the parallel (N_θ):

$$N_f = \frac{\rho \cdot r^2}{6} \cdot \left(5 + \frac{2 \cdot \cos^2 f}{1 - \cos f} \right) \quad [3.11]$$

$$N_\theta = \frac{\rho \cdot r^2}{6} \cdot \left(1 - 6 \cdot \cos f - \frac{2 \cdot \cos^2 f}{1 - \cos f} \right) \quad [3.12]$$

$$N_{f\theta} = 0 \quad [3.13]$$

According to equations 3.9 - 3.13, the in-plane load N_f suffers a drastic change of value $2 r^2 \cdot \rho / (3 \sin^2 f_0)$, in the area around the support ring, and the other in-plane load N_θ is decreased in $2 r^2 \cdot \rho / (3 \sin^2 f_0)$.

In Fig. 3.8 - 3.11, in-plane load graphics are represented for some values of f_0 . For all the cases, lines relating N_f and N_θ are located in the range of β (-45/90). Moduli of N_f and N_θ are given in MN/m and correspond to

$$r = 10 \text{ m}$$

$$\rho = 0.01 \text{ MN/m}^3$$

$$f_0 = 90^\circ, 120^\circ, 150^\circ \text{ or } 180^\circ$$

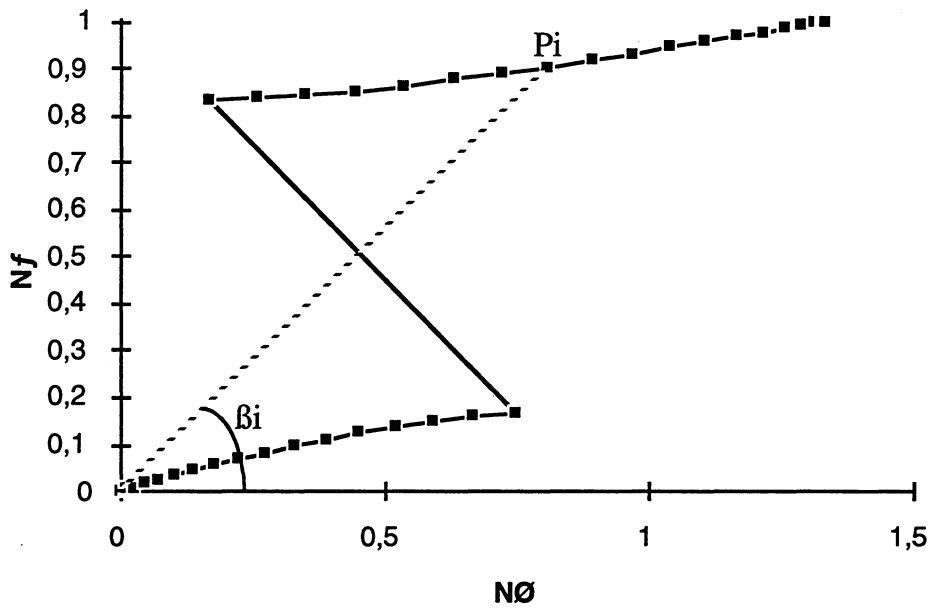


Figure 3.8. Representation of in-plane loads for $f_0 = 90^\circ$.

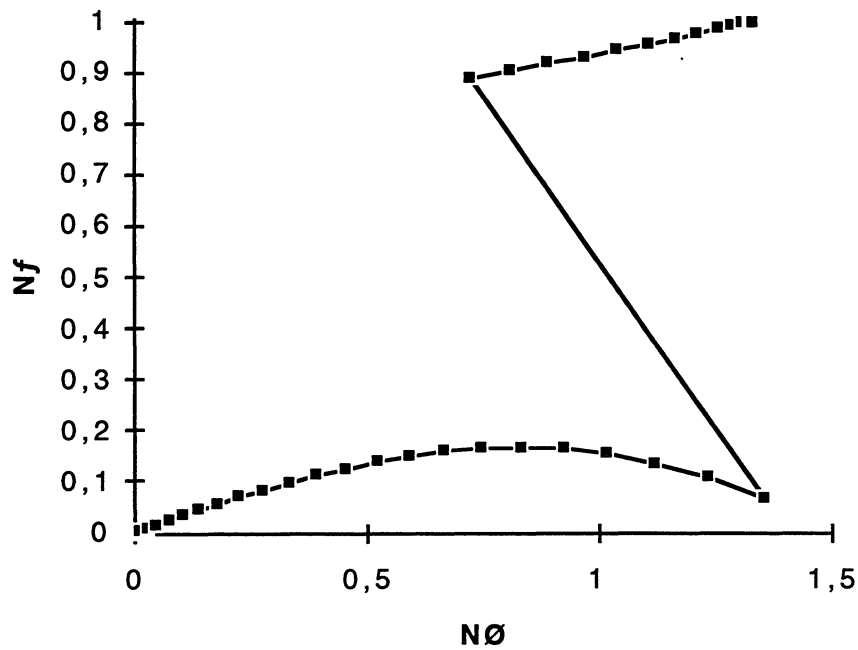


Figure 3.9. Representation of in-plane loads for $f_0 = 120^\circ$.

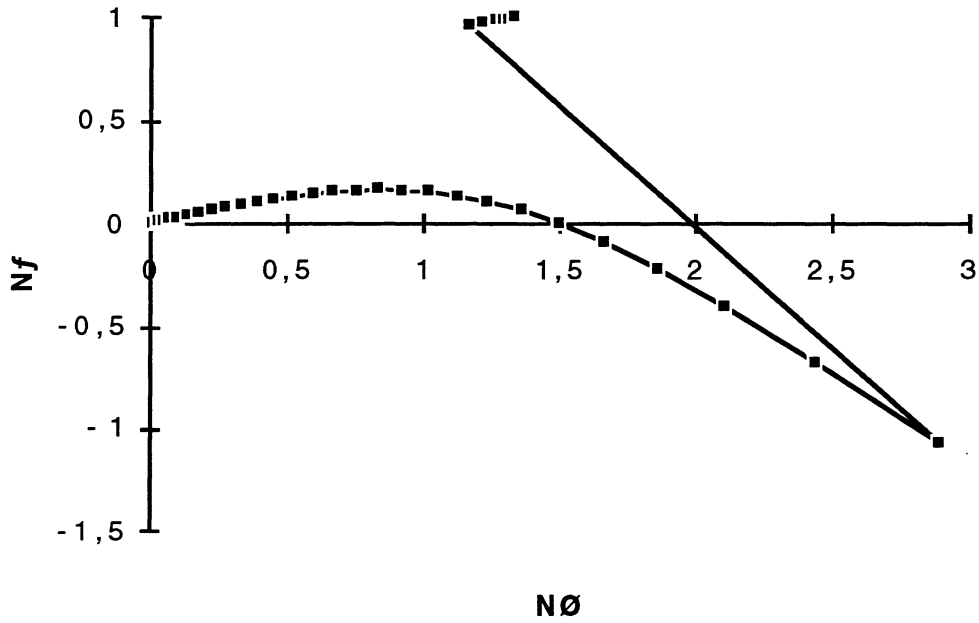


Figure 3.10. Representation of in-plane loads for $f_0 = 150^\circ$.

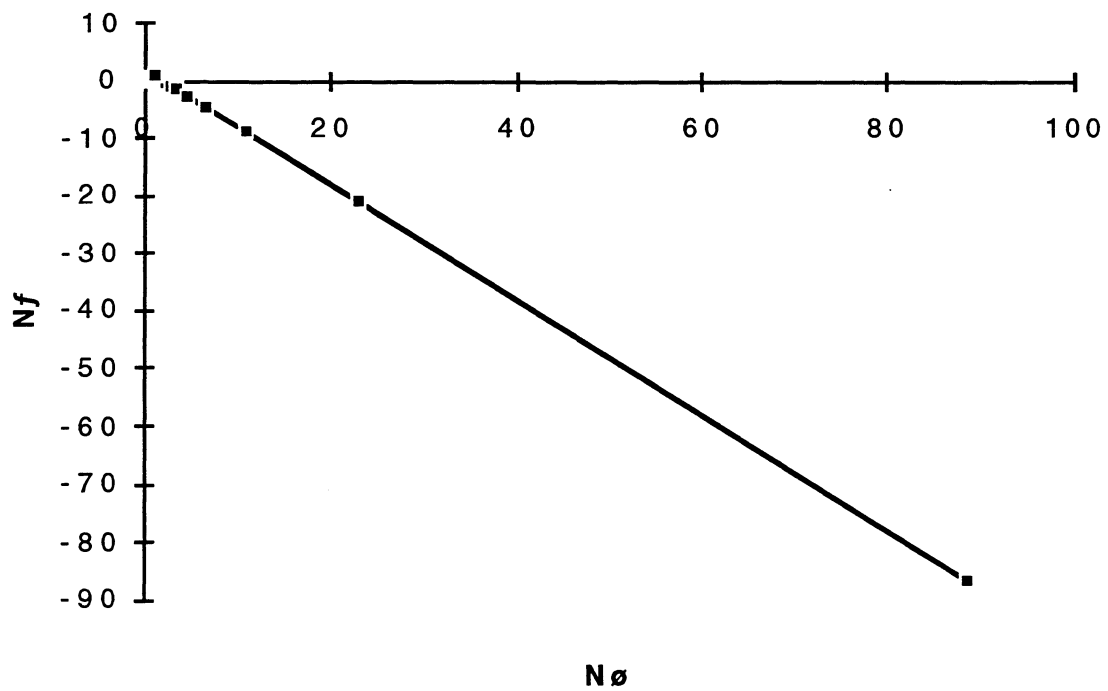


Figure 3.11. Representation of in-plane loads for $f_0 = 180^\circ$.

The relationships between N_f and N_θ shown in Fig. 3.8 to 3.11 depend only upon f , because r and ρ appear in the factor $(\rho \cdot r^2)$ in the expressions of both in-plane loads N_f and N_θ for angles higher and lower than f_0 . Therefore, the weight saving is a function of f . In order to find out which material system is efficient in comparison with a standard

material (A-42 steel), the concept of average weight saving will be used. This parameter is a function of f_0 . Average weight savings for some composite material systems are represented in Fig. 3.12.

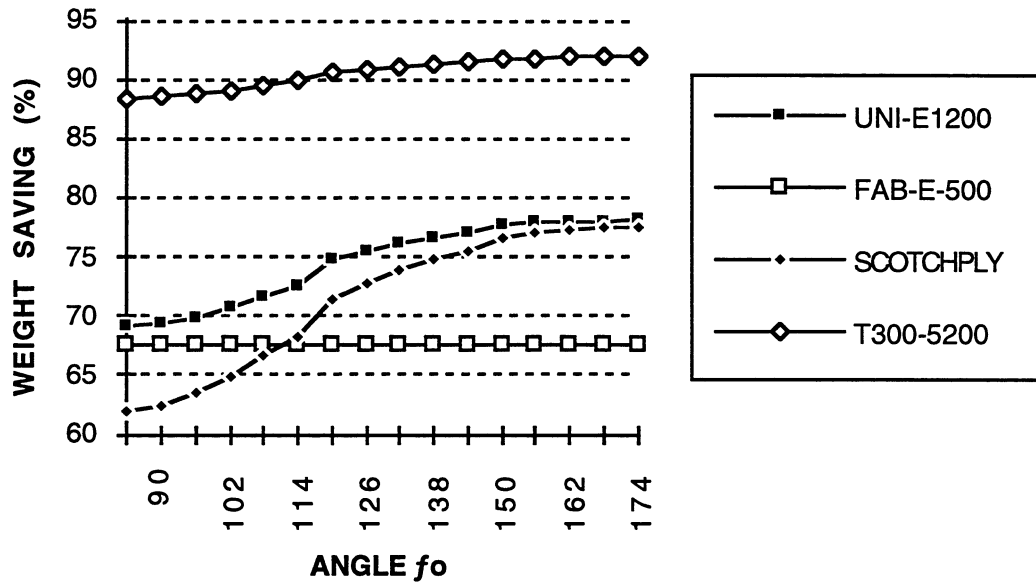


Figure 3.12 Representation of average weight saving for some composite material systems.

Table 3.6 shows the optimum sublaminar for different values of β and for the four material systems analysed above. The angle β ranges from -45° to 90° , according to Fig. 3.8 to 3.11.

Table 3.6 Optimum sublaminar for a spherical vessel

β	UNI-E1200	FAB-E-580	SCOTCH	T300-5208
-45°	4600	0100	8200	6400
-40°	4600	1000	9100	7300
-35°	5500	1000	8200	7300
-30°	5500	1000	8200	7300
-25°	6400	1000	9100	8200
-20°	7300	1000	1000	8200
-15°	8200	1000	1000	1000
-10°	1000	1000	1000	1000
-5°	1000	1000	1000	1000
0°	1000	1000	1000	1000
5°	1000	1000	1000	1000
10°	1000	1000	1000	9100
15°	8200	1000	8200	8200
20°	8200	1000	7300	7300
25°	7300	1000	7300	7300
30°	7300	1000	6400	6400
35°	6400	1000	6400	6400
40°	5500	1000	5500	5500
45°	5500	0100	5500	5500
50°	5500	0100	5500	5500
55°	4600	0100	4600	4600
60°	3700	0100	4600	4600
65°	3700	0100	3700	3700
70°	2800	0100	3700	3700
75°	2800	0100	2800	2800
80°	0100	0100	0100	1900
85°	0100	0100	0100	0100
90°	0100	0100	0100	0100

The following conclusions can be drawn:

- Weight saving does not depend upon the vessel radius nor fluid density. The average weight saving depends only upon the material system:

UNI - E1200: 69 - 78%

FAB - E - 580: 67.5%

SCOTCHPLY: 62 - 77%

T300 - 5208: 88.5 - 92 %

The maximum value is reported for the carbon fibre system. For the case of fabric, the average weight saving is constant and therefore does not depend on the value of f_0 .

- The area below the support ring is subjected to in-plane loads located in the first quadrant ($N_\theta > 0$ and $N_f > 0$), or biaxial. Therefore, unidirectional composite systems will show low values of weight saving. The area above the support ring presents loads whose direction is very close to parallel, or uniaxial, up to an angle f_0 of 135° . Therefore, weight saving for unidirectional composite systems will increase with respect to the area below the support ring.
- For values of f_0 higher than 135° , weight saving increases even more, because the state tension-compression is more favourable for composite materials than the state tension-tension. However, loads moduli increase considerably and therefore, in spite of having an increasing weight saving graphic, the optimum value is reported for $f_0 = 135^\circ$, because the vessel weight increases more rapidly than the weight saving.
- Optimum laminate with all the plies in meridian and parallel directions have been selected. Number of plies in meridian and parallel directions are related to the magnitude of N_f and N_θ in-plane loads respectively.

3.4 Pipeline and submersible hull

This section examines the formulation, in-plane loads and weight saving of two cylindrical shell applications. First, a pipeline (subjected to internal pressure) is analysed (Fig. 3.13), and second, a submersible hull (subjected to external pressure) is also studied (Fig. 3.14).

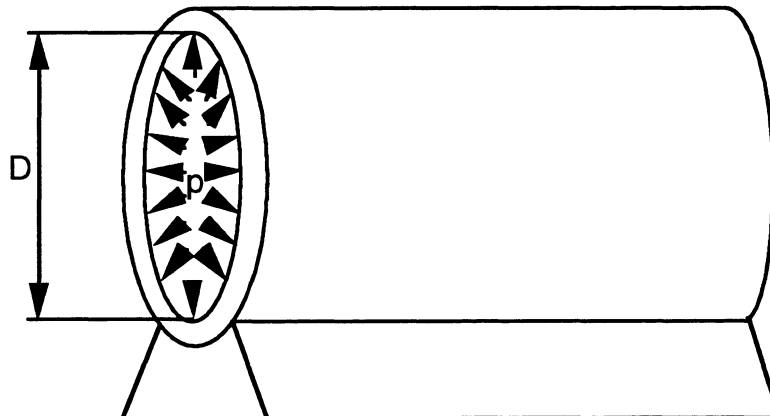


Figure 3.13 Pipeline subjected to internal pressure and the definition of variables.

Mobile underwater vehicles designed for either moderate or extreme depths are likely to require minimisation of structural weight as a basis for increasing the payload and extending operating range. By virtue of their specific compressive strength, fibre reinforced plastics offer major potential weight saving relative to conventional metallic materials. Fibre glass reinforced plastics submersibles fabricated by hand lay-up using polyester resin and E-glass reinforcement have been developed successfully for offshore operations in moderate sea depths. Filament wound S-glass/epoxy and carbon fibre/epoxy shells with helical or polar fibre orientation having compressive strengths of up to 1400 MPa have been extensively researched and appear to offer large potential advantages over high-strength steel, aluminium or titanium in the pressure hulls of high performance submersibles for naval or deep-water exploration purposes.

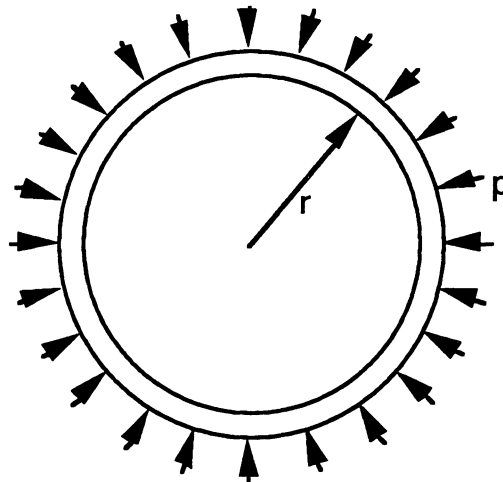


Figure 3.14 Submersible hull structure and definition of variables.

In-plane loads for a pipeline subjected to internal pressure are given by the following expressions:

$$N_x = \frac{p \cdot r}{2} \quad [3.14]$$

$$N_\phi = p \cdot r \quad [3.15]$$

$$N_{x\phi} = 0 \quad [3.16]$$

Consequently, in-plane loads for a submersible hull subjected to external pressure will be similar to those for a pipeline, but in compression:

$$N_x = -\frac{p \cdot r}{2} \quad [3.17]$$

$$N_\phi = -p \cdot r \quad [3.18]$$

$$N_{x\phi} = 0 \quad [3.19]$$

Figure 3.5 shows the in-plane loads for both structures: a pipeline (1st quadrant, $N_x > 0$ and $N_\phi > 0$) and a submersible hull (3rd quadrant, $N_x < 0$ and $N_\phi < 0$). This line is oriented 30° with respect to axes N_ϕ .

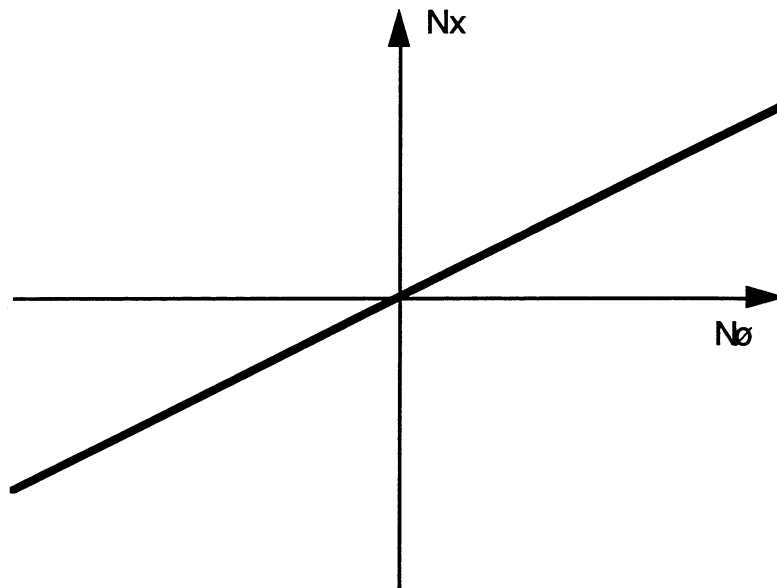


Figure 3.15 Representation of in-plane loads for a pipeline and a submersible hull.

As the weight saving only depends on the angle β , and this is constant for each structure, it is possible to assess the weight saving:

- For a pipeline: $\beta = 30^\circ$
- For a submersible hull: $\beta = 210^\circ$

The weight saving with respect to the A-42 steel, for the four composite material systems seen before is shown in Table 3.7.

Table 3.7 Weight saving for a pipeline subjected to internal pressure

Material	Weight saving, %
UNI-E-1200	64.60
FAB-E-580	68.36
Scotchply	52.02
T300-5208	87.08

For the submersible hull, the weight saving with respect to the HY-100 steel (strength: 690 MPa), for the four composite material systems seen before, is shown in Table 3.8.

Table 3.8 Weight saving for a submersible hull subjected to external pressure

Material	Weight saving, %
UNI-E-1200	-29.50
UNI-R-600	-42.27
UNI-R-1200	-87.65
T300-5208	93.8

A four-digit laminate code for the sublaminates will be used for obtaining the optimum sublaminates. The digits in the code represent the number of plies in the sublaminates, and the order of ply angles selected. The first number represents the number of plies in the sublaminates in the circumferential direction, the second number represents the number of plies in the sublaminates in the longitudinal direction, the third number represents the number of plies at 52° with respect to the meridian circle direction and the fourth number represents the number of plies at - 52° with respect to the meridian circle direction. For a generalised $\pi/4$ laminate code [4211] means [0₄/90₂/52/-52]. These four directions have been selected because 0° and 90° correspond to a polar filament winding process and 52° and - 52° correspond to the principal directions of a cylindrical structure subjected to a uniform radial load (Tables 3.9 and 3.10).

Table 3.9 Optima sublaminates for a pipeline subjected to internal pressure

Material	Sublaminates
UNI-E-1200	4033
FAB-E-580	1000
Scotchply	7300
T300-5208	4033

Table 3.10 Optima sublaminates for a submersible hull subjected to external pressure

Material	Sublaminates
UNI-E-1200	6022
UNI-R-600	6022
UNI-R-1200	1000
T300-5208	5122

The minimum permissible laminate thickness, t_m , to prevent buckling in a submersible hull, shall be determined from the equations 3.21 or 3.23, as appropriate.

If

$$\frac{L}{D_o} \geq 1,35 \cdot \left(\frac{E_{lam\phi}}{p \cdot N} \right)^{0,17} \quad [3.20]$$

where

N: safety factor

p: external pressure (in MPa)

$E_{lam\phi}$: Young's Modulus (in MPa) of laminate under consideration in the circumferential direction

L: effective shell length (in mm)

D_o : outside diameter of shell (in mm)

Then

$$t_m = D_o \cdot \left(\frac{p \cdot N}{2 \cdot E_{lam\phi}} \right)^{0,33} \quad [3.21]$$

And if

$$\frac{L}{D_o} < 1,35 \left(\frac{E_{lam\phi}}{p \cdot N} \right)^{0,17} \quad [3.22]$$

Then

$$t_m = D_o \cdot \left(\frac{0,4 \cdot p \cdot N}{E_{lam\phi}} \cdot \frac{L}{D_o} \right)^{0,40} \quad [3.23]$$

If the proposed design does not meet this requirement, the design should be changed either by redesigning the laminate or by providing additional stiffening rings.

Several particular analyses on composite vessels are shown in references 22-36.

3.5 Conclusions

The following conclusions can be drawn:

- The weight saving of the composite material systems analysed in this sub-section does not depend on the geometric parameters nor the load applied, but remains constant for each application and material system, because the ratio N_f / N_ϕ is constant.
- For a submarine structure, there is no weight saving with respect to HY-100 steel except for the carbon fibre system, which presents an excellent behaviour in terms of compression-compression.
- Optima sublaminates present 40% of plies oriented $\pm 52^\circ$ and the rest of fibres in the circumferential direction for all the fibre glass composite material systems except for the fabric, which has fibres oriented in longitudinal and circumferential directions. The carbon fibre system presents an optimum laminate which is very similar to that obtained for fibre glass systems. The only difference is that there is 10% of plies in the longitudinal direction and 50% in the circumferential direction.
- For a pipeline, all the material systems are competitive with the A-42 steel in terms of weight saving.
- The optimum sublaminates of the unidirectional systems UNI-E-1200 and T300-5208 present 60% of plies at $\pm 52^\circ$ and the rest in the circumferential direction, whereas the SCOTCHPLY and TEJ-E-580 present an optimum sublaminates in longitudinal and circumferential directions.

References

1. Tsai S W , Composites Design, Think Composites, Dayton, OH, 1987.
2. Ahmad S, Curved Finite in the Analysis of Solid Shell and Plate, Ph D thesis, University College of Swansea, Wales, C/Ph/7/69.
3. Zienkiewicz O C, Taylor R L and Too J M, Reduced integration techniques in general analysis of plates and shells, Int J Numer Meth Engng 1971, 3, 275-90.
4. Figueiras J A, Ultimate Load Analysis of Anisotropic and Reinforced Concrete Plates and Shells, Ph D thesis, University College of Swansea, Wales, C/Ph/72/83.
5. Ferreira A J M and Marques A T, Composite Structures Analysis by the Use of a Flat-Shell Element, ICCM-8, Honolulu, 1991.
6. Huang H C, Static and Dynamic Analyses of Plates and Shells, Berlin, 1989.
7. Ferreira A J M, de Sa J C, Marques A T, A Degenerated Shell Element for the Static Linear Analysis of Sandwich Structures, ICCM-9, Madrid, 1993.
8. Tucker J S, 'Glass reinforced plastic submersibles', Trans NEC Inst Engrs & Shipbuilders, 1979, 95.
9. Fried N, 'The potential of filament wound materials for the construction of deep submergent pressure hulls', in Conf on Filament Winding, Plastics Institute, London, 1967.
10. Roberts M L and Smith C S, 'Design of submarine structures', in Proceedings International Conference on Undersea Defence Technology, London, 1988.
11. Smith C S and Chalmers D W, 'Design of Ship Superstructures in Fibre Reinforced Plastic', Trans RINA , 1987, 129.
12. Pegg R L and Reyes H, Composites Promise Navy Weight, Tactical Advantages, Sea Technology (1986), p 31.
13. Wilhelm G F and Schab H W, 'Glass reinforced plastic piping for shipboard applications', Naval Engineers J (1977).
14. Markets and Market Research: a Review of Data Available, in: Proc Annual Conf Reinforced Plastics Inst, SPI (1984)
15. Guide for Quality Assured Fiberglass Reinforced Plastics Structures, Technical & Research Bulletin No 2-23, Panel HS-10 (Plastics), Hull Structure Committee, SNAME, 1977.
16. Crystic Polyester Handbook, Scott Bader Co Ltd, 1980.
17. Guidance Notes on the Manufacture of Glass Fibre Reinforced Polyester Laminates to be Used in Marine Environments, British Plastics Federation, Publication No 220/1, 1978.
18. Smith C S, Design of Marine Structures in Composite Materials, Elsevier Applied Science, London, 1990.
19. Chao C C, Sun C T, Koh S L, 'Strength optimization for cylindrical shells of laminated composites, J of Compos Mater , 1975, 9, 53-66.
20. Tauchert T R, 'Optimum design of a reinforced cylindrical pressure vessels', J of Compos Mater 1981, 15, 390-402.
21. Dong S B, Pister K S and Taylor R L, 'On the theory of laminated anisotropic shells and plates', J. Aerospace Sci., 1962.
22. Chen P C T, 'Nonlinear analysis of a minimum-weight equivalent compound cylinder, ICCM 9, Volume IV, ed. A. Miravete, Woodhead Publishing Limited, Cambridge, UK, 1993, pp 706-15.

23. Witherell M D and Scavullo M A, 'Stress analysis and weight savings of internally pressurized composite-jacketed isotropic cylinders', J of Pressure Vessel Technology, 1990, 112, 397-403.
24. Chen P C T, 'Residual stresses in a prestressed steel pressure vessel wrapped with multilayered composites', in Proceedings of the Sixth Technical Conference of American Society for Composites 1991, pp 980-989.
25. Witherell M D, Weight Reduction of Isotropic Cylinders Using Equivalent Compound Cylinders, ICCM 8, 1-L, Honolulu, July, 1991.
26. Bland D R, 'Elastoplastic thick-walled tubes of work-hardening material subject to internal and external pressures and to temperature gradients', J. Mech. and Phy. of Solids, 1956, 4, pp 209-229.
27. Chen P C T, 'Stress and deformation analysis of autofrettaged high pressure vessels', ASME Pressure Vessels and Piping, 1986, 110, pp 61-67.
28. Wennerstrom H and Backlund J, General Curved Finite Elements for Static Analysis of Sandwich Shell Structures, Dept of Aeronautical Structures and Materials, The Royal Institute of Technology, Report 85-1, Stockholm, 1985
29. Ahmad S, Irons B M and Zienkiewicz O C, 'Curved thick shell and membrane elements with particular reference to axi-symmetric problems', in Proceedings of Second Conference on Matrix Methods in Structural Mechanics, Wright- Patterson Air Force Base, Ohio, 1968.
30. Ahmad S, Irons B M and Zienkiewicz O C, 'Analysis of thick and thin shell structures by curved finite elements', Int J. Numer. Meth. in Eng., 1970, 2, 419-451.
31. Zienkiewicz O C, Taylor R L and Too J M, 'Reduced integration technique in general analysis of plates and shells', Int J. Numer. Meth. in Eng., 1971, 3, 275-290.
32. Pawsey S F and Clough R W, 'Improved numerical integration of thick shell finite elements', Int J. Numer. Meth. in Eng., 1973, 3, 575-86.
33. Pawsey S F, 'Discussion of Papers by O C Zienkiewicz, R L Taylor and J M Too, and S F Pawsey and R W Clough', Int J. Numer. Meth. in Eng., 1973, 4, 449-50.
34. Irons B M and Razzaque A, 'A further modification to ahmad's element', Int J. Numer. Meth. in Eng., 1973, 5, 588-89.
35. Kim C W, Hwang W, Park H C and Han K S, 'An optimal stacking sequence design of laminated composite cylinders', ICCM 9, Volume IV, ed. A. Miravete, Woodhead Publishing Limited, Cambridge, UK, 1993, 661-8.
36. Eschenauer H A, Bellendir K, 'Optimal layout of cylindrical composite shells under non-symmetric loading', ZAMM, 1992, 72, T553-T556.



4 CONSTANT THICKNESS PLATES

4.1 Introduction

Constant thickness composite plates subjected to buckling and transverse loads (uniform or point load) are most used in engineering applications. In most cases, optimum design is required, the weight being the optimisation criterion and the maximum deflection for transverse loads, and critical compressive force for buckling loads being the parameters to be optimised. Usually, stiffness and not strength is used as the optimisation criterion in plates subjected to transverse loads, since failure is associated with very high deflections.

Three studies have been carried out on constant thickness plates subjected to transverse loads: First, three fibre glass composite systems (unidirectional, fabric and chopped strand matting) have been analysed and the influence of several lay-ups on the maximum deflection has been reported for a wide range of aspect ratios. Second, three unidirectional composite systems (carbon, aramid and glass fibres) have been studied and the influence of variation of θ in angle-ply laminates $[\pm\theta]$ has been analysed as a function of the aspect ratio. Finally, the influence of rotation of cross-ply laminates $[0/90]$ on the maximum deflection of the plate has been reported as a function of the aspect ratio for the three material systems described above. A buckling study of constant thickness plates has also been carried out. Uni-, bi-axial and shear loads have been treated for a carbon fibre plate with two boundary conditions: simply supported and clamped along the four sides of the plate. Optimum sublaminates and critical loads are obtained for each case. The behaviour of the optimum angle ply laminates is compared with the isotropic configuration and aluminium, for design optimisation purposes.

4.2 Design optimisation of composite plates in bending

A study of maximum deflection of rectangular composite plates is carried out in this section by means of the theory explained in Chapter 1. A simply supported plate subjected to uniform load is analysed (Figure 4.1). Bending and interlaminar shear effects are taken into account. References 1-23 give several proceedings to optimise composite plates in bending.

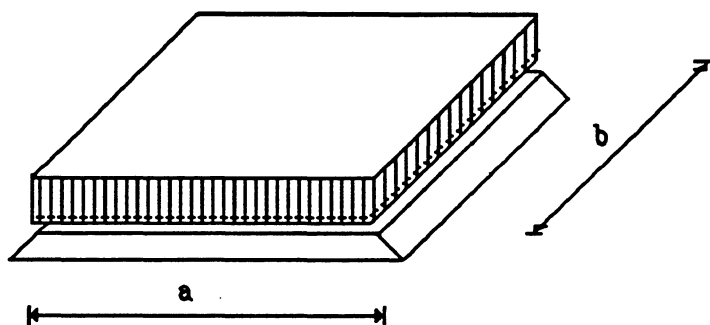


Figure 4.1 A rectangular simply supported plate subjected to a uniform load.

Three fibre glass material systems are considered :

- UNID-E-500 unidirectional fibre glass/polyester system. $V_f = 51.85\%$. $E_y = 10.289$ MPa.

- FAB-E-580 fabric fibre glass/polyester system. $V_f = 40.91\%$. $E_y = 19.817$ MPa.
- CSM-E-600A chopped strand matting system. $V_f = 16.51\%$. $E_y = 7.733$ MPa.

For a uniform load q , the maximum deflection is given by the following expression:

$$f = k \cdot 10^{-2} q a^4 / (E_y t^3) \quad [4.1]$$

For a central load P , the maximum deflection is:

$$f = k \cdot 10^{-2} P a^2 / (E_y t^3) \quad [4.2]$$

4.2.1 Influence of lay-up on maximum deflection

The maximum deflection of square ($a/b = 1$) simply supported and clamped plates subjected to uniform load does not depend upon the lay-up, as shown in Fig. 4.2 and 4.3. For rectangular non-square plates ($a/b > 1$), the optimum lay-up is [90] for simply supported and clamped plates, a substantial difference between the values of k for the optimum lay-up and for the rest of laminates is reported.

For simply supported plates, deflections of laminates [± 45], Q-isotropic and [0/90] are very close for aspect ratios ranged between 1 and 2.5. For aspect ratios higher than 2.5, differences among the deflections of these three laminates increase, the least stiff being [± 45].

For clamped plates, the ranking of laminates in terms of stiffness is [90], [0/90], Q-isotropic and [± 45] for all the aspect ratios considered. The values of k are very similar for a square plate ($a/b = 1$) for the four lay-ups analysed, as shown in Fig. 4.2 and 4.3:

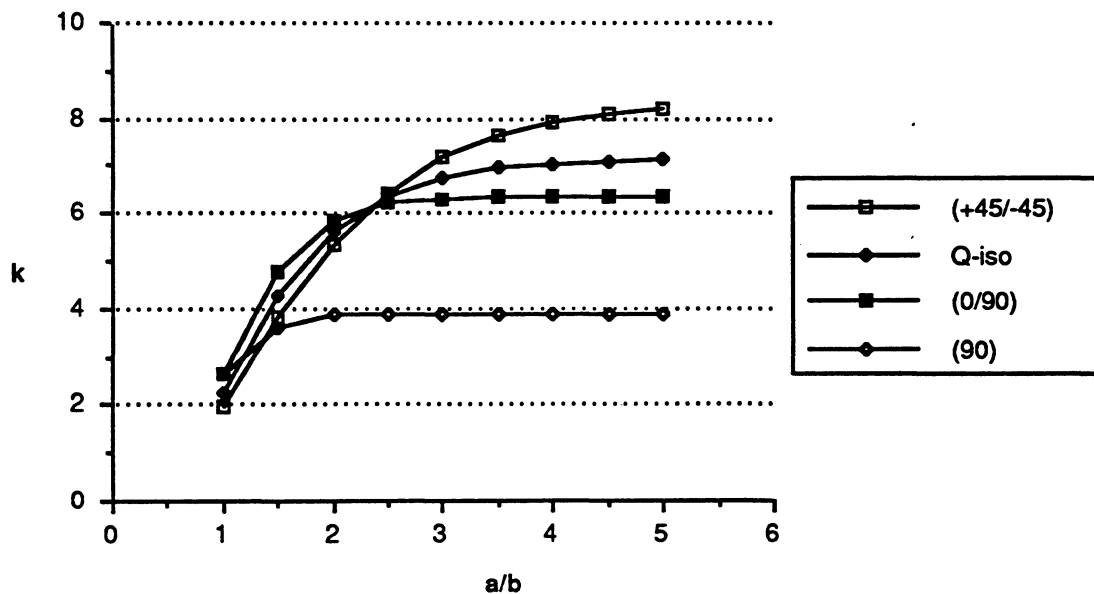


Figure 4.2 Uniform load simply supported plate, UNID-E-500.

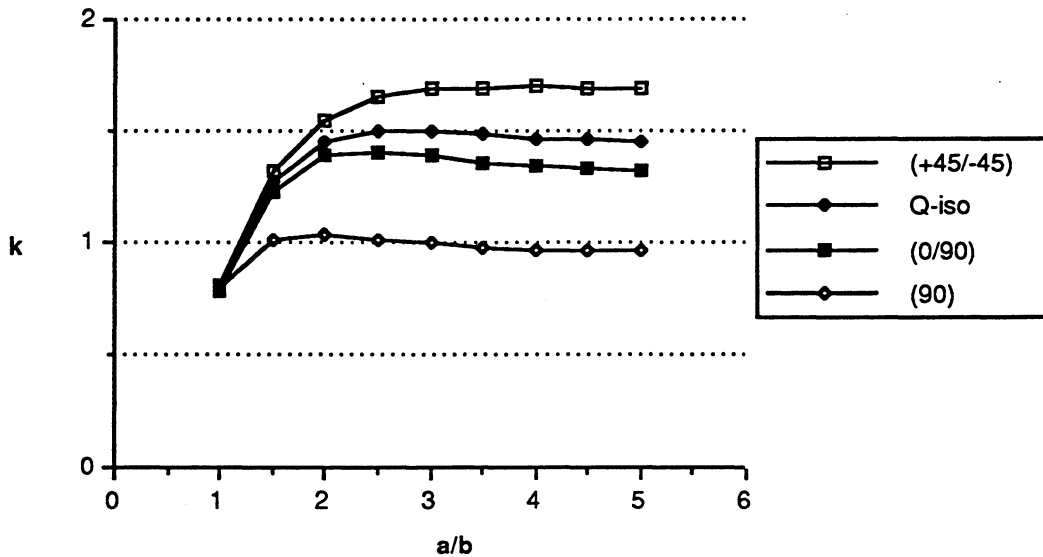


Figure 4.3 Uniform load clamped plate. UNID-E-500.

When the plate is subjected to a central point load, the maximum deflection of square ($a/b = 1$) simply supported and clamped plates depends upon the lay-up, the optimum lay-up being $[\pm 45]$, as it is shown in Fig. 4.4 and 4.5.

For simply supported plates, deflections of laminates $[\pm 45]$, Q-isotropic and $[0/90]$ are very close for aspect ratios ranged between 2.5 and 5. For clamped plates, all the lay-ups considered show very close deflections for all the aspect ratios analysed.

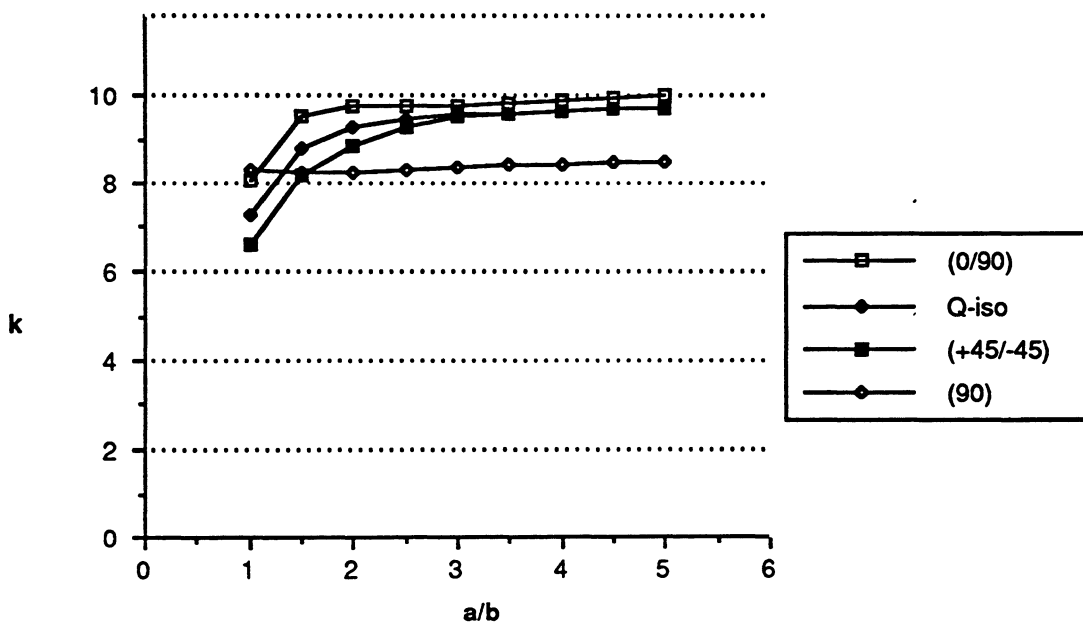


Figure 4.4 Point transverse load, simply supported plate, UNID-E-500.

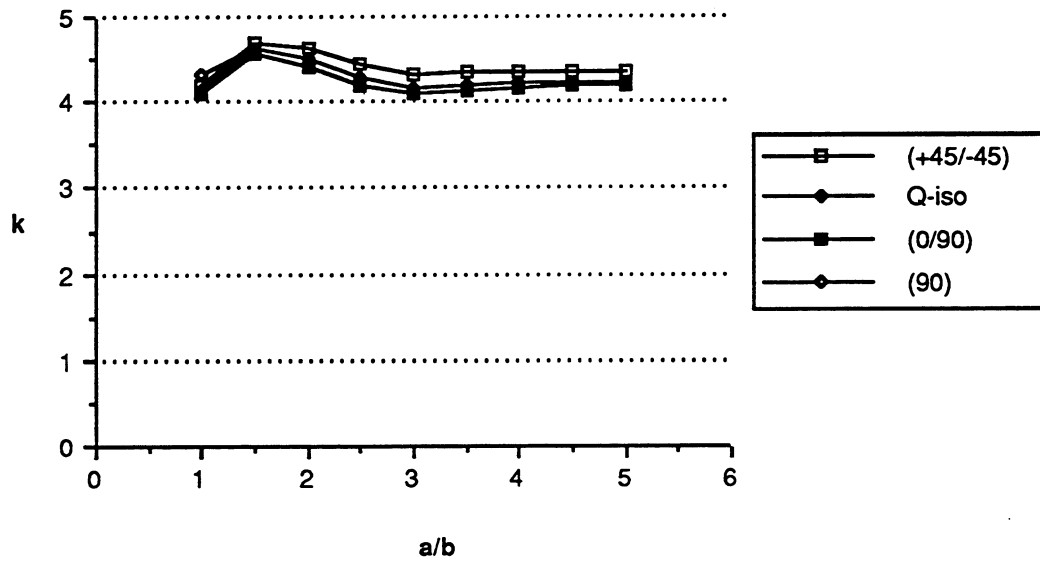


Figure 4.5 Point transverse load clamped plate. UNID-E-500.

Behaviour of the FAB-E-580 fibre glass fabric configuration is similar to the unidirectional mentioned above. Substantial differences exist in the values of k . This parameter for the fabric is 2.5 times higher than the unidirectional configuration, as shown in Fig. 4.6 to 4.9.

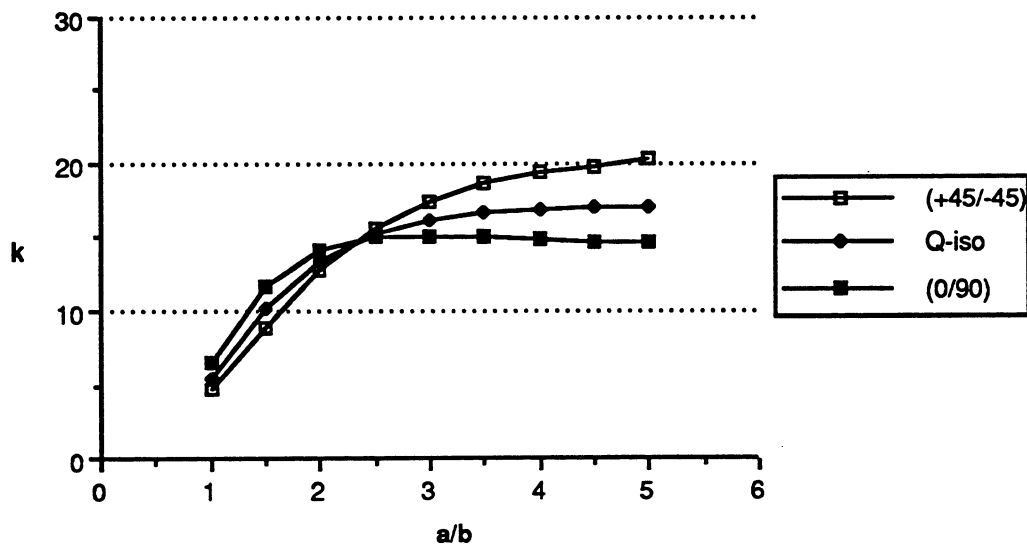


Figure 4.6 Uniform load, simply supported plate, FAB-E-580.

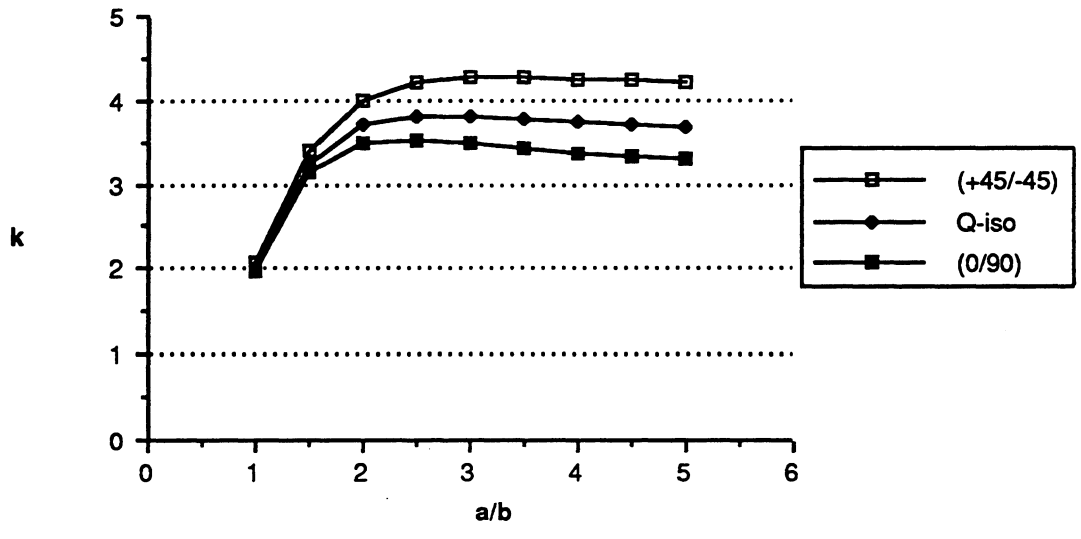


Figure 4.7 Uniform load, clamped plate, FAB-E-580.

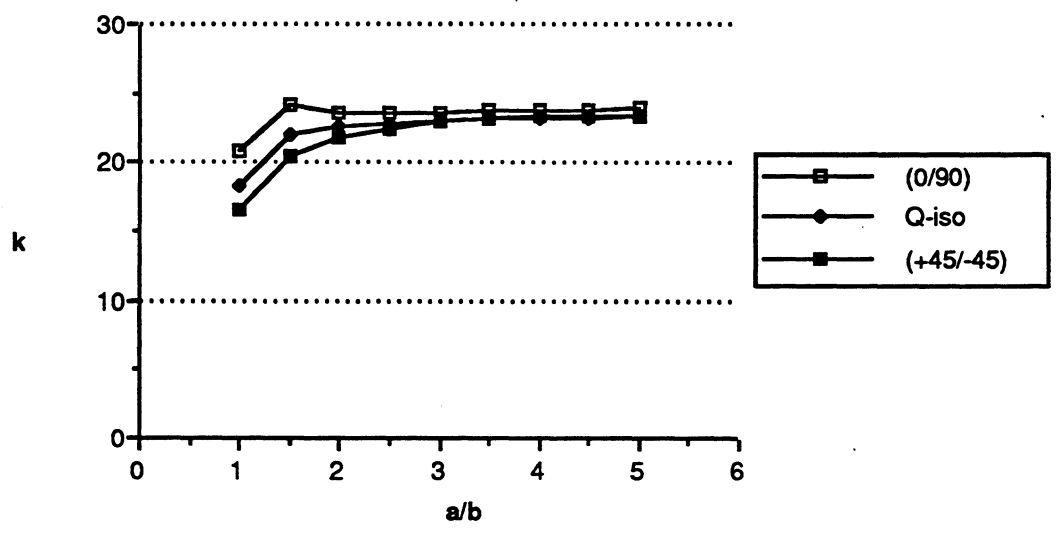


Figure 4.8 Point transverse load, simply supported plate, FAB-E-580.

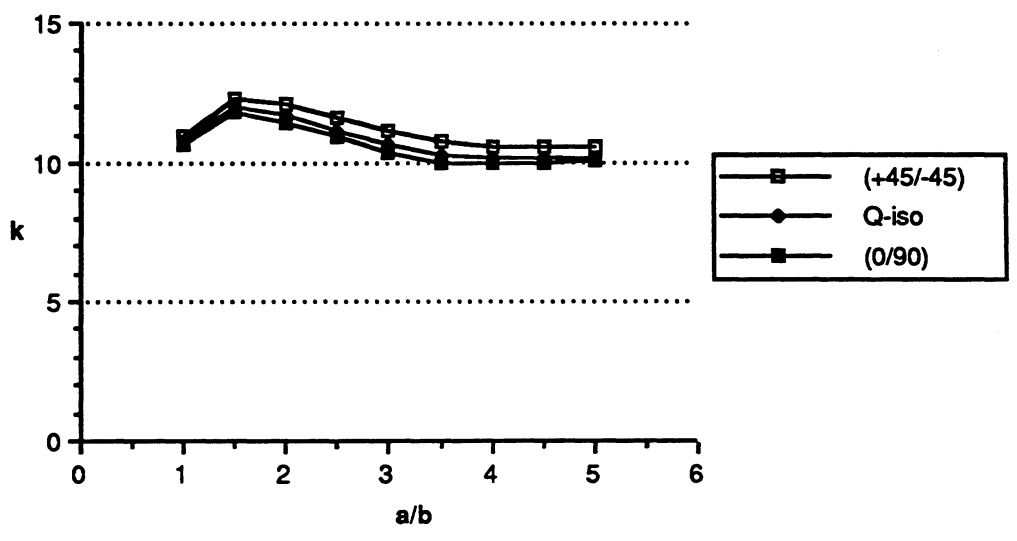


Figure 4.9 Point transverse load, clamped plate, FAB-E-580.

Deflections of chopped strand matting plates subjected to uniform and central load are strongly dependent on the boundary conditions, as shown in Fig. 4.10 and 4.11. For simply supported plates, the stiffness increases substantially for aspect ratios close to 1. Except for the case of a square plate, the deflection of clamped plates does not depend upon the aspect ratio.

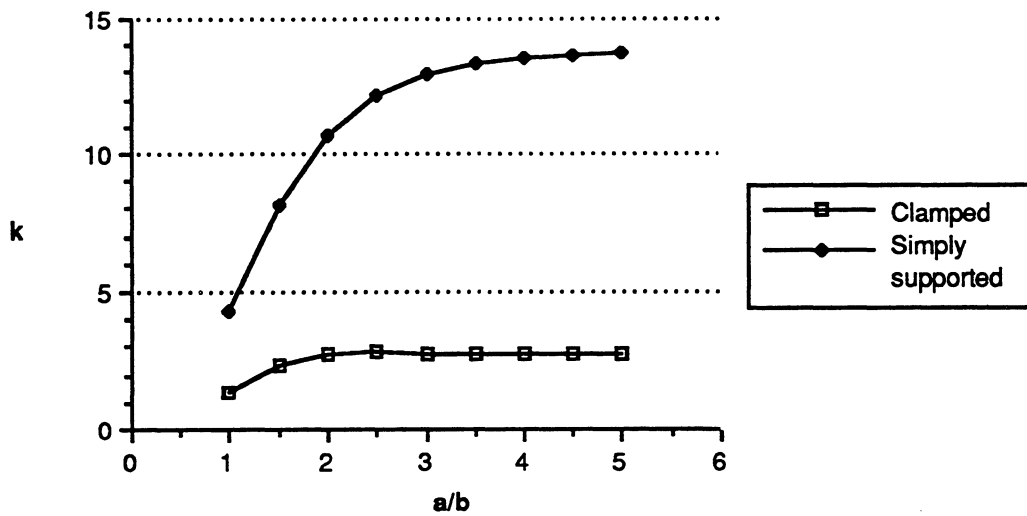


Figure 4.10 Uniform load, CSM-E-600A.

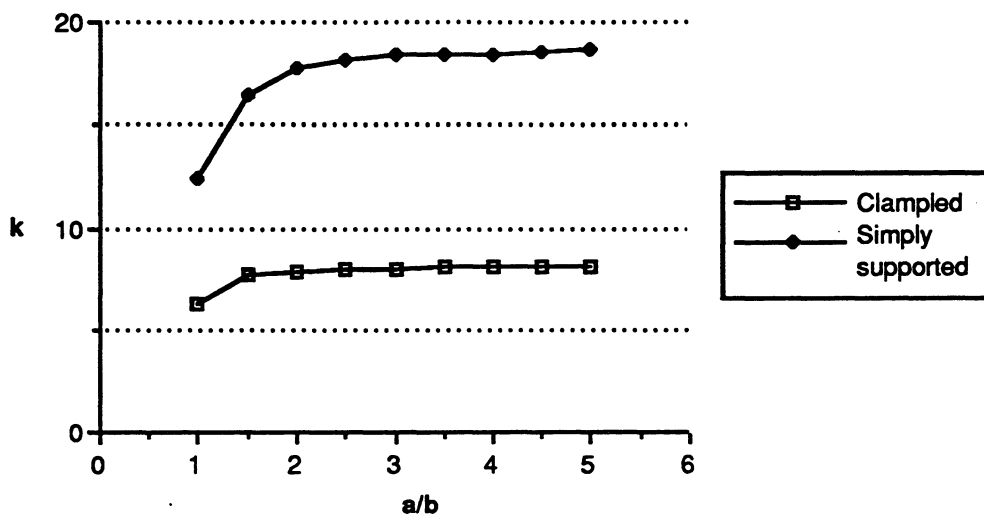


Figure 4.11 Point transverse load, CSM-E-600A.

4.2.2 Maximum deflection of the sublaminates [$\pm\theta$]

The maximum deflection is strongly dependent on the variation of θ on angle-ply laminates, as shown in Fig. 4.12 to 4.17. The stiffest laminate is [90] and the least stiff is [0] for all the aspect ratios considered. Small differences of values of k are reported in the ranges [0] to [± 15] and [± 60] and [90]. Carbon, aramid and glass fibre composite laminates show similar values of k for the lay-up [90] and high aspect ratios. For low values of the aspect ratio, deflections for the glass fibre system become the highest and for the carbon fibre system the lowest.

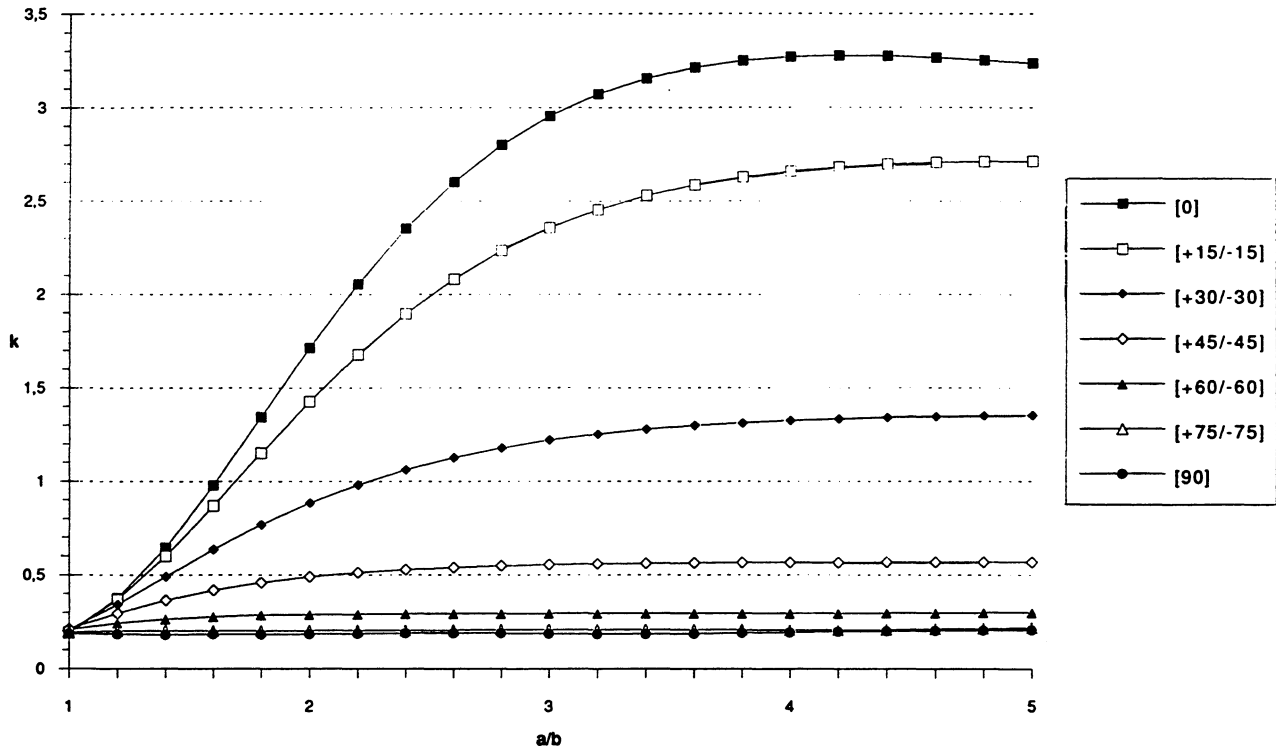


Figure 4.12 T300/5208, rectangular plate, all clamped edges, uniform load, $\{[+\theta/-\theta]_{10}\}_s$.

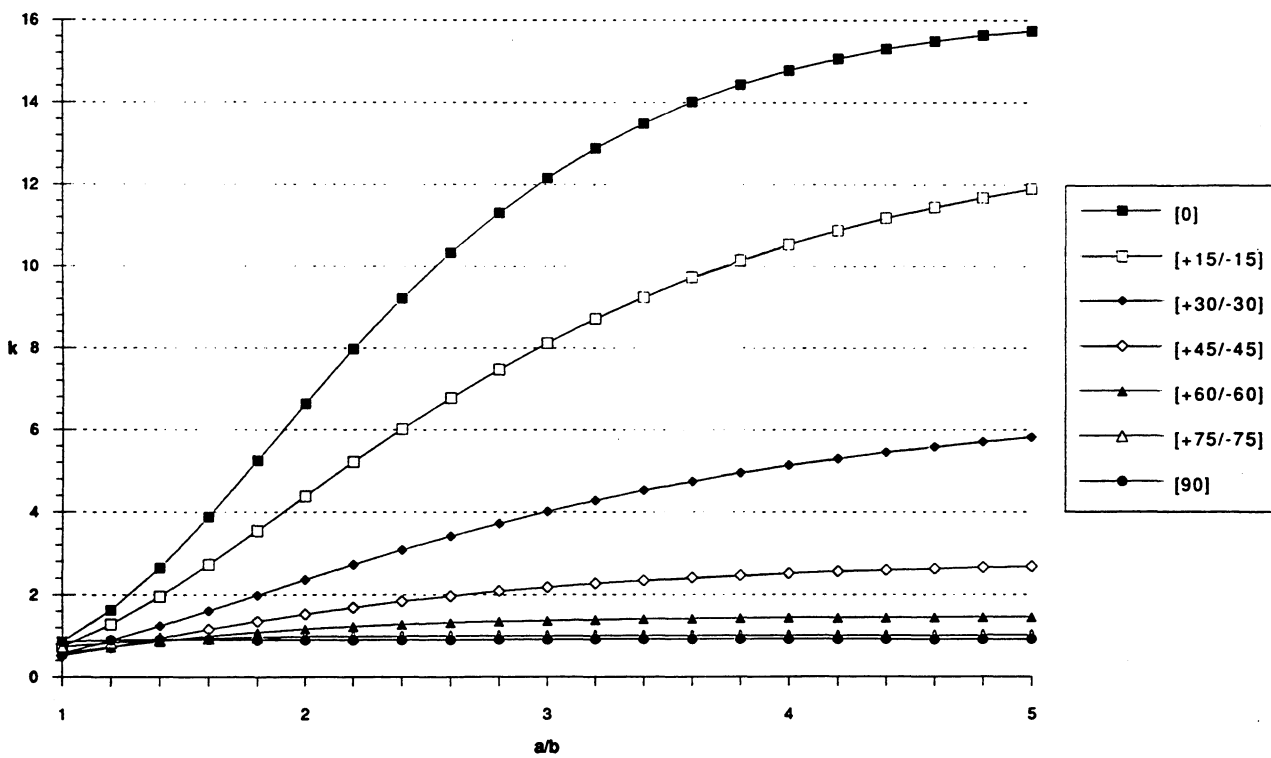


Figure 4.13 T200/5208, rectangular plate, all supported edges, uniform load, $\{[+\theta/-\theta]_{10}\}_s$.

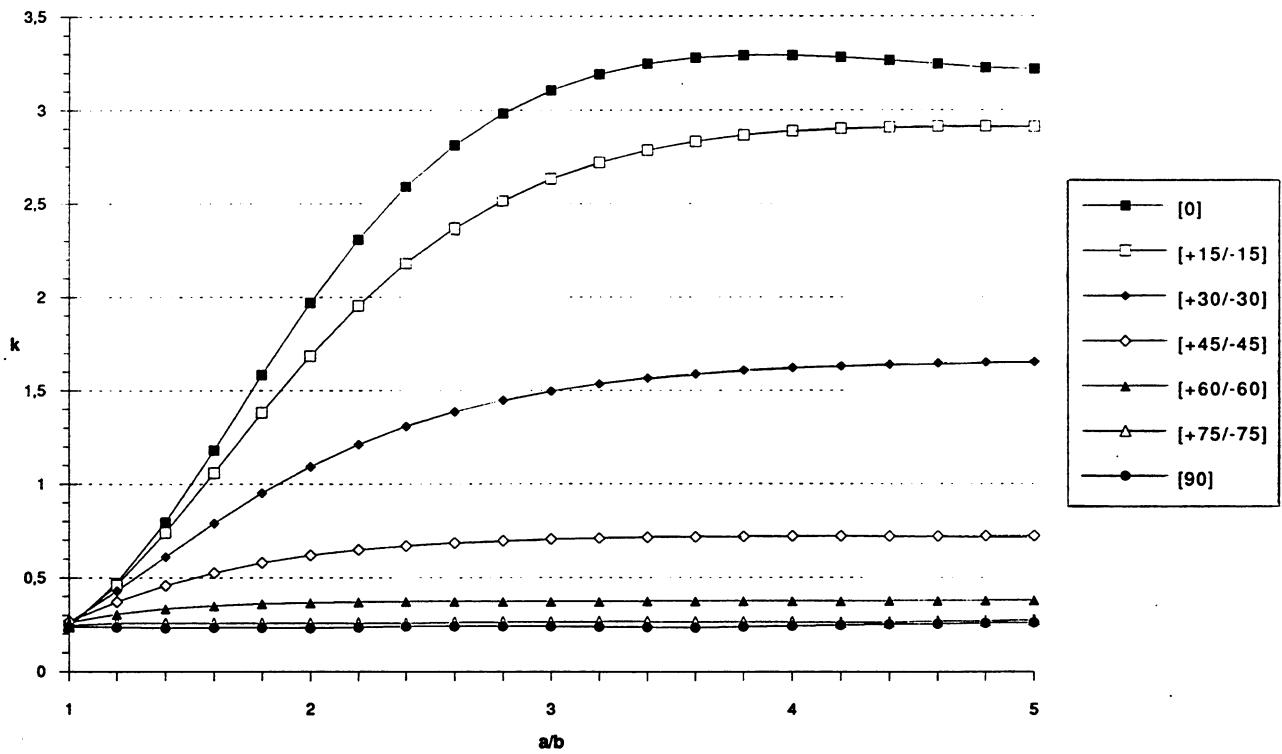


Figure 4.14 Kevlar, rectangular plate, all clamped edges, uniform load, $\{[+\theta/-\theta]_{10}\}_s$.

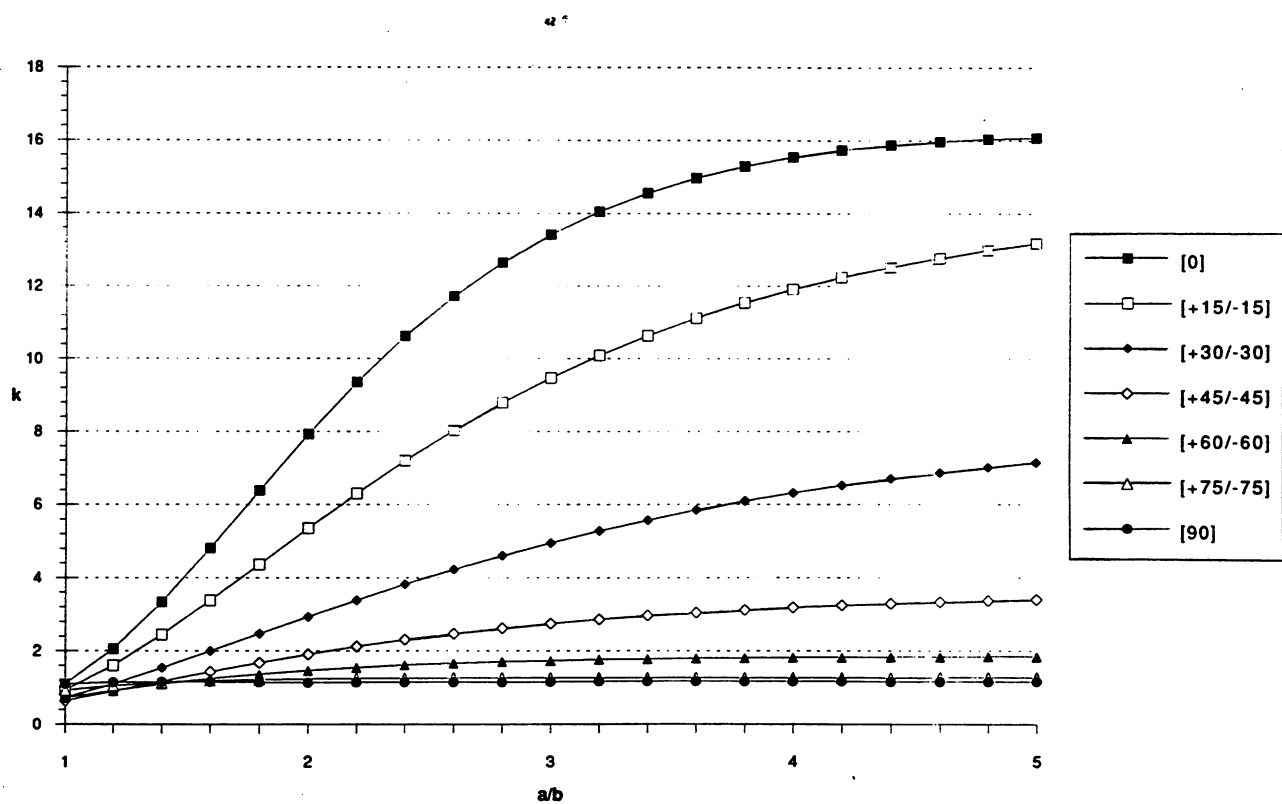


Figure 4.15 Kevlar, rectangular plate, all supported edges, uniform load, $\{[+\theta/-\theta]_{10}\}_s$.

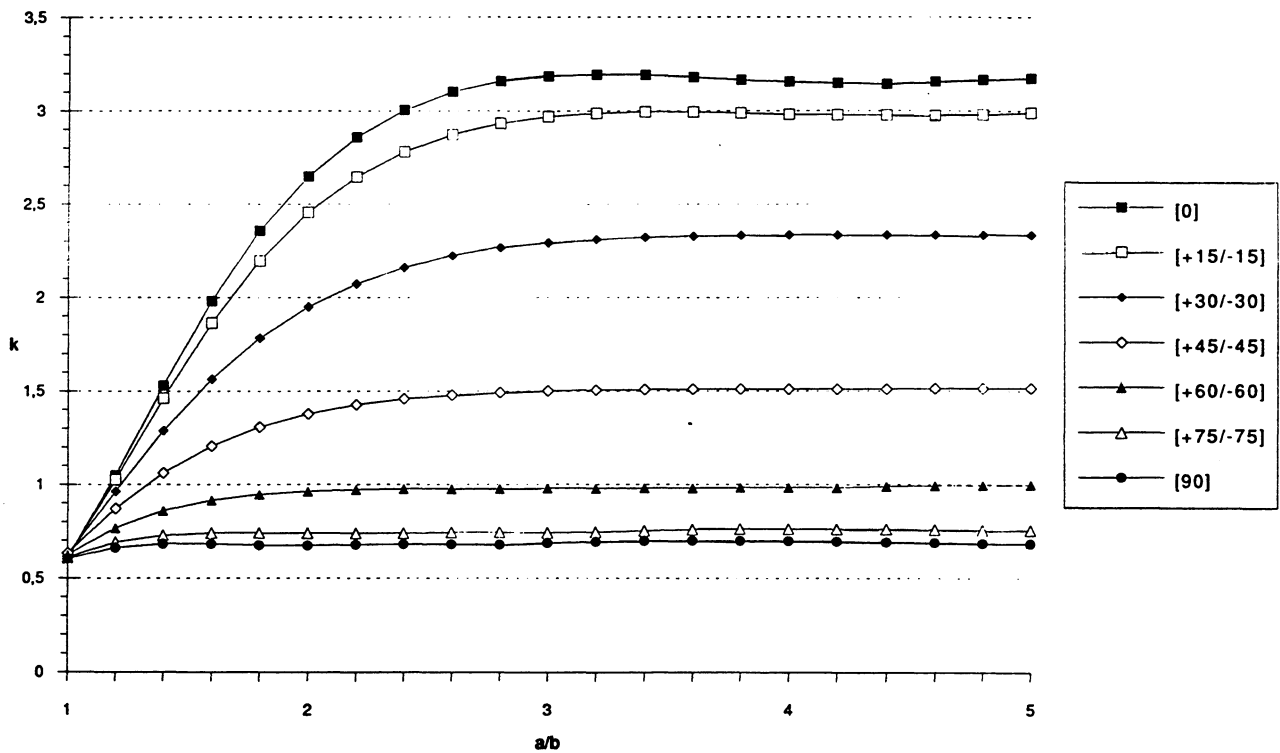


Figure 4.16 Scotchply, rectangular plate, all clamped edge, uniform load, $\{[+\theta/-\theta]_{10}\}_s$.

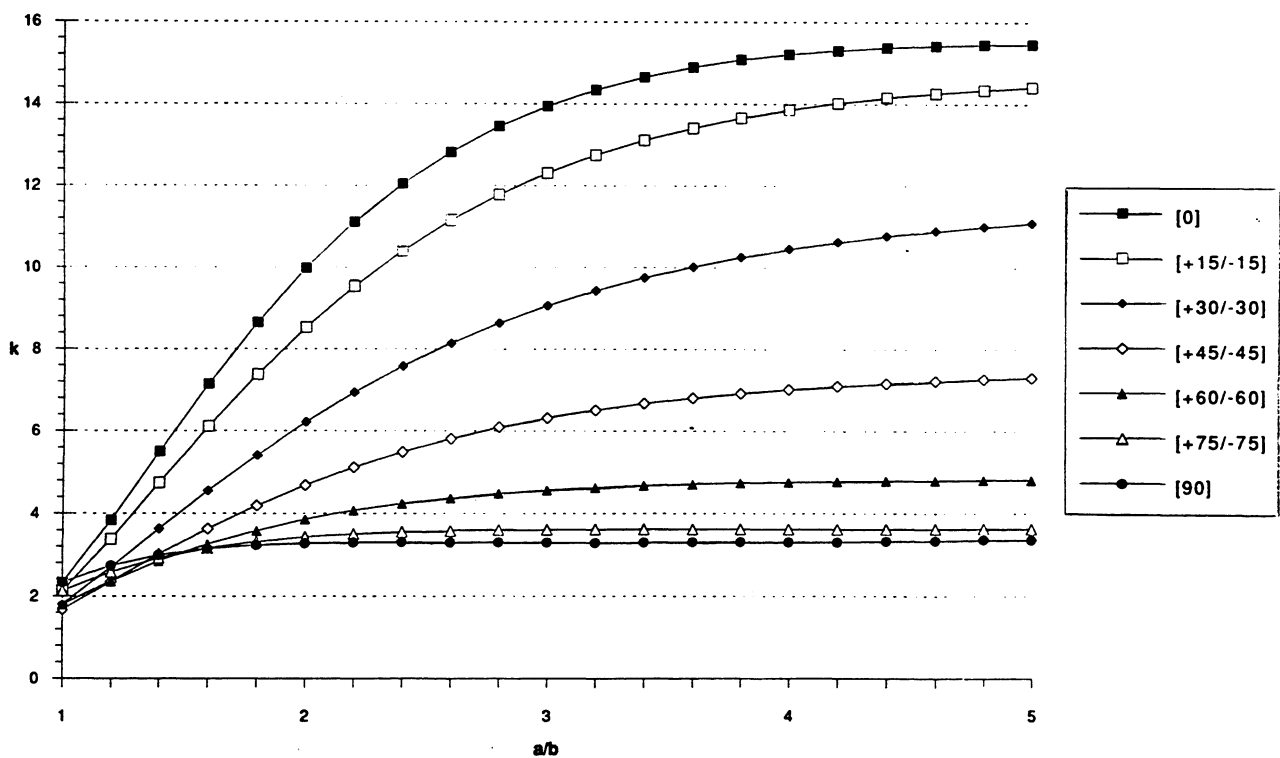


Figure 4.17 Scotchply, rectangular plate, all supported edges, uniform load, $\{[+\theta/-\theta]_{10}\}_s$.

4.2.3 Maximum deflection of rotation of sublaminates [0/90]

In this case, the rotation of cross-ply laminates affects drastically the maximum deflection, as shown in Fig. 4.18 to 4.23. For clamped plates, the stiffest laminate is $[\pm 45]$ and the least stiff is $[0/90]$ for all the aspect ratios and materials considered. For aspect ratios higher than 3, the maximum deflection does not depend on the aspect ratio.

For simply supported plates, two different ranges of aspect ratios are observed for the three material systems studied. For aspect ratios ranged from 1 to 2.5, the optimum lay-up is $[\pm 45]$ and the least stiff is $[0/90]$. For plates whose aspect ratio is 2.5, the maximum deflection does not depend on the aspect ratio. For aspect ratios higher than 2.5, the optimum lay-up is $[0/90]$ and the least stiff is $[\pm 45]$.

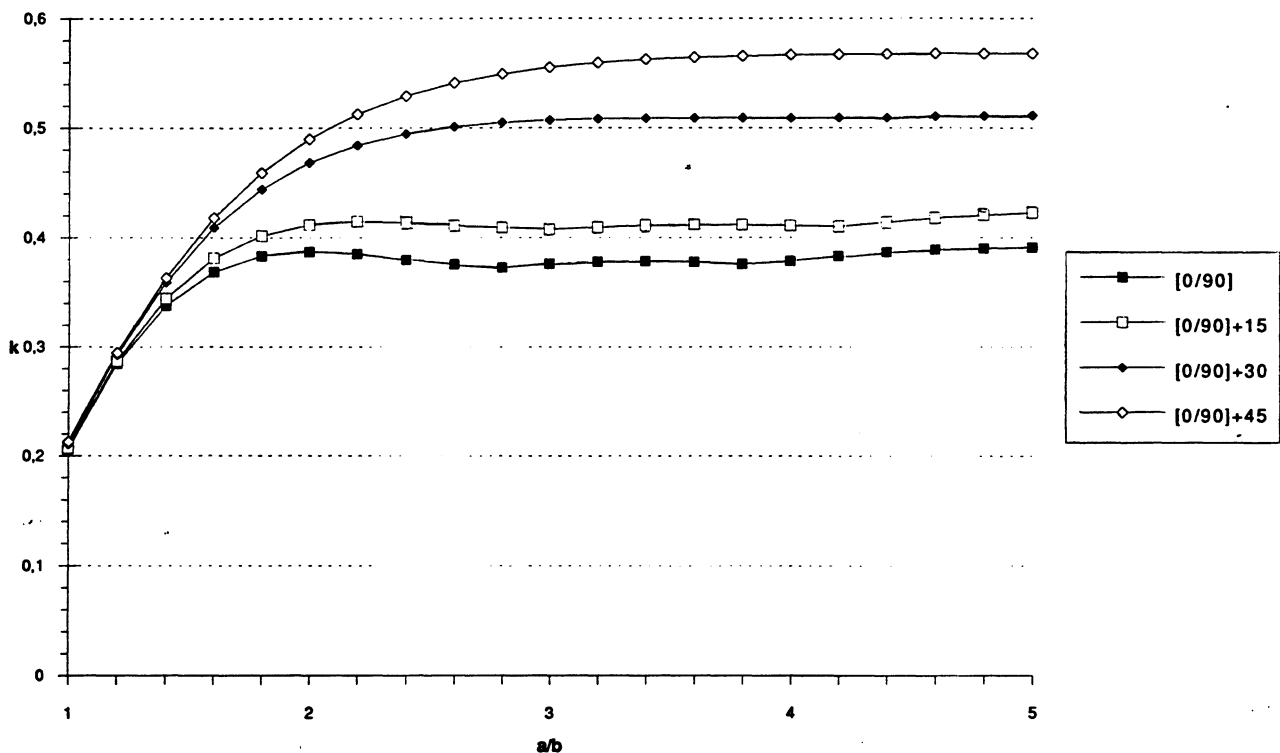


Figure 4.18 T300/5208, rectangular plate, all clamped edges, uniform load, $\{[(0/90) + \theta]_{10}\}_s$.

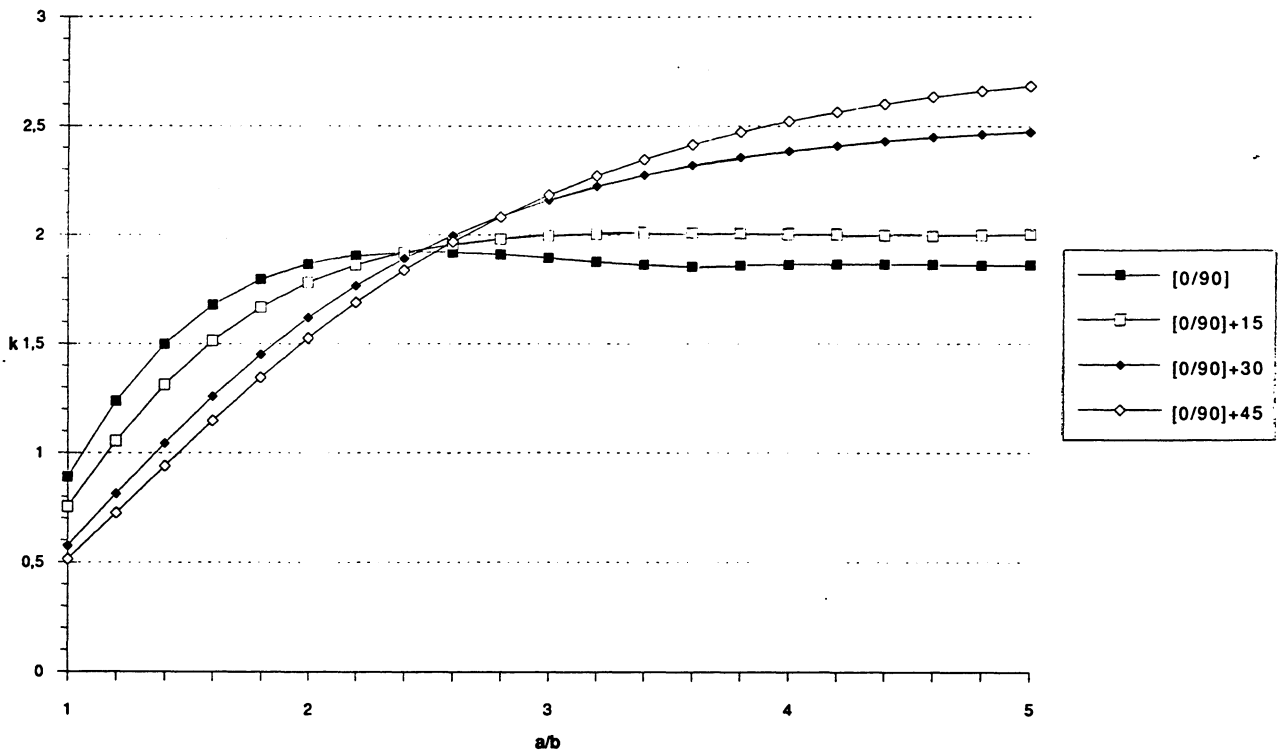


Figure 4.19 T300/5208, rectangular plate, all supported edges, uniform load, $\{[(0/90) + \theta]_{10}\}_s$.

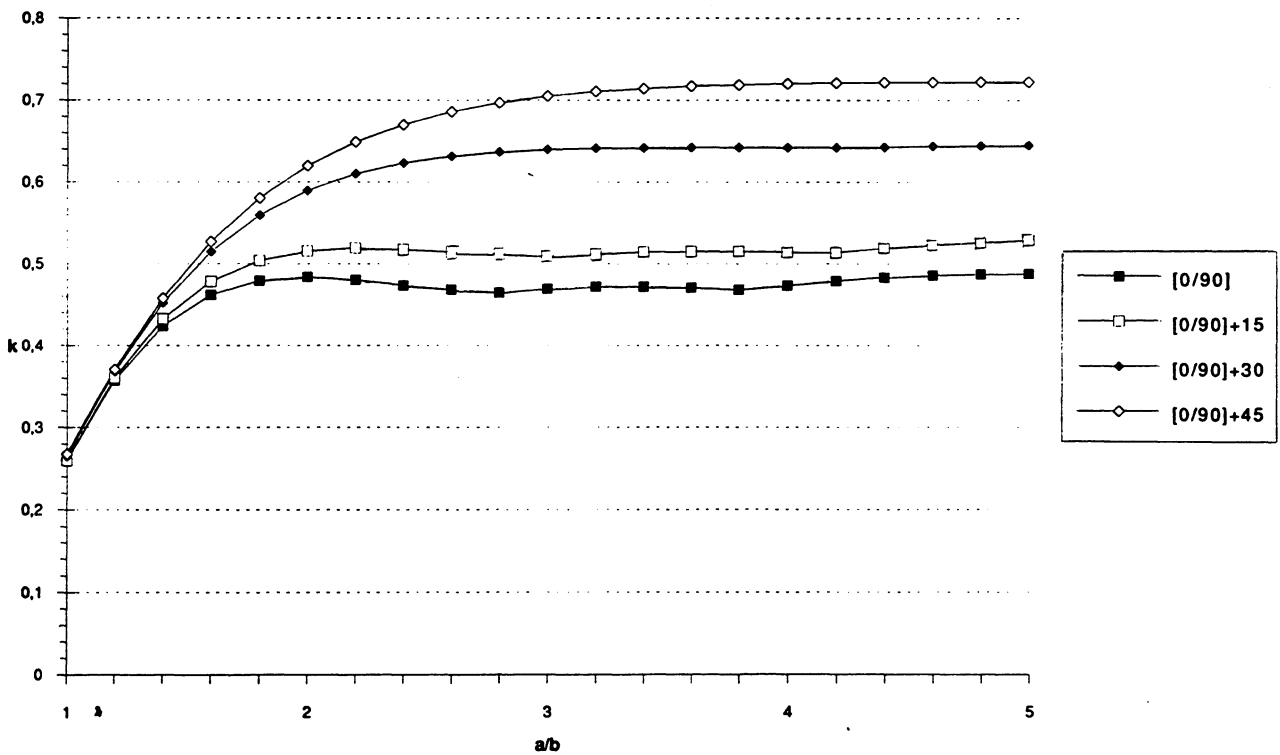


Figure 4.20 Kevlar, rectangular plate, all clamped edges, uniform load, $\{[(0/90) + \theta]_{10}\}_s$.

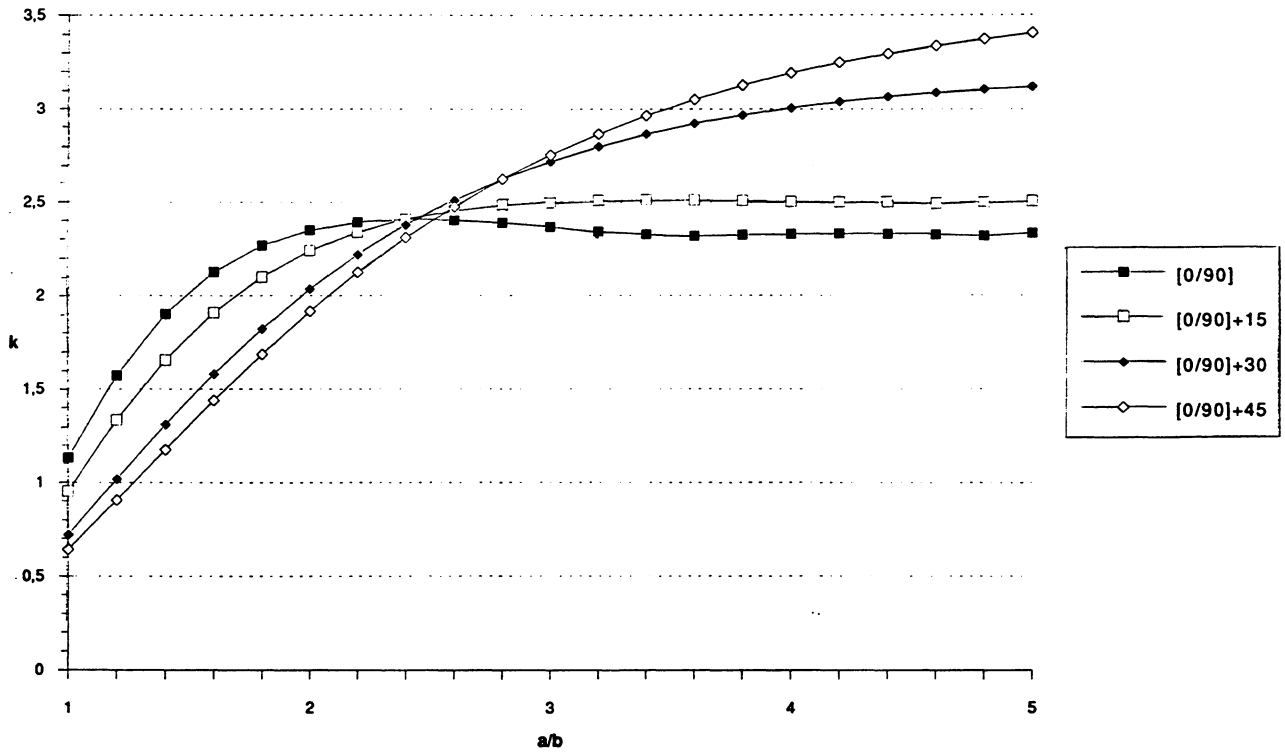


Figure 4.21 Kevlar, rectangular plate, all supported edges, uniform load, $\{[(0/90) + \theta]_{10}\}_s$.

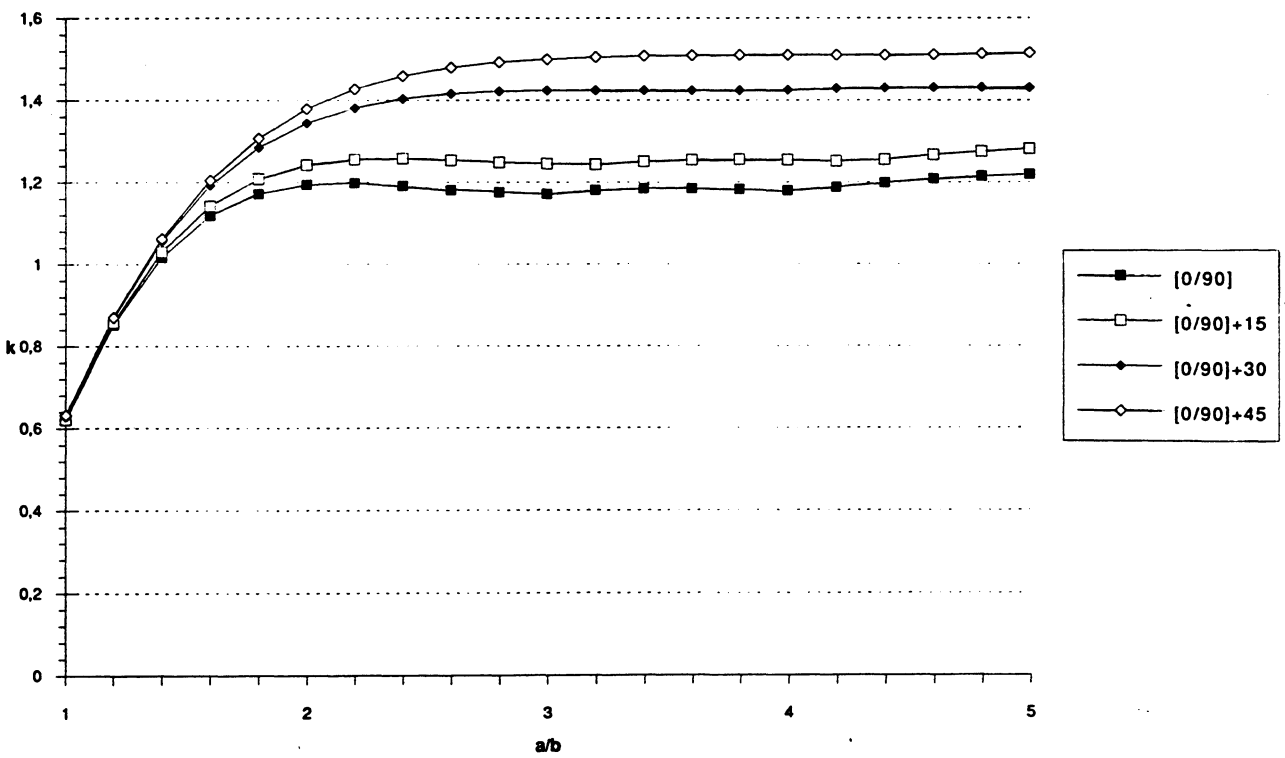


Figure 4.22 Scotchply, rectangular plate, all clamped edges, uniform load, $\{[(0/90) + \theta]_{10}\}_s$.

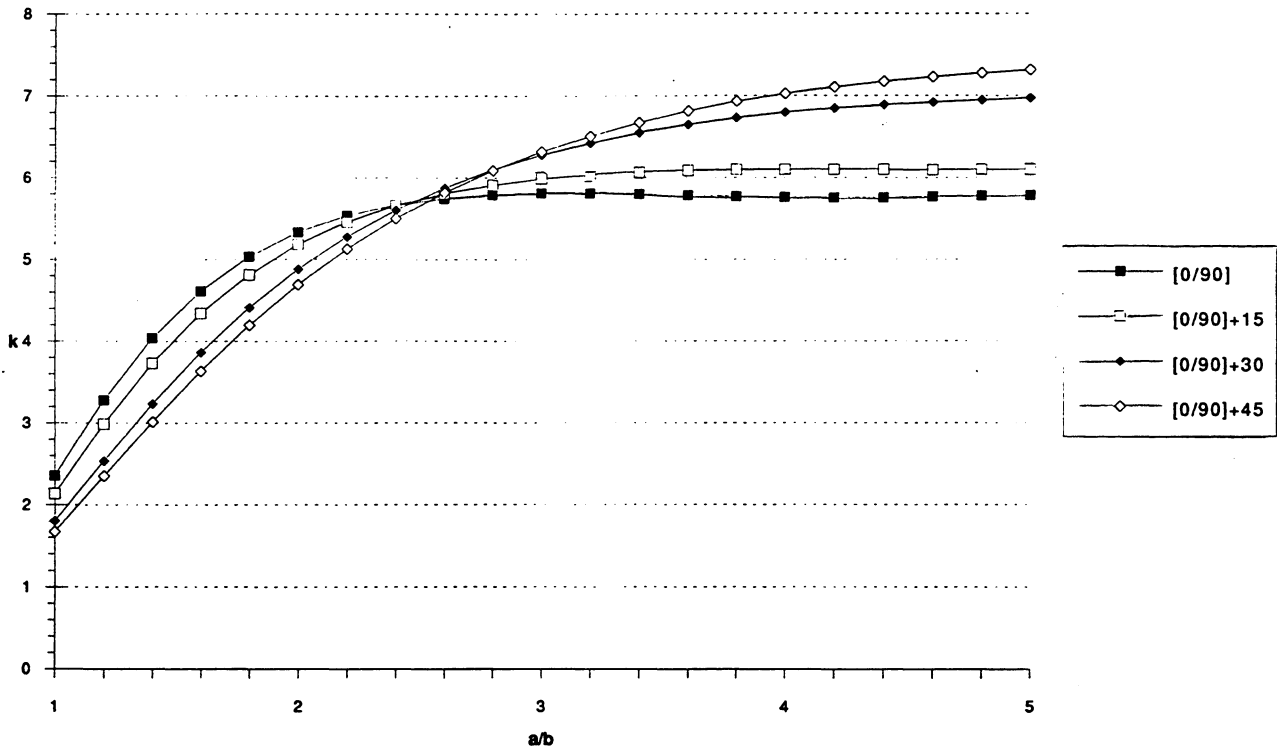


Figure 4.23 Scotchply, rectangular plate, all supported edges, uniform load, $\{[(0/90) + \theta]_{10}\}_s$.

4.3 Design optimisation of composite plates in buckling

The problem analysed here can be defined by the following points:

- The objective is to achieve the minimum weight structure by using critical compressive force as a design criterion.
- Only symmetric and balanced laminates have been considered.
- Boundary conditions are restricted to:
 - simply supported plates along the four edges of the plate;
 - clamped plates along the four edges of the plate.
- Six types of loading have been applied:
 - uniform uniaxial compression load;
 - uniform biaxial compression load ($N_y = N_x/2$);
 - uniform biaxial compression load ($N_y = N_x$);
 - uniform biaxial compression load ($N_y = 2 N_x$);
 - uniform shear load;
 - combined load: uniaxial uniform and uniform shear load.
- The mesh is composed by 400 nodes. The theory used is explained in Chapter 1.

- The material used is T300/N5208.

In Fig. 4.24, a definition of co-ordinates axes for two-dimensional plates subjected to uniform uniaxial, biaxial, shear and combined compression loads is shown.

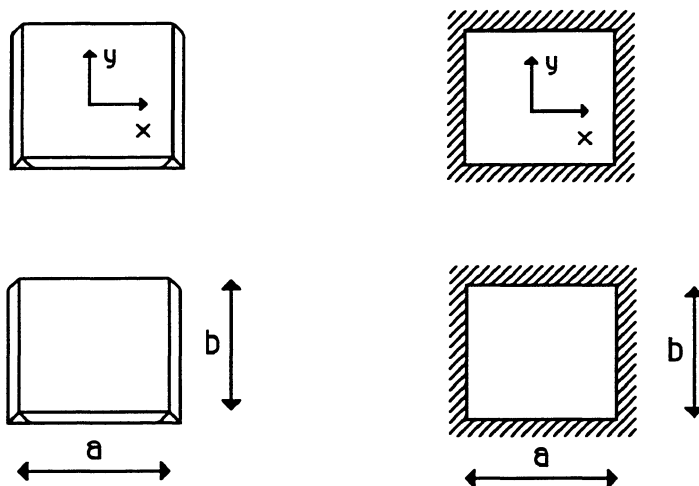


Figure 4.24 Definition of co-ordinates axes for two-dimensional plates subjected to uniform uniaxial compression, biaxial compression, shear or combined load.

4.3.1 Two-dimensional simply supported plates subjected to compression

In Fig. 4.25 and 4.26, critical loads are reported for two-dimensional simply supported plates subjected to uniform loads. The optimum angle can also be seen in Fig. 4.25. Both critical load and optimum angle are a function of the plate aspect ratio, though they present constant values for aspect ratios higher than four. A comparison between the optimum configuration and the Q-isotropic laminate is shown in Fig. 4.26.

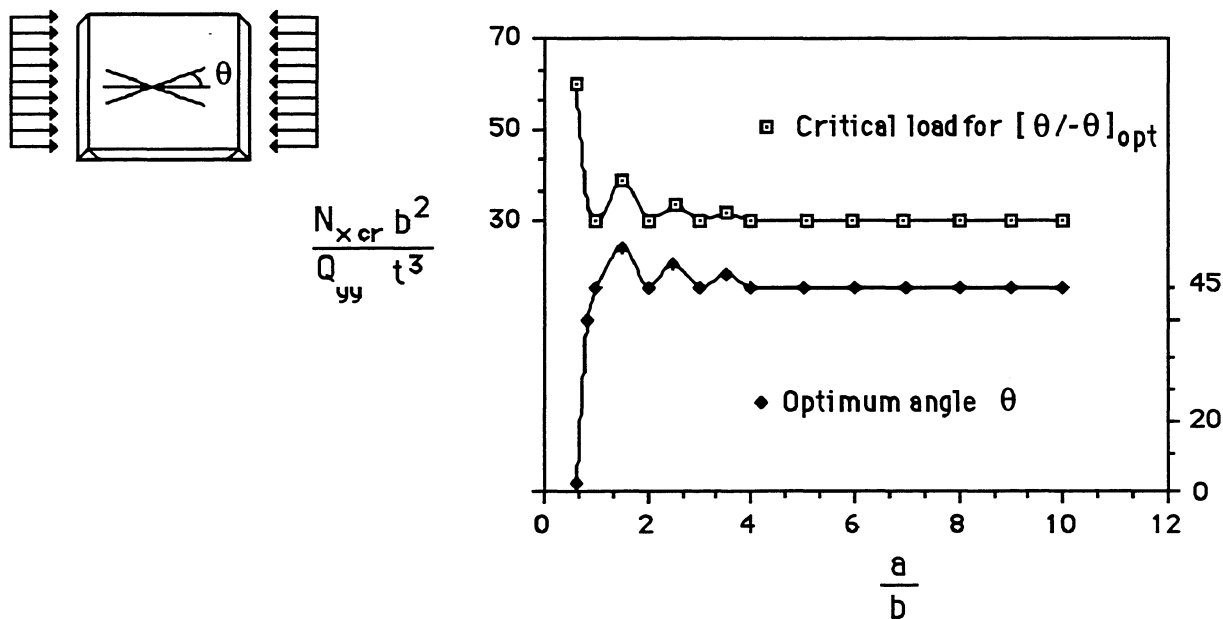


Figure 4.25 Critical load and optimum angle for a simply supported plate subjected to a uniform uniaxial compression load.

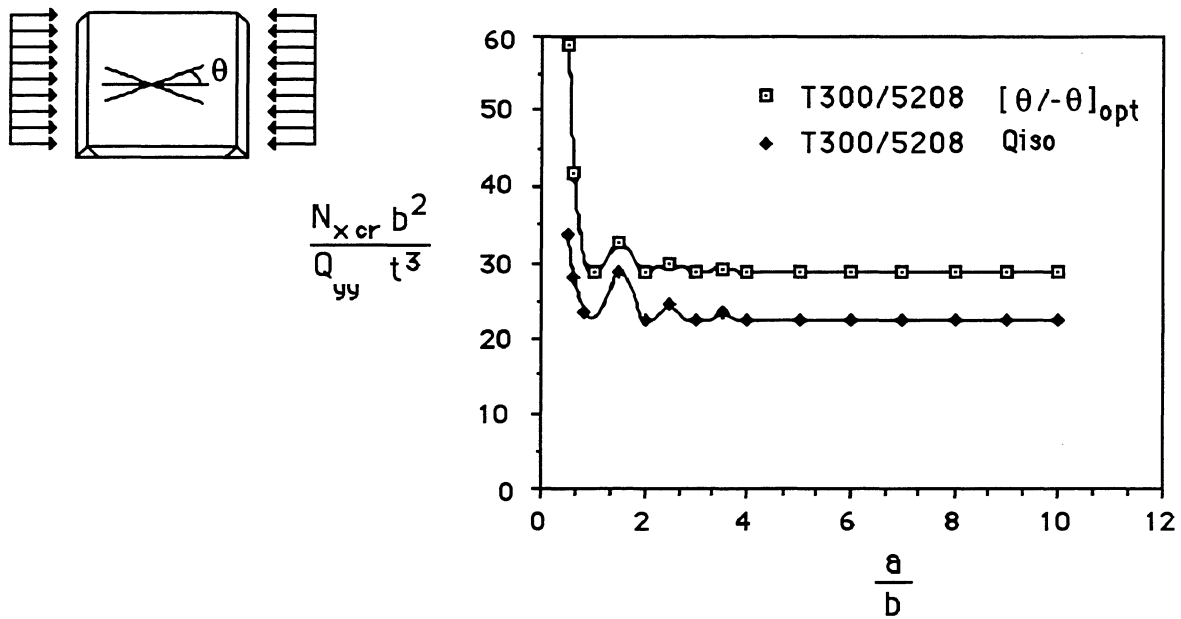


Figure 4.26 Comparison between critical loads of optimum configuration and Q-isotropic laminate (simply supported plates subjected to a uniform uniaxial compression load).

A comparison between critical loads for angle-ply and Q-isotropic laminate as a function of the angle of fibre orientation is shown in Fig. 4.27. For angles between 27° and 66° , the critical load for angle-ply laminates is higher than for Q-isotropic laminates.

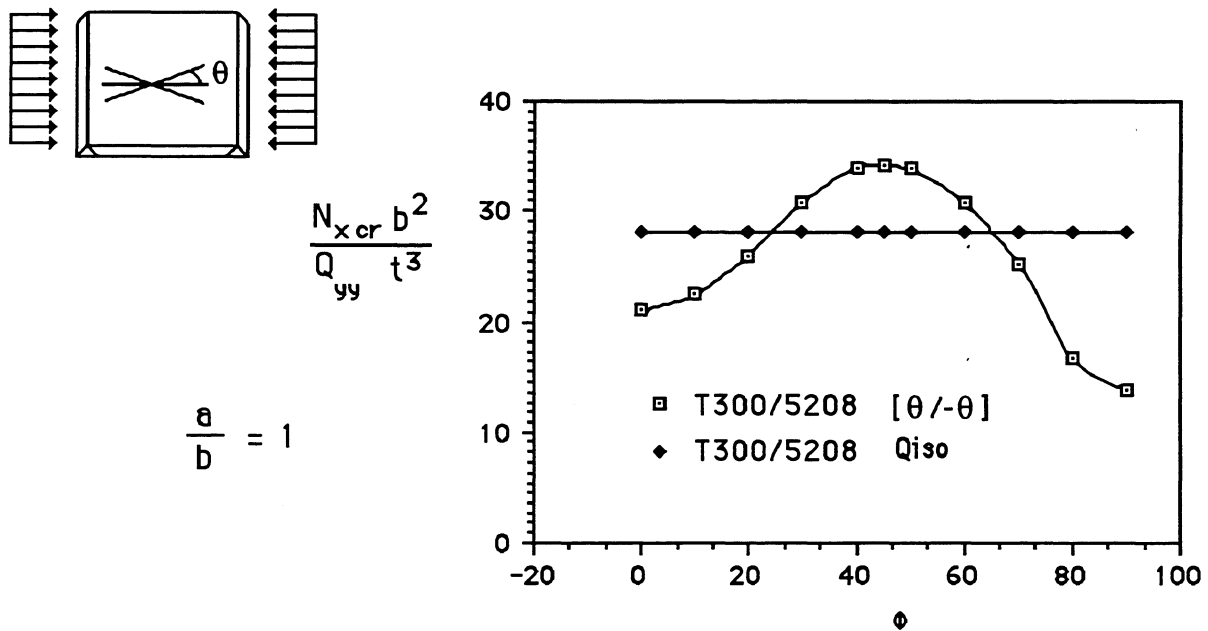
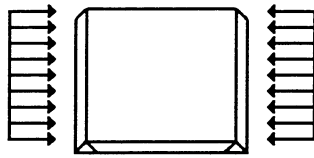


Figure 4.27 Comparison of critical loads for cross-ply and Q-isotropic laminate for a square plate (simply supported plates subjected to a uniform uniaxial compression load).

In Fig. 4.28, normalised weights of aluminium and Q-isotropic T300/N5208 to the optimum laminate of T300/N5208 are reported.



RELATIVE WEIGHT
RESPECT TO
[$\theta / -\theta$] opt

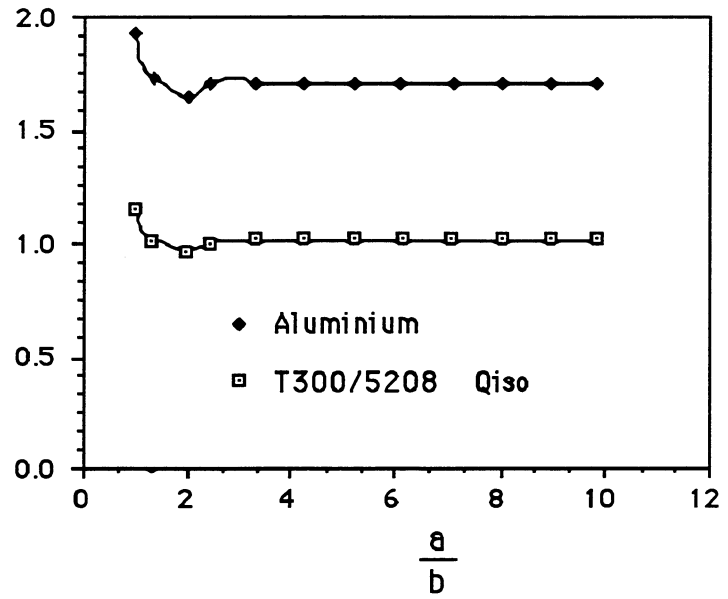


Figure 4.28 Comparison between weights of aluminium and the optimum configuration of T300/N5208 (simply supported plates subjected to a uniform uniaxial compression load).

Similar graphics to the ones represented in Figures 4.25 to 4.28 can be obtained for biaxial compression. The results are shown in Table 4. 1

Table 4.1 Bucking parameters for simply supported plates subjected to biaxial compression

	$N_y=0$	$N_y = N_x/2$	$N_y = N_x$	$N_y = 2 N_x$
Optimum angle (ϕ) for $a/b=1, 2, 3, 4$ and >4	45°	63°	70°	80°
$(N_x \text{ cr } b^2) / (Q_{yy} t^3)$ for $(\phi / -\phi)_{opt}$	28	18	11	5.5
$(N_x \text{ cr } b^2) / (Q_{yy} t^3)$ for Q-isotropic	22	13	7	4
Relative weight of aluminium to $(\phi / -\phi)_{opt}$	1.7	1.8	1.9	2

4.3.2 Two-dimensional clamped plates subjected to compression

When the plate is clamped along the four edges, the critical buckling load decreases as the aspect ratio increases. Figures 4.29 to 4.42 represent optima angles, critical loads for $(\theta / -\theta)_{opt}$ and Q-isotropic configurations and relative weight of aluminium respectively.

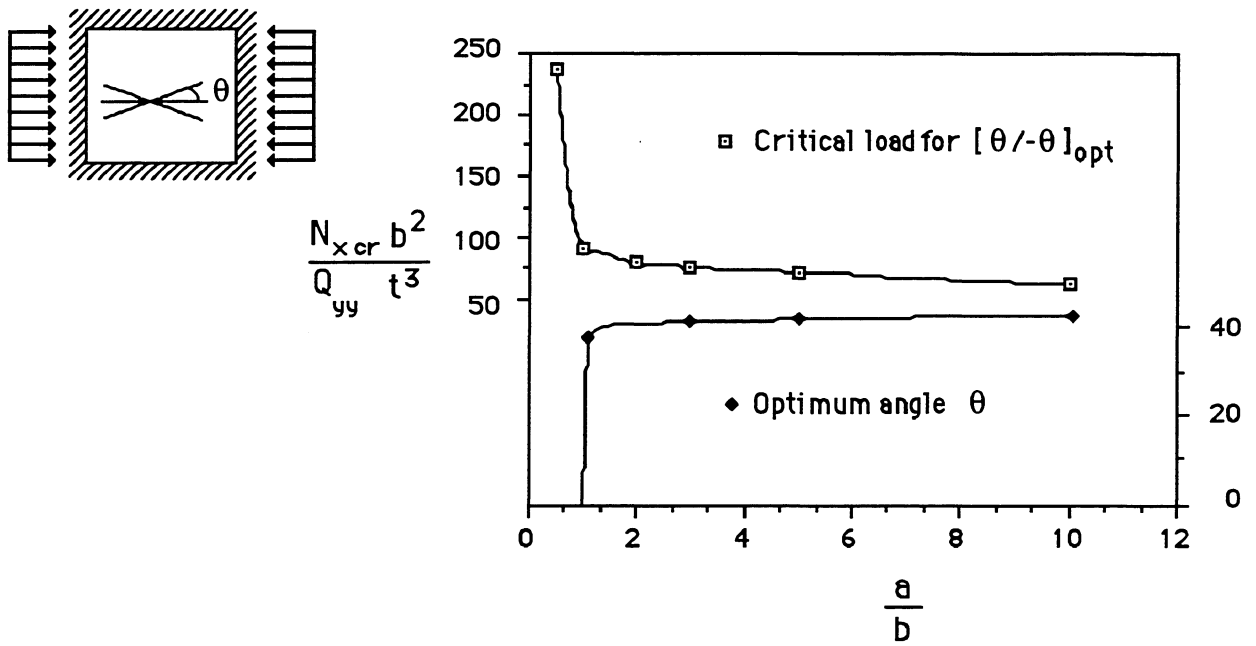


Figure 4.29 Critical load and optimum angle for a clamped plate subjected to a uniform uniaxial compression load.

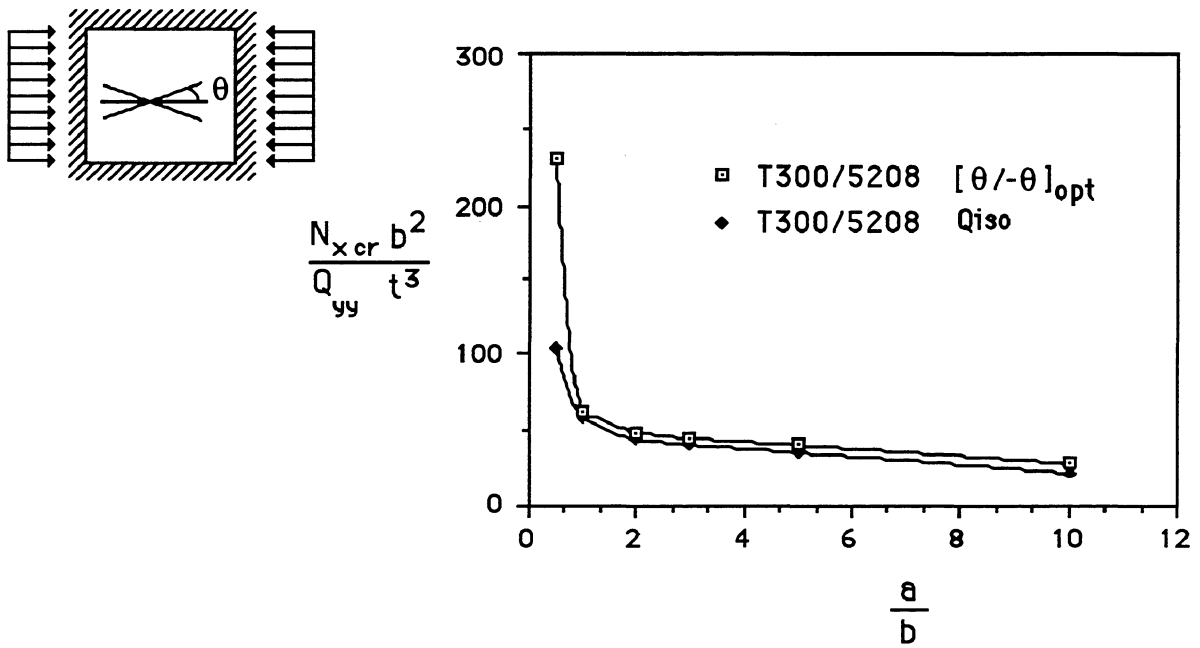


Figure 4.30 Comparison between critical loads of optimum configuration and Q-isotropic laminate (clamped plates subjected to a uniform uniaxial compression load).

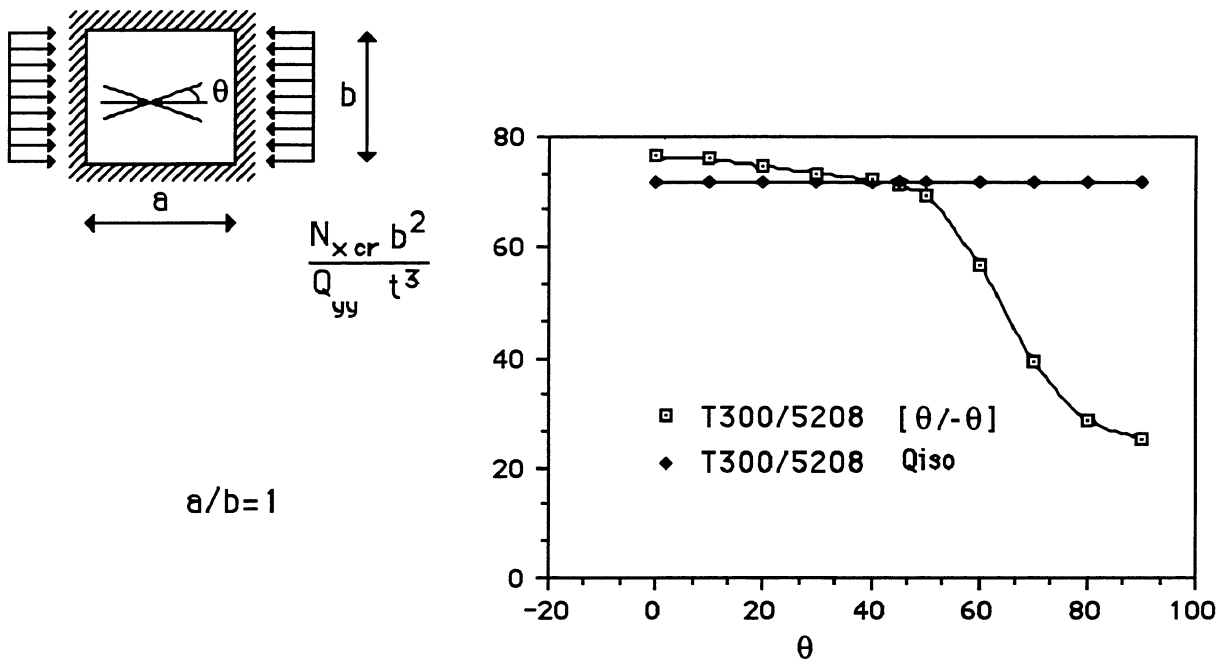


Figure 4.31 Comparison of critical loads for cross-ply and Q-isotropic laminate for a square plate (clamped plates subjected to a uniform uniaxial compression load).

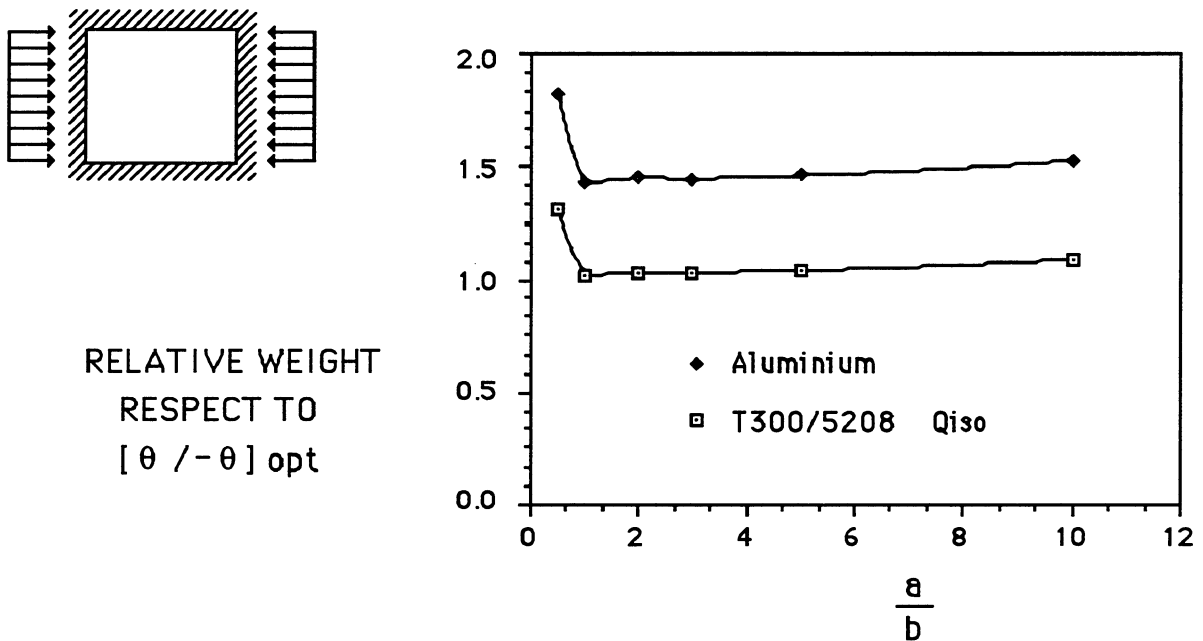


Figure 4.32 Comparison between weights of aluminium and the optimum configuration of T300/N5028 (clamped plates subjected to a uniform uniaxial compression load).

Table 4.2 shows the key value for uniaxial and three biaxial compression load cases.

Table 4. 2 Bucking parameters for clamped plates subjected to biaxial compression

	$N_y = 0$	$N_y = N_x/2$	$N_y = N_x$	$N_y = 2 N_x$
Optimum angle (θ) for $a/b=1$	45°	63°	70°	80°
$(N_x cr b^2) / (Q_{yy} t^3)$ for $(\theta / - \theta)_{opt}$	28	18	11	5.5
$(N_x cr b^2) / (Q_{yy} t^3)$ for Q-isotropic	22	13	7	4
Relative weight of aluminium to $(\theta / - \theta)_{opt}$	1.7	1.8	1.9	2

4.3.3 Two-dimensional simply supported plates subjected to a uniform shear load

The buckling parameters for simply supported plates subjected to a uniform shear load follow similar rules to those plates subjected to compression loads (paragraphs 4.3.1 and 4.3.2). Critical shear buckling loads decreases as the aspect ratio increases (Fig. 4.33 and 4.34). Small differences are reported between the optimum and the Q-isotropic configurations (Fig. 4.34).

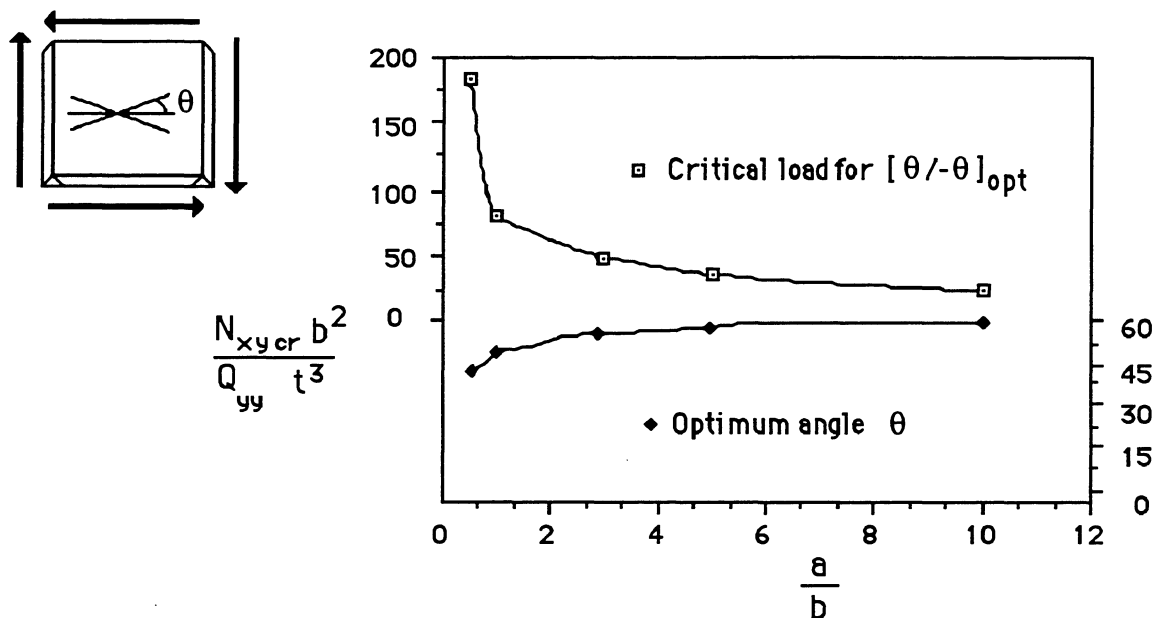


Figure 4.33 Critical load and optimum angle for a simply supported plate subjected to a uniform shear load.

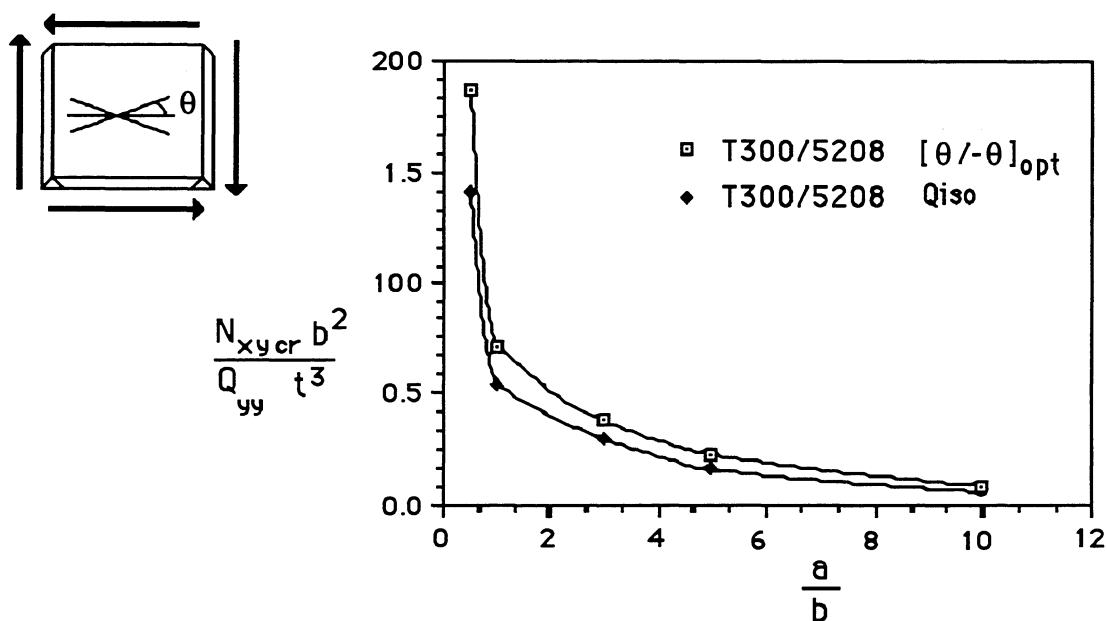


Figure 4.34 Comparison between critical loads of optimum configuration and Q-isotropic laminate (simply supported plates subjected to a uniform shear load).

A comparison between critical loads for angle-ply and Q-isotropic laminate in function of the angle of fibre orientation is carried out in Fig. 4.35. For angles between 27° and 66° , the critical load for angle-ply laminates is higher than for Q-isotropic laminates.

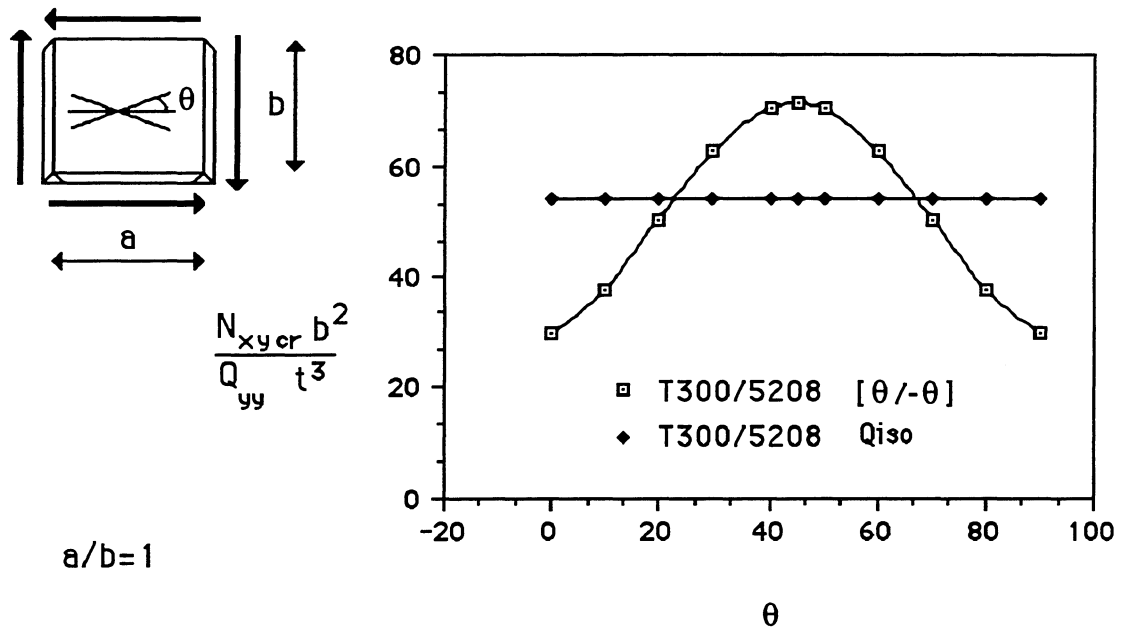


Figure 4.35 Comparison of critical loads for cross-ply and Q-isotropic laminate for a square plate (simply supported plates subjected to a uniform shear load).

In Fig. 4.36, normalised weights of aluminium and Q-isotropic T300/N5208 to the optimum laminate of T300/N5208 are shown.

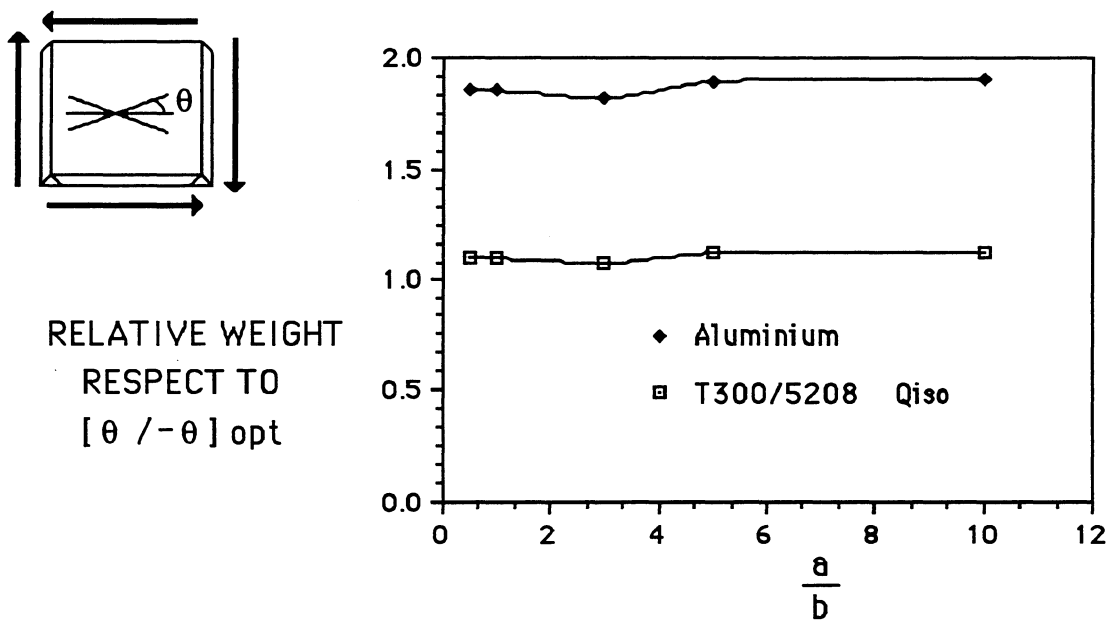


Figure 4.36 Comparison between weights of aluminium and the optimum configuration of T300/N5208 (simply supported plates subjected to a uniform shear load).

4.3.4 Two-dimensional clamped plates subjected to a uniform shear load

The behaviour of clamped plates subject to a uniform shear load is quite similar to that registered for simply supported plates, as shown in Fig. 4.37 to 4.40.

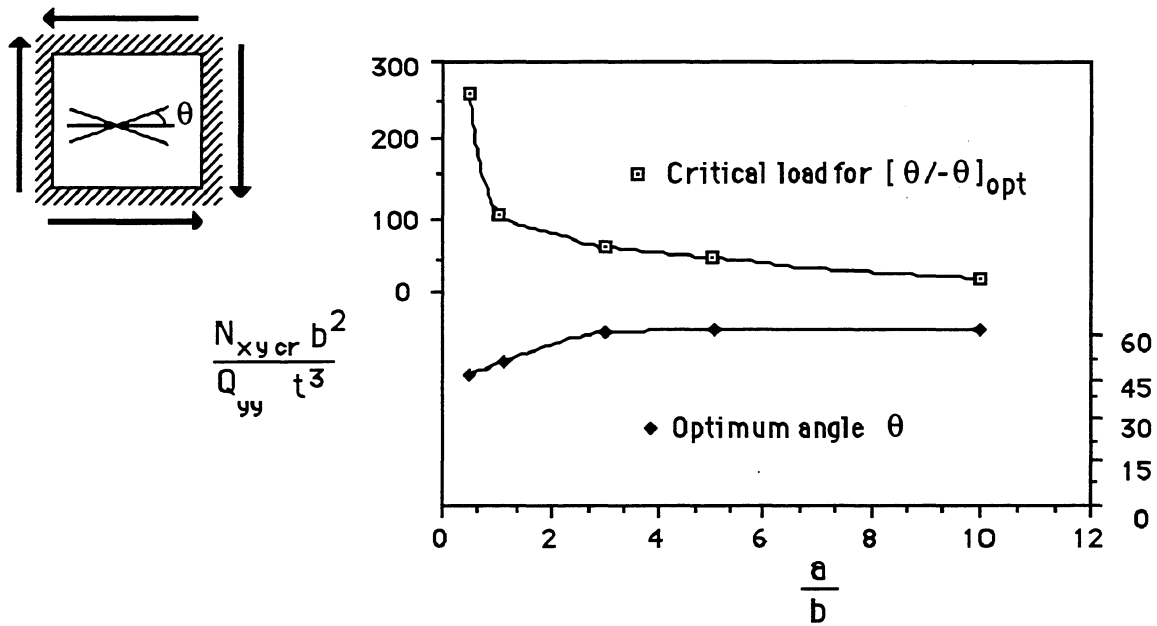


Figure 4.37 Critical load and optimum angle for a clamped plate subjected to a uniform shear load.

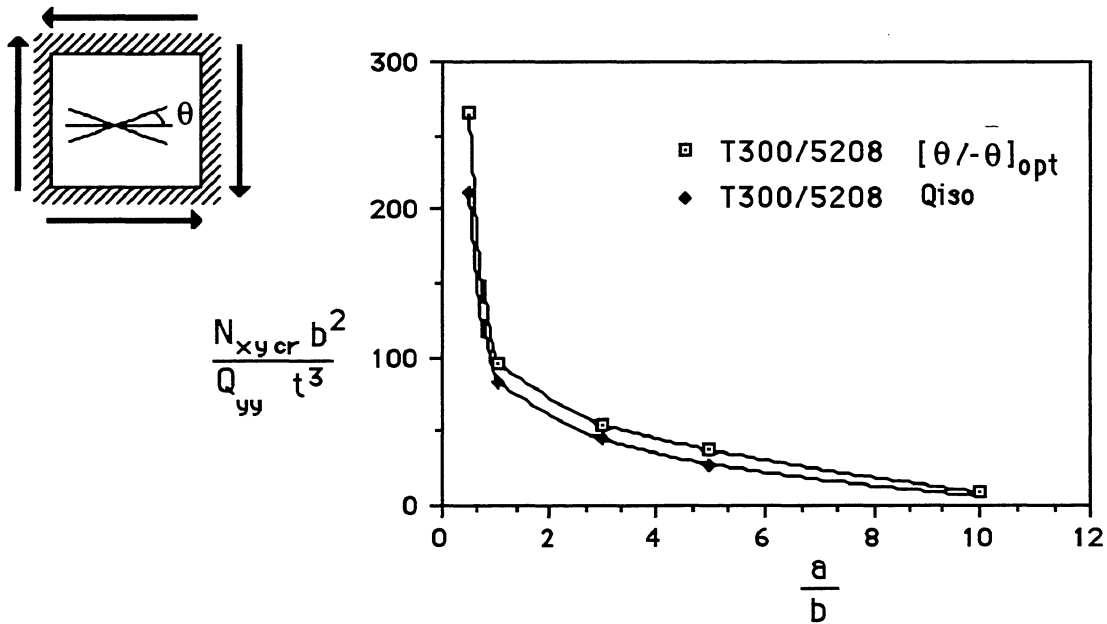


Figure 4.38 Comparison between critical loads of optimum configuration and Q-isotropic laminate (clamped plates subjected to a uniform shear load).

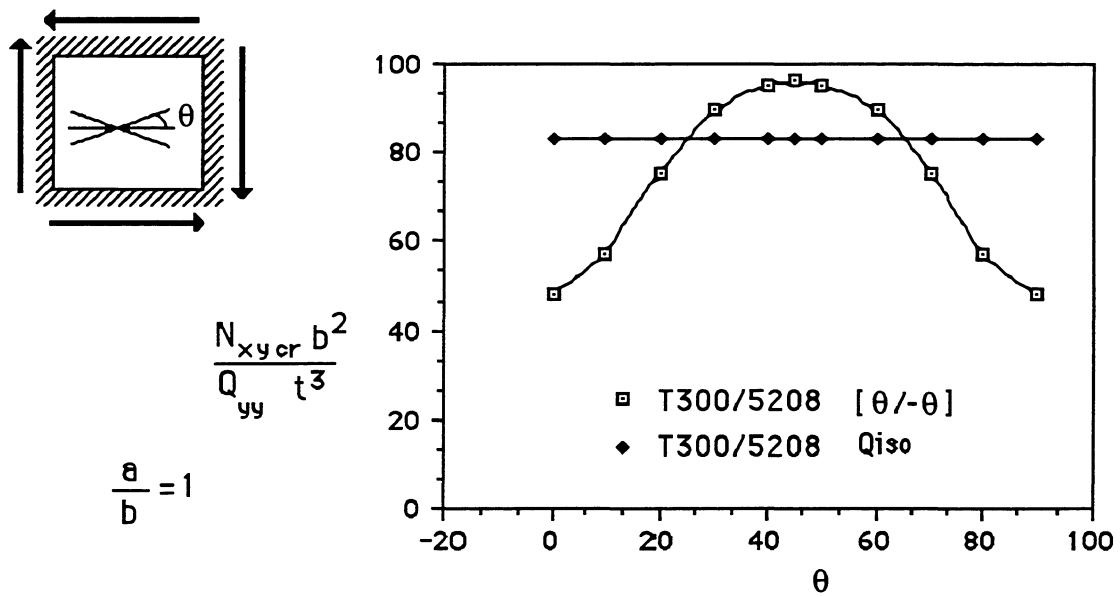


Figure 4.39 Comparison of critical loads for cross-ply and Q-isotropic laminate for a square plate (clamped plates subjected to a uniform shear load).

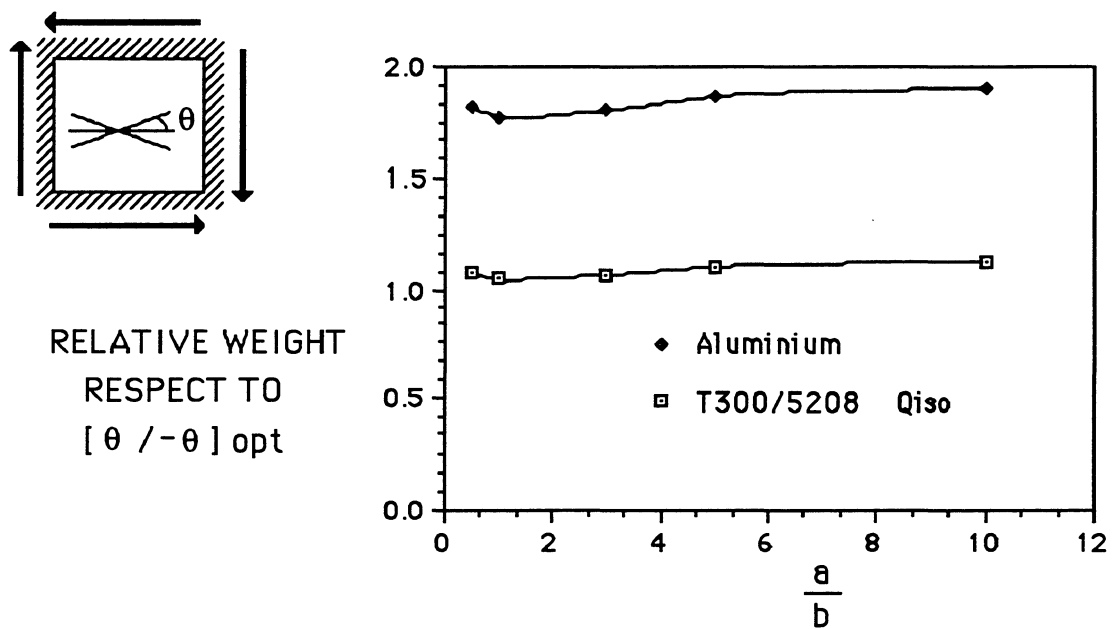


Figure 4.40 Comparison between weights of aluminium and the optimum configuration of T300/N5208 (clamped plates subjected to a uniform shear load).

4.3.5 Two dimensional plates subjected to combined loads

Finally, Fig. 4.41 and 4.42 represent the buckling parameters for simply supported and clamped plates subjected to combined uniform uniaxial compression and shear, respectively.

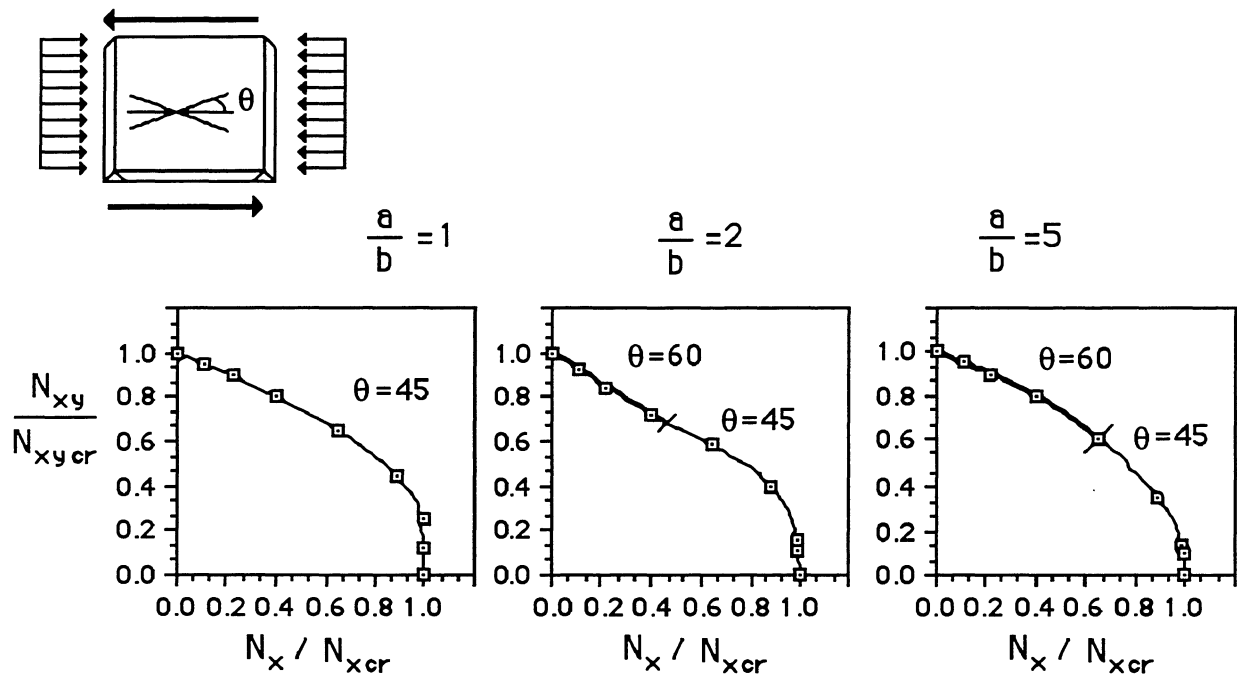


Figure 4.41 Buckling parameters for simply supported plates subjected to combined uniform uniaxial compression and shear.

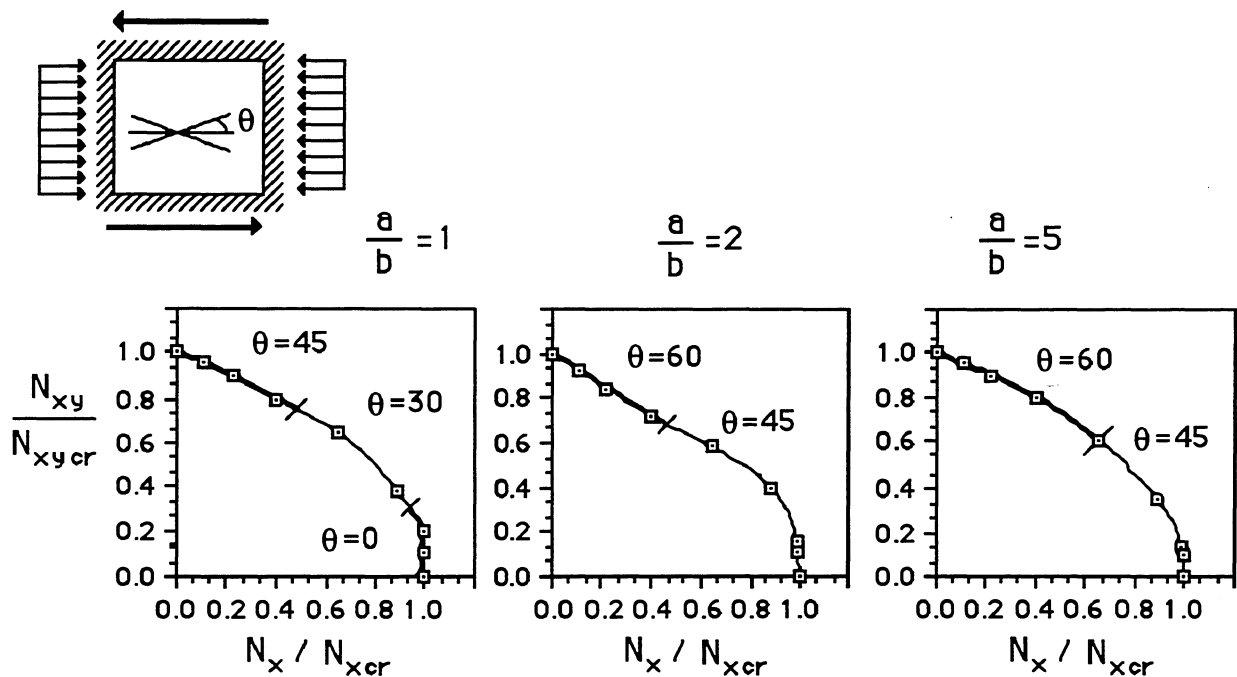


Figure 4.42 Buckling parameters for clamped plates subjected to combined uniform uniaxial compression and shear. Further information can be obtained in references 24-54.

4.4 Conclusions

Constant thickness composite plates subjected to buckling and transverse loads (uniform or point load) are used most in engineering applications. In most cases, optimum designs are required, the weight being the optimisation criterion and

the maximum deflection (transverse loads) or critical compressive force (buckling) being the parameters to be optimised.

Three studies have been carried out on sections of constant thickness plates subjected to transverse loads. First, three fibre glass composite systems (unidirectional, fabric and chopped strand matting) have been analysed and the influence of several lay-ups on the maximum deflection has been reported for a wide range of aspect ratios. Second, three unidirectional composite systems (carbon, aramid and glass fibres) have been studied and the influence of variation of θ in angle-ply laminates $[\pm\theta]$ has been analysed as a function of the aspect ratio. Finally, the influence of rotation of cross-ply laminates $[0/90]$ on the maximum deflection of the plate has been reported as a function of the aspect ratio for the three material systems described above.

The maximum deflection of square ($a/b = 1$) simply supported and clamped plates subjected to uniform load does not depend upon the lay-up. For rectangular non-square plates ($a/b > 1$), the optimum lay-up is $[90]$ for simply supported and clamped plates, a substantial difference between the values of k for the optimum lay-up and for the rest of laminates is reported.

For simply supported plates, deflections of laminates $[\pm 45]$, Q-isotropic and $[0/90]$ are very close for aspect ratios ranged between 1 and 2.5 and for aspect ratios higher than 2.5, differences between the deflections of these three laminates increase, the least stiff being $[\pm 45]$.

For clamped plates, the ranking of laminates in terms of stiffness is $[90]$, $[0/90]$, Q-isotropic and $[\pm 45]$ for all the aspect ratios considered. The values of k are very similar for a square plate ($a/b = 1$) for the four lay-ups analysed. Behaviour of the FAB-E-580 fibre glass fabric configuration is similar to the unidirectional mentioned above. There exist substantial differences in the values of k . This parameter for the fabric is 2.5 times higher than that reported for the unidirectional configuration.

Deflections of chopped strand matting plates subjected to uniform and central load are strongly dependent on the boundary conditions. For simply supported plates, the stiffness increases substantially for aspect ratios close to 1. Except for the case of a square plate, clamped plates show a deflection, which does not depend upon the aspect ratio.

Maximum deflection is strongly dependent on the variation of θ of angle-ply laminates. The stiffest laminate is $[90]$ and the least stiff is $[0]$ for all the aspect ratios considered. Small differences of values of k are reported in the ranges $[0]$ to $[\pm 15]$ and $[\pm 60]$ and $[90]$. Carbon, aramid and glass fibre composite laminates show similar values of k for the lay-up $[90]$ and high aspect ratios. For low values of the aspect ratio, deflections for the fibre glass system become the highest and for the carbon fibre system become the lowest.

Maximum deflection is strongly dependent on the rotation of cross-ply laminates. For clamped plates, the stiffest laminate is $[\pm 45]$ and the least stiff is $[0/90]$ for all the aspect ratios and materials considered. For aspect ratios higher than 3, the maximum deflection does not depend on the aspect ratio.

For simply supported plates, two different ranges of aspect ratios are observed for the three material systems studied. For aspect ratios ranged from 1 to 2.5, the optimum lay-up is $[\pm 45]$ and the least stiff is $[0/90]$. For plates whose

aspect ratio is 2.5, the maximum deflection does not depend on the aspect ratio. For aspect ratios higher than 2.5, the optimum lay-up is [0/90] and the least stiff is [± 45].

A buckling study of constant thickness plates has also been carried out. Uni, bi-axial and shear loads have been treated for a carbon fibre plate with two boundary conditions: simply supported and clamped along the four sides of the plate.

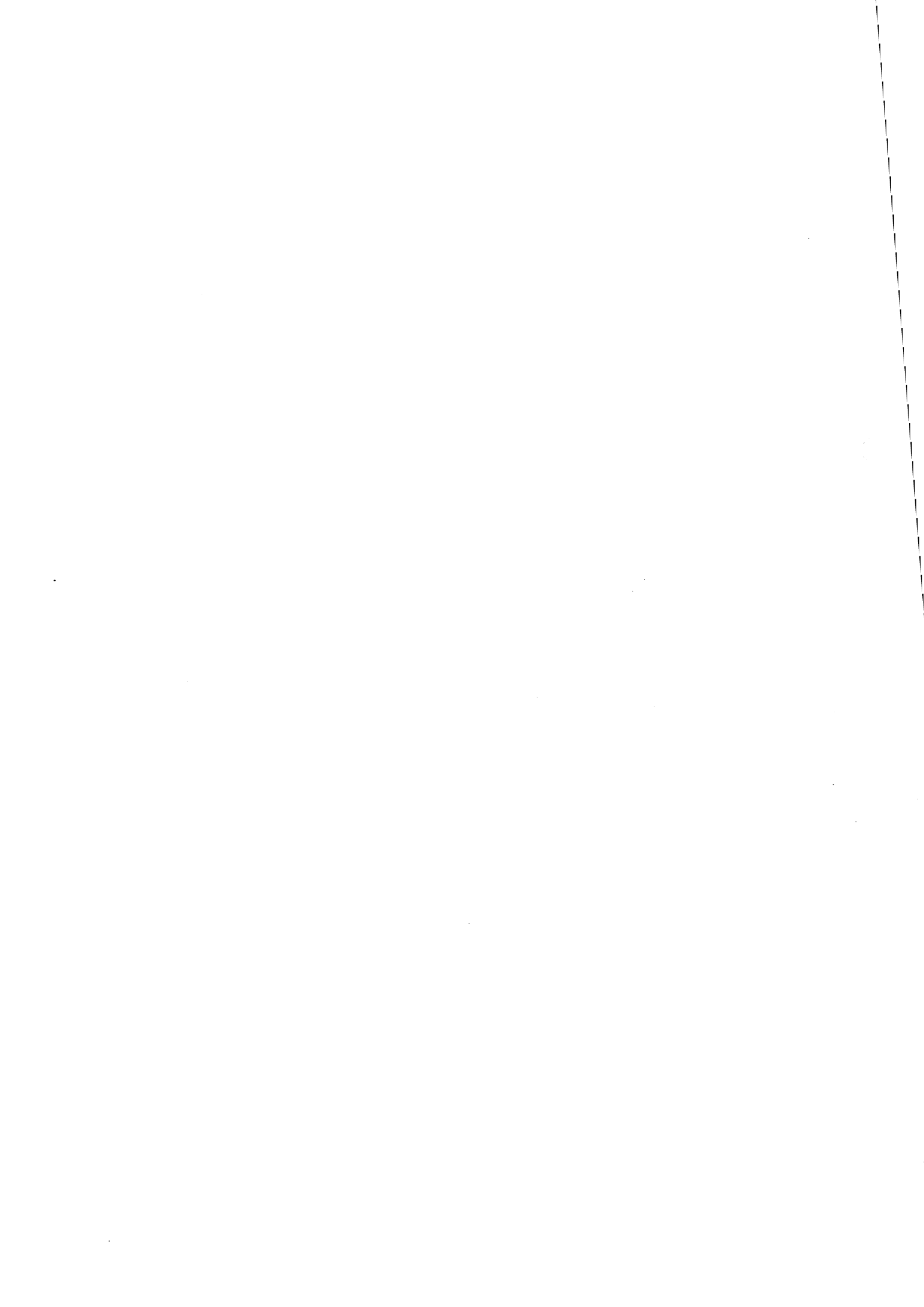
Optimum sublaminates and critical loads have been obtained for each case. The behaviour of the optimum angle ply laminates has been compared with the Q-isotropic configuration and aluminium and substantial weight savings have been reported.

References

1. Hirano Y, 'Optimum design of laminated plates under axial compression', J. AIAA, 1979, 17, 1017.
2. Bert CW, 'Optimal design of a composite material plate to maximize its fundamental frequency', J. Sound & Vibration, 1977, 50, 229.
3. Bert CW 'Design of clamped composite material plates to maximize fundamental frequency', J. of Mech. Des. ASME, 1978, 100, 274.
4. Adali S 'Design of shear-deformable antisymmetric angle-ply laminates to maximize the fundamental frequency and frequency separation', Comp. Struct., 1984, 2, 349.
5. Pedersen P, 'On Sensitivity Analysis and Optimal Design of Specially Orthotropic laminates', Proc. ASI CAD, Troia, Portugal, pp. 170, 1986.
6. Pedersen P, 'On sensitivity analysis and optimal design for laminates', In Mechanical Behavior of Composites and Laminates, ed. Green and Micunovic, Elsevier, 1987, 274.
7. Joshi SP, Iyengar NGR 'Studies on optimization of laminated composite plates', Proc 13 ICAS Cong, AIAA Sys Conf, pp 607, 1982.
8. Soni PJ and Iyengar NGR 'Optimal design of clamped laminated plates', J. Fibre Sci & Tech, 1983, 19, 281.
9. Joshi SP and Iyengar NGR 'Optimal design of laminated composite plates under axial compression', Trans Can Soc Mech Eng, 1986, 9, 45.
10. Khot NS, Computer Program (OPTCOMP) for Optimization of Composite Structures for Minimum Weight Design, AFFDL TR-76-149, Wright-Patterson Air Force Base, Dayton, OH, 1977.
11. McKeown JJ, 'Optimal composite structures by deflection-variable programming', Comput. Meth. Appl. Mech. Eng., 1977, 112, 155.
12. Starnes JH and Haftka RT, 'Preliminary Design of Composite Wings AIAA, ASME Structures', Structural Dynamics and Material Conference, Bethesda, MD, 1978.
13. Schmit LA and Mehrinfar M, 'Multilevel optimum design of structures with fiber-composite stiffened-panel components', J. AIAA, 1980, 16, 5.
14. Sobieszczanski-Sovieski J, An Integrated Computer Procedure for Sizing Composite Airframe Structures, NASA TP 1300, NASA Langley Research Center, Hampton, VA, 1979.
15. Park JW, An Optimal Design of Simple Symmetric Laminates Under the First Ply Failure Criteria, AFWAL-TR-81-4175, Air Force Materials Laboratory, 1982.
16. Donaldson S, 'Simplified weight saving techniques for composite panels', J. Reinf Plastics and Composites, 1983.

17. Wurzel DP, On the Optimal Design of Bidirectional Composites, AFWAL-TR-83-4060, Air Force Materials Laboratory, 1983.
18. Massard TN, 'Computer sizing of composite laminates for strength', J. Reinf. Plastics and composites, 1984, 3, 300.
19. Maksimovic S, 'Optimum design of composite structures', Proc. 3rd Conf. Comp. Struct., Paisley, pp 148, 1985.
20. Tsai SW, Composites design, (eds. Tsai, S W, Massard, T N, Susuki, I), 1985.
21. Watkins RI and Morris AJ, 'A multicriteria objective function optimization scheme for laminated composites for use in multilevel structural optimization schemes', Comp. Meth. in Eng. 1987, 160, 233.
22. Iyengar NGR, 'Optimal Design of Fiber Reinforced Composite Plates', Proc Advances in Aerospace structures, Madras, 1988, 71.
23. Pedersen, P, 'On optimal orientation of orthotropic materials', (in press).
24. Leissa AW, Buckling of Laminated Composite Plates and Shell Panels, AFWAL-TR-85-3069, 1985.
25. Muc, A, 'Optimal fibre orientation for simply-supported, angle-ply plates under biaxial compression', Comp. Struct, 1988, 9, 161.
26. Timoshenko SP and Woinowsky-Krieger S, Theory of Plates and Shells, McGraw- Hill, New York, 1959.
27. Cook RD, Concepts and Applications of Finite Element Analysis, John Wiley, New York, 1981.
28. Reissner E, 'The effect of transverse shear deformation on the bending of elastic plates', ASME. J. Appl. Mech. 1945, 12, A69-A77.
29. Mindlin RD, 'Influence of rotatory inertia and shear deformation on flexural motions of isotropic elastic plates', ASME. J. Appl. Mech., 1951, 18, 31.
30. Khalil M and Ramahefarison E, 'Optimum design of composite laminates subjected to multiple loads', in ICCM 9, Volume IV, ed. A. Miravete, Woodhead Publishing Limited, Cambridge, 1993, pp 643-50.
31. Shin YS, Haftka RT, Watson LT and Plaut RH, 'Design of laminated plates for maximum buckling load', J. of Comp. Mater., 1989, 23, 348-369.
32. Vanderplaats GA, Numerical Optimization Techniques for Engineering Design with Applications, McGraw-Hill, New York, 1984, 26-54, 104-116, 121-140.
33. Minoux M, Programmation Mathématique: Théorie et Algorithmes, Tome I Dunod, 1983, pp 31-53, 95-11.
34. Park WJ, 'An optimal design of simple symmetric laminates under the first ply failure criterion', J. of Comp. Mater., 1982, 16, 341-355.
35. Schmit LA, The Structural Synthesis Concept and its Potential Role in the Design with Composites, in: Mechanics of Composite Materials, Proceedings of the Fifth Symposium of Naval Structural Mechanics, May 8-10, 1976.
36. Vanderplaats GA, and Weisshaar TA, 'Optimum design of composite structures', Int. J. for Numer. Meth. in Eng. 1989, 27, 437-448.
37. Flanagan G, Palazotto AN, 'Composite laminate optimization program suitable for microcomputers', Computers & Structures 1986, 22, 995-1009.
38. Wurzel DP, 'On the design and optimization of bidirectional composites', J. Reinforced Plastics and Composites 1983, 2, 178-195.

39. Khalil M and Ramahefarison E, OPTICOM: Un Logiciel d'Optimisation des Stratifiés Composites sur Micro-ordinateur, in: Proceedings of STRUCOME 92, Paris, November 16-19, 1992, pp 489-501.
40. Gay D, Matériaux Composites, Hermes, Paris, 1987, pp 48-63, 398-409.
41. Harper BD, 'The effects of moisture induced swelling upon the shapes of antisymmetric cross-ply laminates', J. of Compos. Mater. 1987, 21, 36-48.
42. Mukhopadhyay AK and Sierakowski RL, 'On sandwich beams with laminate facings and honeycomb cores subjected to hygrothermal loads', J. of Compos. Mater. 1990, 24, 382-400.
43. Manera M, Massot JJ, Morel G and Verchery G, Manuel de Calcul des Composites Verre/Résine, Pluralis, Paris, 1988, pp 147-151.
44. Eschenauer H A, 'Aspects on finding optimal layouts of structures made of composite materials', in ICCM 9, Volume IV, ed. Antonio Miravete, Woodhead Publishing Limited, Cambridge, UK, 1993, pp 651-660.
45. Bremicker M, Eschenauer H A and Post PU, 'Optimization procedure SAPOP - A general tool for multicriteria structural designs', in Multicriteria Design Optimization, ed. H A Eschenauer, J Koski and A Osyczka, Berlin, 1990.
46. Eschenauer HA, Schumacher G and Hartzheim W, 'Multidisciplinary design of composite aircraft structures by Lagrange', Computers and Structures, 1992, 44, 877-93.
47. Eschenauer HA, Koski J and Osyczka A (eds), Multicriteria Design Optimization, Berlin, Heidelberg, New York, 1990.
48. Eschenauer HA, Bellendir K, 'Optimal layout of cylindrical composite shells under non-symmetric loading', ZAMM, 1992, 72, T553-T556.
49. Eschenauer H, Schnell W, Elastizitätstheorie - Grundlagen, Flächentragwerke, Strukturoptimierung, Mannheim, Leipzig, Wien: BI-Wissenschaftsverlag, 3 völlig überarbeitete u erweiterte Aufl 1993.
50. Geilen J, Optimierungsmodellbildung und Auslegung dickwandiger, gemischter Composite-Bauweisen mit stark gekrümmten Bereichen, Diss Universität-GH Siegen 1992 TIM-Forschungsberichte, Nr T02-0992.
51. Jones RM, Mechanics of Composite Materials, Scripta Book Company, Washington DC, 1975.
52. Kim CW, Hwang W, Park H C and Han K S, 'An optimal stacking sequence design of laminated composite cylinders', ICCM 9, Volume IV, ed A. Miravete, Woodhead Publishing Limited, Cambridge, UK, 1993, pp 661-8.
53. Schmit A Jr and Farshi B, 'Optimum design of laminated fiber composite plates', Int. J. for Numerical Meth. in Eng., 1977, 11, 623-640.
54. Graesser DL, Zabinsky ZB, Tuttle ME and Kim GI, 'Designing laminated composites using random search techniques', Composite Structures, 1991, 18, 311-325.



5 CONSTANT THICKNESS SANDWICHES

5.1 Introduction

A typical sandwich consists of two thin, high-strength facings bonded to a thick, lightweight core. The sandwich concept produces extremely stiff and strong structures at minimum weight. Thus, the sandwich structure is a key configuration in terms of design optimisation with composite materials.

Dramatic structural improvements in honeycomb and foam cores seem unlikely unless radically new materials are found (high-modulus low density fibres; foams with tubular transverse cells). Steady improvements in non-structural properties of foams are sought (stability, fire-resistance, low creep, non-toxicity, low CFC involvement). There is scope for new types of manufactured cores (tubes and heavy welded steel). The biggest advances are likely in fabrication methods for cores, faces, sandwich panels (continuous production lines), complete structures (fuselages, hulls, aerogenerator blades, reflectors) and in the design of connections.

Core material properties are described at the beginning of this chapter. Four material systems will be reviewed: PVC, polyurethane foam, aluminium honeycomb and aramid honeycomb. Design optimisation on sandwich structures will be undertaken. Special attention will be drawn to the design of skins, cores and reinforcements.

Both bending and buckling analysis will be carried out, showing in each case the optimum sublaminate, weight saving and critical load. In order to obtain lightweight structures, the possibilities of increasing the thickness of the sandwich and reinforcing the sandwich structure will be studied.

5.2 Core materials

A sandwich structure is composed of two skins and a core. The composite material systems used for the skins were described in Chapter 2 (carbon, aramid and glass fibres and epoxy, vinylester and polyester resins). Four types of materials are mainly used for sandwich structure cores:

- Polychlorure of vinyl foam (PVC)
- Polyurethane foam (PUR)
- 5052 aluminium alloy honeycomb
- Aramid fibre/phenolic resin honeycomb

The following four sections present the mechanical properties of these four material systems as a function of the core density, which is critical for design purposes. Compression strength, compression modulus, shear strength and shear modulus are obtained as a function of the core density (Fig. 5.1-5.20).

5.2.1 PVC

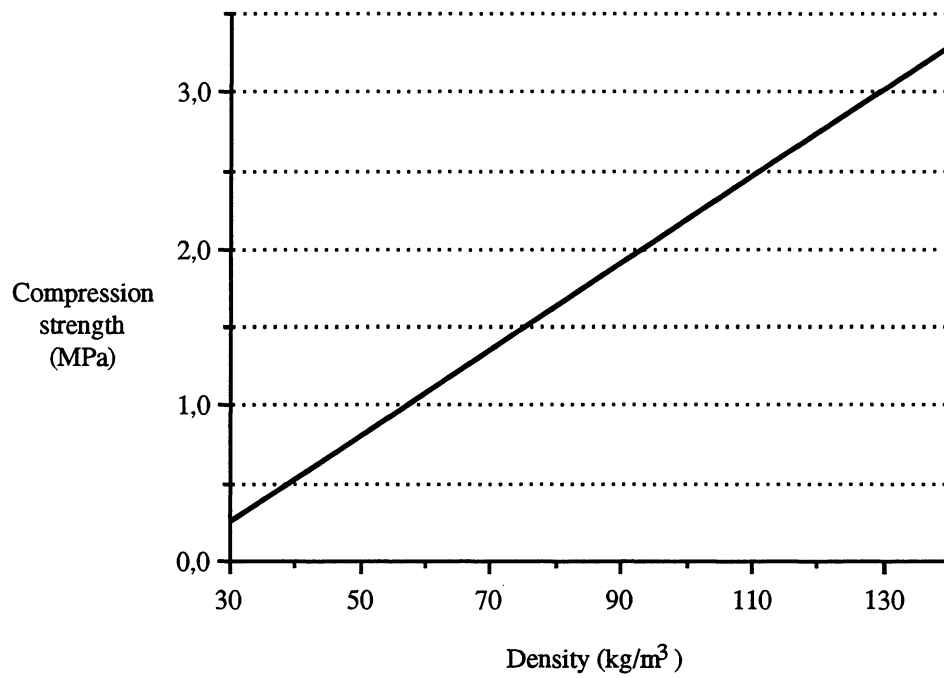


Figure 5.1 Compression strength of PVC foam versus density.

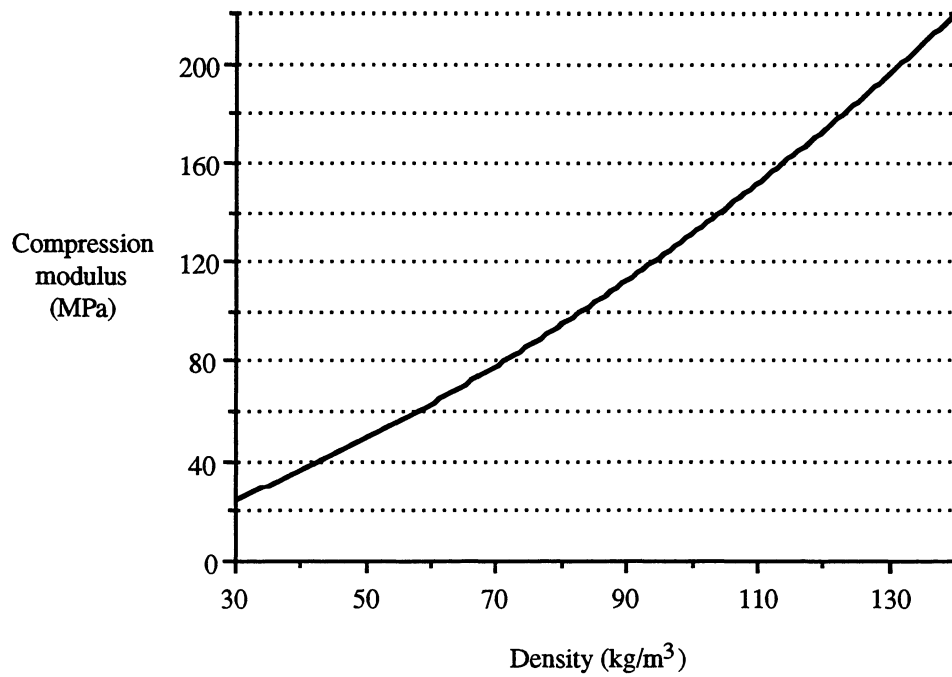


Figure 5.2 Compression modulus of PVC foam versus density.

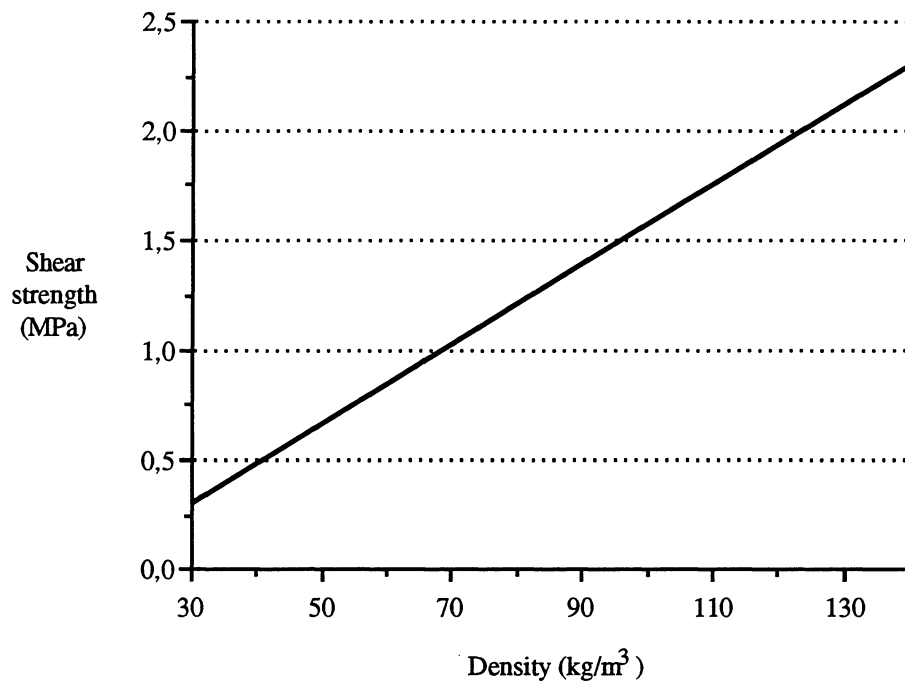


Figure 5.3 Shear strength of PVC foam versus density.

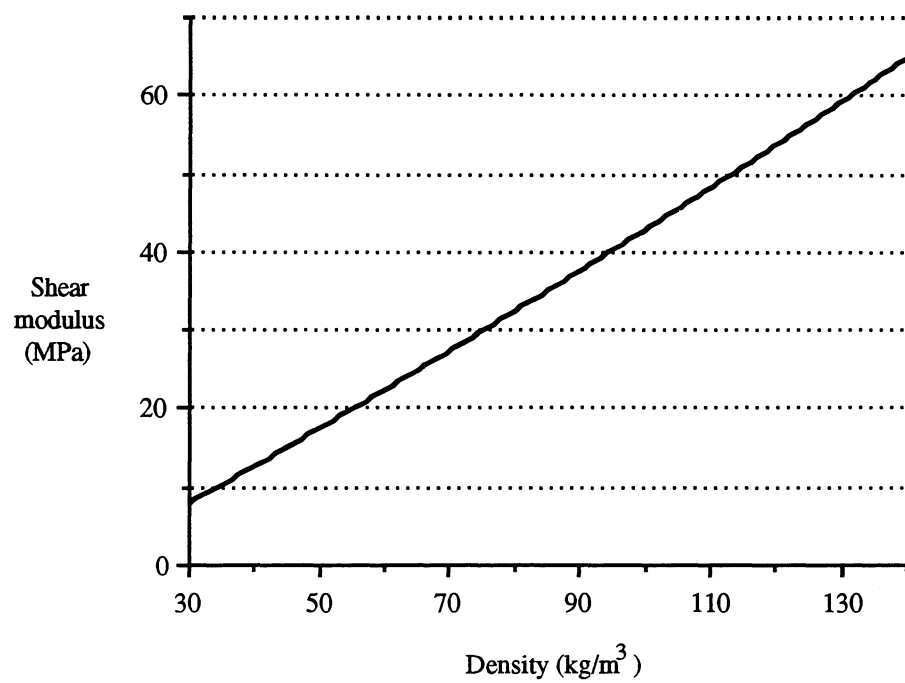


Figure 5.4 Shear modulus of PVC foam versus density.

5.2.2 Polyurethane foam

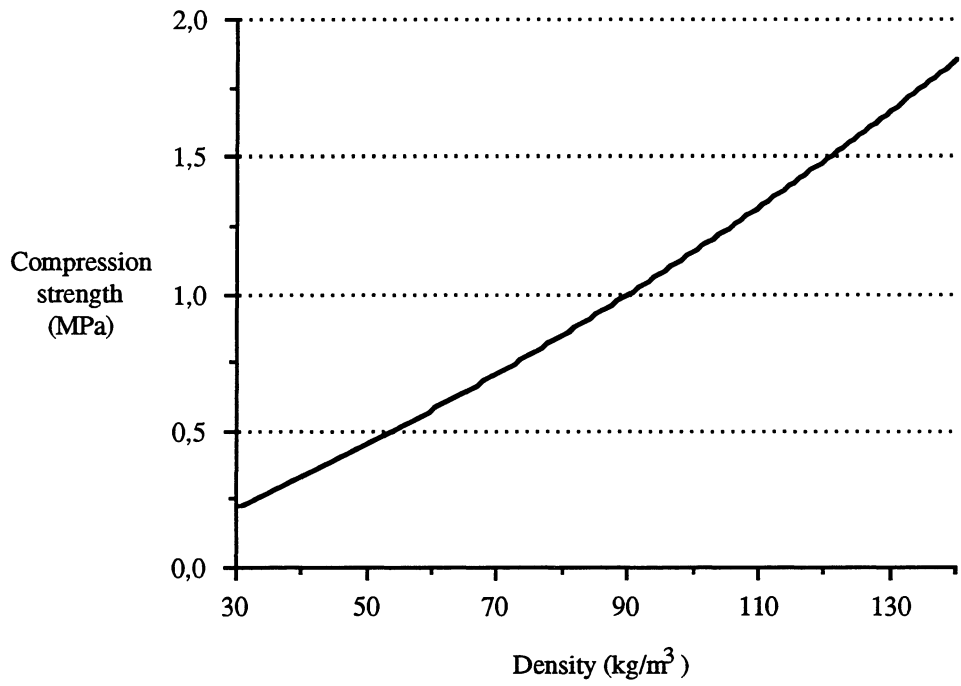


Figure 5.5 Compression strength of PUR foam versus density.

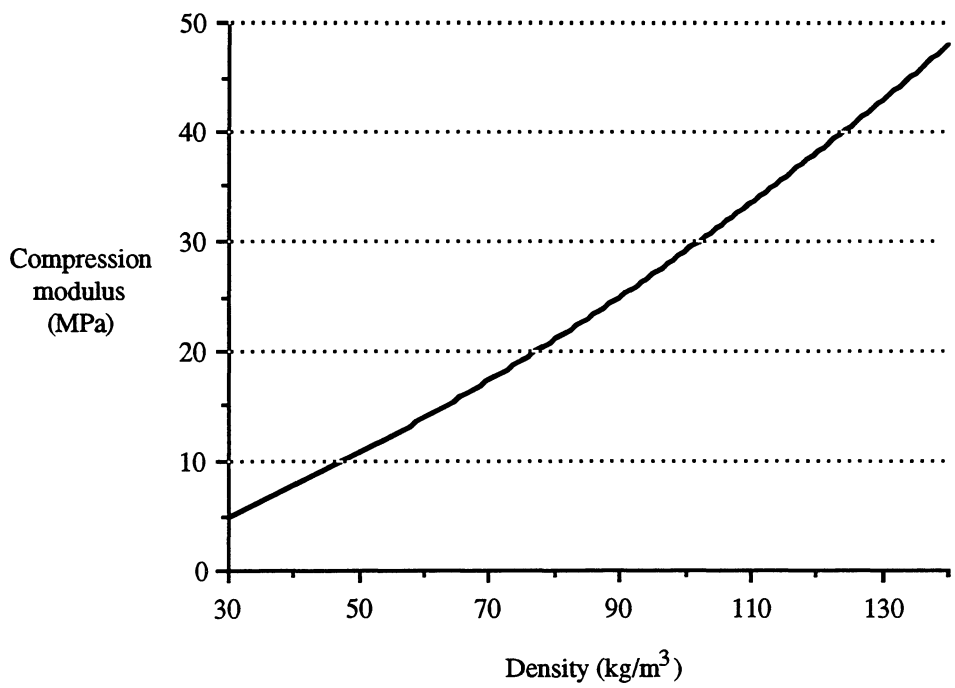


Figure 5.6 Compression modulus of PUR foam versus density.

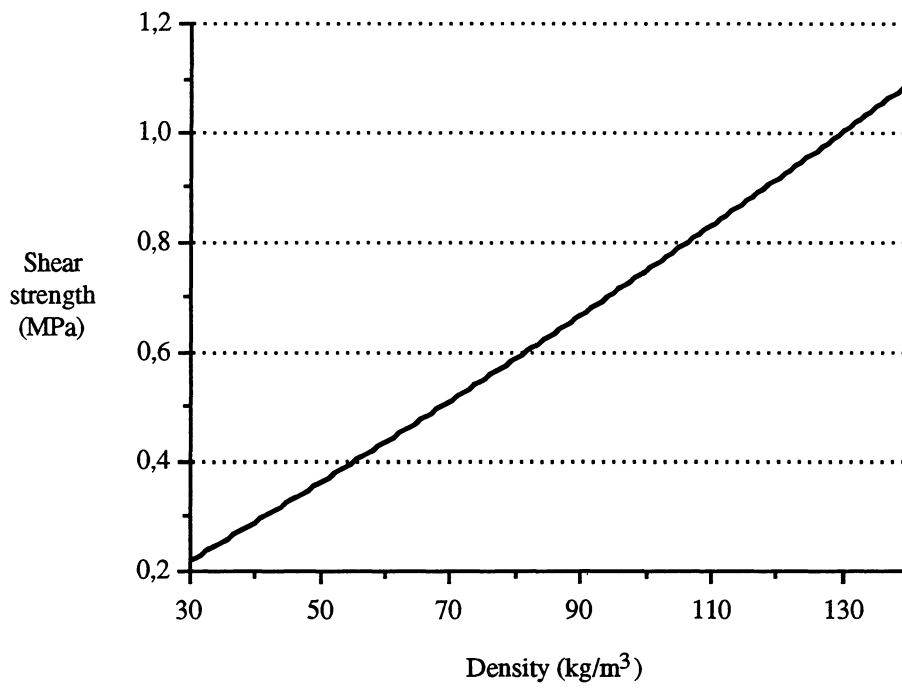


Figure 5.7 Shear strength of PUR foam versus density.

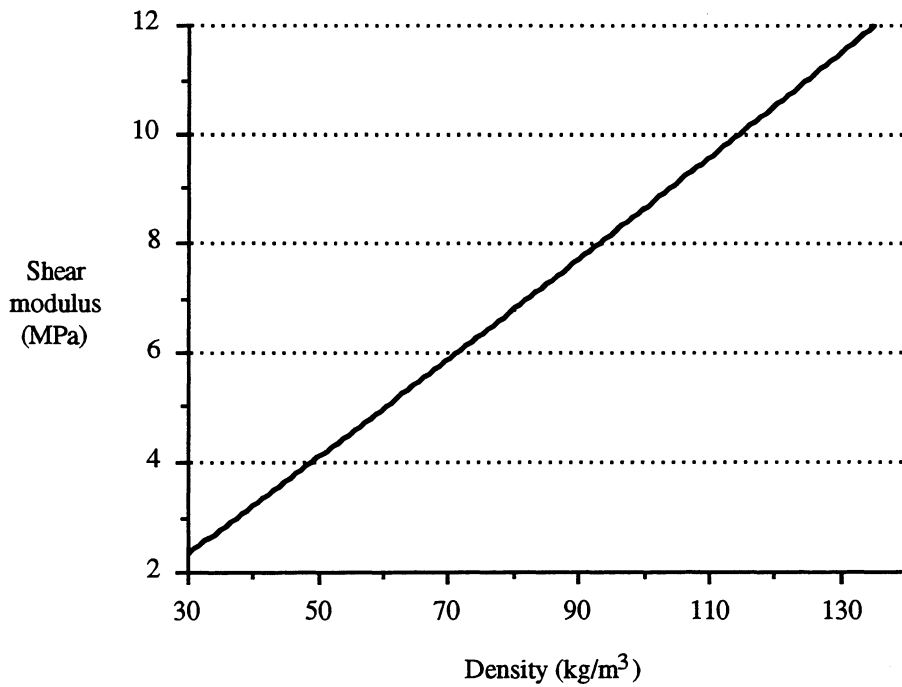


Figure 5.8 Shear modulus of PUR foam versus density.

5.2.3 Aluminium honeycomb

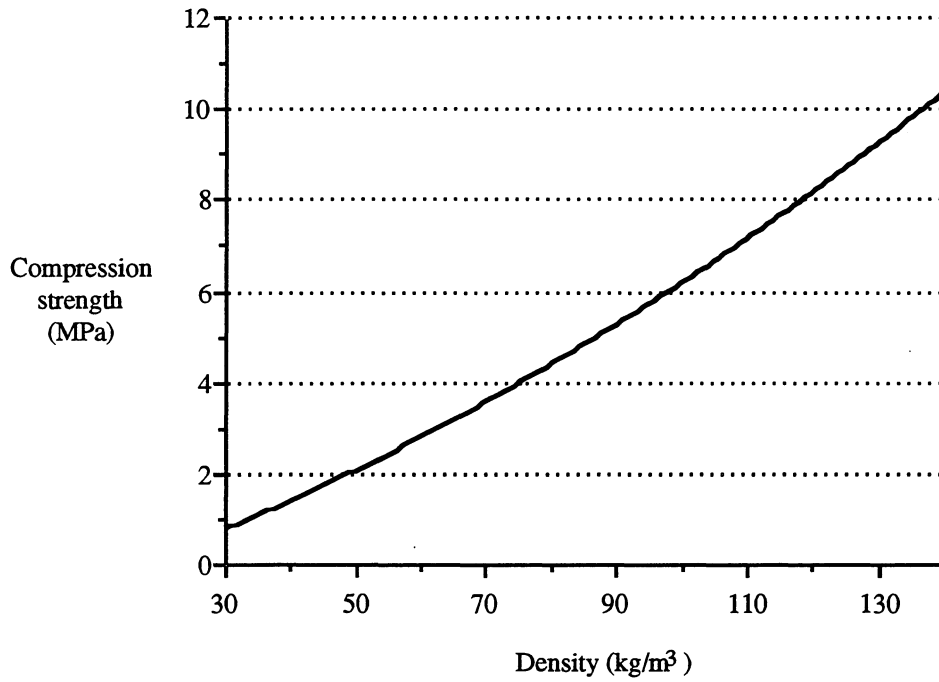


Figure 5.9 Compression strength of 5052 aluminium alloy honeycomb versus density.

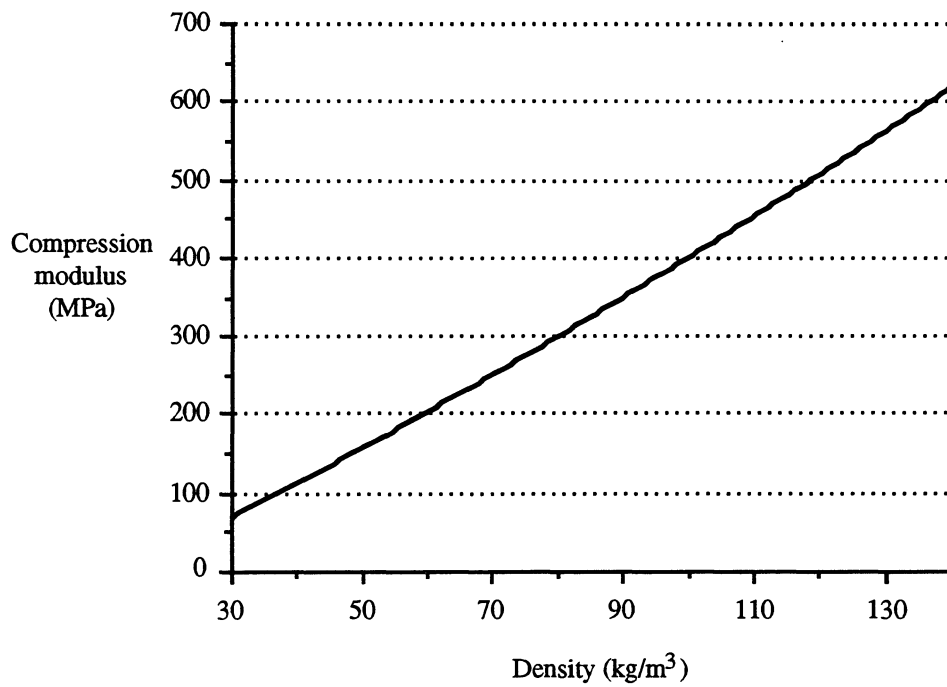


Figure 5.10 Compression modulus of 5052 aluminium alloy honeycomb versus density.

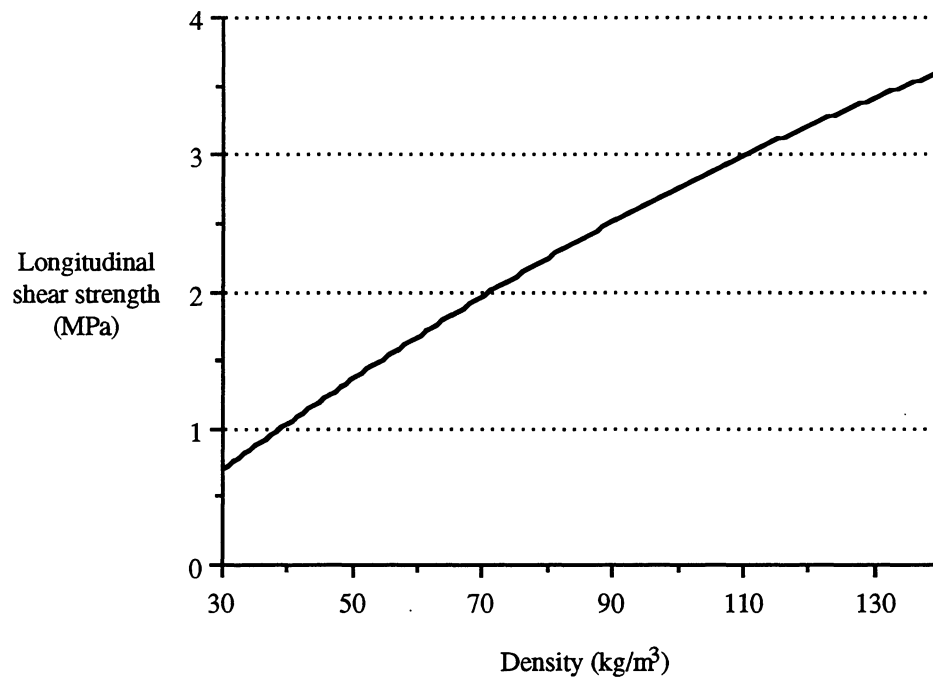


Figure 5.11 Longitudinal shear strength of 5052 aluminium alloy honeycomb versus density.

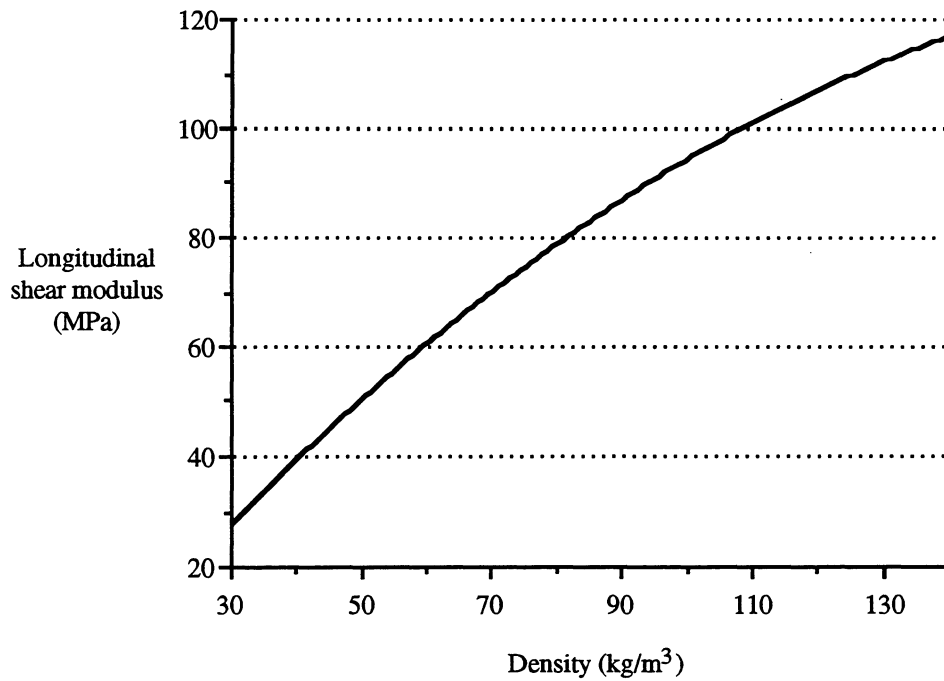


Figure 5.12 Longitudinal shear modulus of 5052 aluminium alloy honeycomb versus density.

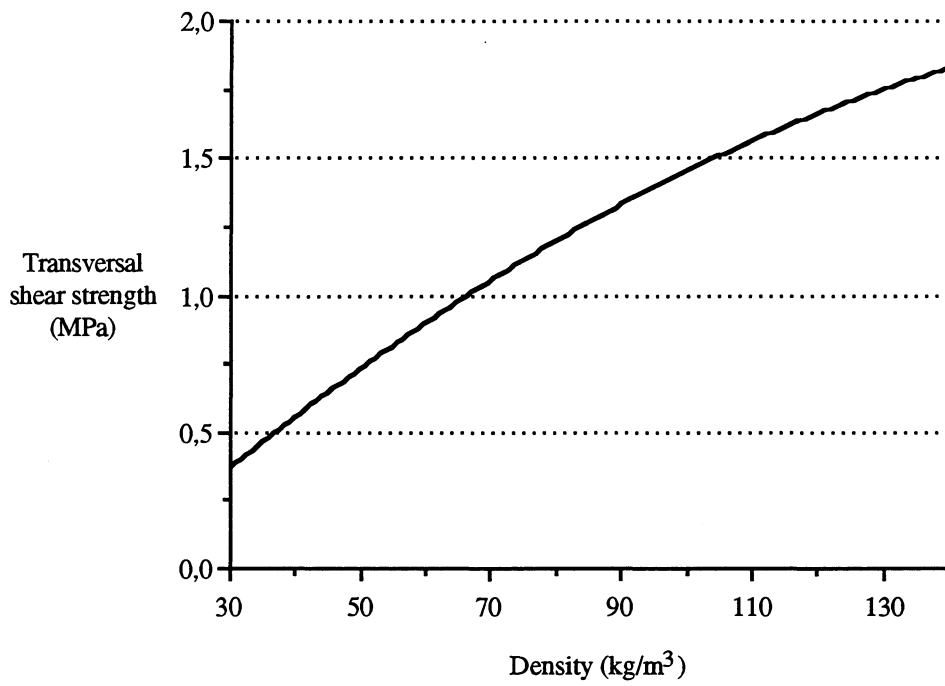


Figure 5.13 Transverse shear strength of 5052 aluminium alloy honeycomb versus density.

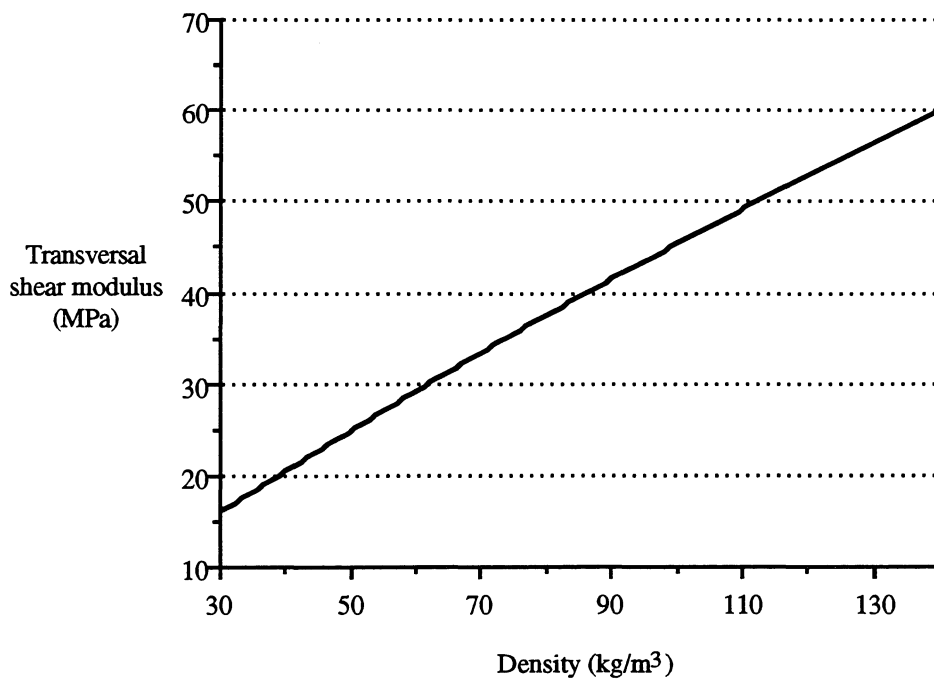


Figure 5.14 Transverse shear modulus of 5052 aluminium alloy honeycomb versus density.

5.2.4 Aramid honeycomb

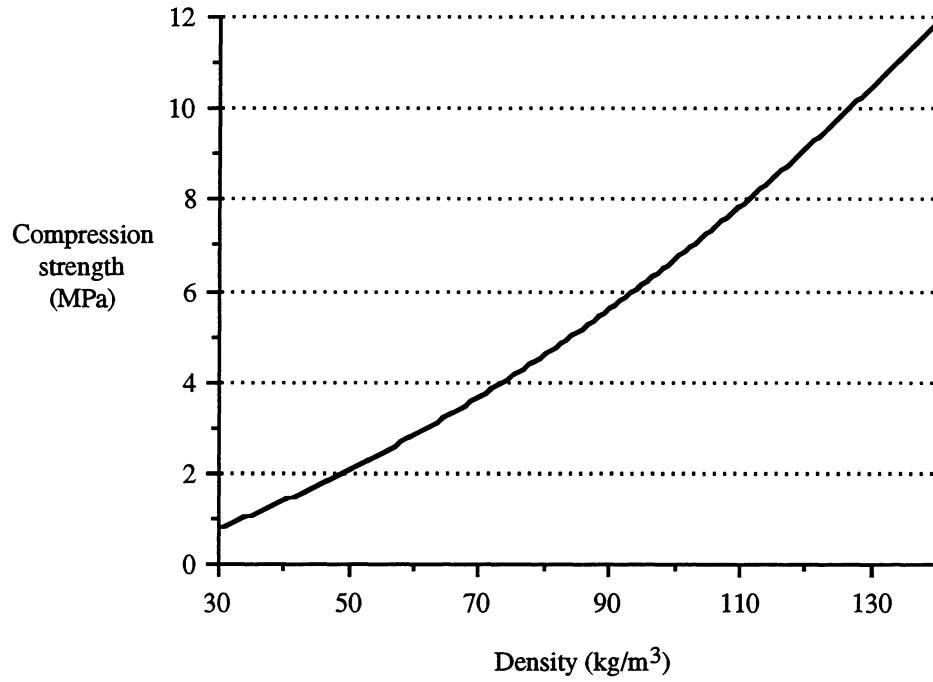


Figure 5.15 Compression strength of aramid fibre/phenolic resin honeycomb versus density.

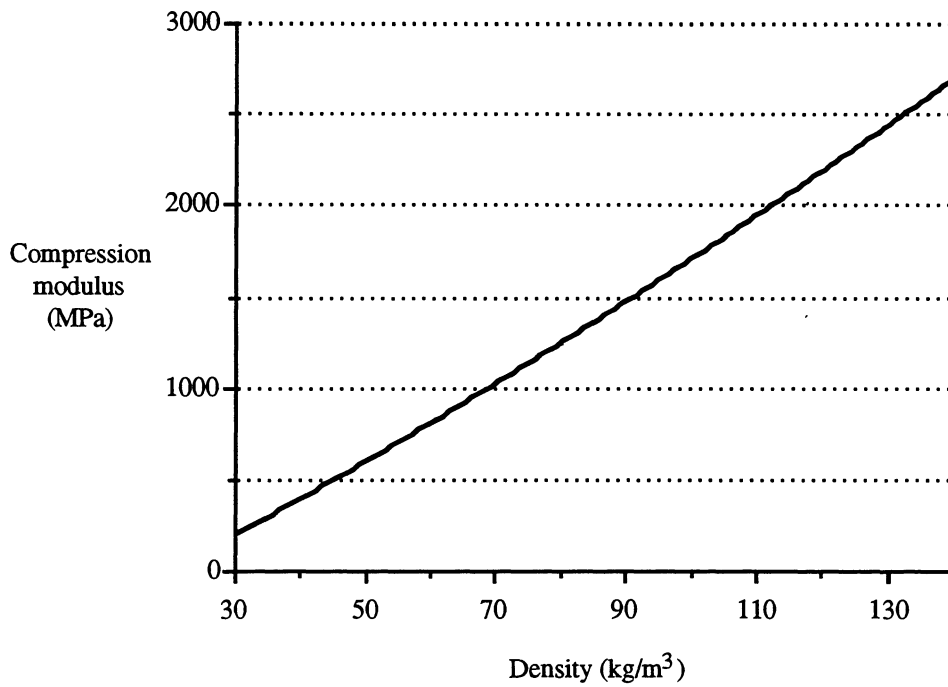


Figure 5.16 Compression modulus of aramid fibre/phenolic resin honeycomb versus density.

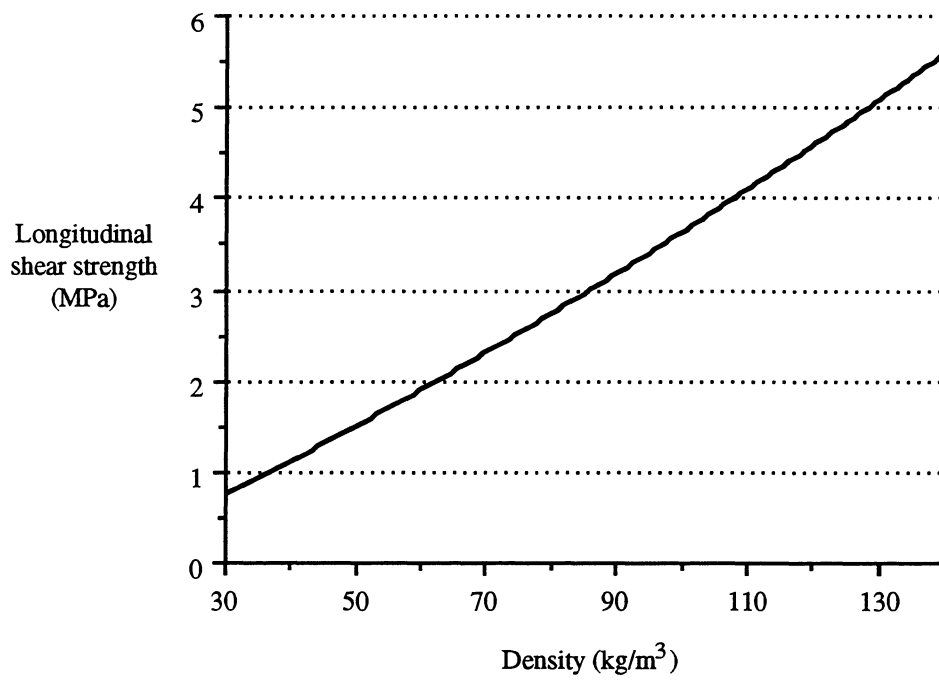


Figure 5.17 Longitudinal shear strength of aramid fibre/phenolic resin honeycomb versus density.

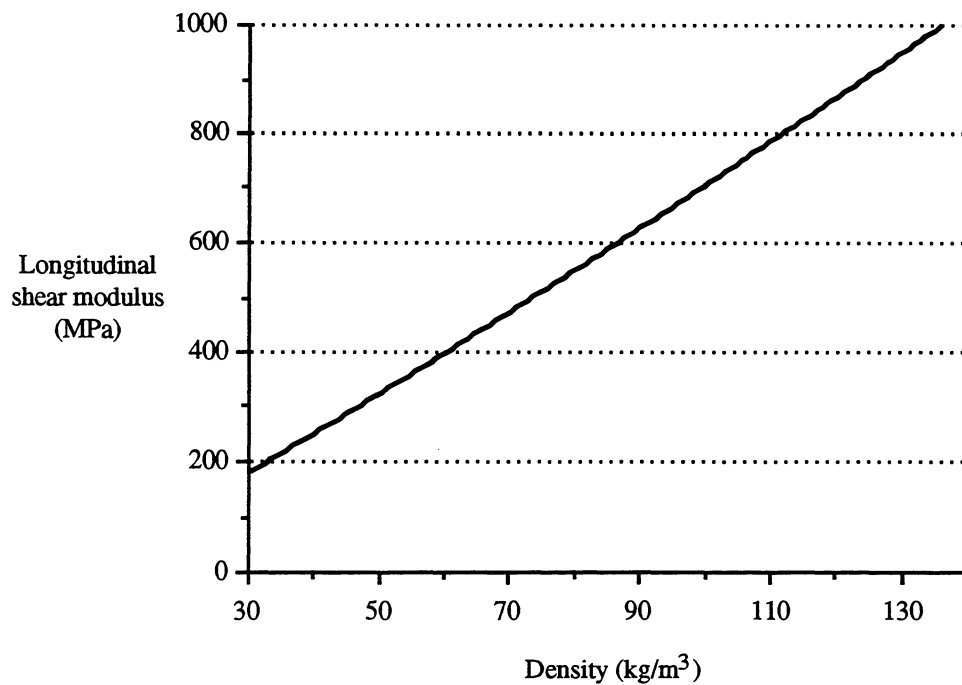


Figure 5.18 Longitudinal shear modulus of aramid fibre/phenolic resin honeycomb versus density.

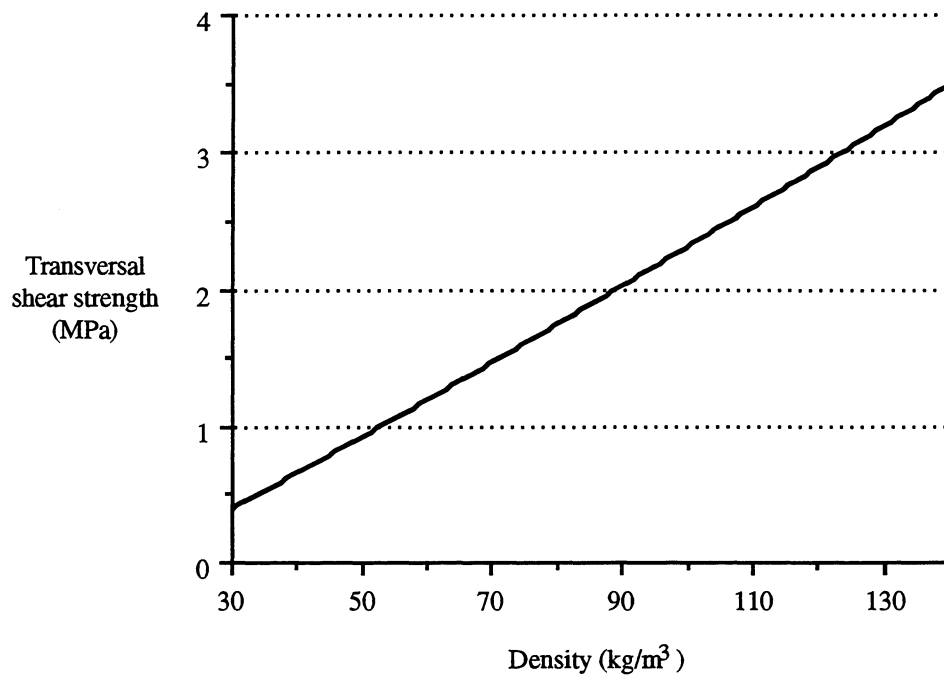


Figure 5.19 Transverse shear strength of aramid fibre/phenolic resin honeycomb versus density.

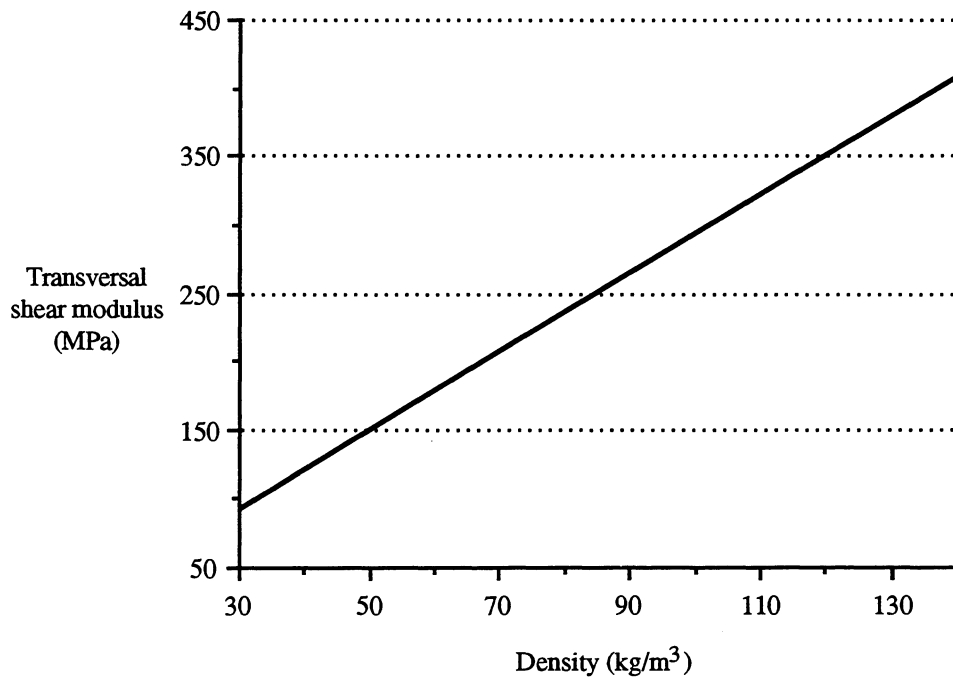


Figure 5.20 Transverse shear modulus of aramid fibre/phenolic resin honeycomb versus density.

5.3 Optimum design of sandwich constructions

The main causes for sandwich failure are:

- Tensile or compression failure of the facings.
- Shear failure of the core.
- Failure under general instability.
- Failure under local instability.

These types of failure must be adequately taken into account and avoided in a strength design.

5.3.1 Facings design

The actual stress in a sandwich is of course given by the algebraic sum of the components due to the bending moment and the shear force. The presence of the shear force therefore causes a stress increase in one facing and simultaneously a stress decrease in the other. If the stresses exceed the corresponding ultimate stresses of the constitutive materials of the facings, the latter will fail in a catastrophic way.

In design calculations, the strength verification of the facings is usually carried out by comparing the stresses caused by external loads with the allowable stresses for the constitutive materials of the facings. The allowable stresses are obtained by dividing the strengths by suitable factors of safety which take into account the variable properties of the materials, the approximations in the structure schematic design, the accidental loads, fatigue phenomena, etc.

When the calculated stresses exceed the allowable stresses, a change in the sandwich sizing is required. In such a case one may:

- Use a material with higher allowable stresses for the facings.
- Increase facings thickness, thus reducing the applied stresses.
- Increase core thickness; this method too will decrease the stresses in the facings.

The increase of core thickness is often the most suitable way to solve the problem; on the other hand a higher-density (therefore stiffer) core does not affect the stresses in the facings.

5.3.2 Core design

The sandwich core is then subjected to shear stress only. If the value of the shear stress is greater than the shear strength of the core material, the latter fails causing failure of the structure. The shear verification is carried out by comparing the calculated stress generated by the design loads with the allowable stress, which is calculated by dividing the shear strength of the core material by a suitable factor of safety. If the calculated stress exceeds the allowable stress, one may:

- Use a core material with higher allowable shear stress.
- Increase the core thickness, thus reducing the shear stress.

On the other hand, using a different material for the facings or increasing their thickness does not affect the shear stress in the core.

5.3.3 Stiffness and strength versus core properties

Stiffness and strength of sandwich structures are strongly dependent on core thickness and core density. A number of sandwich structures have been calculated by means of the theory described in Chapter 1. Deflections, R-values (safety factor) and weight have been represented as a function of the core density and core thickness for uniformly loaded, square sandwiches (Fig. 5.21-5.27).

Carbon fibre / aluminium honeycomb and glass fibre / polyurethane foam systems have been analysed.

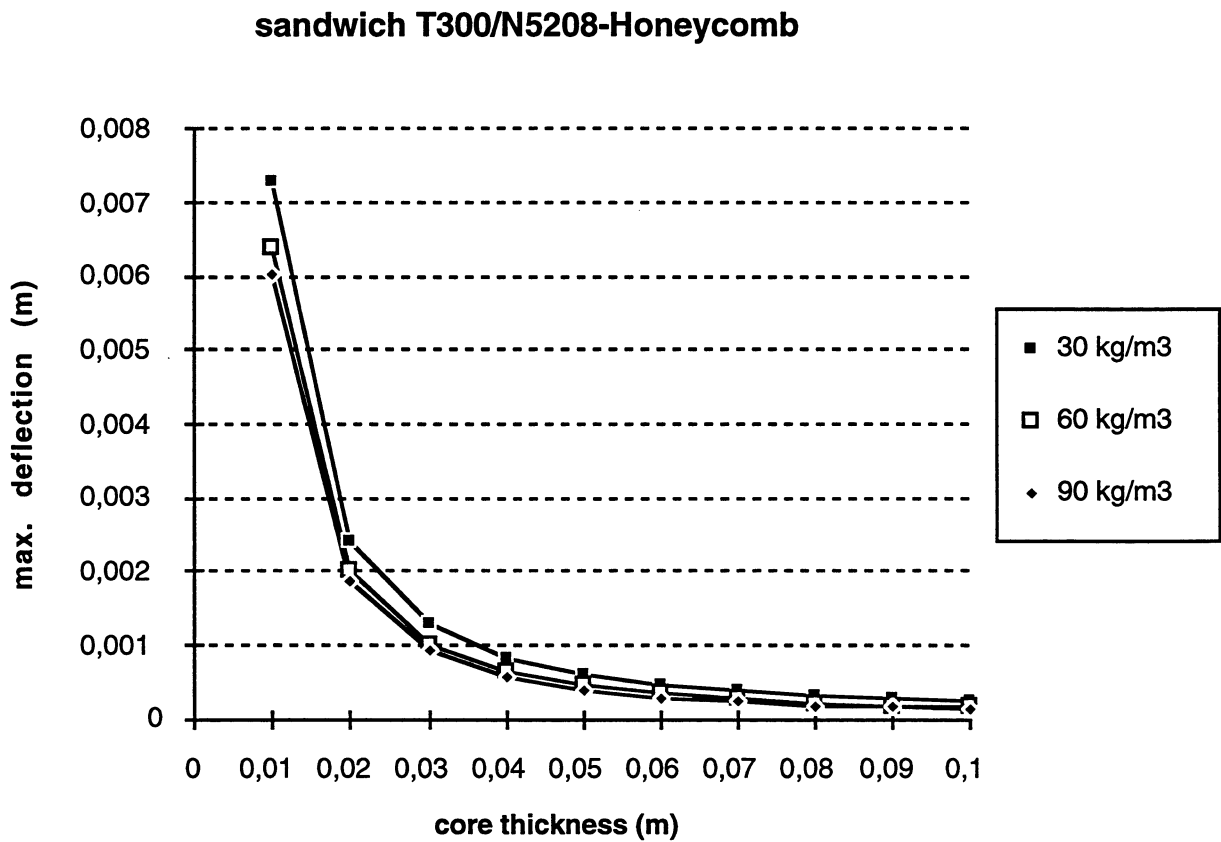


Figure 5.21 Maximum deflection versus core thickness for some core foams. Carbon fibre and aluminium honeycomb core.

sandwich SCOTCHPLY-PUR

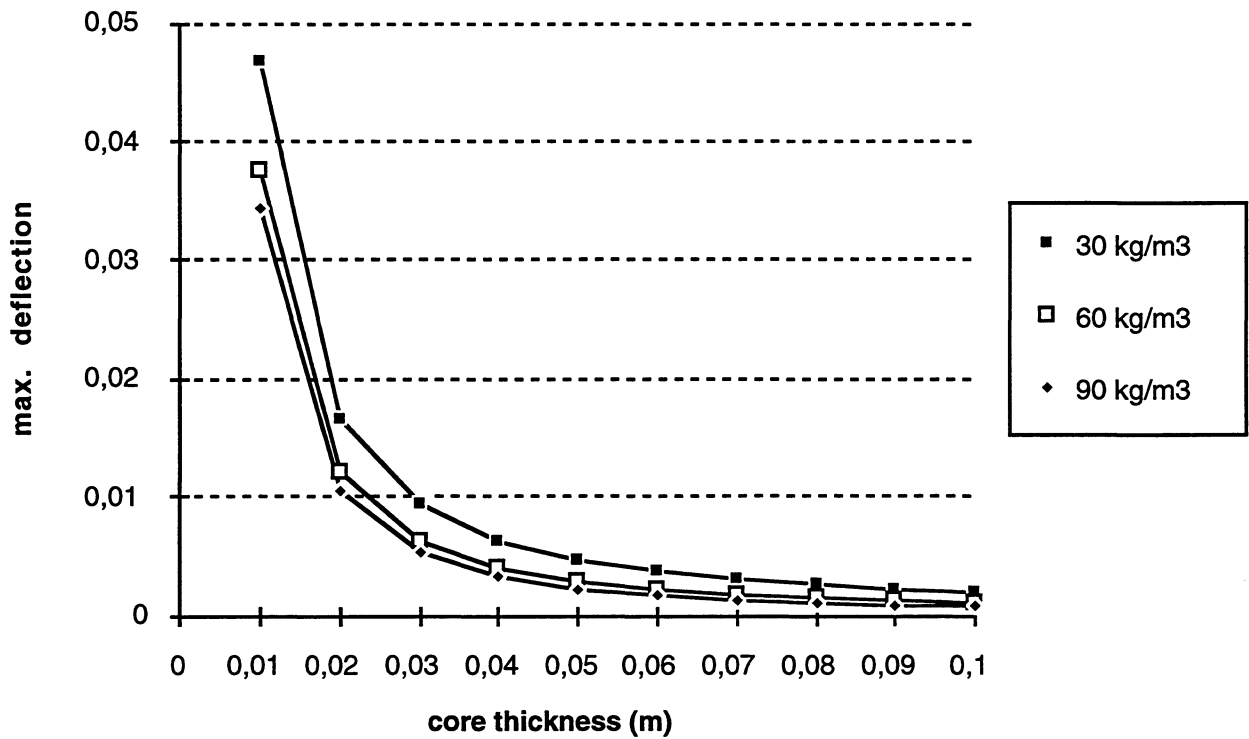


Figure 5. 22 Maximum deflection versus core thickness for some core foams. Glass fibre and polyurethane foam core.

sandwich T300/N5208-Honeycomb

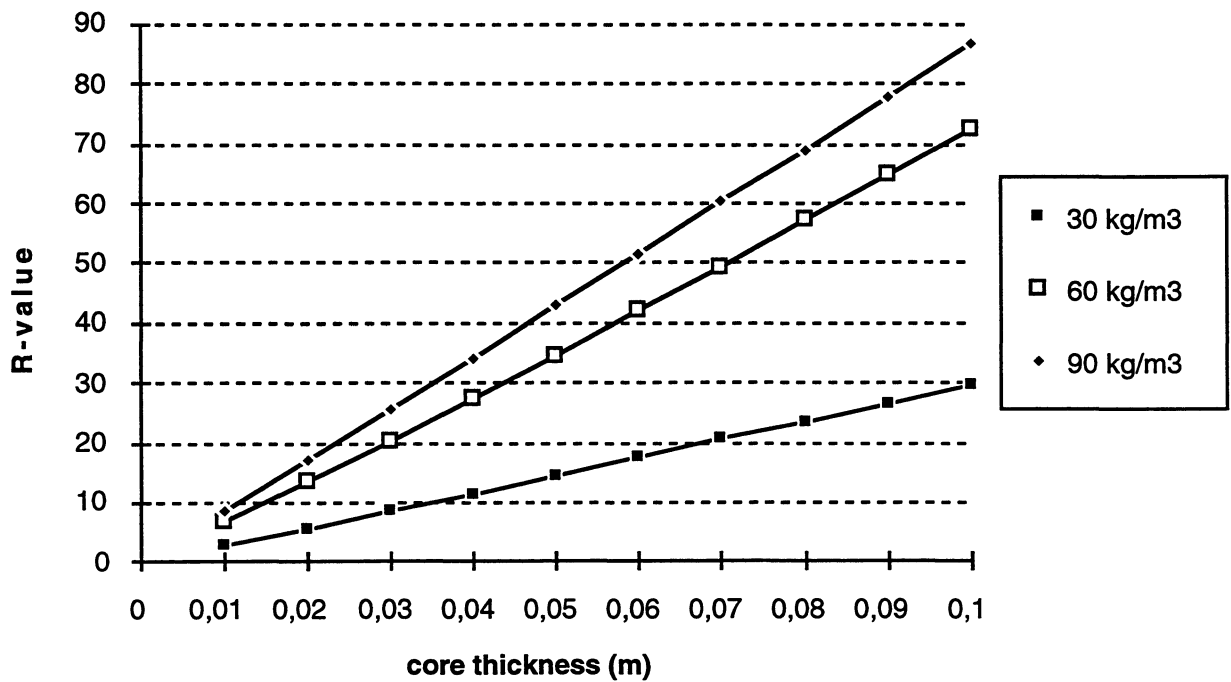


Figure 5. 23 R-value versus core thickness for some core foams. Carbon fibre and aluminium honeycomb core.

sandwich SCOTCHPLY-PUR

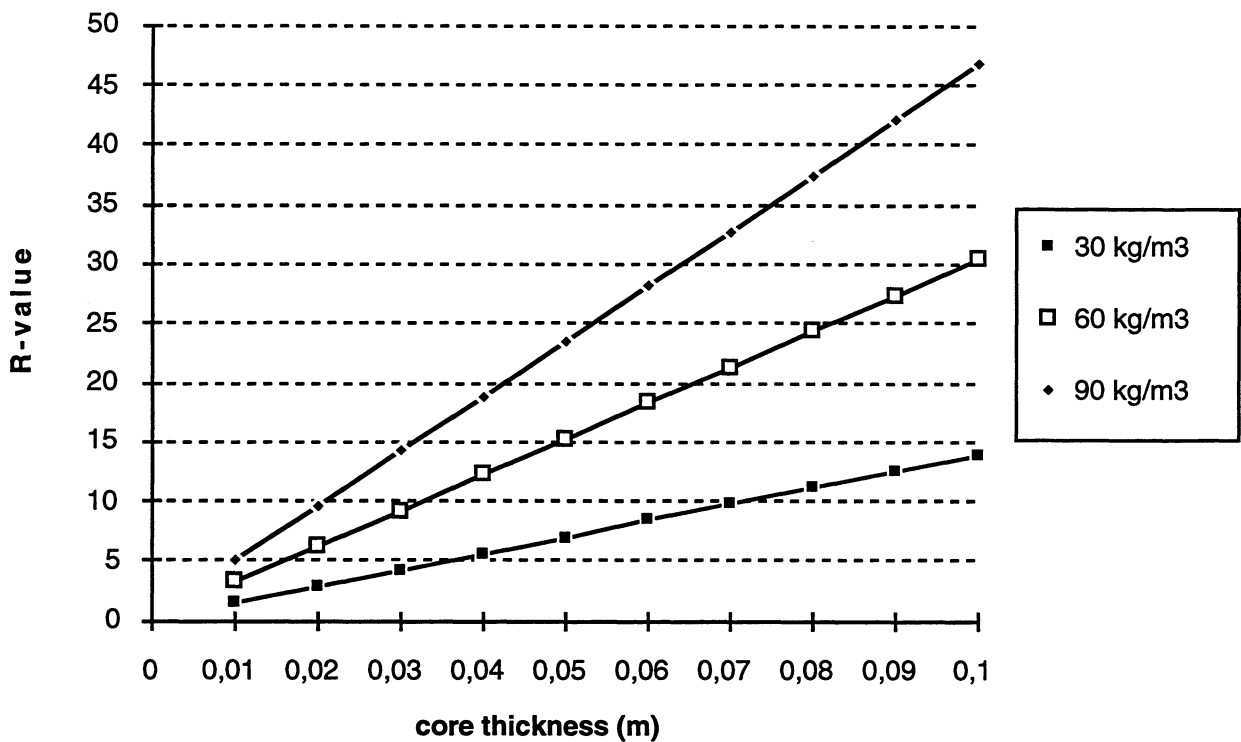


Figure 5. 24 R-value versus core thickness for some core foams. Glass fibre and polyurethane foam core.

sandwich T300/N5208-Honeycomb

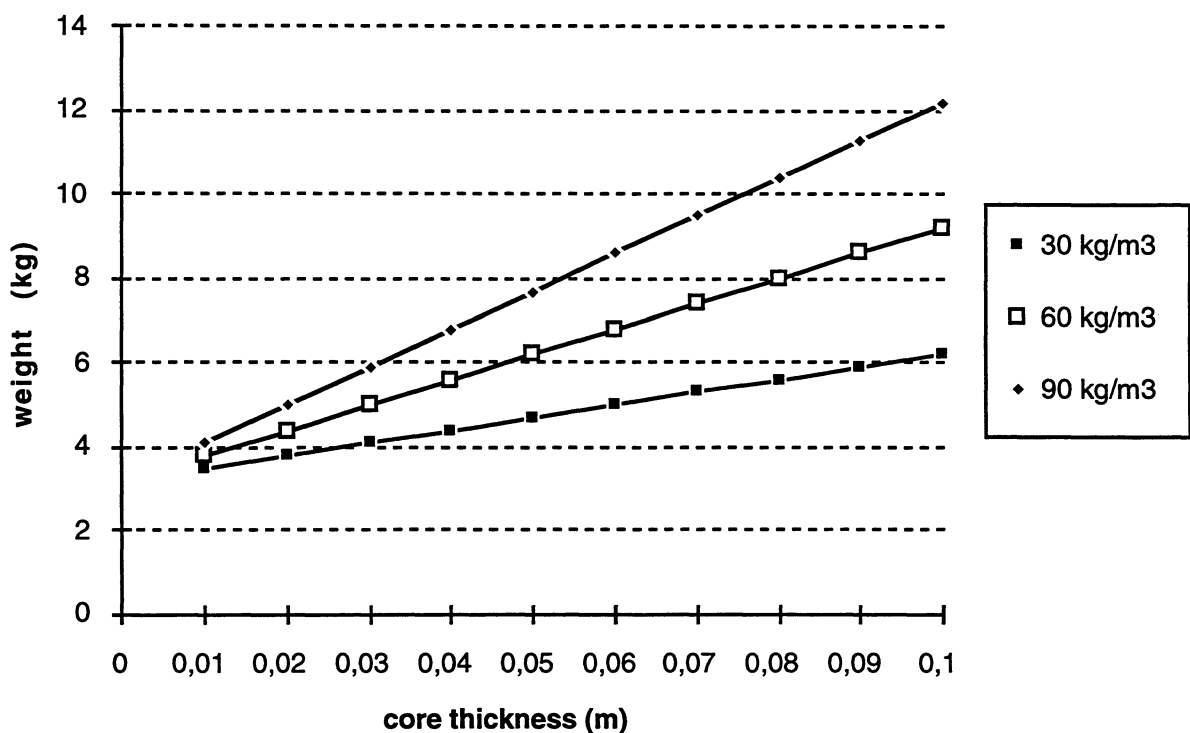


Figure 5. 25 Weight versus core thickness for some core foams. Carbon fibre and aluminium honeycomb core.

sandwich SCOTCHPLY-PUR

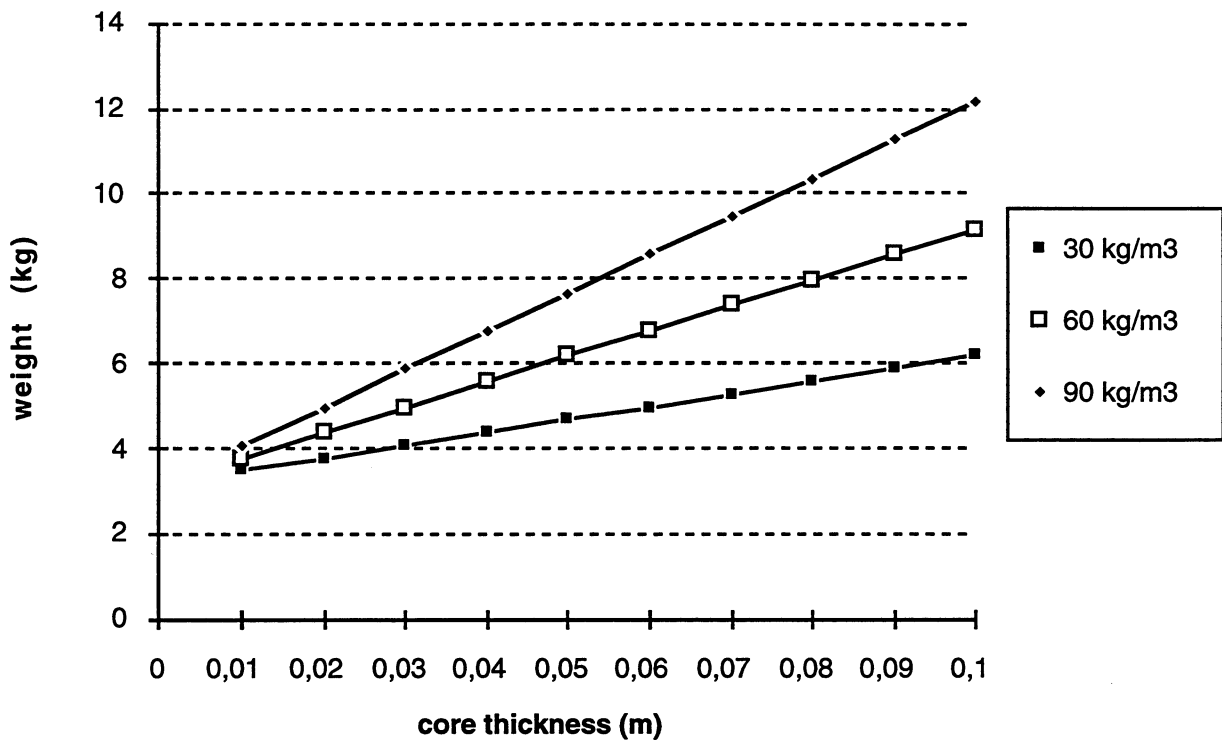


Figure 5. 26 Weight versus core thickness for some core foams. Glass fibre and polyurethane foam core.

As shown in Fig. 5.27, the weight of the structure decreases dramatically in a certain range of core thickness (90-150 mm). If the core thickness is increased from the upper limit of this range (thickness higher than 150 mm), the weight of the structure decreases very slowly. Therefore, in terms of weight saving, there is a range (90-150 mm) where increasing the core thickness is a very efficient design possibility, but in the range of core thicknesses higher than 150 mm, other designs, such as implementing reinforcements in the sandwich, must be considered.

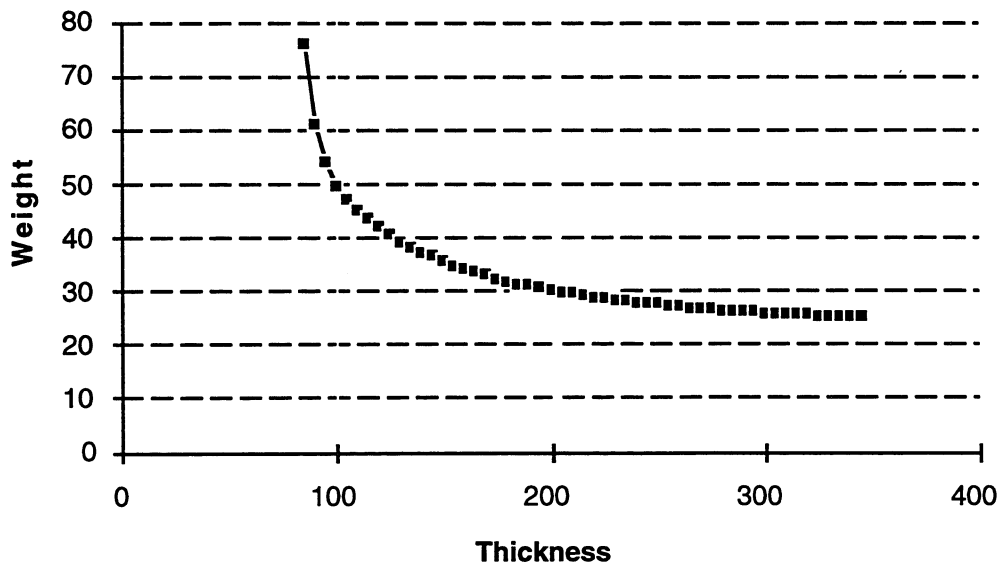


Figure 5.27 Weight (kg/m) versus core thickness. Glass fibre and polyurethane foam core 2 m width with uniform load (10 MPa)

Although Fig. 5.27 demonstrates a design curve for a particular sandwich geometry and fibre/resin type, many such curves can be derived from a knowledge of the sandwich behaviour of different geometries and fibre/resin types as a function of the sandwich thickness.

5.3.4 Optimum design of reinforced sandwich constructions

Simple reinforcements are especially efficient for those applications where there is a unidirectional stress, for instance in narrow simply supported plates subjected to uniform loads (Fig. 5.28 and 5.29). For square plates, there are stresses in the transverse and longitudinal directions, and therefore reinforcement should be used in both directions. Great difficulties can be encountered when joining perpendicular reinforcements.

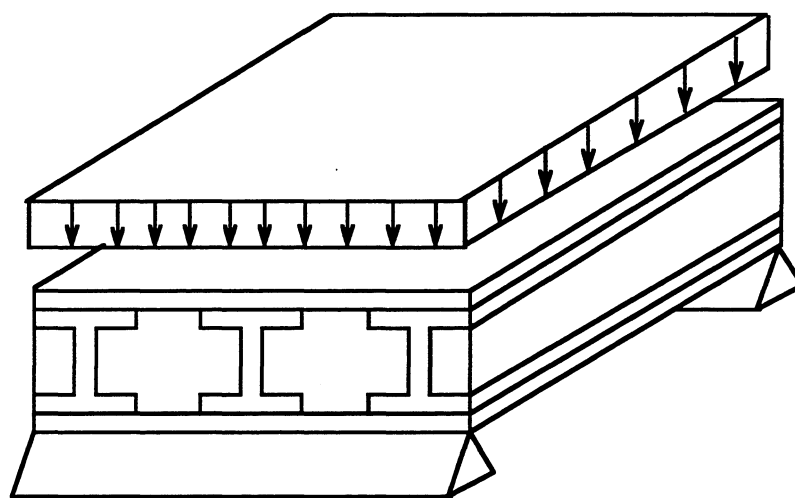


Figure 5.28 The structure.

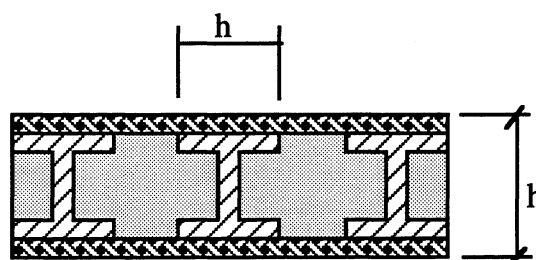


Figure 5.29 The sandwich and reinforcement.

Weight is the optimisation criterion and the maximum deflection should not be higher than the ratios span/250 or span/500 for fibreglass and carbon fibre skins, respectively. This is a rule used in engineering applications design to take account of stiffness and strength of the sandwich structure.

Skin thickness, reinforcement thickness, foam density and number of reinforcements per unit width have been optimised. For carbon fibre skins and aluminium honeycomb, with a 2.5 m span and a 30 MPa load, the reinforced design is considerably better than the non-reinforced one for sandwich thicknesses between 110 and 280 mm (Fig. 5.30). For thicknesses between 80 and 110 mm, one solution exists for reinforced sandwiches but it is not possible to meet

the requirements with non-reinforced sandwiches. For thicknesses greater than 280 mm, results from reinforced and non-reinforced sandwiches are similar (the weight saving is 22%). The optimum number of reinforcements is three per metre in all cases. Thus, the efficiency of the implementation of reinforcements depends on the sandwich thickness.

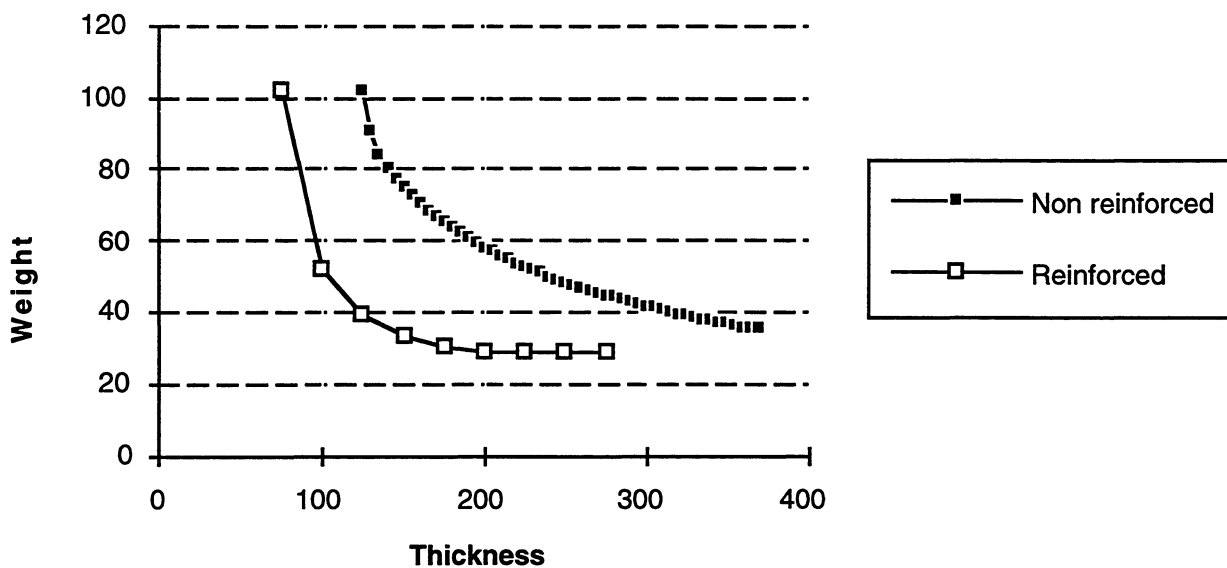


Figure 5.30 Carbon aluminium honeycomb. Weight (kg/m) versus thickness for a sandwich 2.5 m width with uniform load (30 MPa).

Similar graphics are obtained by varying the load magnitude, span and the material system. Results are shown in the table below:

Table 5.1 Optimisation of reinforced sandwich constructions

Facing material	Core material	Span (m)	Load (MPa)	Minimum	Minimum	Minimum	Minimum		
				thickness for reinforced sandwich (mm)	thickness for non-reinforced sandwich (mm)	weight for reinforced sandwich (Kg/m)	weight for non-reinforced sandwich (Kg/m)		
Carbon/epoxy	Alum. honeycomb	2.5	30	78	122	28	36	WS: 22 %	
		2.5	50	100	183	35	51	WS: 31%	
		2.5	70	124	241	42	74	WS: 43%	
	30k/m ³	2	2	30	73	100	18	22	WS: 18%
			2	50	78	144	23	32	WS: 28%
			2	70	100	186	27	40	WS: 32%
		1.5	1.5	30	40	75	10	13	WS: 23%
			1.5	50	54	100	13	18	WS: 28%
			1.5	70	70	133	15	23	WS: 35%
			1	30	30	50	4	6	WS: 33%
1	50	32	68	6	8	WS: 25%			
1	70	34	95	7	10	WS: 30%			

Facing material	Core material	Span (m)	Load (MPa)	Minimum	Minimum	Minimum	Minimum	
				thickness	thickness	weight	weight	
				for reinforced sandwich (mm)	for non-reinforced sandwich (mm)	for reinforced sandwich (Kg/m)	for non-reinforced sandwich (Kg/m)	
E-glass polyester	PUR 30K/m ³	2.5	10	55	105	30	40	WS: 25%
		2.5	30	100	248	43	90	WS: 48%
		2.5	50	120	380	55	140	WS: 61%
		2	10	50	83	18	25	WS: 28%
		2	30	68	200	28	62	WS: 55%
		2	50	88	300	36	95	WS: 62%
		1.5	10	53	63	10	14	WS: 28%
		1.5	30	63	145	18	34	WS: 47%
		1.5	50	70	215	20	50	WS: 60%
		1	10	34	40	5	6	WS: 8%
		1	30	36	100	7	14	WS: 50%
		1	50	38	140	10	22	WS: 55%

It has been shown that the weight saving obtained by using reinforced sandwiches is strongly dependent on the load. The higher the load, the higher the weight saving. Variations of weight saving with the span of the plate are not significant.

5.4 Buckling

5.4.1 General buckling

A sandwich beam subjected to compression may fail because of a condition of instability that involves the whole beam. For this reason it is called 'general buckling' (Fig. 5.31 (a)).

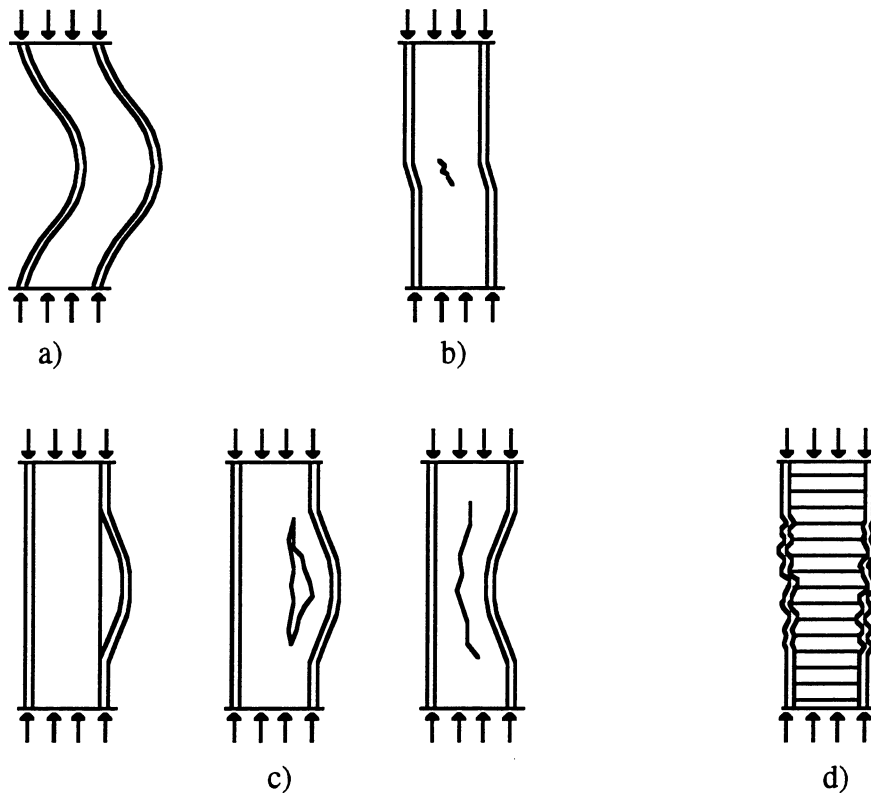


Figure 5.31 Sandwich failures due to a buckling load: (a) general buckling; (b) crimping; (c) wrinkling; (d) dimpling.

General buckling may also occur when the stress in the facings and in the core is lower than the allowable stress. The load that determines sandwich instability depends on such parameters as the beam in-plane size and the constraint conditions, which can only be partially modified at the design stage. Other quantities, which are equally important for the definition of buckling load, depend directly on the type of sandwich.

They are:

- Flexural rigidity of the sandwich.
- Thickness of the facings.
- Elastic properties of the facings.
- Core thickness.
- Shear modulus of the core.

To avoid this type of failure, it is necessary to ensure that the general buckling load is higher, according to a suitable factor of safety, than the predicted compression stress. When choosing the safety factor one must take into account that the theoretical formulae used to predict the general buckling critical load are less reliable than those for the calculation of sandwich stresses.

If general buckling is feared, one may:

- Use facings with a higher elastic modulus material.
- Increase facings thickness.

- Increase core thickness.
- Use a core material with higher shear modulus.

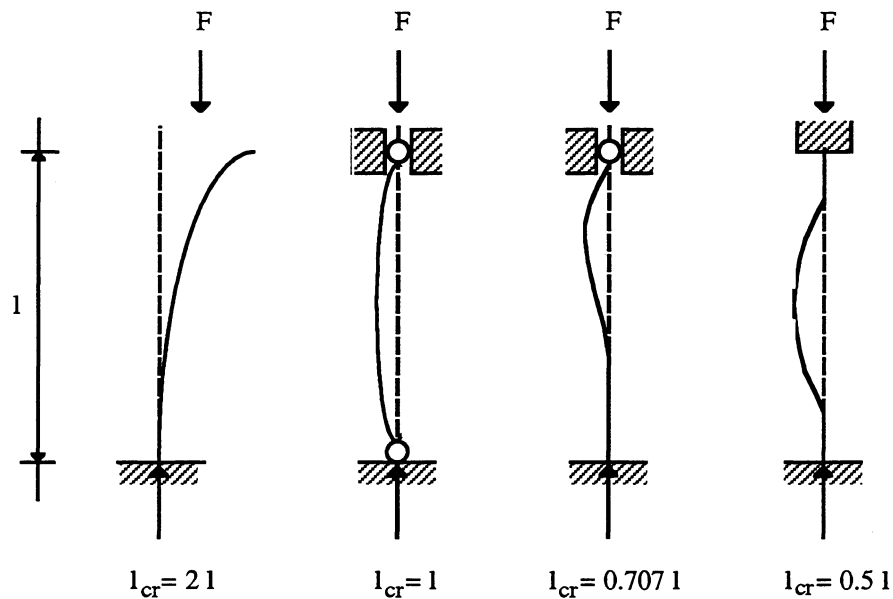


Figure 5.32 General buckling of a sandwich structure and critical lengths of some boundary conditions.

In the case of a sandwich with a relatively low length/thickness ratio and where shear rigidity is small in comparison with flexural rigidity, sandwich general buckling will assume a typical configuration, (Fig. 5.54 (b)). This failure mode, typical of sandwich structures, is called 'shear crimping'. The total load per unit length capable of producing crimping is practically independent of facing properties. On the other hand, it increases linearly with the following parameters:

- Core thickness.
- Shear modulus of the core.

To increase the total critical crimping load, one should:

- Increase core thickness.
- Use a higher shear modulus for the core.

5.4.1.1 General buckling of a sandwich beam

It has been shown by Teti¹ that the critical stress causing the general buckling of a sandwich beam under compressive load (Fig. 5.55) is given by:

$$\sigma_{cr b} = \frac{1}{2 b S_F \left(1 + \frac{H^2 E I}{l_{cr}^2 G A} \right)} \frac{\pi^2 E I}{l_{cr}^2} \quad [5.1]$$

where:

$$S_{Ft} = S_{F1} + S_{F2} \quad [5.2]$$

and

- $\sigma_{cr b}$ = critical buckling stress (N/mm²)
- EI = sandwich flexural rigidity (N/mm²)
- b = beam width (mm)
- $S_{F1,2}$ = thickness of facings 1,2 (mm)
- l_{cr} = free length of the sandwich beam (mm)
- G_A = sandwich shear rigidity (N)

It is easily verified that, when $l_{cr}^2 GA \ll EI$, equation 5.1 reduces to:

$$\sigma_{cr b} = \frac{G_A S_A}{S_{Ft}} \quad [5.3]$$

In this case a particular mode of general buckling occurs, usually called 'shear crimping' (Fig. 5.54 (b)). Considering that the quantity $\sigma_{cr b} S_{Ft}$ represents the total crimping load per unit width of the sandwich, it can be concluded from equation 5.3 that this load is only dependent on the shear rigidity G_A .

5.4.1.2 General buckling of a rectangular plate compressively loaded along two opposite edges

The critical stress causing the general buckling of an isotropic rectangular sandwich plate with equal facings and isotropic core, subjected to a compressive load along two opposite edges, is given by the following equation:

$$\sigma_{cr p} = K_d \frac{\pi^2}{4} \frac{E_F}{1-\nu_F^2} \left(\frac{S_A}{b} \right)^2 \quad [5.4]$$

where:

$$S_A = S_A^* + S_F \quad [5.5]$$

and

- $\sigma_{cr p}$ = critical buckling stress (N/mm²)
- K_d = buckling factor, to be evaluated from Fig. 5.56 and 5.57
- E_F = facing compression modulus (N/mm²)
- ν_F = facing Poisson's ratio
- b = length of the plate loaded edge (mm)
- S_A = distance between the facings centroids (mm)
- S_A^* = core thickness (mm)
- S_F = facing thickness (mm)

It is easily seen, from the graphs in Fig. 5.56 and 5.57, that the so-called 'shear deformation factor', S , must be evaluated in order to define the buckling factor K_d . S is given by:

$$S = \frac{\pi^2 E_F S_F S_A}{2 G_A b^2 (1-\nu_F^2)} \quad [5.6]$$

where:

G_A = core shear modulus (N/mm^2)

K_d is given by Fig. 5.56 and 5.57 for simply supported and clamped sandwich structures, respectively.

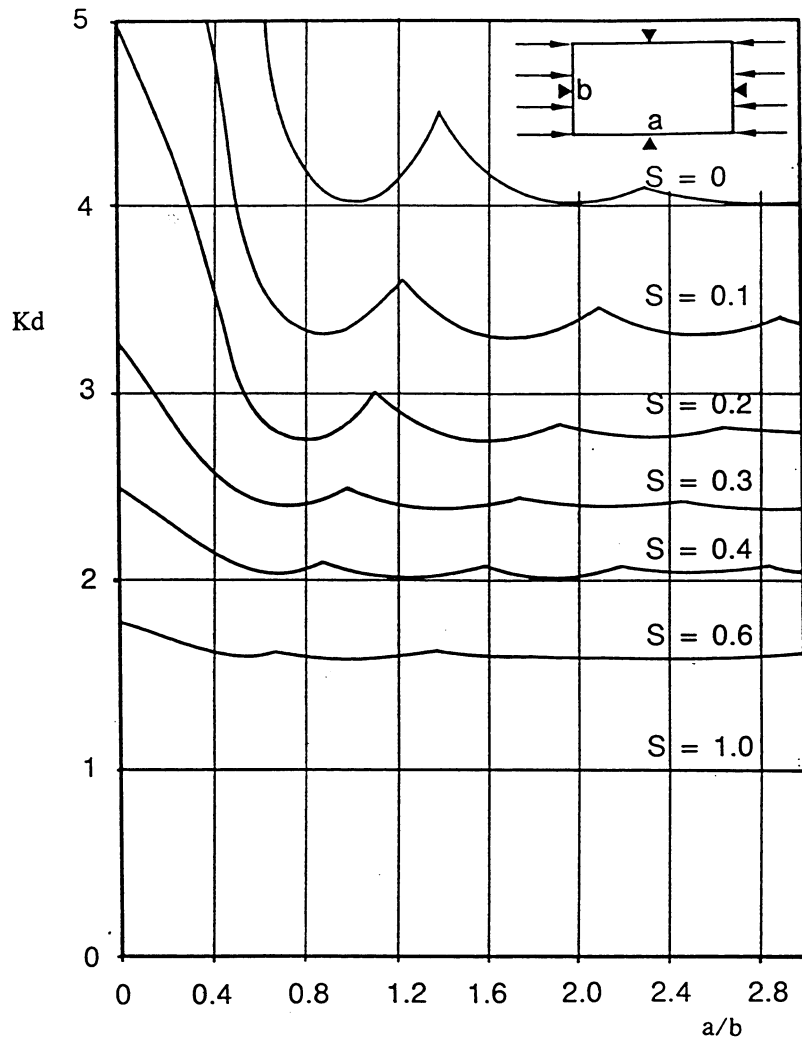


Figure 5.33 Values of K_d as a function of S and the aspect ratio for a simply supported sandwich structure.

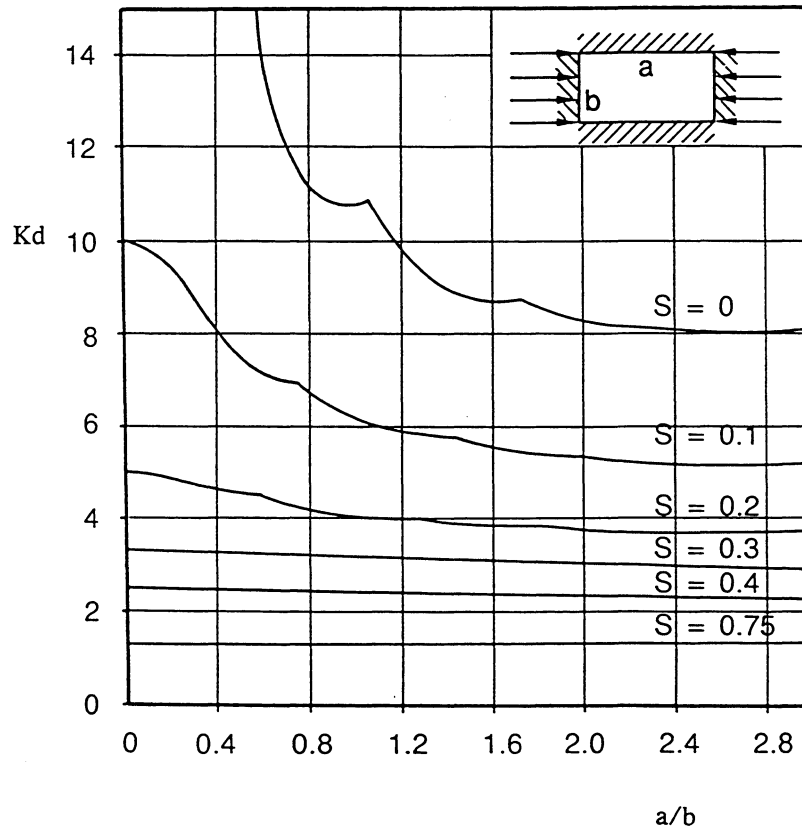


Figure 5.34 Values of K_d as a function of S and the aspect ratio for a clamped sandwich structure.

5.4.2 Local buckling in the sandwich

Sandwich facings, when considered on their own (i.e. separate from the core) tend to lose stability because of their reduced thickness. The buckling of the facings is prevented by the core which, when the facings are subjected to compression, supports them laterally. It may happen, however, that when the compression stress on the facings exceeds a certain limit, the core will not be able to prevent their buckling. In this case, a local buckling occurs in the sandwich. This type of buckling is called 'local' because it does not depend on the geometry of the structure nor on the constraint conditions, but only on local phenomena or interaction between facings and core. Local buckling may assume two different forms, according to the kind of core used for the sandwich construction. If the core is made of foam, it supports the external facings with continuity, i.e. the contact between facings and core occurs practically on the entire interface surface. In this case, each facing behaves like a plate on elastic foundation and its buckling necessarily involves (Fig. 5.54 (c)) the failure of the bonding at the interface with the core and/or the failure under tension or compression of the core itself. This type of failure, called 'wrinkling', is therefore catastrophic and is mainly influenced by the following parameters:

- Elastic modulus of the facings.
- Elastic modulus of the core.
- Shear modulus of the core.

To prevent local wrinkling phenomena, it must be verified that the compression stress in the sandwich is lower than the critical buckling stress, according to a suitable safety factor. When choosing the value of the safety factor, it must be borne in mind that the available formulae for the calculation of the critical stress for local wrinkling are approximate. If local wrinkling is feared, one may:

- Use a facing material with a higher elastic modulus.
- Use a core material with higher elastic properties.

With regard to the second solution, it should be noted that a foamed polymeric material usually presents higher elastic and shear moduli with higher density. As the two moduli both affect the critical stress for local instability, a higher core density is twice as efficient in the prevention of this phenomenon.

When the core is made of honeycomb, the bonding between facings and core is obtained only on honeycomb cells' external borders. When facings are subjected to compression, they may therefore undergo buckling in the free spaces within the single cells, generating a 'dimpling' phenomenon (Fig. 5.54 (d)). Dimpling depends mainly on the following factors:

- Facing elastic modulus.
- Facing thickness.
- Core cell size.

When it is necessary to increase the critical dimpling stress, one should:

- Use a material for the facings with higher elastic modulus.
- Use thicker facings.
- Use a core with smaller cells.

It is important to note that, differently from the case of wrinkling, the phenomenon of dimpling does not determine the failure of the structure. This type of buckling, therefore, is not necessarily catastrophic. It is, however, advisable to take dimpling into account at the design stage because it may be a prelude to wrinkling failure and it may also produce irreversible deformations in the structure.

Two different local buckling modes may occur in a sandwich structure under compressive load, depending on the type of core. In the case of a core supporting facings continuously (foamed core), facings may buckle as a plate resting on an elastic foundation. This type of buckling is called 'wrinkling', and results in debonding at the core-facing interface or tensile (compressive) failures in the core (Fig. 5.54 (c)).

When the core supports the facings discontinuously (honeycomb core), facings may buckle into the spaces between cell walls; this phenomenon, which does not necessarily lead to failures, is called 'dimpling' (Fig. 5.54 (d)).

5.4.2.1 Wrinkling

It has been shown by Teti¹ that the critical wrinkling stress (Fig. 5.54 (c)) of a sandwich facing supported continuously by an isotropic core and subjected to a compressive loading is approximately given by:

$$\sigma_{cr w} = Q \sqrt[3]{\frac{E_F E_A G_A}{(1 - \nu_F^2)}} \quad [5.7]$$

where:

$\sigma_{cr w}$ = critical buckling stress (N/mm²)

E_F = facing compression modulus (N/mm²)

E_A = core compression modulus (N/mm²)

G_A = core shear modulus (N/mm²)

ν_F = facing Poisson's ratio

Q = wrinkling parameter, to be evaluated from Fig 5.58

In order to compute Q , the quantities q and K , appearing in Fig 5.58, must be calculated in advance. These quantities are defined by the following formulae:

$$q = (S_A/S_F) G_A \sqrt[3]{\frac{(1 - \nu_F^2)}{E_F E_A G_A}} \quad [5.8]$$

$$K = \frac{\delta E_A}{S_A F_A}$$

where

S_A = distance between the facings centroids (mm)

S_F = facing thickness (mm)

d = facing initial deflection (mm)

F_A = flatwise strength of the sandwich (the lower value between compression and tensile strength) (MPa)

Besides:

$$S_A = S_A^* + (S_{F1} + S_{F2})/2 \quad [5.9]$$

where:

S_A^* = core thickness (mm)

$S_{F1,2}$ = thickness of the facings 1, 2 of the sandwich (mm)

At present it is not possible to measure the facing initial deflection, d , directly. This quantity must be therefore experimentally determined, by carrying out compression test on sandwich panels. In this way, experimental values of the critical wrinkling stress are obtained, and using these a Q value can be calculated from equation 5.7. From Fig. 5.58, a K value which matches the experimental data, is found. Finally, d is calculated by equation 5.9. It can be assumed, in the design stage, that d is constant for all the sandwiches obtained by the same fabrication procedure.

It is important to note that equation 5.7 is only approximate, and can only be used in designing to give reference values of the wrinkling stress. Experimental tests should therefore be performed to support the design. If no information is available on d , a reference value $d = 0.5$ is suggested for an approximate estimate of the wrinkling stress.

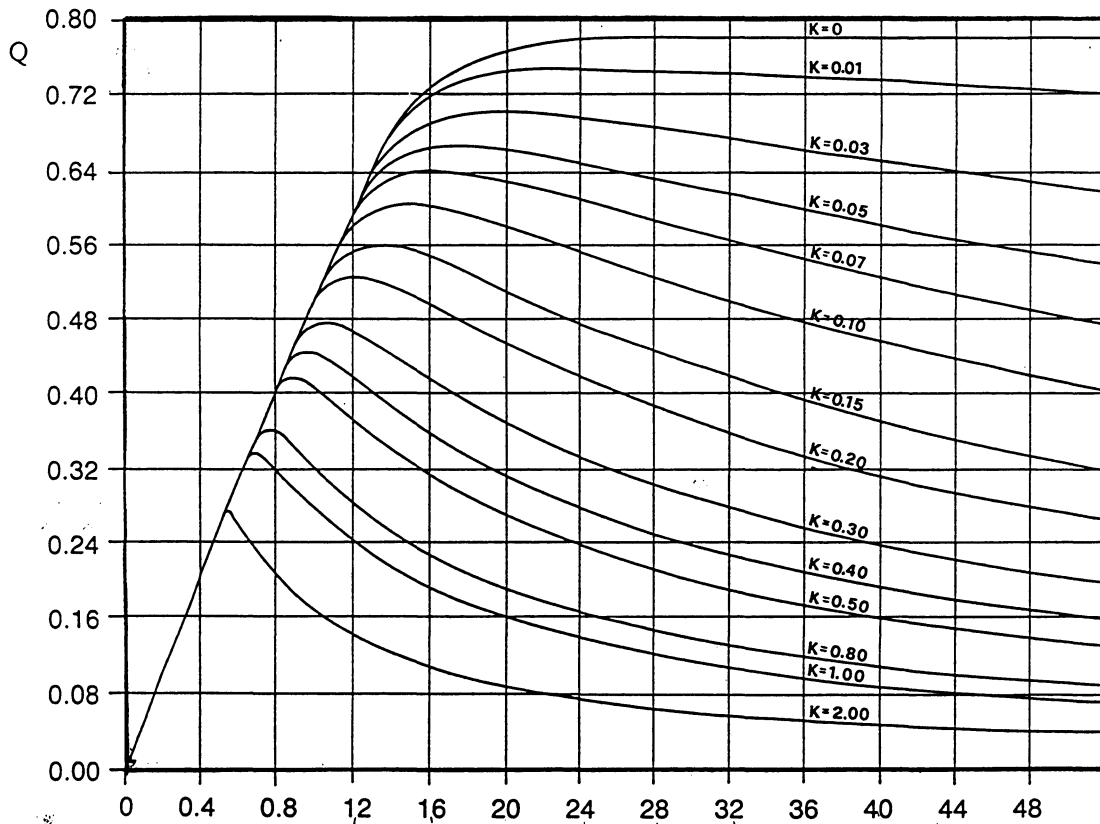


Figure 5.35 Wrinkling parameter Q as a function of q and K factors

5.4.2.2 Dimpling

It has been shown by Teti¹ that the critical stress for dimpling (Fig. 5.54 (d)) of a sandwich facing supported by a honeycomb core is calculated by the following empirical formula:

$$\sigma_{cr d} = \frac{E_F}{(1 - \nu_F)^2} \left(\frac{S_F}{S_C} \right)^2 \quad [5.10]$$

where:

$\sigma_{cr d}$ = critical dimpling stress (N/mm²)

S_C = core cell size, given by the diameter of the inscribed circle (mm)

5.5 Conclusions

Design optimisation on sandwich structures has been carried out. Special attention has been drawn to the design of skins, cores and reinforcements. Core properties of PVC, polyurethane foam, aluminium honeycomb and aramid honeycomb material systems have been shown.

When the calculated stresses exceed the allowable stresses, a change in the sandwich sizing is required. In such cases:

- Use a material with higher allowable stresses for the facings.
- Increase facings thickness, thus reducing the applied stresses.
- Increase core thickness; this method too will decrease the stresses in the facings.

The increase of core thickness is often the most suitable way to solve the problem; on the other hand a higher-density (therefore stiffer) core does not affect the stresses in the facings. The sandwich core is then subjected to shear stress only. If the value of the shear stress is greater than the shear strength of the core material, the latter fails causing the failure of the structure.

The shear verification is carried out by comparing the calculated stress generated by the design loads with the allowable stress, which is calculated by dividing the shear strength of the core material by a suitable factor of safety. If the calculated stress exceeds the allowable stress, one may:

- Use a core material with higher allowable shear stress.
- Increase the core thickness, thus reducing the shear stress.

On the other hand, using a different material for the facings or increasing their thickness does not affect the shear stress in the core.

In order to obtain lightweight structures, one can increase the thickness of the sandwich. This option is efficient for low-medium values of thickness. From a certain thickness, the weight does not decrease substantially by increasing the sandwich thickness. Another option is to reinforce the sandwich structures. This design leads to drastic weight saving in most cases.

It has been shown that the weight saving obtained by using reinforced sandwiches is strongly dependent on the load. The higher the load, the higher the weight saving. Variations of weight saving with the span of the plate are not significant. The optimum number of reinforcements is three per metre in all cases. In general, as the number of reinforcements increases, the minimum weight decreases. However, the weight saving obtained by using four reinforcements per metre instead of three is insignificant.

Optimum buckling design is a function of the type of load (uni or bi-axial) and boundary conditions. It is extremely difficult to predict the optimum sublaminate and the critical loads. Thus, the graphs in this chapter are recommended for the optimisation design of sandwich structures.

Further information can be found in refs. 2-36.

References

1. Teti G C R, Sandwich Structures: Handbook, Ed. Il Prato, 1989.
2. Esping B, Holm D, Campion F, Clarin P, Ljunggren L and Romell O, 'Integrated modular software of design optimization with structural and multidisciplinary objectives', in OPTI' 93 - Computer Aided Design of Structures, Zaragoza, Spain, July 7-9, 1993.

3. Esping B and Holm D, A CAD approach to structural optimization, in Computer Aided Optimal Design: Structural and Mechanical Systems, Ed. C A Mota Soares, 1987.
4. Esping B and Holm D, 'Structural shape optimization using OASIS', Structural Optimization, Ed. G I N Rozvany and B L Karahaloo, Kluwer Publishers, 1988.
5. Esping B, Holm D and Romell O, 'The OASIS-Aladdin structural optimization system', in International Series of Numerical Mathematics, 110, Birkhauser Verlag, Basel, 1993, pp 159-85.
6. Svanberg K, 'The method of moving asymptotes (MMA) with some extensions', in Optimization of Large Structural Systems, NATO, Berchtesgaden, Germany, 1991.
7. Wennerstrom H and Backlund J, Plate Finite Elements for Static Analysis of Stiffened Sandwich Construction, Dept of Aeronautical Structures and Materials, The Royal Institute of Technology, Report 83-6, Stockholm, 1983.
8. Wennerstrom H and Backlund J, Cylindrical Finite Elements for Static Analysis of Stiffened Sandwich Construction, Dept of Aeronautical Structures and Materials, The Royal Institute of Technology, Report 84-3, Stockholm, 1984.
9. Holm D, Esping B, Campion F, 'An inverse problem in designing laminated composite structures', in ICCM 9, Volume IV, Ed. A. Miravete, Woodhead Publishing Limited, Cambridge, 1993, pp 690-7.
10. Mirza S and Alizadeh Y, On Dynamics of Triangular Orthotropic Plates with a Crack Along the Support, inpress.
11. Gorman D J, 'A highly accurate analytical solution for free vibration analysis of simply supported right triangular plates', Journal of Sound and Vibration, 1983, 89, 1, pp 107-18.
12. Gustafson P N, Stokey W F and Zorowski C F, 'An experimental study of natural vibrations of cantilevered triangular plates', Journal of Aeronautical Sciences, 1953, 20, pp 331-7.
13. Leissa A W, 'Plate vibration research, 1976-1980: Classical Theory', The Shock and Vibration Digest, 1981, 13, 11-22.
14. Leissa A W, 'Recent studies in plate vibrations, 1981-1985: Part i Classical theory', The Shock and Vibration Digest, 1987, 19, 11-18.
15. Midlin R D, 'Influence of rotary inertia and shear of flexural motion of isotropic elastic plates', J. Apl. Mech., 1951, 18, 31-38.
16. Bakos D, Kyriakopoulos M, Kostopoulos V and Papanicolaou G C, 'Interfacial fracture toughness in aluminum-composite sandwich beams', in ICCM-9, Volume IV, Ed. A. Miravete, Woodhead Publishing Ltd, Cambridge, 1993, pp 376-83.
17. Ruhmann D C, Bates W F, Dexter H B and June R, 'New materials drive high-performance aircraft', Aerospace America, August, 1992, 46-9.
18. Frostig Y and Baruch M, 'Bending of sandwich beams with transversely flexible core', AIAA Journal, 1990, 28, 523-31.
19. Bakos D and Papanicolaou G C, 'The effect of skin treatment on the bending behaviour of sandwich beams', Composites Science and Technology, 1993.
20. Christopoulos G C, Papanicolaou G C, Friedrich K and Wittich W, 'Interlaminar fracture of fabric reinforced composites', Proceedings of The Second Interlaminar Symposium on Composite Materials and Structures, Beijing, China, July, 1992.
21. Raju I S, Crews J H and Aminopour M A, 'Convergence of strain energy release rate components for edge delaminated composites', Eng. Fracture Mech., 1988, 30, 383.

22. Ozdil F, Carlsson L A, 'Finite element analysis of interleaved DCB specimen', Eng. Fracture Mech., 1992, 41, 475-85.
23. Broek D, Elementary Engineering Fracture Mechanics, 4th Ed., Kluwer Academic, Dordrecht, 1986.
24. Malhotra S K, 'Some studies on end connection of composite sandwich panels', in ICCM9, Volume IV, Ed. A. Miravete, Woodhead Publishing Ltd, Cambridge, 1993, pp 384-91.
25. MIL HDBK 23A, Structural Sandwich Composites, Chapter 14, Dec. 1968.
26. Chen R-S and Wu P-C, 'Analysis of the special finite element model of honeycomb composites', in ICCM/9, Volume IV, Ed. A. Miravete, Woodhead Publishing Ltd, Cambridge, 1993, pp 392-7.
27. Johns R M, Mechanics of Composite Materials, Scripta Book Company, Washington D C.
28. Withney J M, 'Stress analysis of thick laminated composite and sandwich plates', Journal of Composite Materials, 1972, 6, 426-40.
29. Vinson J R, 'Optimum design of composite honeycomb sandwich panels subjected to uniaxial compression', AIAA Journal 1986, 24, 1690-6.
30. Kanematsu H H and Iyama H, 'Bending and vibration of CFRP-faced rectangular sandwich plates', Composite Structures, 1988, 10, 145-63.
31. Azar J J, 'Bending theory for multilayer orthotropic sandwich plates', AIAA Journal, 1968, 6, 2166-9.
32. Reissner E, 'Finite deflection of sandwich plates', Journal of Aerospace Sciences, 1948, 15, 435-40.
33. Folie G M, 'Bending of clamped orthotropic sandwich panels', Journal of the Engineering Mechanics Division, Proceedings of ASCE, 1970, EM3, 243-65.
34. Liaw B-D and Little R W, 'Bending of multilayer sandwich plate', AIAA Journal, 1967, 5, 301-4.
35. Pagano N J, 'Exact solutions for rectangular bidirectional composites and sandwich plates', Journal of Composite Materials, 1970, 4, 20-34.
36. Crisfield M A, 'A quadratic midlin element using shear constraints', Computers & Structures, 1984, 18, 833-52.

6 DESIGN OPTIMISATION OF VARIABLE THICKNESS COMPOSITE STRUCTURES

6.1 Introduction

Composite materials have been increasingly used over the last few decades to lighten structures in fields such as aeronautics and space. Two steps are essential in the process of taking advantage of these materials: design and optimisation.

Optimisation of composite structures is a recent issue, because both optimisation techniques and composite structures have been developed over the last few decades and therefore, the conjunction of them is even more recent. Composite materials are an expensive but efficient technology to achieve minimum weight structures. It is logical to attempt to find out how to design optimum laminated composite plates with no reduction in their strength. A general scheme is depicted in Fig. 6.1.

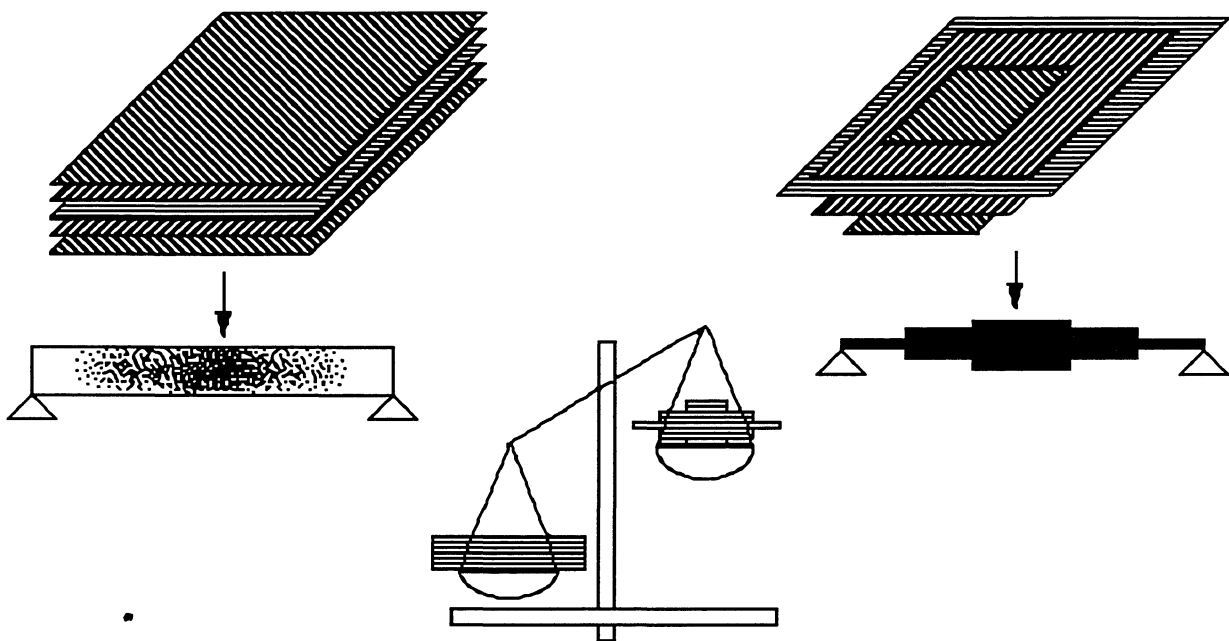


Figure 6.1 Schematic representation of a variable-thickness composite plate.

This chapter deals with the design optimisation of variable thickness laminated composite structures subjected to a transverse load. The study of the optimisation of laminated composite plates subjected to this type of load is extremely complex. On the one hand, the whole stress tensor must be considered: the three in-plane stress components are present owing to the bending effects, and so are the two interlaminar shear stress components, due to the shear effects. Finally, the interlaminar normal stress component must also be considered because of the variable thickness, as equilibrium equations predict. References 1-8 give further details about these aspects.

Firstly, the variable thickness problem is analysed. The behaviour of a bidimensional plate with variable thickness is extremely difficult to understand, because it is a 3-D problem, and because bending, shear, and variable thickness effects appear simultaneously. Therefore, a one-dimensional plate with variable thickness is studied here by means of a 2-D plane strain finite element model. Results are easy to analyse, and some conclusions about variable thickness laminated composite plates can be drawn. Second, the failure mechanisms are identified.

One-dimensional laminated composite plates are studied by applying the 2-D plane strain model mentioned above. Optimum configurations and weight savings are reported for several types of plates, loads, and boundary conditions.

Two-dimensional laminated composite plates are also analysed. Since the 2-D plane strain model can only be used for the 1-D case, a more general model based on a higher order shear theory is used. This method is efficient and accurate, not only because the analysis is carried out very fast, but also because the required number of nodes of the mesh is not large, and the results from the shear deformation theory used here and the 2-D plane strain model are very close.

Variable thickness beams, plates and sandwich constructions will be analysed in subsequent chapters.

6.2 Variable thickness laminate stress distribution

The aim of this study is to find out what happens inside the laminate when the laminate thickness varies and one transverse load is applied. The behaviour of a 2-D plate with variable thickness is extremely difficult to understand because it is a 3-D problem, and because bending, shear and variable thickness effects appear simultaneously. In other words, the whole stress tensor must be considered: the three in-plane stress components are present owing to the bending effects, and so are the two interlaminar shear stress components because of the shear effects. Finally, the interlaminar normal stress component must also be considered because of the variable thickness effect. To simplify the problem and to understand the variable thickness phenomenon, a 1-D plate with variable thickness is studied here by means of a 2-D plane strain finite element model.

The next section refers to attempts at obtaining through-thickness stresses distributions in a cross section where the laminate thickness varies. Once the stress level is known, the laminate failure will be predicted by means of a quadratic failure criterion. The aim of this study is to analyse theoretically the influence of the different parameters on the mechanical behaviour of variable-thickness laminated composite plates.

An investigation is performed to study the damage in variable thickness laminated composites caused by a transverse load. The major objective of the study is to understand the fundamental failure mechanisms in composites caused by transverse loads, and to identify the essential parameters causing the damage in composites.

Finally, an experimental study will be carried out to assess the accuracy of the theory, as well as to analyse experimentally the influence of the different parameters on the mechanical behaviour of variable-thickness laminated composite plates. By using this method, the results are easy to analyse and some conclusions about variable thickness laminated composite plates can be drawn.

6.2.1 Model assumptions and method of analysis

The model is used with the following assumptions:

- This study is limited to one-dimensional laminated composite plates, in order to avoid 3-D effects and to analyse properly the consequences of the variable thickness effect.
- The fibre orientation is longitudinal (x -direction). This is the optimal direction for 1-D laminated composite plates.

- The material used is graphite/epoxy AS4/3501-6.

The following method of analysis was used:

- A 2-D plane strain finite element model.
- The mesh is composed by 1891 nodes.
- Different types of loading and boundary conditions have been studied to analyse the variable thickness problem from a theoretical point of view as well as to obtain through-thickness stress distributions.
- A three point bending model has been used for theoretically analysing the influence of the different parameters on the mechanical behaviour of variable-thickness laminated composite plates.
- A three point bending test in fatigue and static conditions has been carried out for identifying the failure mechanisms.
- A three point bending test in static conditions has been used to verify the theoretical model, and to analyse experimentally the influence of the different parameters on the mechanical behaviour of variable-thickness laminated composite plates.

6.2.2 Through-thickness stress distribution

This section refers to the attempts which have been made to obtain through-thickness stress distribution in a cross section, where the laminate thickness varies from t to $t-t_1$.

The solution of the problem is a function of a number of parameters:

- θ : angle of variation of thickness.
- t/t_1 : thickness ratio.
- Stacking sequence.
- Bending moment distribution.
- Shear force distribution.
- Characteristic length / laminate thickness ratio.
- Material

The model described in section 6.2.1 has been applied to different cases in order to find out what happens inside the laminate when the laminate thickness varies and to study the sensitivity of the parameters mentioned above. Thus, once the relationship between each parameter and the mechanical behaviour of the plate is known, some design changes can be made in order to improve the mechanical characteristics of the plate.

Fig. 6.2-6.4 show the distribution of σ_1 , σ_3 and σ_5 through unidimensional, two-sides tapered plates and linear bending moment distributions with $\partial M/\partial x > 0$. These stress components present remarkable differences with respect to

the constant-thickness plate distributions, especially those related to σ_3 and σ_5 , because σ_5 has two maxima near the top and bottom surfaces and σ_3 reaches much higher values than in the case of constant-thickness.

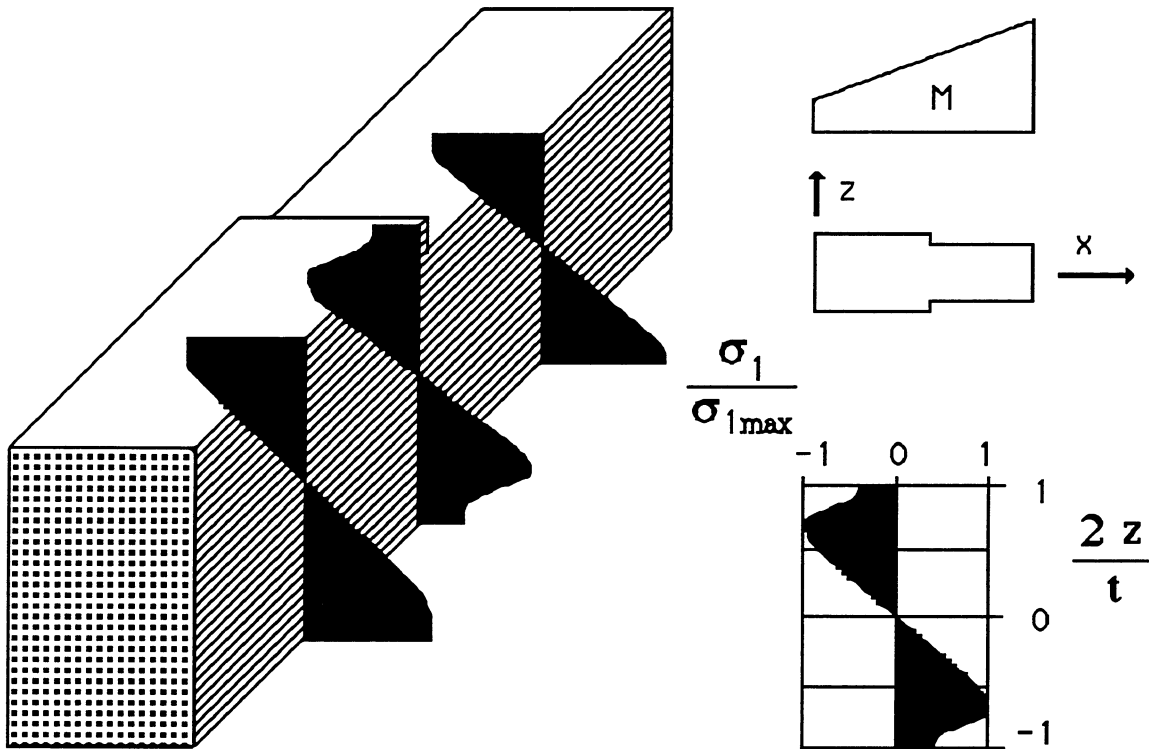


Figure 6.2 Distribution of σ_1 for a two-sides tapered plate and $\partial M/\partial x > 0$.

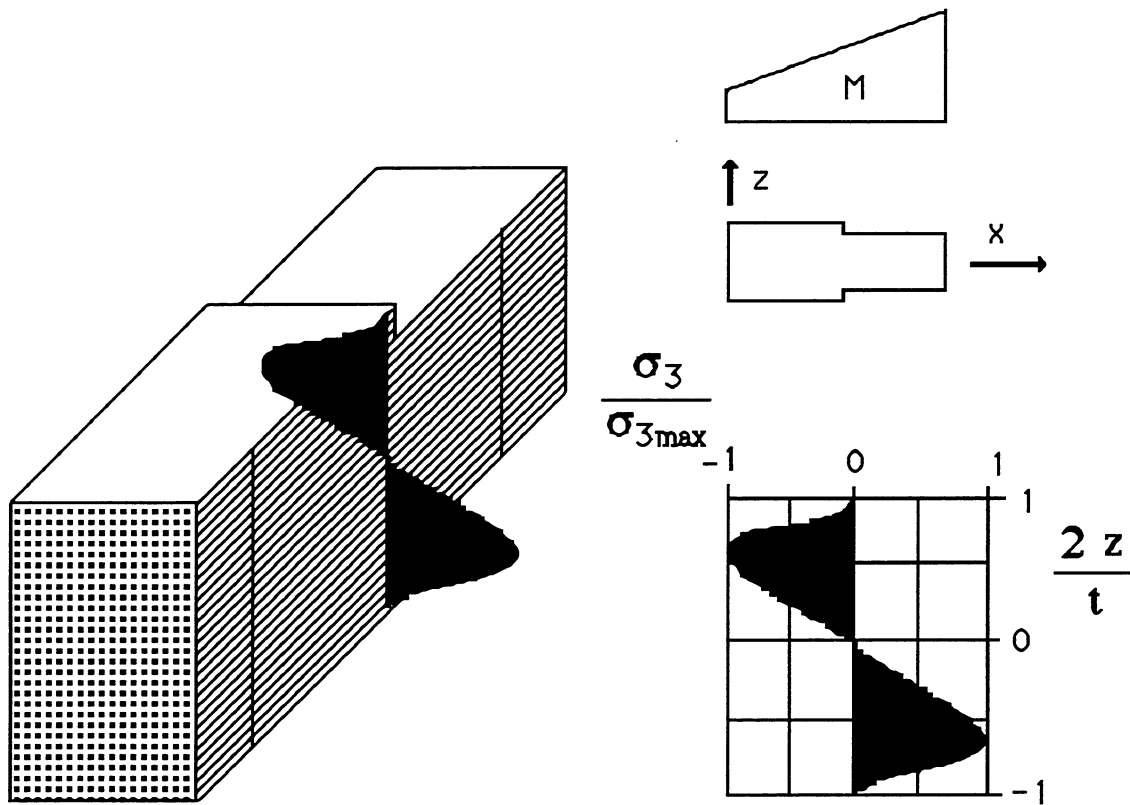


Figure 6.3 Distribution of σ_3 for a two-sides tapered plate and $\partial M/\partial x > 0$.

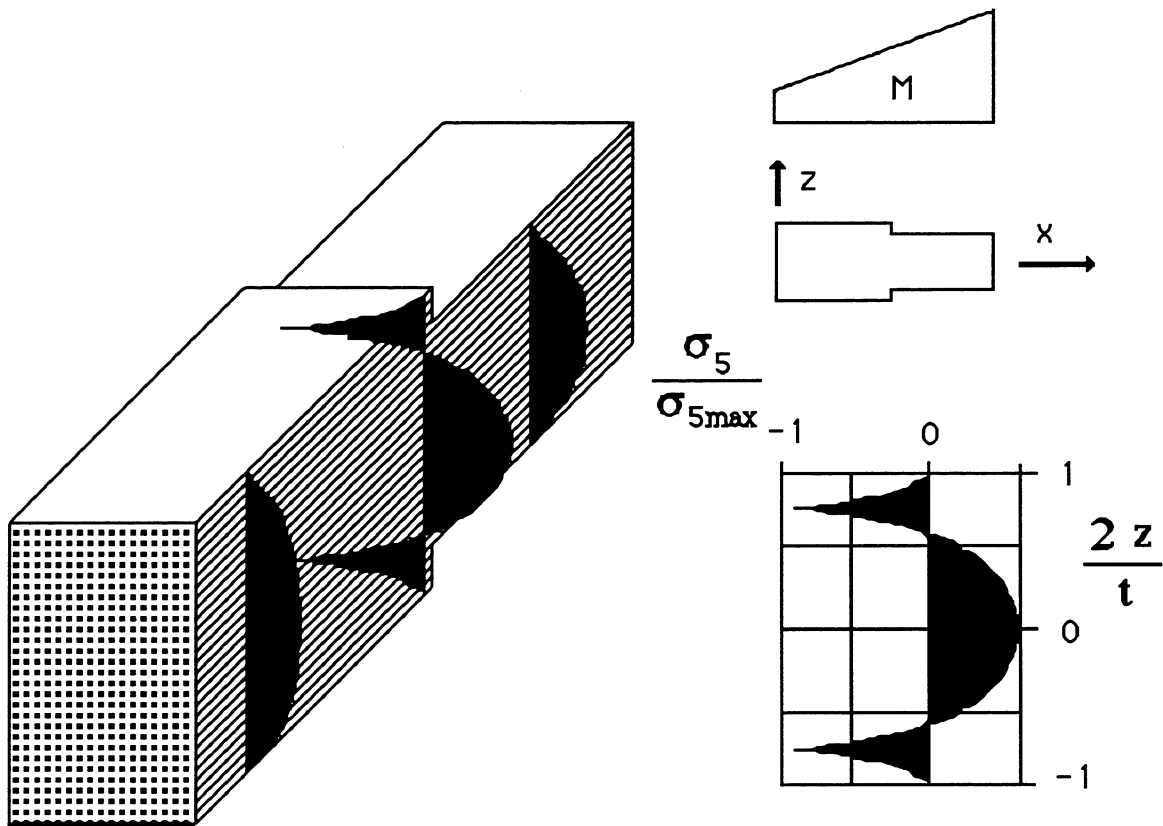


Figure 6.4 Distribution of σ_5 for a two-sides tapered plate and $\partial M/\partial x > 0$.

In Fig. 6.5-6.7, the distributions of σ_1 , σ_3 and σ_5 through the thickness for unidimensional one-side tapered plates and linear bending moment distributions with $\partial M/\partial x > 0$ are shown. Obviously, to taper the plate on just one side leads to non-symmetrical distribution with peaks of interlaminar stresses near the surface which is tapered.

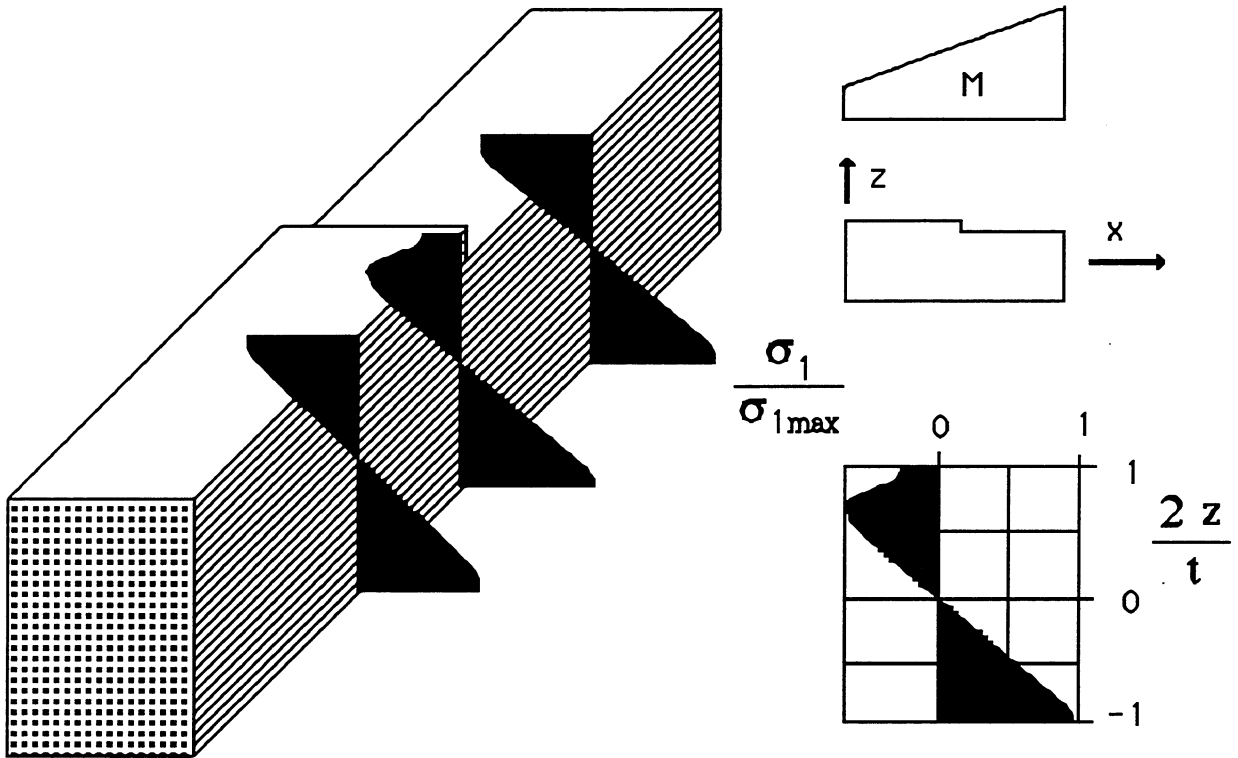


Figure 6.5 Distribution of σ_1 for a one-side tapered plate and $\partial M/\partial x > 0$.

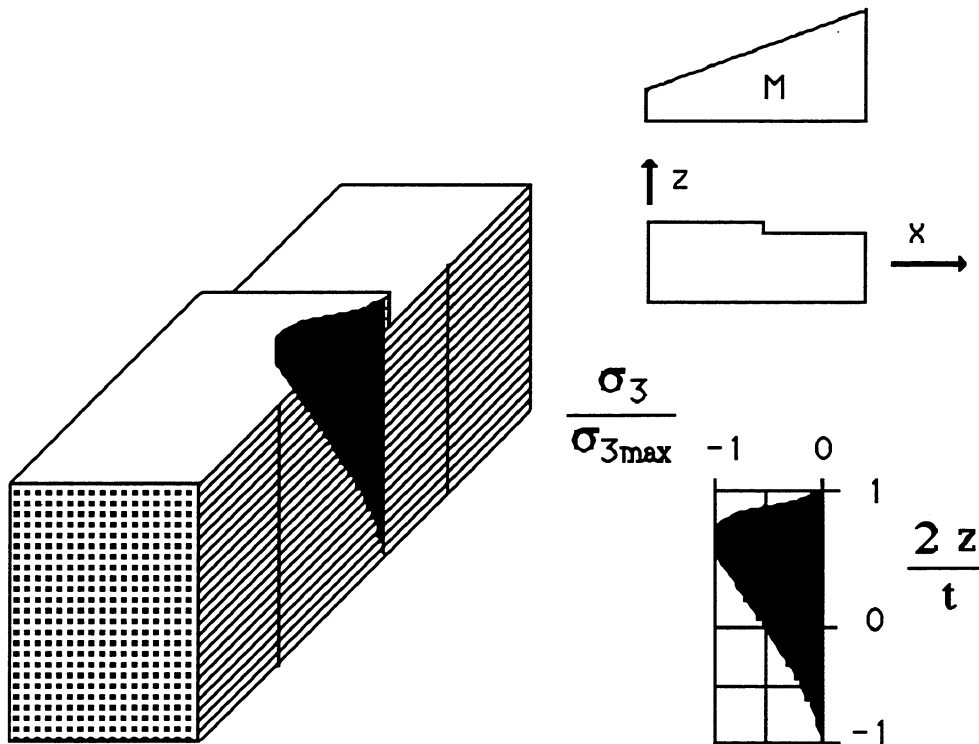


Figure 6.6 Distribution of σ_3 for a one-side tapered plate and $\partial M/\partial x > 0$.

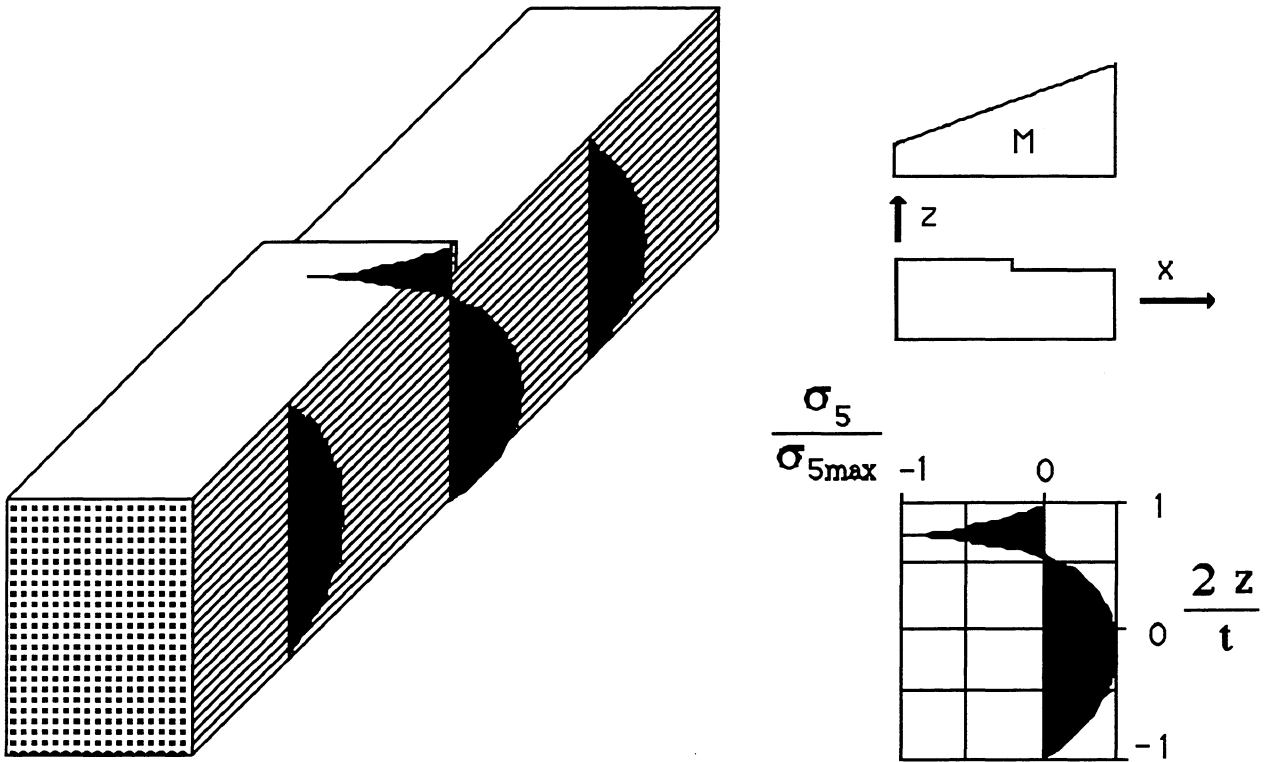


Figure 6.7 Distribution of σ_5 for a one-side tapered plate and $\partial M/\partial x > 0$.

Figures 6.8-6.10 show the distributions of σ_1 , σ_3 and σ_5 through unidimensional two-sides tapered plates and linear bending moment distributions with $\partial M/\partial x < 0$. It is apparent that the sign of $\partial M/\partial x$ has a strong influence on the distributions of longitudinal and interlaminar stresses.

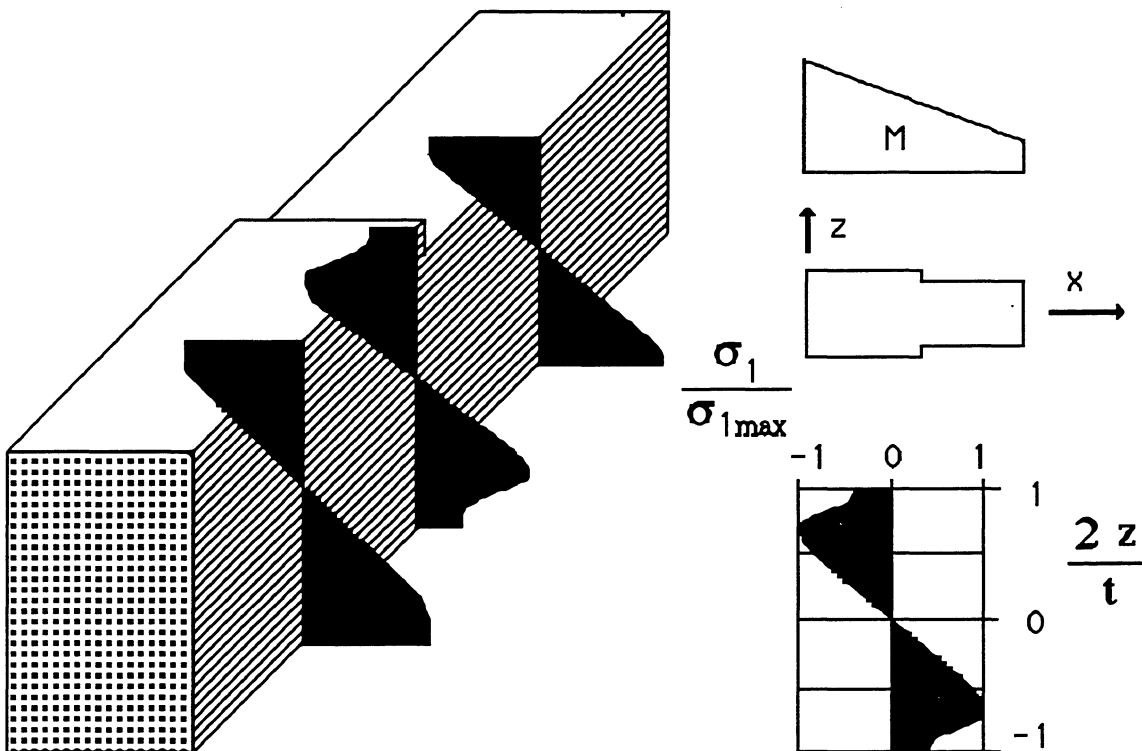


Figure 6.8 Distribution of σ_1 for a two-sides tapered plate and $\partial M/\partial x < 0$.

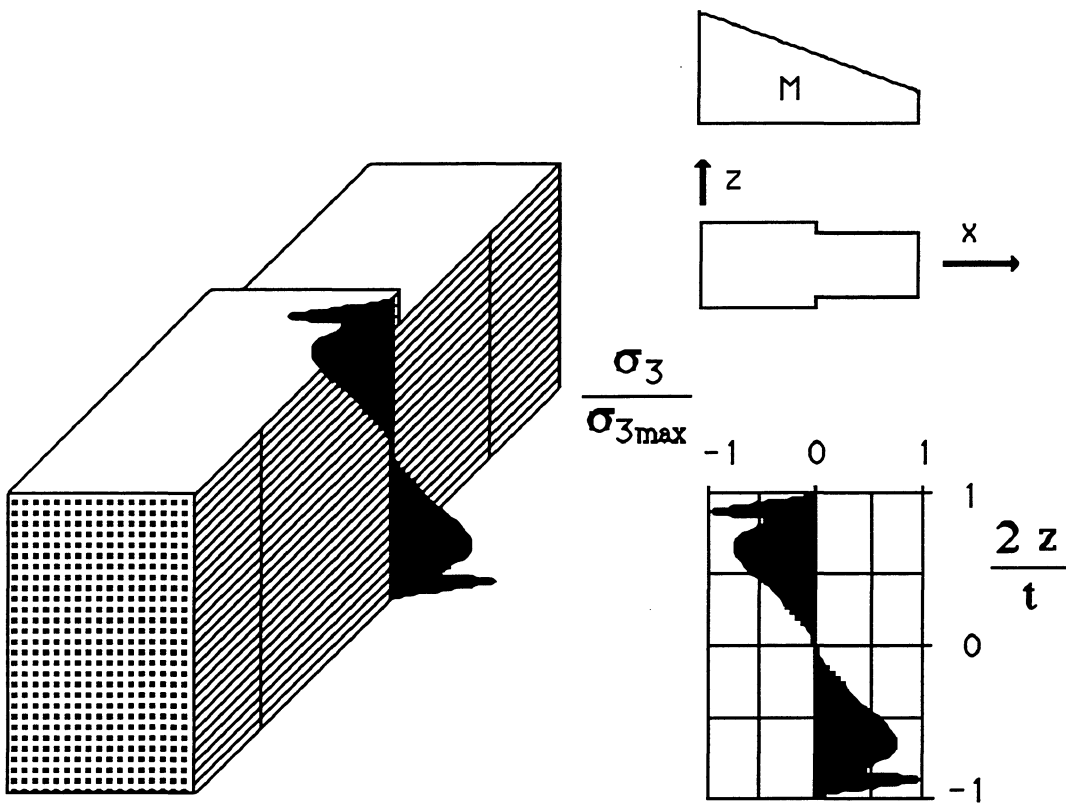


Figure 6.9 Distribution of σ_3 for a two-sides tapered plate and $\partial M/\partial x < 0$.

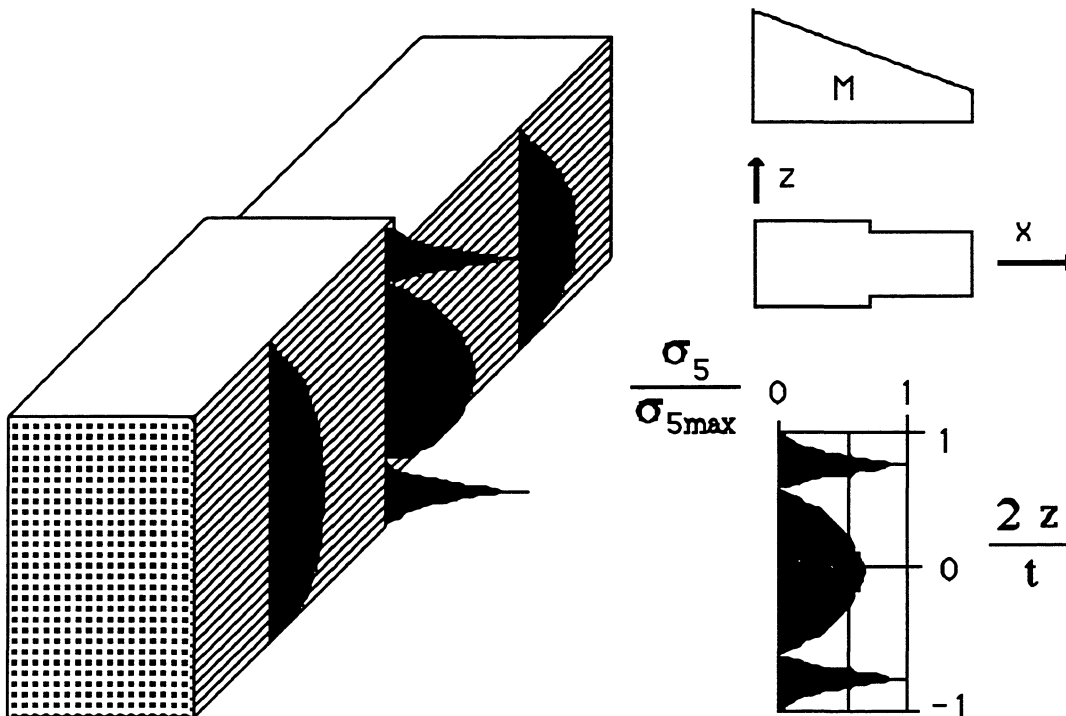


Figure 6.10 Distribution of σ_5 for a two-sides tapered plate and $\partial M/\partial x < 0$.

Finally, Fig. 6.11 to 6.13 represent the distributions of σ_1 , σ_3 and σ_5 through unidimensional one-side tapered plates and linear bending moment distributions with $\partial M/\partial x < 0$.

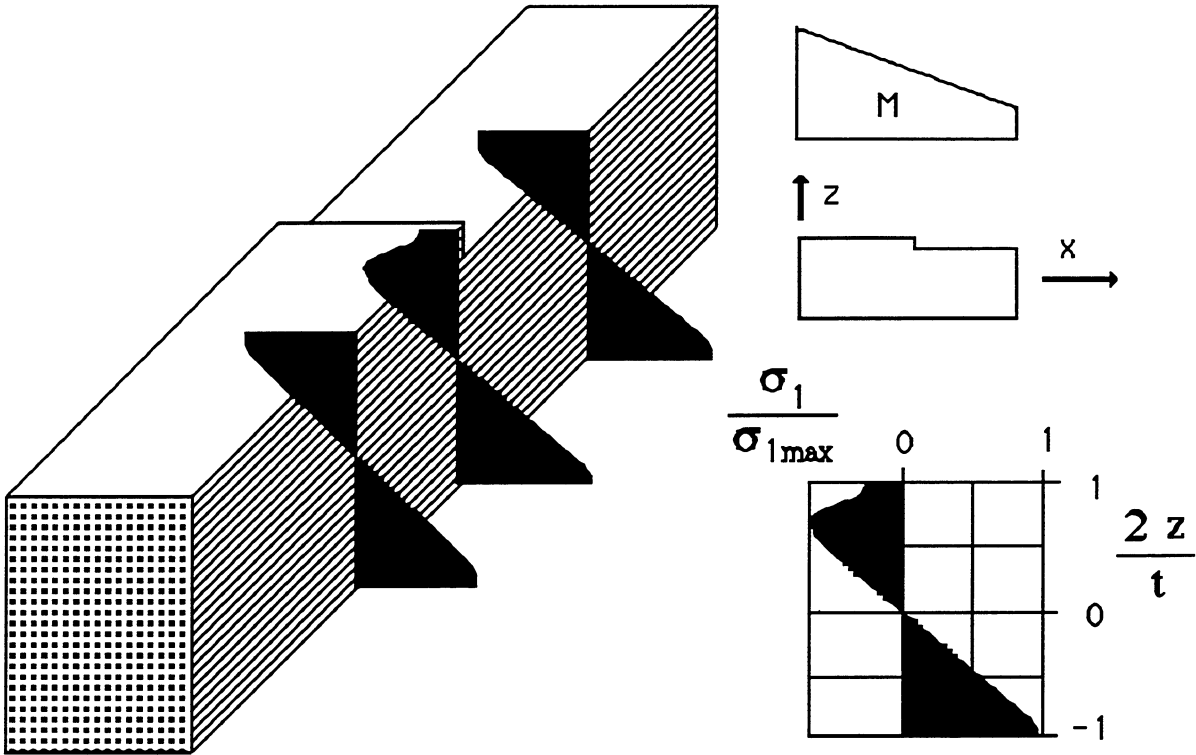


Figure 6.11 Distribution of σ_1 for a one-side tapered plate and $\partial M/\partial x < 0$.

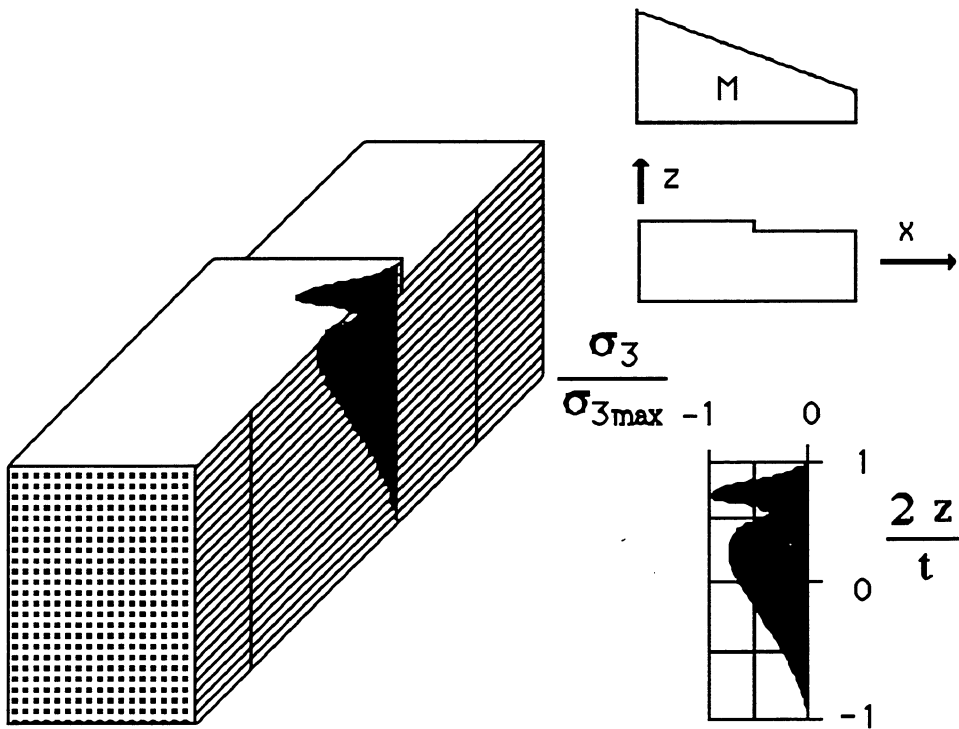


Figure 6.12 Distribution of σ_3 for a one-side tapered plate and $\partial M/\partial x < 0$.

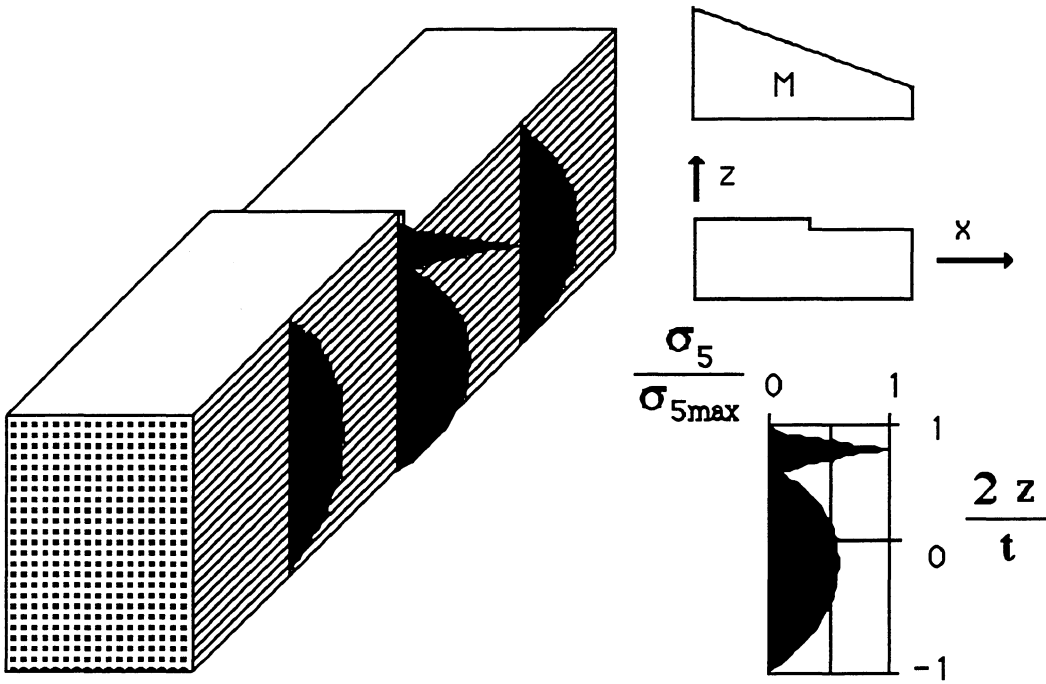


Figure 6.13 Distribution of σ_5 for a one-side tapered plate and $\partial M/\partial x < 0$.

In Fig. 6.14-6.16, σ_1 , σ_3 and σ_5 distributions are represented for $t_1/t=0.3$, $M/Pt=5$ and $\partial M/\partial x < 0$, respectively. Two angles of variation of thickness have been considered: 15° and 90° . Reducing the angle of variation of thickness from 90° to 15° leads to a considerable decrease in the values of the peaks in the distributions of σ_1 , σ_3 and σ_5 , especially these last two.

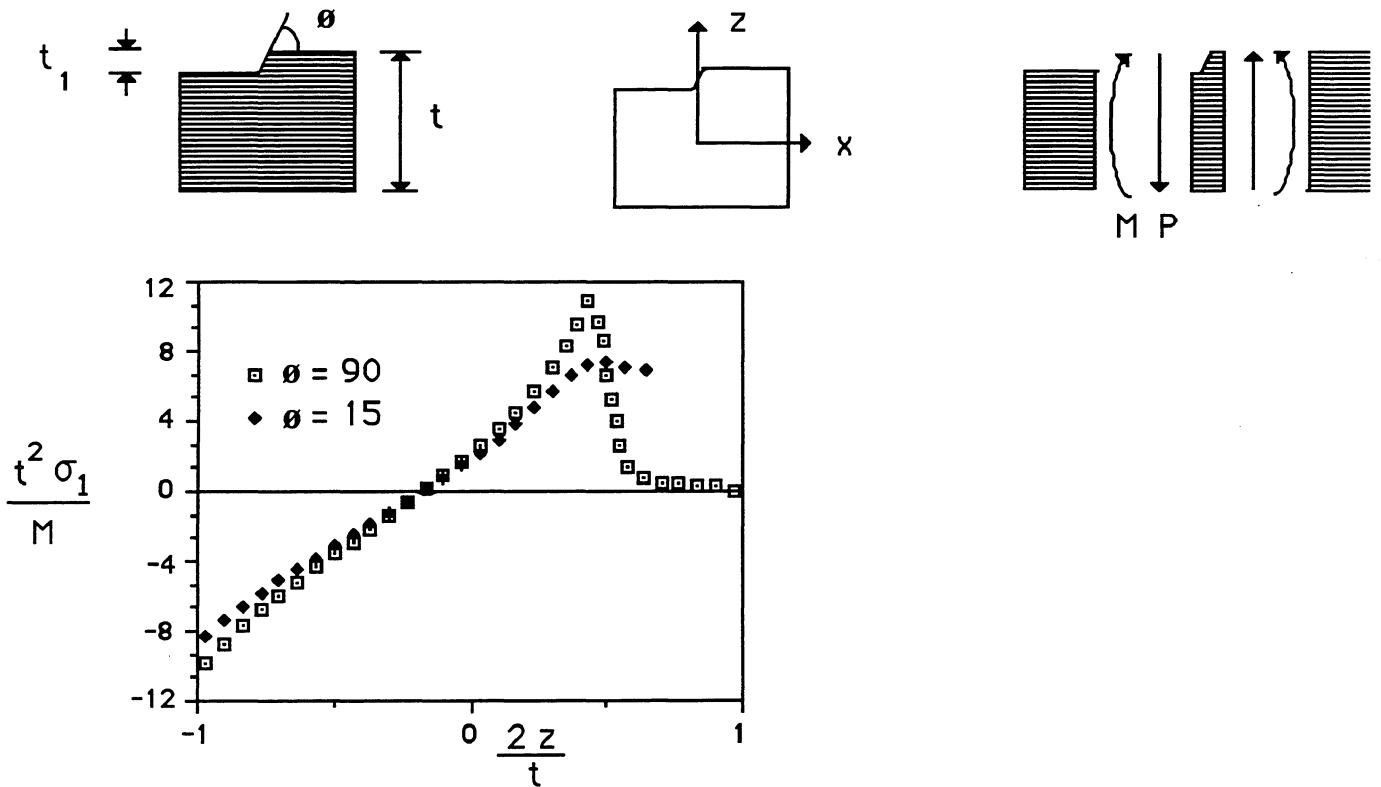


Figure 6.14 Distribution of σ_1 for a one-side tapered plate, $t_1/t=0.3$, $M/Pt=5$ and $\partial M/\partial x > 0$.

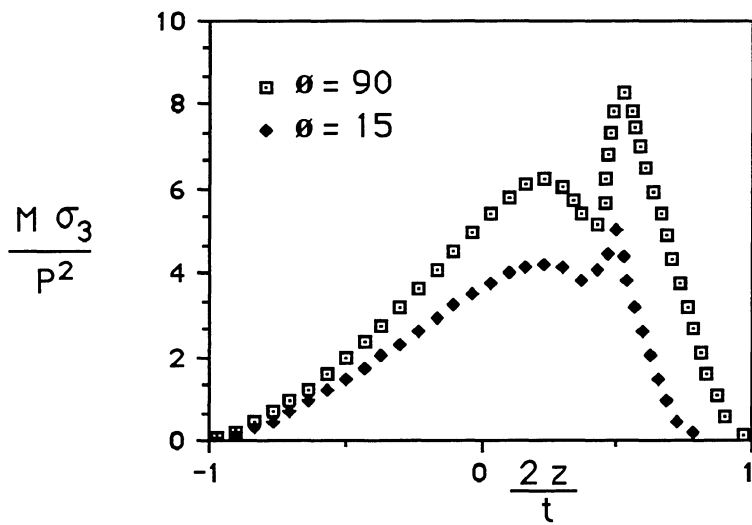


Figure 6.15 Distribution of σ_3 for a one-side tapered plate, $t_1/t=0.3$, $M/Pt=5$ and $\partial M/\partial x > 0$.

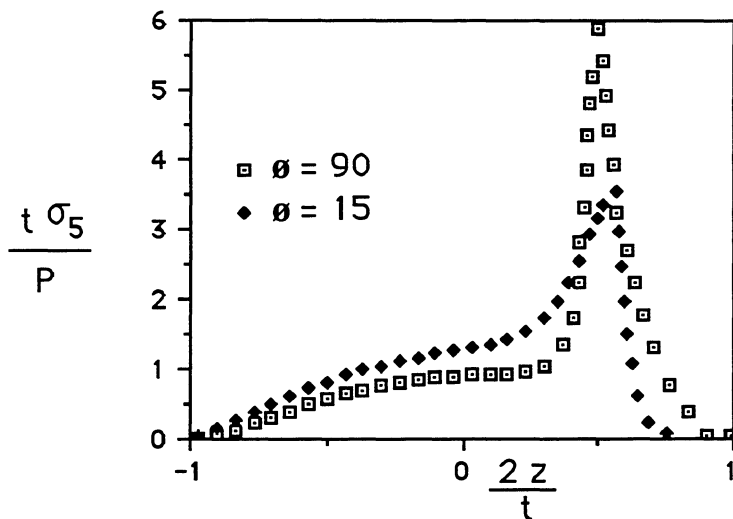
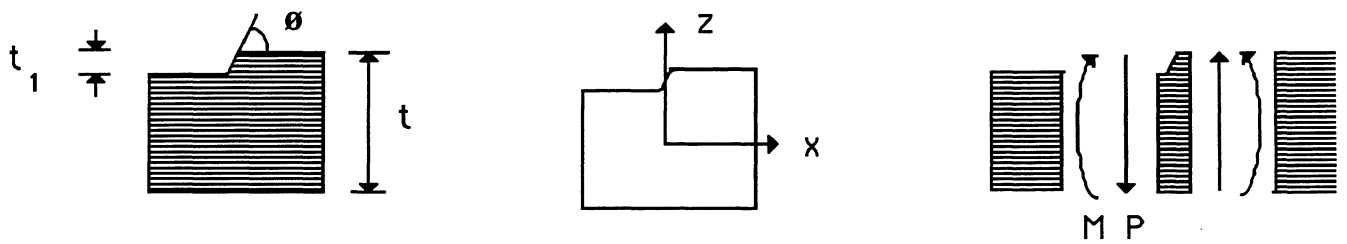


Figure 6.16 Distribution of σ_5 for a one-side tapered plate, $t_1/t=0.3$, $M/Pt=5$ and $\partial M/\partial x > 0$.

Figures 6.17-6.19 show the distributions of σ_1 , σ_3 and σ_5 for $t_1/t=0.2$, $M/Pt=5$ and $\partial M/\partial x < 0$, respectively. As

expected, maximum values decrease considerably with respect to Fig. 6.14 to 6.16, because of the smaller value of t_1/t .

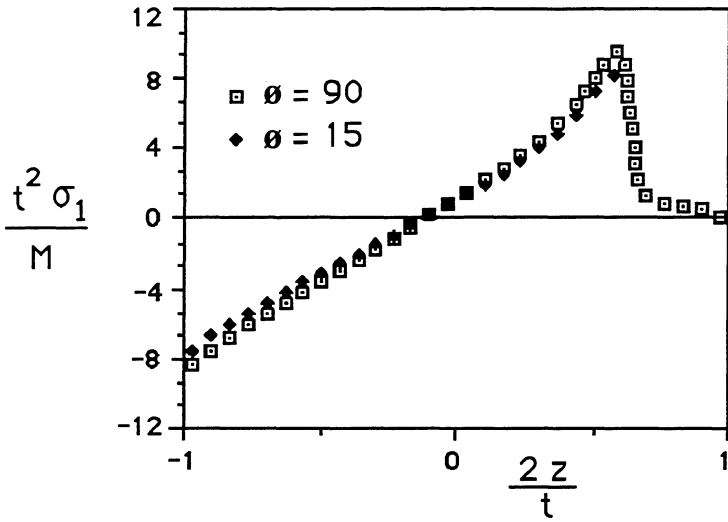


Figure 6.17 Distribution of σ_1 for a one-side tapered plate, $t_1/t=0.2$, $M/Pt=5$ and $\partial M/\partial x > 0$.

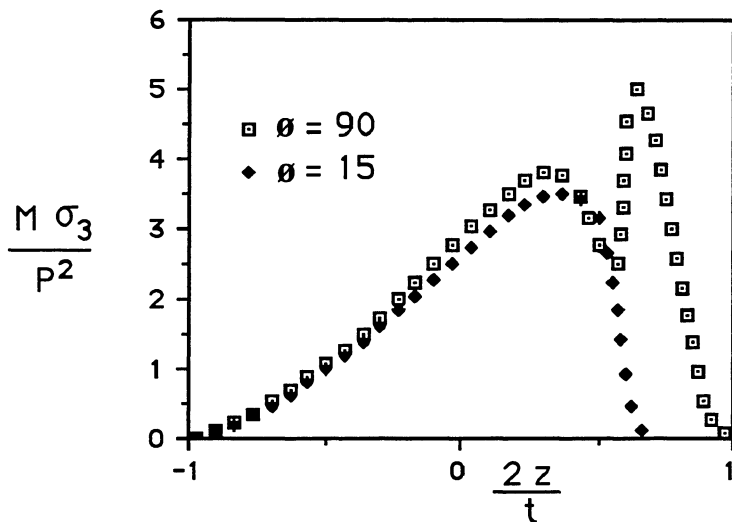
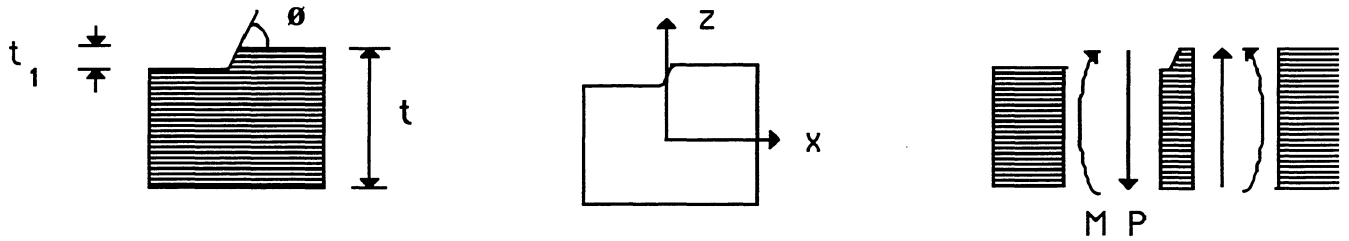


Figure 6.18 Distribution of σ_3 for a one-side tapered plate, $t_1/t=0.2$, $M/Pt=5$ and $\partial M/\partial x > 0$.

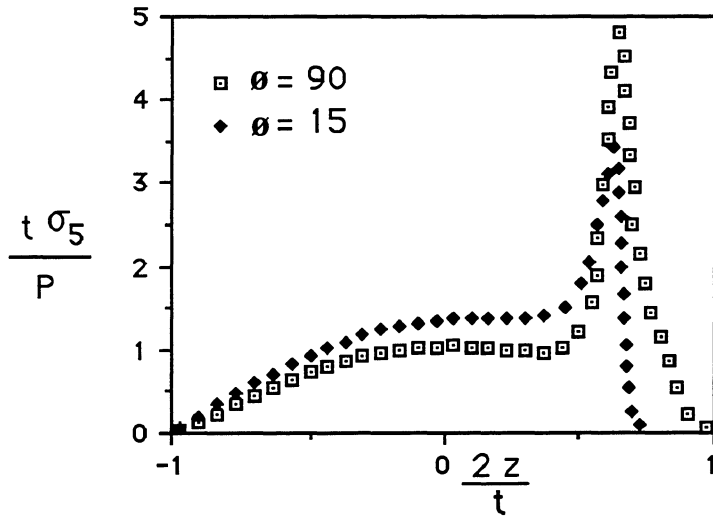


Figure 6.19 Distribution of σ_5 for a one-side tapered plate, $t_1/t=0.2$, $M/Pt=5$ and $\partial M/\partial x > 0$.

Distributions of σ_1 , σ_3 and σ_5 for $t_1/t=0.1$, $M/Pt=5$ and $\partial M/\partial x < 0$ are presented in Fig. 6.20-6.22, respectively. Numerical values keep decreasing because of the value of $t_1/t=0.1$. Also, the effect of the angle of variation of thickness can be seen by comparing the distributions for $\theta=90^\circ$ and $\theta=15^\circ$.

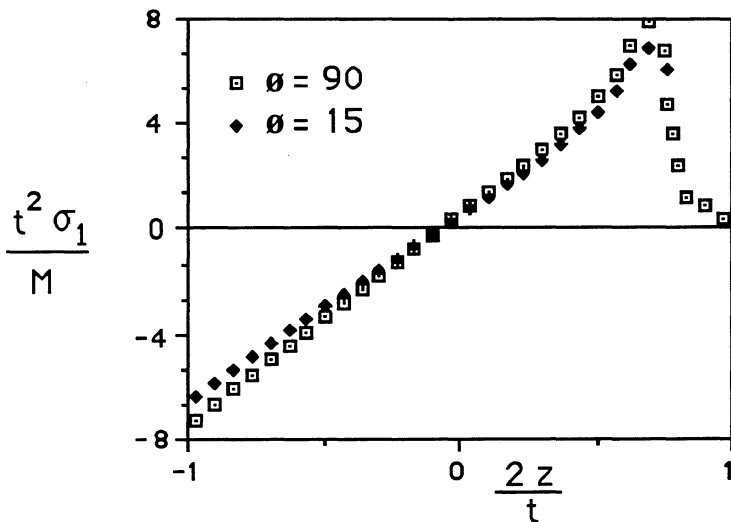
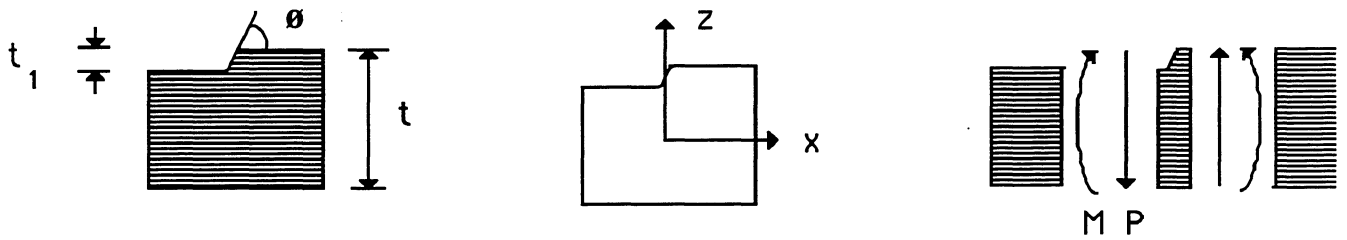


Figure 6.20 Distribution of σ_1 for a one-side tapered plate, $t_1/t=0.1$, $M/Pt=5$ and $\partial M/\partial x > 0$.

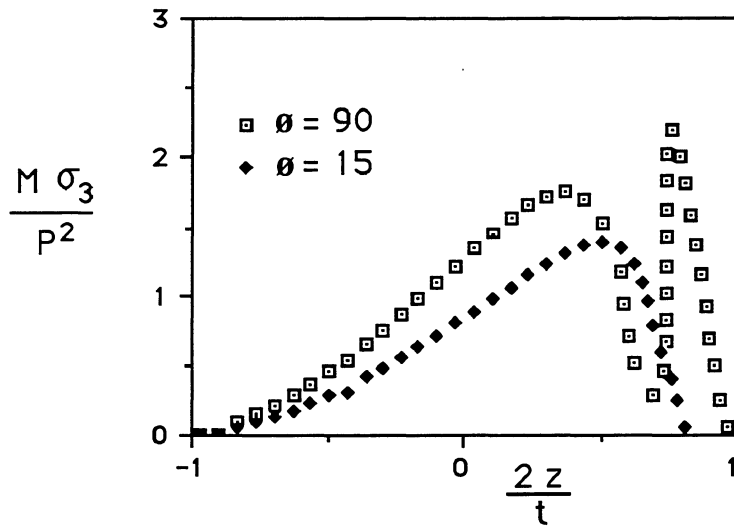


Figure 6.21 Distribution of σ_3 for a one-side tapered plate, $t_1/t=0.1$, $M/Pt=5$ and $\partial M/\partial x > 0$.

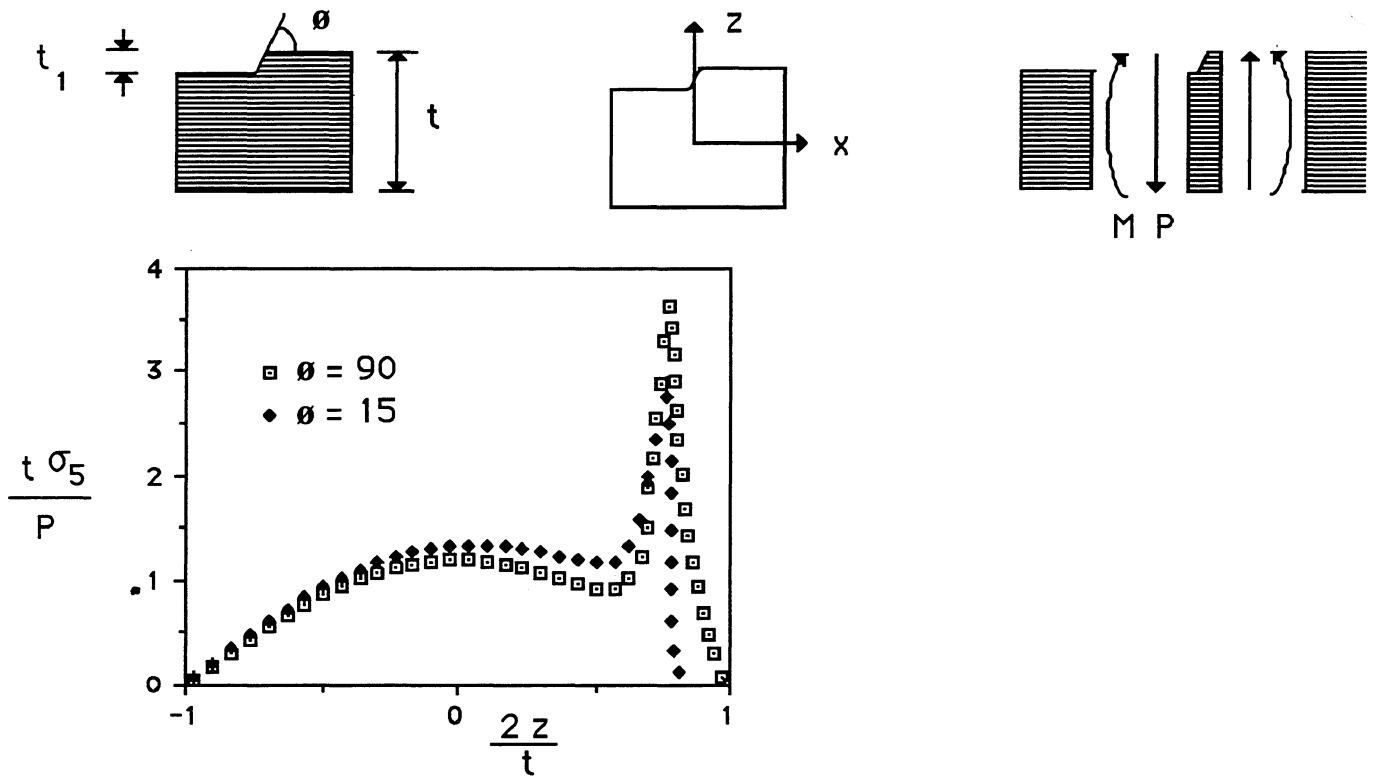


Figure 6.22 Distribution of σ_5 for a one-side tapered plate, $t_1/t=0.1$, $M/Pt=5$ and $\partial M/\partial x > 0$.

The following conclusions can be drawn after analysing the results described above:

- The examination of Fig. 6.2-6.13 leads to the conclusion that the variable-thickness effect presents a strong influence on the distributions of longitudinal and interlaminar stresses. High peaks of interlaminar stresses appear near the areas of change of thickness.
- It is also noticeable by comparison of Fig. 6.2-6.4 and Fig. 6.5-6.7, that the distributions of the through-thickness stresses vary as a function of the sign of $\partial M/\partial x$.

- Stress distributions are strongly dependent on t/t_1 , the thickness ratio, as the comparison between Fig. 6.14-6.16, 6.17-6.19 and 6.20-6.22, reflect.
- ϕ , the angle of variation of thickness has a remarkable influence on interlaminar stress distributions through the laminate thickness. This can be seen in Fig. 6.14-6.22.

Focusing on optimisation of laminated composite plates, the last four parameters in the above list will be input data, and the optimisation procedure will determine the other parameters on the list except for the angle of variation of thickness. Therefore, the study of this parameter becomes more and more important since the angle of variation of thickness is critical for the mechanical behaviour of variable thickness plates.

6.2.3 Failure mechanisms

A variable thickness unidimensional laminated composite plate exhibits a variety of failure mechanisms when subjected to transverse loads. Knowledge of these modes is very important to understand what happens inside the laminate. Once we know the critical failure mechanisms, we will be able to identify the strain components associated with them.

Different types of laminated composite plates were tested in fatigue and static conditions:

- AS4/3501-6 graphite/epoxy was used for this work.
- The types of testing performed were three point static and dynamic bending.
- The load rate for the static testing was 0.06 in/min (0.001524 m/min).
- For fatigue testing, the frequency was 5 cycles/second, and the load was 60 % of the static failure load. The vertical displacement was controlled.

Figure 6.23 shows the three-point bending testing.

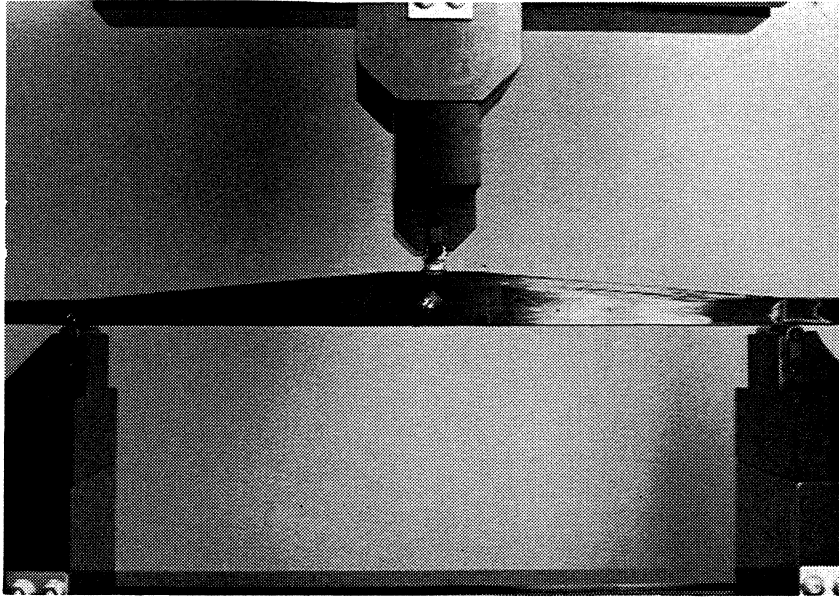


Figure 6.23 Three point bending test.

After studying the results, the following failure mechanisms have been reported:

- 1 Delamination. This is the most usual failure mode when the angle of variation of thickness is high. It is due to the fact that a sharp thickness variation generates a peak of interlaminar shear stress near the areas of change of thickness. In Fig. 6.24, a delamination failure in a tapered surface is shown. This mechanism can also be detected in thick plates, though the angle of variation of thickness is low. A representation of this failure mechanism is shown in Fig. 6.25.

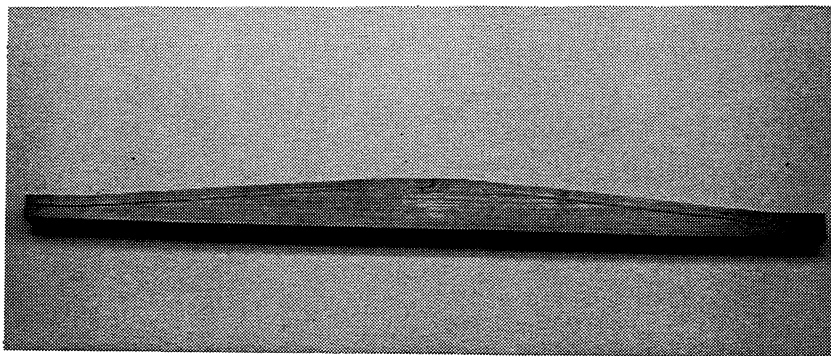


Figure 6.24 Delamination failure in the midplane.

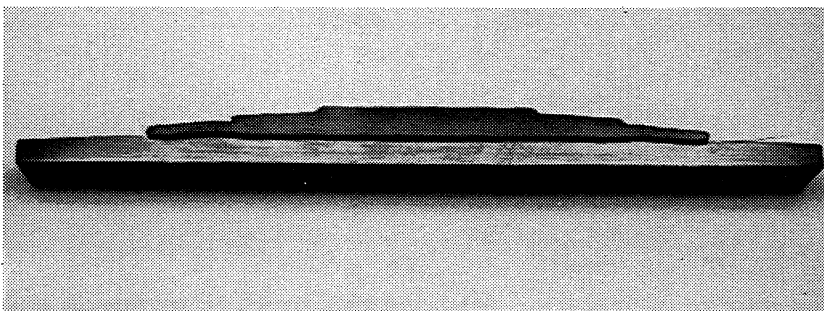


Figure 6.25 Delamination failure in the tapered surface.

2 Bending modes (compression). This mechanism occurs when the plate is very thin, the variable thickness effect is negligible, and the compression strength is lower than the tension strength in the fibre direction. The following in-plane compression failure modes can be distinguished:

- (a) Induced transverse tensile failure. Unidirectional composites can fracture along the fibres when loaded by compression by a transverse tensile failure mode, because of the weakness of the matrix and the fibre-matrix interface, compared with the strength of the fibres.
- (b) Compressive delamination failure. If a fibre buckles, the fibre-matrix interface may fracture in shear and lead to ultimate failure.
- (c) Euler failure. If the matrix is ductile and the interface is strong, the fibre can bend without matrix failure and eventually fracture in bending.
- (d) Microbuckling. A more likely failure mode of unidirectional composite laminates associated with fibre microbuckling and fibre kinking, is shear crippling. Macroscopically, shear crippling looks like a shear failure on a plane at an angle to the direction of loading. Microscopic inspection, however, indicates that shear crippling is frequently the result of kink-band formation.
- (e) Strength failure. The final failure mode exhibited in unidirectional composites is associated with pure compression failure of the fibres. In this case, the fracture surface is likely to be at an angle to the loading direction, usually about 45° .

3 Bending modes (tension). This mechanism occurs when the plate is very thin, the variable thickness effect is negligible, and the compression strength is higher than the tension strength in the fibre direction. The following in-plane tension failure modes can be distinguished:

- (a) Unidirectional composite subjected to longitudinal tensile load. Brittle failure. In this mode, stress concentrations created at the broken fibre ends lead to specimen separation at a given cross section.
- (b) Unidirectional composite subjected to longitudinal tensile load. Brittle failure with fibre pullout. Variations in bond strength and local load transfer mechanisms from matrix to fibre can lead to the pull-out of the fibres from the matrix at fracture.
- (c) Unidirectional composite subjected to longitudinal tensile load. Brittle failure with debonding and/or matrix failure. Finally, in other cases, cracks at different cross sections of the laminate may join together at fracture through fibre-matrix debonding or by shear failure of the matrix. This interfibre matrix shear failure and fibre-matrix debonding can occur either independently or in combination; i.e., portions of the failure path may exhibit debonding, while matrix shear failure is evident in other regions.

4 Mixed modes. A mixed failure mechanism has been detected in the regions close to the application of the load.

There exists a compressive delamination failure due to the bending mode (compression), and crushing due to a compressive peeling or interlaminar normal stress. This mechanism was observed in three-point bending testing, after 50 000 cycles. In Fig. 6.26, a representation of this mixed mode is shown. This mixed mode does not appear in the four point bending testing and it can also be avoided by placing a hard rubber pad (60-80 durometer) between the load point and the specimen (Fig. 6.27).

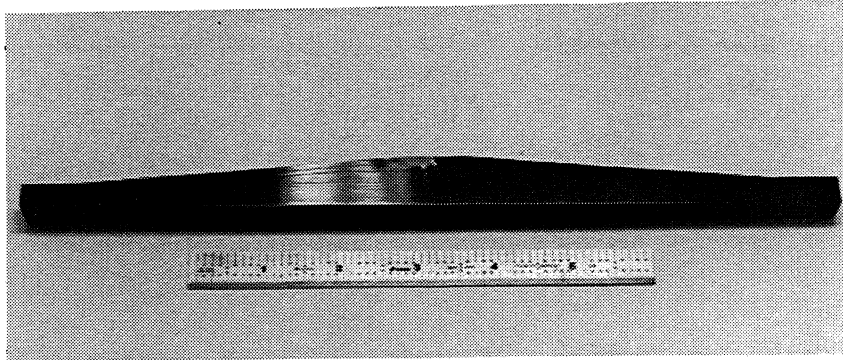


Figure 6.26 A mixed compression-interlaminar normal failure mode.

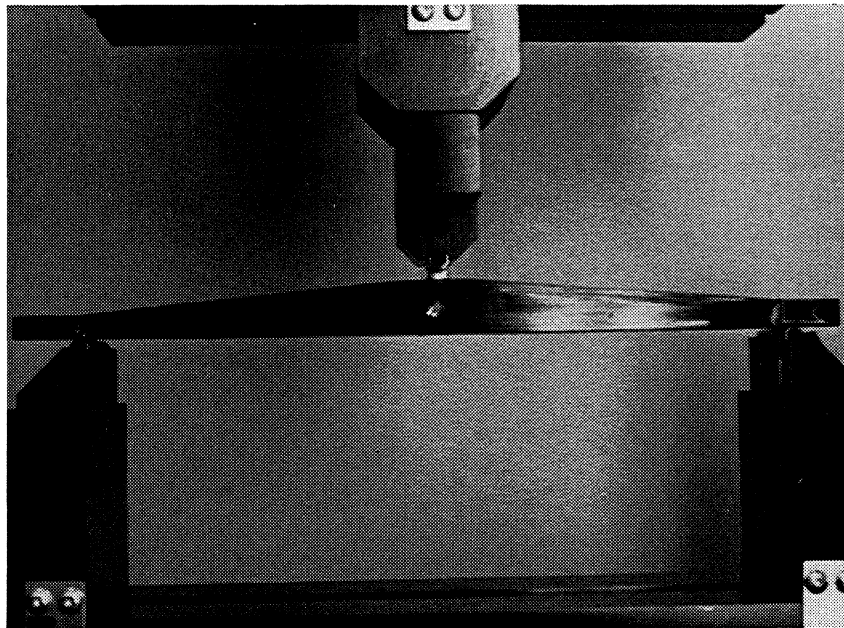


Figure 6.27 A 3P test bending with a hard rubber pad between the load point and the specimen.

After analysing the failure mechanisms described above, the following conclusions can be drawn:

- The critical failure modes are related to two strain components: ϵ_1 or longitudinal normal strain and ϵ_5 or interlaminar shear strain.
- The bending (compression or tension) modes are likely to occur when the plate is thin and the variable thickness effect is negligible.

- The delamination mechanisms are usual in cases where the variable thickness effect is critical (sharp change of thickness). The failure appears in the tapered surface. This mechanism also occurs when the plate is thick, even if the variable thickness is negligible. In this case, the failure appears near the middle plane of the laminate.
- The mode related to interlaminar normal strains (mixed modes) are due to stress concentrations in the areas near the application of the load. This mechanism can be easily avoided by means of the solutions mentioned above.

6.3 Conclusions

A study on variable thickness composite structures has been carried out. This chapter focused on the distribution of stresses through the laminate thickness and failure modes. The following conclusions have been obtained:

- The variable thickness effect has a remarkable influence on the behaviour of a tapered laminated composite plate. The distributions of through-thickness stresses are very sensitive to the thickness ratio (t/t_1) and the angle of variation of thickness. In particular, the interlaminar shear stress reaches very high values in the areas of change of thickness. The peak value can be controlled by modifying some parameters: thickness ratio, angle of variation of thickness, type of loading, etc. The distributions of interlaminar stresses vary with the sign of the bending moment.
- The failure mechanisms reported in variable-thickness composite plates can be grouped in three general modes:
 - Interlaminar shear mode: This is due to interlaminar shear stresses, and appears in the tapered surfaces when the change of thickness is sharp (high angles of variation of thickness) . It can also appear in the mid-plane, in thick plates.
 - Bending modes: These are due to bending stresses. These modes are usual in thin plates, very low angles of variation of thickness and low thickness ratios. They are the typical failure modes in thin, untapered plates.
 - Mixed modes: A compression-interlaminar normal mode has been found in the area of application of the load in the fatigue testing. This mode does not appear in the four-point bending test.

References 9-13 analyse aspects related to failure of these types of structures.

The following chapters will be devoted to the optimisation of variable thickness beams, plates and sandwich constructions.

References

1. Foye R, 'Advanced Design Concepts for Advanced Composite Frames', Volume I-II Air Force Materials

Laboratory, Wright Patterson Air Force Base, Ohio, AFML-TR-68-91, 1968.

2. Waddoups ME, 'Structural Airframe Application of Advanced Composite Materials-Analytical Methods', Volume IV Air Force Materials Laboratory, Wright Patterson Air Force Base, Ohio, AFML-TR-69-101, 1969.
3. Waddoups ME, McCullers LA., Olsen FO. and Ashton JE , " Structural synthesis of anisotropic plates ", Presented at AIAA/ASME 11th Structures, Structural Dynamics and Material Conference, Denver, Colorado, 1970.
4. Schmit, LA., " Structural Design by Systematic Synthesis", Proceedings of 2nd National Conference on Electrical Computation, Structure Division, ASCE , pp. 105, 1960.
5. Schmit LA, Kicher TP and Morrow WM., 'Structural synthesis capability for integrally stiffened waffle plates', AIAA Journal, 1963, 1, 2820-36.
6. Kicher TP, 'Structural synthesis of integrally stiffened cylinders', Journal of Spacecraft and Rockets, 1968, 5, 62-8.
7. Schmit LA., Morrow WM., and Kicher TP, "Structural Synthesis Capability for Integrally Stiffened Cylindrical Shell Shells", AIAA Paper 68-327, Palm Springs, California, 1968.
8. Tsai SW and Hahn HT, 'Introduction to Composite Materials', Technomic, Westport Com., 1980, pp. 457.
9. Tsai SW and Wu EM, 'A general theory of strength for anisotropic materials', J. Composite Mat, 1971, 5, 58.
10. Roy AK and Tsai SW, '3-D Effective moduli of laminated orthotropic plates', to appear in Journal of Applied Mechanics.
11. Ashton JE, 'Analysis of anisotropic plates II', J. Composite Mat., 1969, 3, 470.
12. Miravete A., 'Analisis del Comportamiento Resistente de Laminados de Poliéster Reforzado y su Aplicación a los Medios de Transporte', Ph D University of zaragoza, Spain, 1984.
13. Miravete A., 'Caracterisation et mise au Point d'un Element Fini de Grande Precision Applicable a des Lamines de Polyester Renforce avec Fibres de Verre', Composites. 1986, 4, 20.

7 VARIABLE THICKNESS BEAMS

7.1 Introduction

In this chapter, a study of optimisation of variable thickness laminated composite beams subjected to transverse loads is carried out. Generally speaking, a beam subjected to a transverse load presents a level of stress which varies substantially from one cross section to another. Therefore, the variation of thickness represents a possibility for reducing the weight of the structure by adapting the thickness of the section to the stress level. There are many applications where this philosophy has been successfully applied. For instance, the weight of the non-suspended part (suspension system) is critical for the stability of a vehicle. The stability of the vehicle increases by lightening the suspension system.

There are several possibilities to tailor a beam in order to optimise the design (Fig. 7.1). The best design consists of a constant width and variable thickness beam composed of a non-continuous fibre internal part and continuous fibre laminates at the external part. If the external part is non-fibre continuous, delamination takes place at a very low stress level. If the cross-section is constant, (width and thickness variable) delamination also takes place.

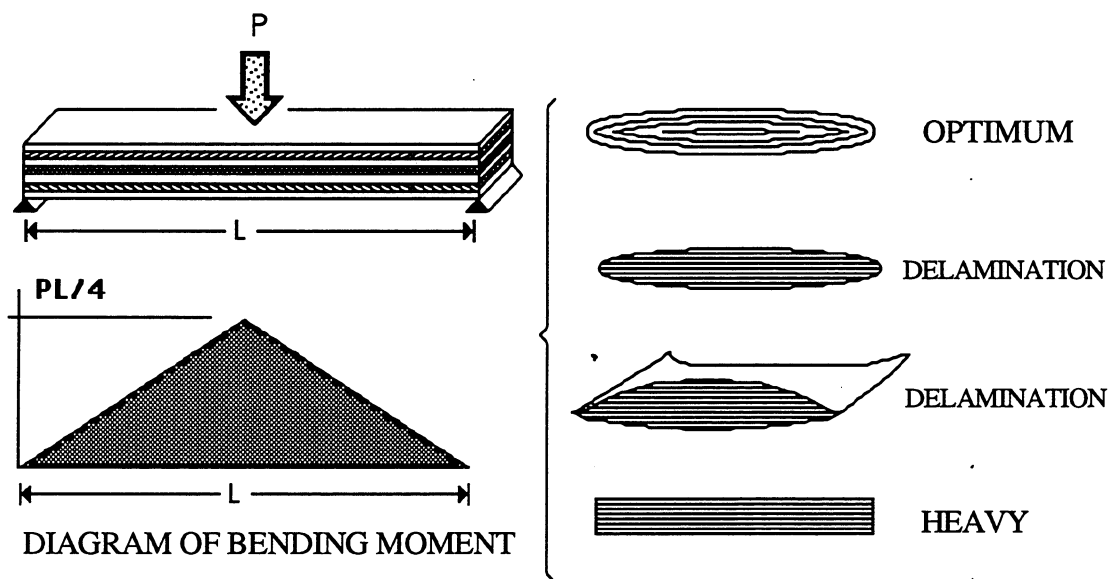


Figure 7.1 Scheme of variable thickness composite beams.

This chapter is divided into two parts. The first part deals with the behaviour of variable thickness composite beams. An experimental analysis of three types of beams is described and the results of a correlation study between the model defined in Chapter 6 and this experimental analysis will be shown. The second part of this chapter is devoted to the optimisation of variable thickness composite beams. Solutions for different types of beams, loads and boundary conditions are given.

7.2. Behaviour of variable thickness composite beams

An experimental study has been carried out in order to assess the accuracy of the theoretical model, as well as to find out the influence of the angle of variation of thickness on the strength of a composite plate.

- AS4/3501-6 graphite/epoxy was used for this work.
- The type of testing performed was three point static bending.
- The load rate was 0.06 in/min (0.001524 m/min).
- Three types of specimens were tested. Maximum, minimum thickness and span were the same for the three specimens. The only variable parameter was the angle of variation of thickness:
 - Specimen OLCP_7001. Angle of variation of thickness: 6°.
 - Specimen OLCP_7002. Angle of variation of thickness: 45°.
 - Specimen OLCP_7003. Angle of variation of thickness: 90°.
- The span was 8 in (0.2032 metres).
- The maximum thickness was at the centre of the beam: 0.66 in (0.0167 metres).
- The minimum thickness was at the end of the beam: 0.28 in (0.007 metres).
- Longitudinal and interlaminar strains were measured by using strain gauges. The situation of the gauges is reported in Table 7.1. The choice of the points was carried out as a function of the theoretical analysis. Strain gauges were placed at those points whose strain value was critical, according to the results from the finite element method applied to variable thickness laminated composite plates.

Table 7.1 Co-ordinates x and y of strain gauges. Values are expressed in inches (metres)

POINT	x		y	
1	0.0	(0.0000)	0.100	(0.00254)
2	0.0	(0.0000)	0.200	(0.00508)
3	1.0	(0.0254)	0.350	(0.00889)
4	2.0	(0.0508)	0.415	(0.01054)
5	3.0	(0.0762)	0.600	(0.01524)
6	4.0	(0.1016)	0.510	(0.01295)
7	4.0	(0.1016)	0.350	(0.00889)
8	4.0	(0.1016)	0.000	(0.00000)

According to the results of the study on failure mechanisms, critical strain components are the longitudinal strain ϵ_1 and the interlaminar shear strain ϵ_5 . Therefore, both components are analysed for the three types of specimens described above.

The scheme of the specimen OLCP_7001 is shown in Fig. 7.2. This specimen was made by tapering the inner part of the plate (Fig. 7.4). The angle of change of thickness is 6° . The failure load was 4950 lb (22 000N). The upper surface does not present any failure, in spite of being tapered. Instead of that, a crack appears near the middle plane at the end of the plate where interlaminar shear strains are maximum. The reason for this is that the angle of variation of thickness is very low. A scheme of the situation of the gauges is depicted in Fig. 7.3. The numerical results of the specimen OLCP_7001 are presented in Tables 7.2-7.4. Tables 7.2 and 7.3 show longitudinal and interlaminar shear strains in the critical points for the failure load, respectively. The maximum value is registered in point number 1 ($\epsilon_5=0.0131$).

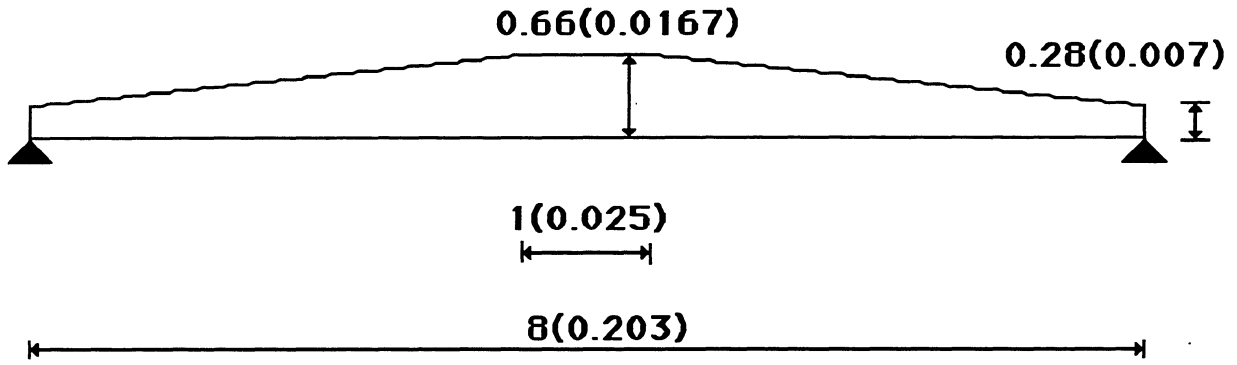


Figure 7.2 Scheme and measurements of specimen OLCp_7001 in inches (metres).

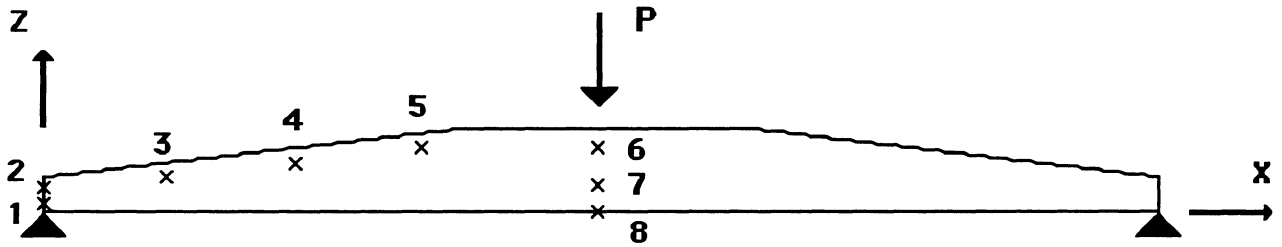


Figure 7.3 Representation of specimen OLCp_7001 and position of gauges.

Table 7.2 Longitudinal strains in specimen OLCp_7001. Load: 4950 lb (22 000 N).

POINT	$\epsilon_1 \times 1E-3$ TESTING	$\epsilon_1 \times 1E-3$ THEORY
8	8.9	8.6

Table 7.3 Interlaminar shear strains in specimen OLCP_7001. Load: 4950 lb (22 000 N).

POINT	$\xi_5 * 1E-3$ TESTING	$\xi_5 * 1E-3$ THEORY
1	13.1 (FAILURE)	12.5
2	9.0	8.1
3	6.3	7.3
4	5.7	6.7
5	4.2	5.8
6	3.7	3.1
7	12.7	12.1

The maximum vertical displacement is reported in Table 7.4. In both fields, strains and displacements, an excellent agreement is found between the data and the prediction.

Table 7.4 Maximum vertical displacement in specimen OLCP_7001. Load: 4950 lb (22 000 N).

POINT	d_z TESTING	d_z THEORY
8	- 0.173 (0.00439)	- 0.161 (0.00409)

The scheme of specimen OLCP_7002 is shown in Fig. 7.5. The angle of change of thickness is 45°. Six steps were designed along the specimen. The failure load was 2960 lb (13 150 N). Owing to the fact that the angle of variation of thickness is high, failure appears at the upper surface in the thinnest area of change of thickness. Failure mechanism is a kind of interlaminar shear mode. As theoretical results predict, there is a peak of interlaminar shear strains in the places where the thickness changes. The position of the gauges is shown in Fig. 7.6. The numerical results of the specimen OLCP_7002 are presented in Tables 7.5-7.7. Tables 7.5 and 7.6 show longitudinal and interlaminar shear strains in the critical points for the failure load, respectively. The maximum value is registered in point number 3 ($\epsilon_5=0.0131$).

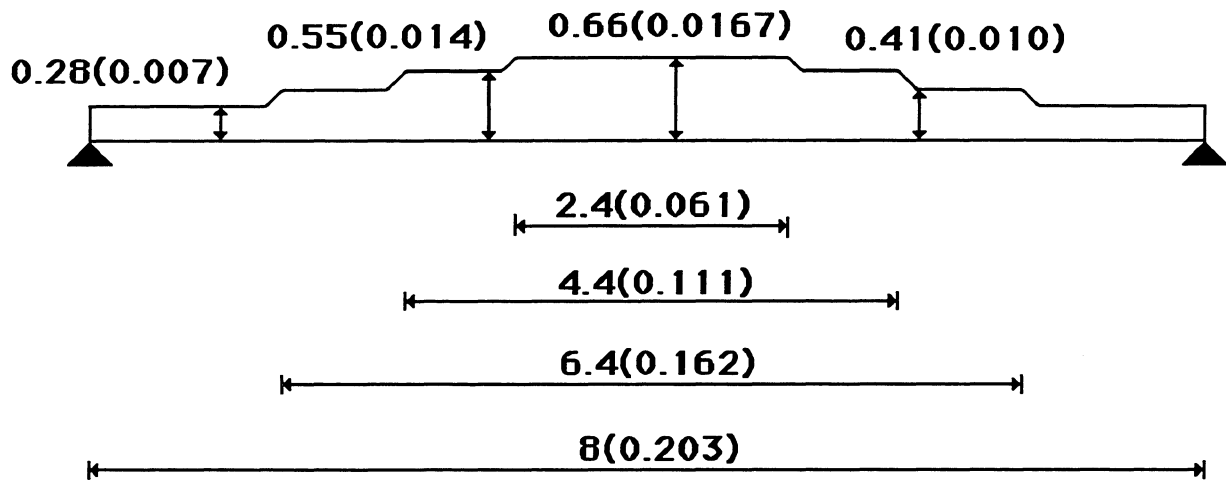


Figure 7.4 Scheme and measurements of specimen OLCP_7002 in inches (metres).

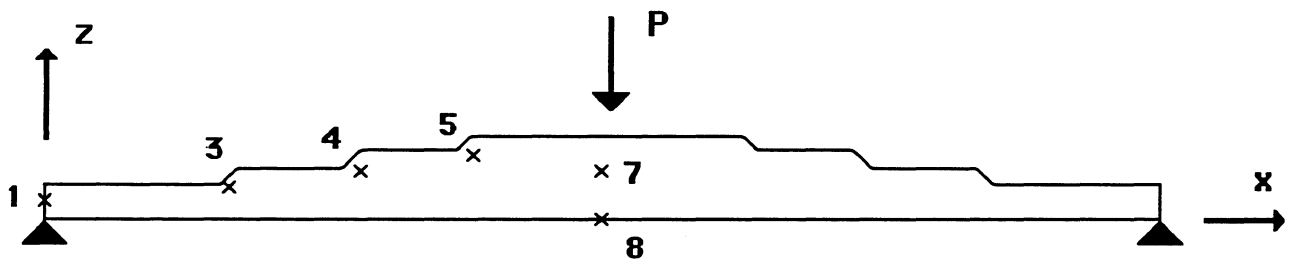


Figure 7.5 Representation of specimen OLCP_7002 and position of gauges.

Table 7.5 Longitudinal strains in specimen OLCP_7002. Load: 2960 lb (13150 N).

POINT	$\epsilon_1 * 1E-3$ TESTING	$\epsilon_1 * 1E-3$ THEORY
8	4.4	3.96

Table 7.6 Interlaminar shear strains in specimen OLCP_7002. Load: 2960 lb (13150 N).

POINT	$\epsilon_5 \times 1E-3$ TESTING	$\epsilon_5 \times 1E-3$ THEORY
1	6.0	5.7
3	13.1 (FAILURE)	12.5
4	11.0	11.6
5	10.0	9.8
7	2.8	2.3

The maximum vertical displacement is reported in Table 7.7. In both fields, strains and displacements, an excellent agreement is found between the data and the prediction.

Table 7.7 Maximum vertical displacement in specimen OLCP_7002. Load: 2960 lb (13150 N).

POINT	d_z TESTING	d_z THEORY
8	- 0.157 (0.004)	- 0.141 (0.0036)

The scheme of specimen OLCP_7003 is shown in Fig. 7.6. The angle of change of thickness is 90°. Six steps were designed along the specimen. The failure load was 2485 lb (11 046 N). Owing to the fact that the angle of variation of thickness is very high, failure appears at the upper surface in the thinnest area of change of thickness at a low failure load. As occurred with specimen OLCP_7002, failure mechanism is a kind of interlaminar shear mode. As theoretical results predict, there is a remarkable peak of interlaminar shear strains in the places where the thickness changes. The position of the situation of the gauges is shown in Fig. 7.8. The numerical results of the specimen OLCP_7003 are presented in Tables 7.8-7.10. Tables 7.8 and 7.9 show longitudinal and interlaminar shear strains in the critical points for the failure load, respectively. The maximum value is registered in point number 3 ($\epsilon_5=0.0139$).

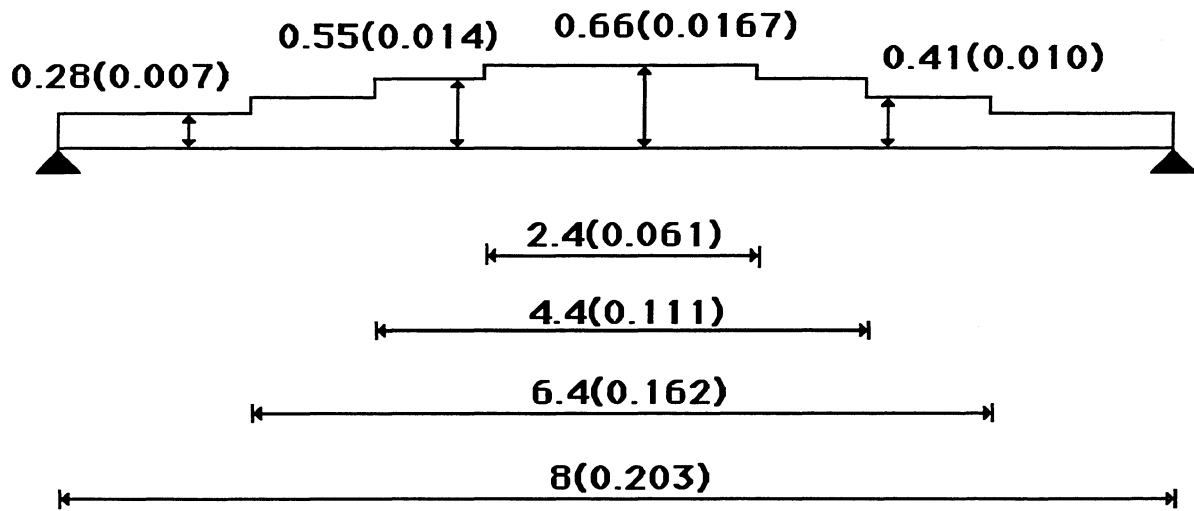


Figure 7.6 Scheme and measurements of specimen OLCP_7003 in inches (metres).

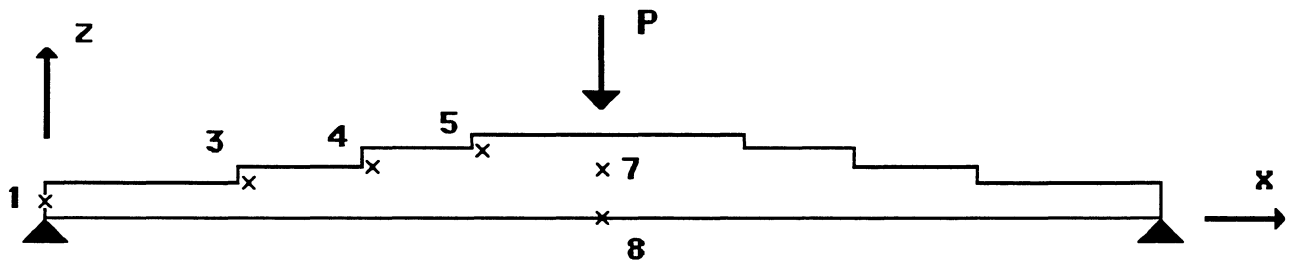


Figure 7.7 Representation of specimen OLCP_7003 and position of gauges.

Table 7.8 Longitudinal strains in specimen OLCP_7003. Load: 2485 lb (11046 N).

POINT	$\epsilon_1 * 1E-3$ TESTING	$\epsilon_1 * 1E-3$ THEORY
8	5.13	4.6

Table 7.9 Interlaminar shear strains in specimen OLCP_7003. Load: 2485 lb (11 046 N).

POINT	$\epsilon_5 * 1E-3$ TESTING	$\epsilon_5 * 1E-3$ THEORY
1	7.25	7.5
3	13.9(Failure)	12.5
4	12.18	11.6
5	11.02	9.8
7	3.77	3.4

The maximum vertical displacement is reported in Table 7.7. In both fields, strains and displacements, an excellent agreement is found between the data and the prediction.

Table 7.10 Maximum vertical displacement in specimen OLCP_7003. Load: 2485 lb (11046 N).

POINT	d_z TESTING	d_z THEORY
8	- 0.171 (0.00432)	- 0.157 (0.004)

Tables 7.11-7.13 show the values of longitudinal, interlaminar shear strains and maxima vertical displacements, respectively, for a load of 1000 lb (4445 N) for the three specimens.

**Table 7.11 Longitudinal strains in specimens OLCP_7001, OLCP_7002 and OLCP_7003.
Load: 1000 lb (4445 N).**

POINT	$\epsilon_1 * 1E-3$ OLCP_7001	$\epsilon_1 * 1E-3$ OLCP_7002	$\epsilon_1 * 1E-3$ OLCP_7003
8	1.78	1.77	1.76

As expected, the longitudinal strains at the inner surface in the middle of the span are very similar for the three specimens tested. The reason for this is that the three specimens present the same thickness at the middle of the span and, therefore, the longitudinal strains and stresses are very close in all three cases.

Table 7.12. Interlaminar shear strains in specimens OLCP_7001, OLCP_7002 and OLCP_7003.
Load: 1000 lb (4445 N).

POINT	$\xi_5 * 1E-3$ OLCP_7001	$\xi_5 * 1E-3$ OLCP_7002	$\xi_5 * 1E-3$ OLCP_7003
1	2.62	2.5	2.4
3	1.26	4.8	5.24
4	1.14	4.2	4.4
5	0.84	3.8	4.0
7	2.54	1.3	1.12

Table 7.12 shows very good results. On the one hand, the maximum values are registered in specimens OLCP_7002 and OLCP_7003, whose angles of variation of thickness present high values (45° and 90°, respectively). On the other hand, in these two cases, the values given by gauges numbers 3, 4 and 5 are critical, which means that the upper surface is the critical one from the failure point of view. However, specimen OLCP_7001 does not present its maximum value in any of these points and, therefore, the tapered surface is not critical at all.

Table 7.13 Maximum vertical displacement in specimens OLCP_7001, OLCP_7002 and OLCP_7003. Load: 1000 lb (4445 N).

POINT	d_z OLCP_7001	d_z OLCP_7002	d_z OLCP_7003
8	- 0.0346 (0.00087)	- 0.059 (0.00149)	-0.0628 (0.00159)

The results reported in Table 7.13 highlight the higher stiffness of specimen OLCP_7001 with respect to the other two. The lower the angle of variation of thickness, the better the fibre works. Hence, according to these results, there is no linearity, and the angle of variation of thickness must be very low in order to get a high quality design from the point of view of stiffness and strength.

Figures 7.8 and 7.9 can be used to compare the distributions of interlaminar strains through the laminate thickness. Both graphs refer to the three-point bending test and the specimen OLCP_7001 described above. Figure 7.9 shows the theoretical and experimental distributions of interlaminar shear strain ξ_5 in section AA. As we can see in Fig. 7.10, section AA corresponds to the end of the beam. This section is critical because the laminate thickness is minimum. Figure 7.9 represents the same distributions of ξ_5 in section BB, at the middle of the span (Fig. 7.10). In both cases, theoretical and experimental distributions are very close.

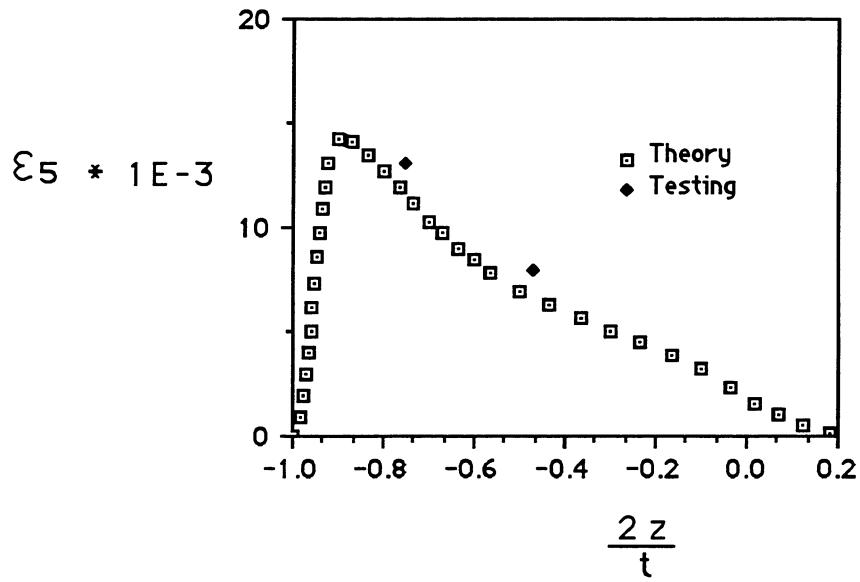


Figure 7.8 Distribution of ϵ_5 through the thickness in section AA

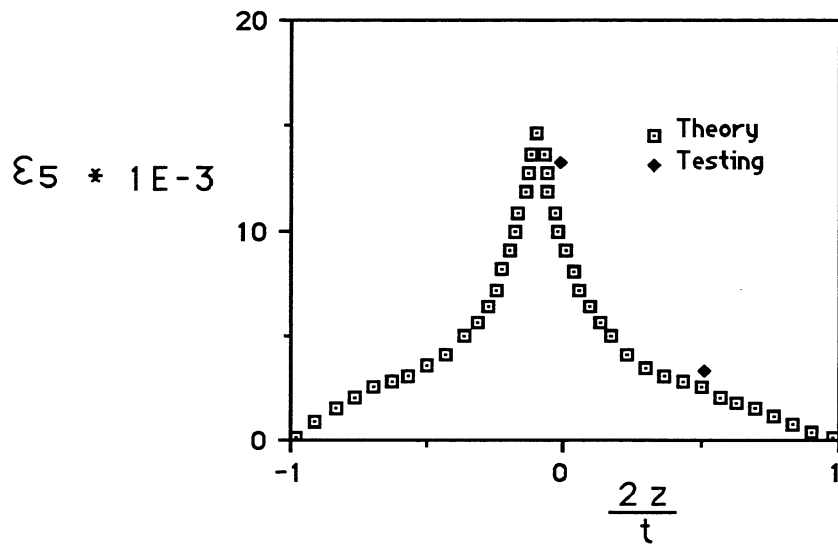


Figure 7.9 Distribution of ϵ_5 through the thickness in section BB.

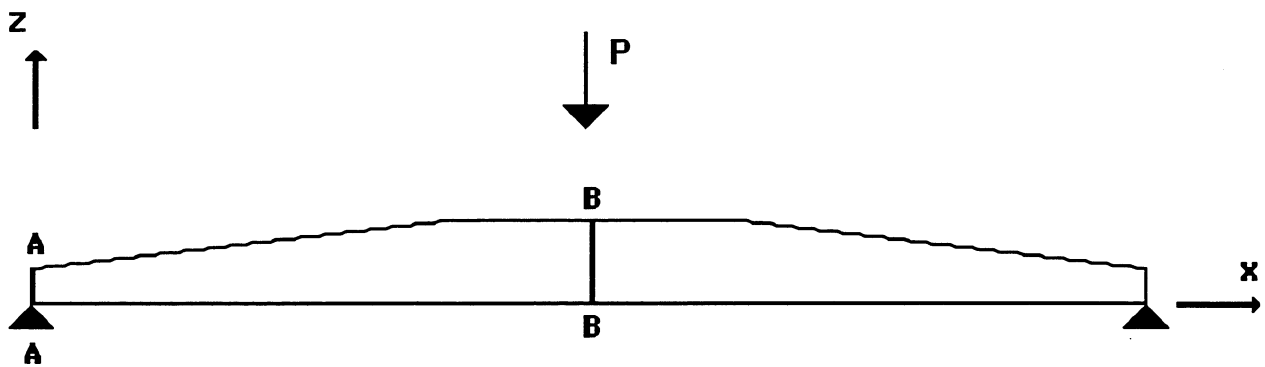


Figure 7.10 Representation of sections AA and BB.

7.3 Optimisation of variable thickness composite beams

The problem analysed here can be formulated by means of the following points:

- The objective is to get the minimum weight structure by using strength as a design criterion.
- The laminate used is $[0]_n$ because it is the optimum for one-dimensional laminated composite plates subjected to transverse loads.
- Two side tapered laminates have been considered.
- Two kinds of plates have been analysed:
 - thin plates ($l/t \gg 10$).
 - thick plates ($l/t \ll 10$).
- Boundary conditions are restricted to:
 - simply supported plates.
 - clamped plates.
 - cantilever plates.
- Two types of loading have been applied:
 - uniform load
 - point load, at the centre of the beam for simply supported and clamped plates, and at the free end of the plate for cantilever plates.
- The mesh was composed by 400 nodes.
- The material used is T300/N5208.

In Fig. 7.11 the definition of axis co-ordinates and the shaded key for one-dimensional plates are shown.

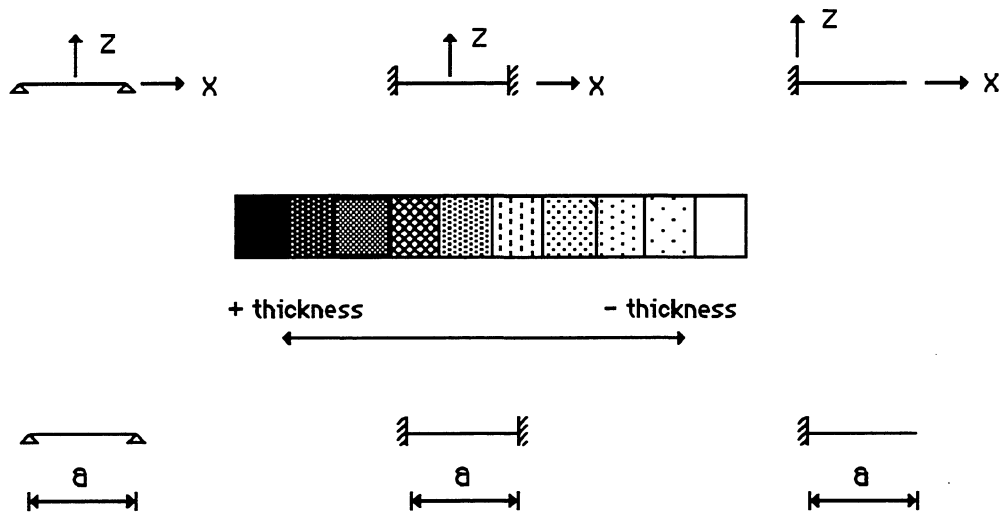


Figure 7.11 Definition of axis co-ordinates and shaded key for one-dimensional plates.

7.3.1 Thin plates subjected to a uniform load

Optimum thin plates subjected to a uniform load are shown in Fig. 7.13. Whatever the boundary conditions, the optimum laminate thickness is:

$$t = 2 k a (P/X)^{1/2} \quad [7.1]$$

where a is the plate span, P is the load applied, X is the uniaxial tensile strength of a ply along the x -axis, and k is a coefficient that varies in function of x . The value of the non-dimensional coefficient k in function of x is given for the following boundary conditions: simply supported, clamped and cantilever one-dimensional plate. Also, the weight savings (WS) are reported for these three cases. The 45.7 % WS for the cantilever plate is remarkable.

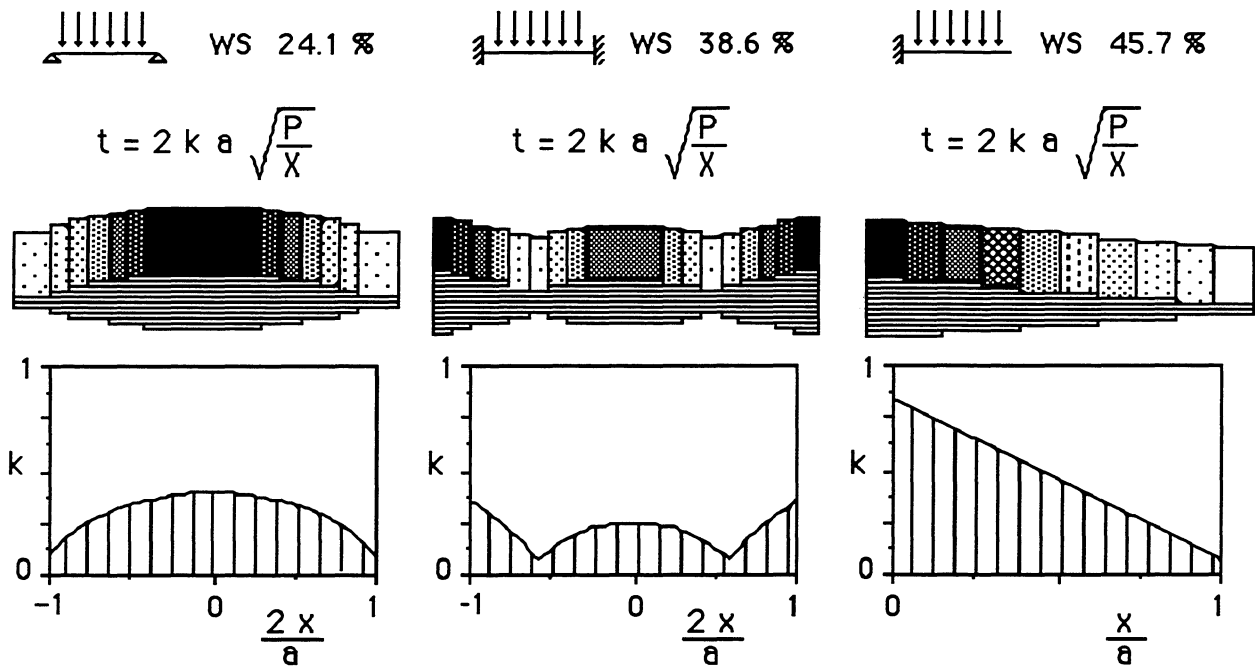


Figure 7.12 Representation of optimal thin one-dimensional plates subjected to a uniform distributed transverse load.

7.3.2. Thick plates subjected to a uniform load

Fig. 7.13 shows the optimum thick plates subjected to a uniform load. In this case, the optimum laminate thickness is:

$$t = 2 k a P/S \quad [7.2]$$

where S is the shear strength in the xy - or 12 -plane of a ply. The value of the non-dimensional coefficient k is a function of x and the optimum configurations are given for the boundary conditions mentioned above. The weight saving is the same for the three boundary conditions: 45.7 %.

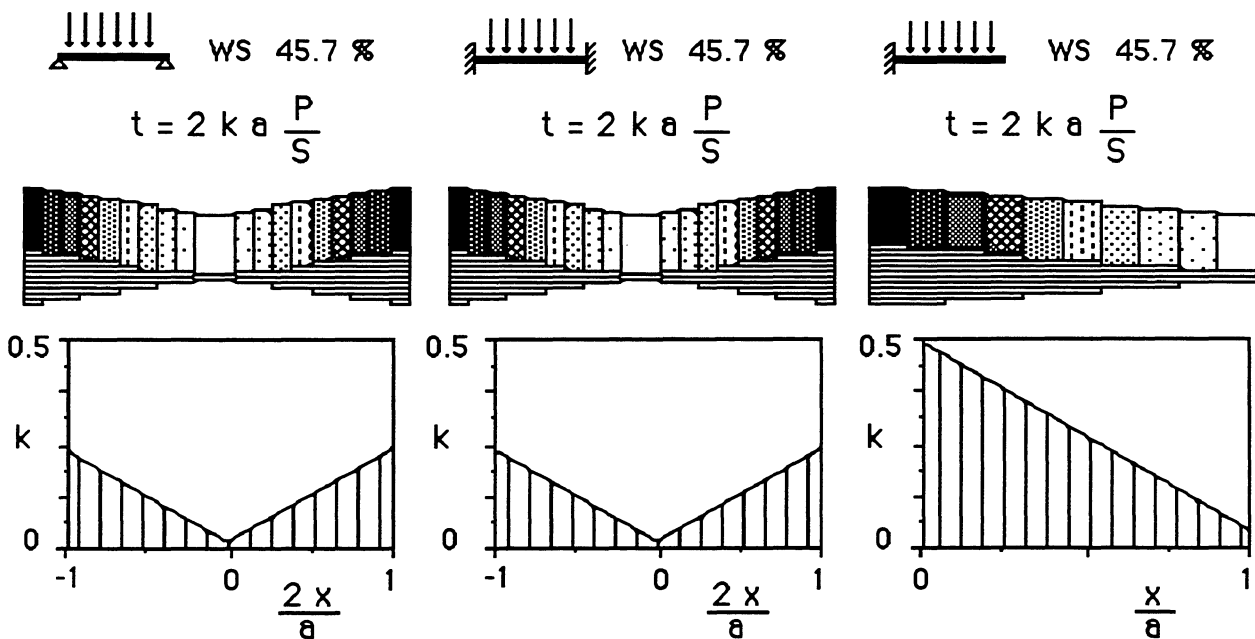


Figure 7.13 Representation of optimal thick one-dimensional plates subjected to a uniform distributed transverse load.

7.3.3 Thin plates subjected to a point load

Optimum thin plates subjected to a point load are shown in Fig. 7.14. Whatever the boundary conditions, the optimum laminate thickness is :

$$t = 2 k (P a/X)^{1/2} \tag{7.3}$$

The value of the non-dimensional coefficient k in function of x is given for the following boundary conditions: simply supported, clamped and cantilever one-dimensional plate. Also, the weight savings (WS) are reported for these three cases. The 44.0 % WS for clamped plates is remarkable.

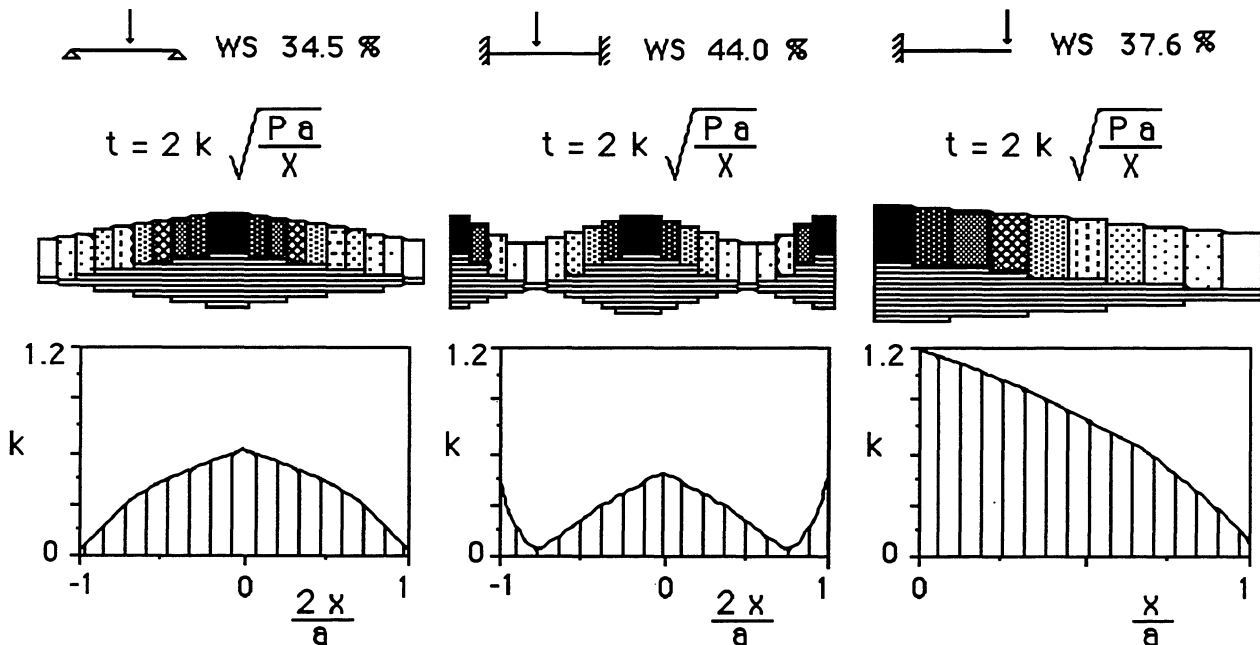


Figure 7.14 Representation of optimal thin one-dimensional plates subjected to a point transverse load.

7.3.4 Thick plates subjected to a point load

Figure 7.15 shows optimal thick plates subjected to a point load. In this case, the optimum laminate thickness is :

$$t = 2 k P/S \tag{7.4}$$

The value of the non-dimensional coefficient k as a function of x and the optimum configurations are given for the boundary conditions mentioned above. There is no weight saving in this case for any boundary conditions.

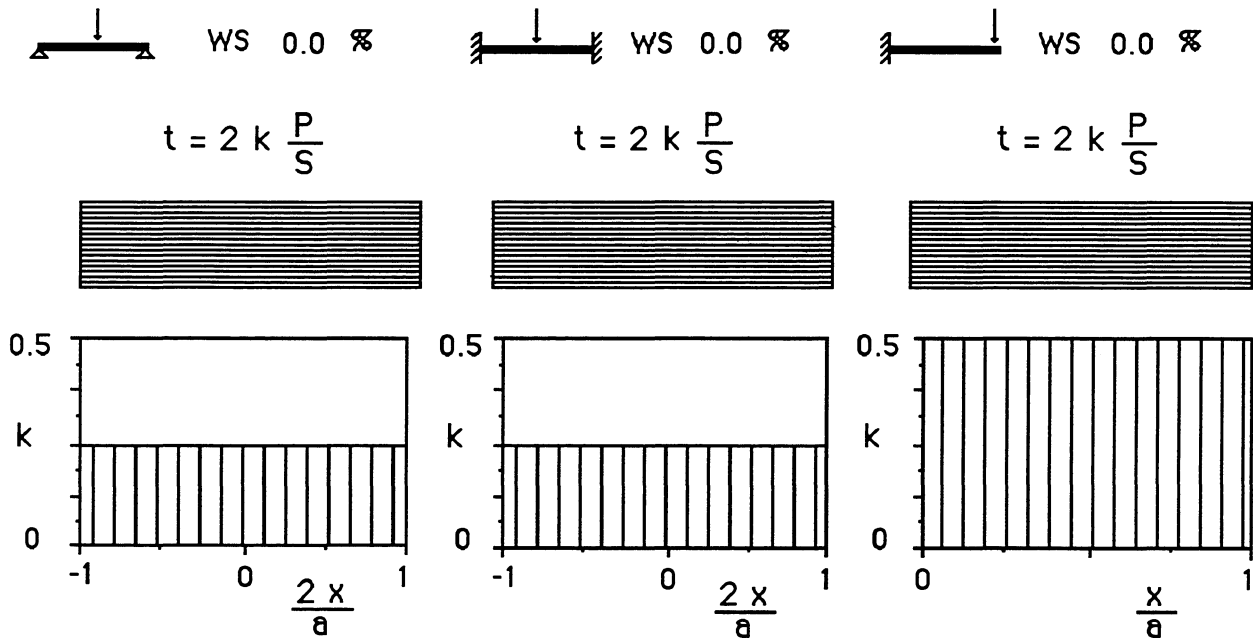


Figure 7.15 Representation of optimal thick one-dimensional plates subjected to a point transverse load.

7.4 Conclusions

The results of the correlation study between the theoretical model and the experimental analysis described in the first part of this chapter are excellent in both fields: deflection and failure mode. Three types of beams were analysed, the difference between them being the angle of variation of thickness. Strain gauge values also reflect an excellent correlation between theoretical and experimental strains.

The main conclusion of this study is that the external part of the beam must be fibre-continuous to avoid delamination at a low stress level. The angle of variation of thickness must be as low as possible. The 90° angle specimen shows very weak resistance in terms of delamination.

Another conclusion of the study described in this chapter is that the critical stress components in terms of failure for high angles of variation of thickness are the interlaminar shear ones. A comparison analysis between theoretical and experimental interlaminar shear stress distributions has been carried out, the conclusion being that the correlation is excellent in the two cross sections considered: at the middle of the span and at the end of the beam.

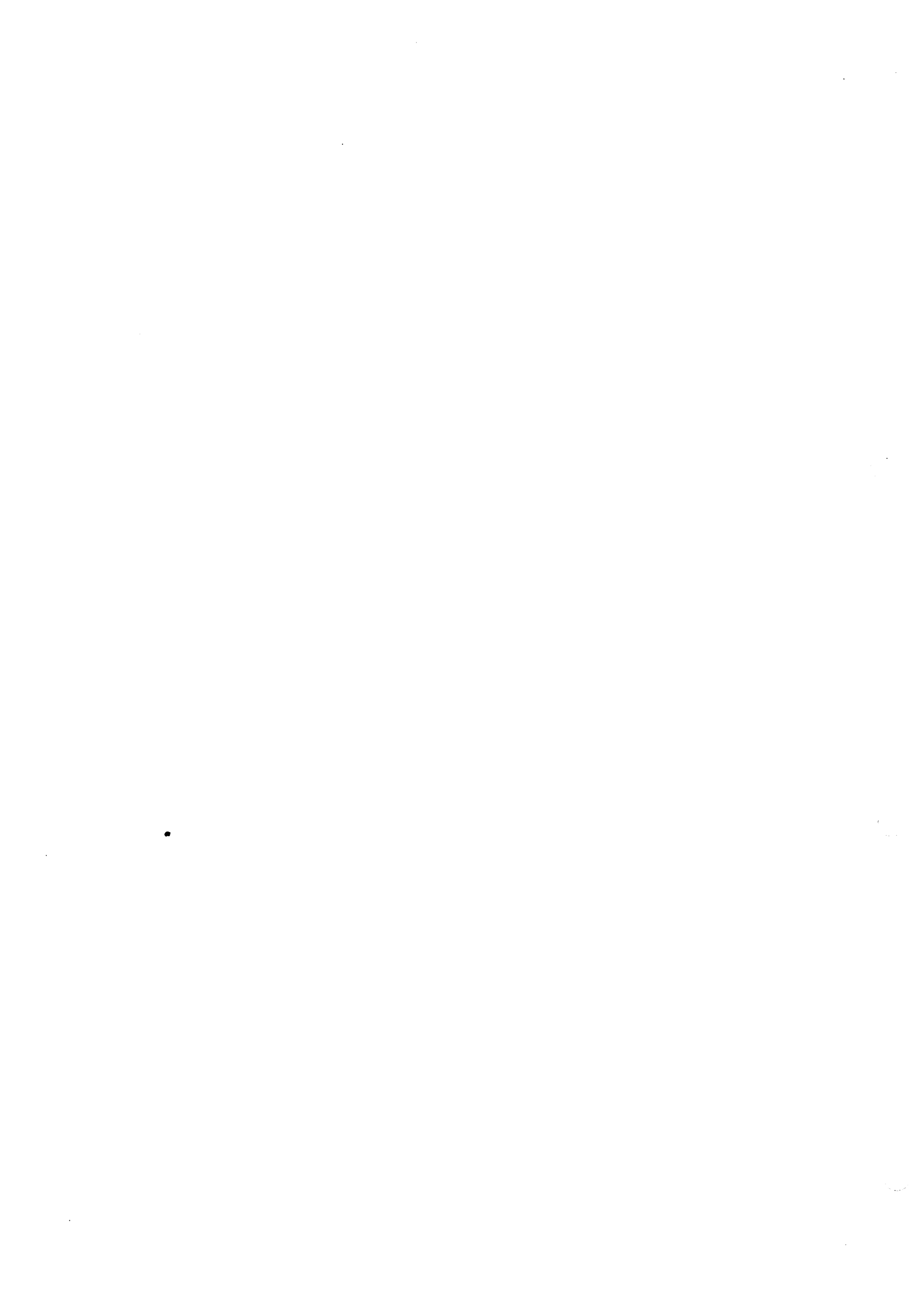
Variable thickness composite beams with different types of transverse loading and boundary conditions have been analysed and optimised throughout this chapter. Analytical solutions have been obtained for all the cases and weight savings and optimum sublaminates are reported. For uniform load and thin beams, the weight savings vary in the range between 45.7 % and 24.1% , depending on the boundary conditions. Thick beams present a 45.7% of weight saving for the three boundary conditions considered.

For uniform load and thin beams, the weight saving varies in the range 44 % and 34.5% , depending on the boundary conditions. Thick beams do not present weight saving with respect to the constant thickness beam for the three boundary conditions considered.

Finally, the weight savings reported are very high but they also depend substantially on these two aspects (boundary conditions, type of beam and load).

References

1. Kicher T P. and Chao T L, 'Minimum weight design of stiffened fiber composite cylinders', Journal of Aircraft, 1971, 7, 562-8.
2. Verette R M, 'Stiffness, Strength and Stability Optimization of Laminated Composite', Report NOR-70-138, Northrop Aircraft Corp., Hawthorne, California, 1970.
3. Morz Z, 'Optimal Design of Structures of Composite Materials', Int. J. Solids & Struct., 1970, 6, 559.
4. Bryzgalin, G J 'On some optimal design criteria of inhomogeneous anisotropic bodies', J. Appl. Maths & Mech., 1972, 36, 716.
5. Love P G and Melchers R E, 'On the theory of optimal constant thickness fiber reinforced plates', Int. J. Mech. Sc., 1972, 19, 311.
6. Lai Y S and Achenbach J D, 'Optimal Design of Layered Structures under Dynamic Loading', Int. J. Mech. Sc., 1973, 3, 559.
7. Khot N S and others, 'Optimization of fiber reinforced composite structures', J. Solids & Struct., 1973, 19, 1225.
8. Schmit Jr L A and Farshi B, 'Optimum laminate design for strength and stiffness', Int. J. Numer. Meth. Eng., 1973, 4, 519.
9. Schmit Jr L A and Farshi B, 'Optimum design of laminated fiber composite plates', Int. J. Numer. Meth. Eng., 1977, 7, 623.
10. Hayashi T, 'Optimization for elastic buckling strength of fiber reinforced composite structures-columns, plates and cylinders', Proc.Soc. Mat. Sc. Japan, 399, 1974.
11. Chao C C and others, 'Optimization of buckling and yield strengths of laminated composites', J. AIAA, 1975, 12, 1131.
13. Hayashi T, 'Optimization Design of Cross- and Angle-Plied Laminated Composite Plates under Compression', Proc. Composite Materials Structures. Japan, pp. 18, 1974.
14. Bert C W, 'Optimal Design of Composite Materials Panels for Business Aircraft Meeting', Wichita, Kansas, Vol.1, 1977.
15. Housner J M and Stein M., 'Numerical Analysis and Parametric Studies of the Buckling of Composite Orthotropic Compression and Shear Panels', NASA TN D-7996, 1975.



8 VARIABLE THICKNESS PLATES

8.1 Introduction

This chapter provides numerical results for variable thickness laminated composite plates. First, the method of analysis used is reported. The conclusions drawn in the last section are the key to the formulation of the present problem. Because the results obtained from the 2-D plane strain model are very close to the data given by the experimental study, this model can be directly applied for analysing one-dimensional laminated composite plates. And that model can also be the base for a more general one, applicable to the analysis of two-dimensional laminated composite plates.

Once the method of analysis is known, the different input data required for the calculation must be obtained. In a structural optimisation problem, there are two types of input data: geometric ones and those related to the material itself. There is no problem in obtaining the geometric data of the plate, but the elastic constants and strengths of the material require special treatment. In-plane constants are given in the literature though some doubt exists with regard to compression strength. However, through-thickness properties are difficult to obtain, and even some constants like interlaminar normal and interlaminar shear moduli are a function of the stacking sequence. Therefore, the elastic constants and strengths will be obtained for the material used in this work.

Finally, variable thickness laminated composite plates are studied, and a number of figures will show the optimum configurations for different types of plates, loads and boundary conditions. References 1-21 give some information about the analysis of variable thickness plates.

8.2 Model assumptions and method of analysis

In the last chapter, a 2-D plane strain model was verified by means of an experimental study. Hence, there are two options to optimise bidimensional plates:

- Generalising to a 3-D model, by using a tridimensional finite element theory.
- Using a 2-D model, by applying a shear deformation plate theory.

The first option is expensive, especially from the point of view of the optimisation and, therefore, the subsequent application of an iterative procedure. The second option is efficient, because the analysis is carried out very fast and the required number of nodes of the mesh is not large. However, the following question remains to be answered: is the 2-D shear deformation plate theory accurate enough to study bidimensional plates with variable thickness? This question has two possible answers:

- If the angle of variation of thickness is 90° , there are discontinuities in the exterior surface(s) of the laminated composite plates, there are free-edge effects, and a 3-D finite element theory should be used.
- If the angle of variation of thickness is low, and the plate exterior surfaces are continuous, as shown in Fig. 8.1, a bidimensional plate with variable thickness can be studied very accurately by means of a 2-D shear deformation theory. This fact is based on a number of verifications made between 2-D plane strain models and 1-D models using a shear deformation plate theory. In all cases, deflections were very close and,

according to the conclusions of failure mechanisms, the critical stress components σ_1 and σ_5 presented very small differences. One verification is presented in Fig. 8.1-8.3. The geometry is shown in Fig. 8.1. In Fig. 8.2 and 8.3, distributions of σ_1 and σ_5 from both models are depicted, respectively.

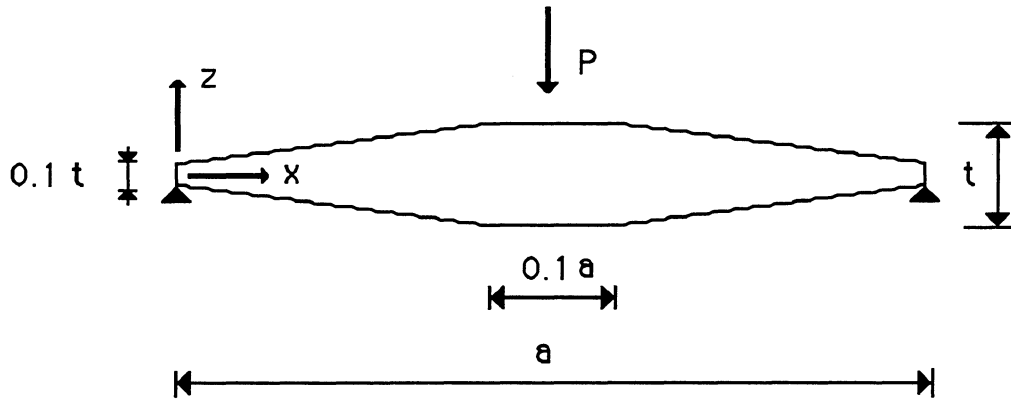


Figure 8.1 Structure used to compare both 2-D plane strain model and shear deformation plate model.

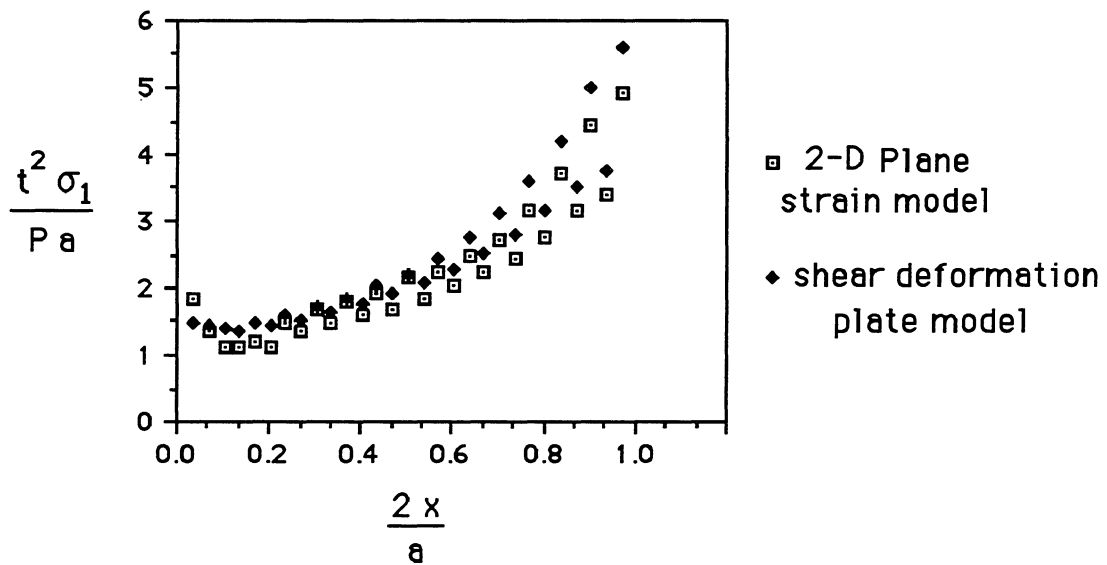


Figure 8.2 Distribution of σ_1 through the thickness from a 2-D plane strain model and a shear deformation plate model.

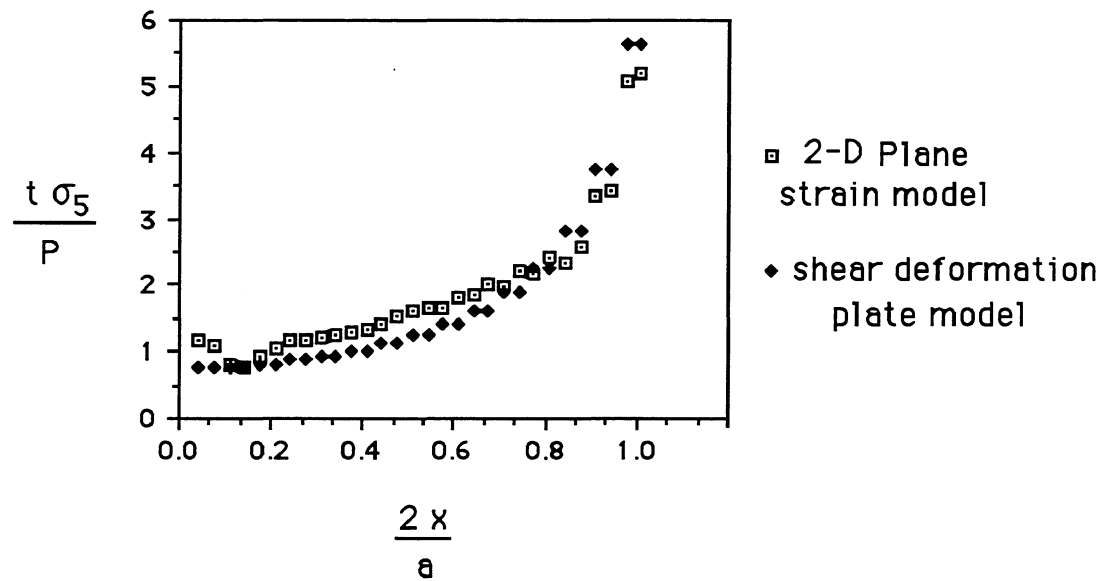


Figure 8.3 Distribution of σ_5 through the thickness from a 2-D plane strain model and a shear deformation plate model.

Both theoretical and experimental studies about variable thickness (Section 3.2) showed that the angle of variation of thickness has a strong influence on the failure load, and that the lower the angle, the higher the failure load. Hence, it is logical to design tapered plates with low angles of variation of thickness and continuous exterior surfaces. In this case, a 2-D shear deformation plate theory is applicable.

The finite element used here is based on the higher order shear theory [22] and on the penalty function theory. This scheme makes it possible to analyse thin and thick plates, due to its general formulation. The results given by the finite element method are optimised by means of an iterative procedure. Laminate thickness and fibre orientation are the design variables. Laminate thickness is modified in each step by means of an iterative procedure based on optimality criteria to design a minimum weight structure. In order to assess the stress level, a quadratic failure criterion is applied in each element. If the stresses in all the elements satisfy this criterion, the process is over. If they do not, another iteration starts. Usually, around ten iterations are needed to achieve convergence.

The optimisation of fibre orientations is complex due to the following points:

- Due to practical considerations, only four angles have been used : 0° , 45° , -45° and 90° .
- Also due to practical considerations, the optimum laminate should be defined as a function of repetitive sublaminates.
- The stacking sequence has a strong influence on the strain and stress level, due to bending and interlaminar effects.

No acceptable result was obtained by using the optimisation procedures available. Hence, since the 2-D shear deformation model is so fast and is able to consider discrete variables, all the possible combinations were tried as

possible optimum sublaminates.

Finally, the following assumptions have been made in the development of the analysis:

- The analysis is static.
- The theory applied is valid for small deformations.
- The material used is supposed to be elastic.

8.3 Determination of elastic constants and strengths

The analysis and optimisation of a composite structure require the determination of elastic constants and strengths. T300/N5208 is a unidirectional graphite/epoxy laminate. Thus, each layer can be considered as a transversely isotropic material. The stiffness matrix for such material is represented in Table 8.1. There are 5 independent constants and 12 non-zero components.

Table 8.1 Stiffness matrix for a transversely isotropic material

	ϵ_1	ϵ_2	ϵ_3	ϵ_4	ϵ_5	ϵ_6
σ_1	C_{11}	C_{12}	C_{12}	0	0	0
σ_2	C_{21}	C_{22}	C_{23}	0	0	0
σ_3	C_{21}	C_{32}	C_{22}	0	0	0
σ_4	0	0	0	$(C_{22} - C_{23})/2$	0	0
σ_5	0	0	0	0	C_{66}	0
σ_6	0	0	0	0	0	C_{66}

The five independent constants present the following values :

C_{11}	=	181.8	GPa
C_{12}	=	2.90	GPa
C_{22}	=	10.35	GPa
C_{23}	=	7.05	GPa
C_{66}	=	7.17	GPa

For a laminate, the components that relate σ_3 / ϵ_3 and σ_5 / ϵ_5 are a function of the stacking sequence. According to Roy and Tsai,² Fig. 8.4 gives some values of the interlaminar normal modulus as a function of m and n in a laminate T300/N5208 $[90_m / 0_n]_s$.

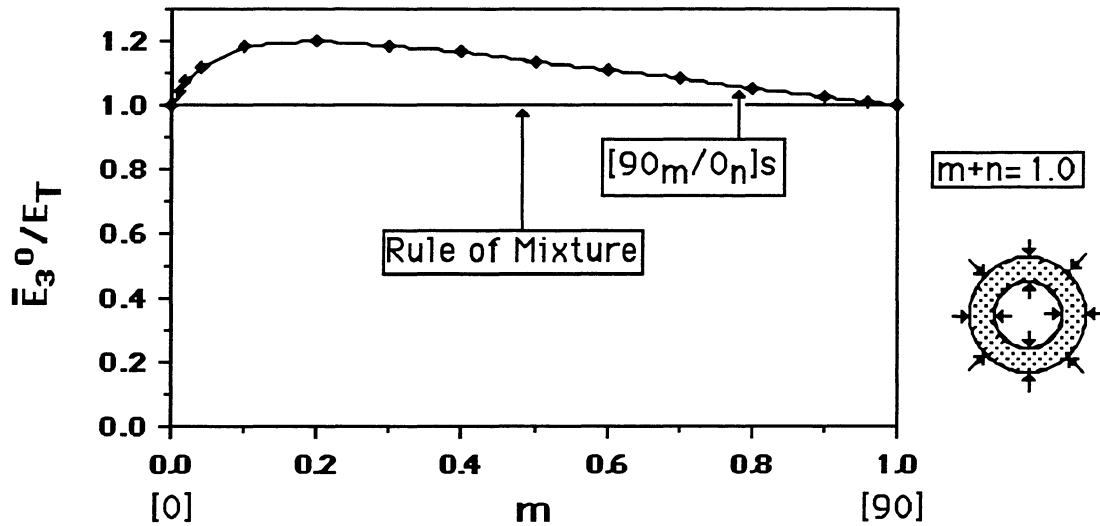


Figure 8.4 Variation of interlaminar normal modulus as a function of m and n in a laminate T300/N5208 $[90_m/0_n]_s$.

Figure 8.5 shows the variation of the interlaminar shear modulus as a function of ϕ in a laminate T300/N5208 $[+\phi/-\phi]_s$.

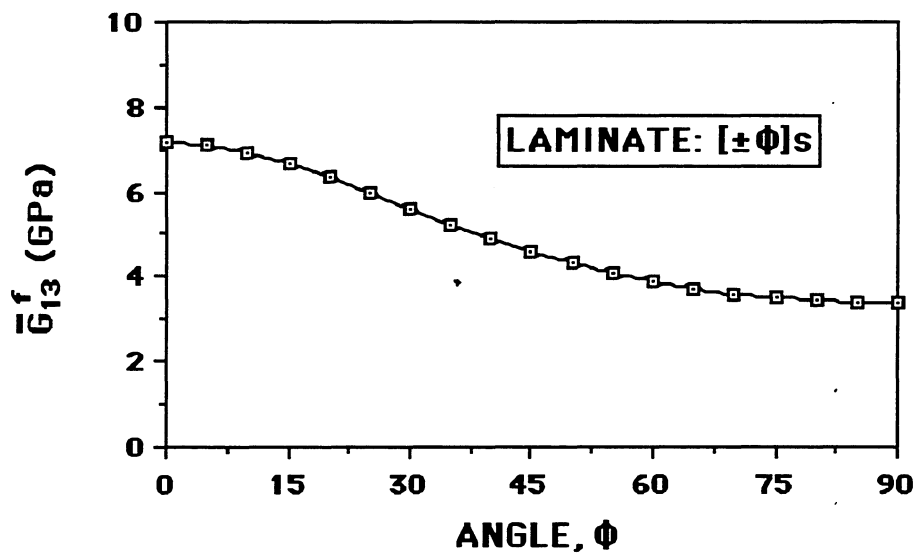


Figure 8.5 Variation of interlaminar shear modulus as a function of ϕ in a laminate T300/N5208 $[+\phi/-\phi]_s$.

The strengths for this material are given by the following values:

X	=	1500	MPa
X'	=	1500	MPa
Y	=	40	MPa
Y'	=	246	MPa
Z	=	40	MPa
Z'	=	246	MPa
S	=	68	MPa

$$S' = 68 \text{ MPa}$$

8.4 Optimisation of variable thickness laminated composite plates

The problem analysed here can be formulated by the following:

- The objective is to get the minimum weight structure by using strength as a design criterion.
- The laminate used is $[0]_n$ because it is the optimum for one-dimensional laminated composite plates subjected to transverse loads.
- Two side tapered laminates have been considered.
- Two kinds of plates have been analysed:
 - thin plates ($l/t > 10$);
 - thick plates ($l/t < 10$).
- Boundary conditions are restricted to :
 - simply supported plates along the four edges of the plate.
 - clamped plates along the four edges of the plate.
- Two types of loading have been applied:
 - uniform load;
 - point load, at the centre of the plate for simply supported and clamped plates, and at the free end of the plate for cantilever plates.
- The mesh was composed by 400 nodes.
- The material used is T300/N5208.

8.4.1 Thin, simply supported plates subjected to a uniform load

Weight saving and normalised deflection for thin, simply supported, uniform loaded plates are shown in Fig. 8.7. As we can see, the weight saving is a function of the aspect ratio, the maximum value being 27% for a square plate. The optimum sublaminates also varies as a function of the aspect ratio:

- $[45/-45]$ for b/a between 1 and 1.75.
- $[0/45/-45]$ for b/a between 1.75 and 2.25.
- $[0_5/45/-45]$ for b/a between 2.25 and 3.5.

- [0] for b/a higher than 3.5.

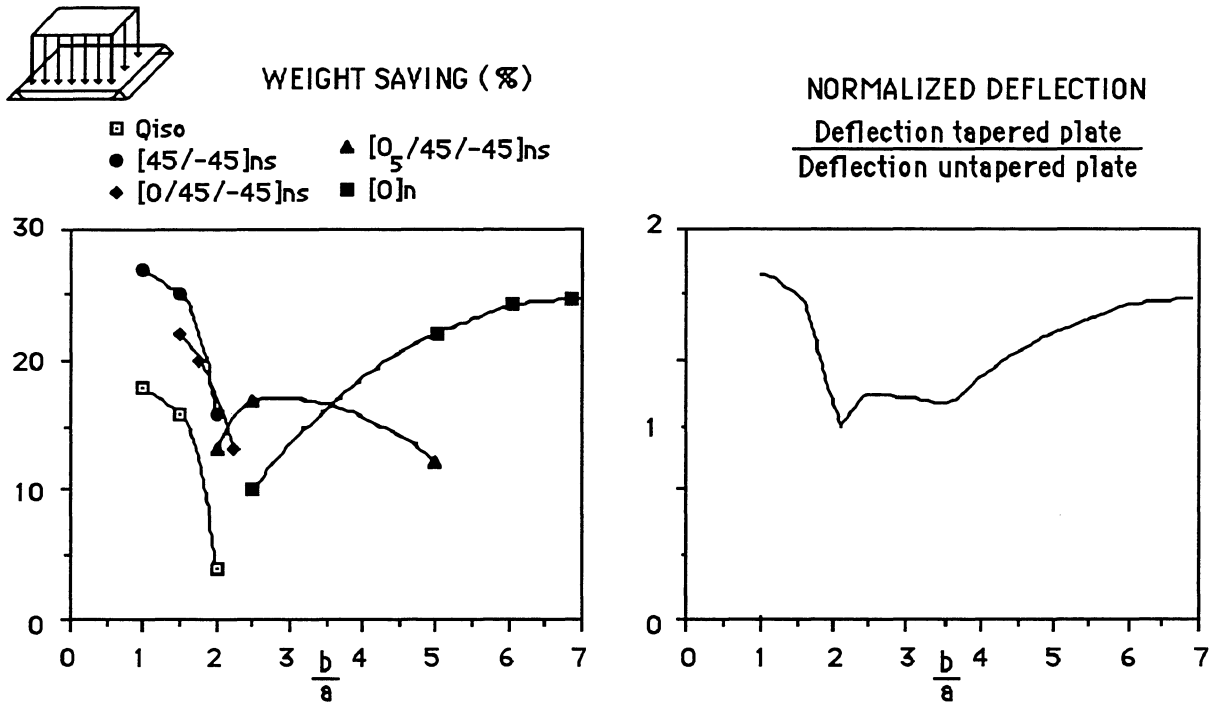


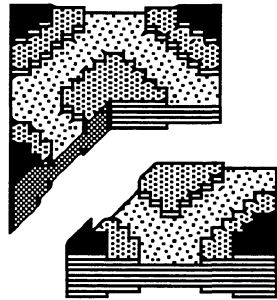
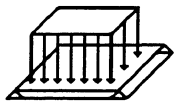
Figure 8.6 Weight saving and normalised deflection for a thin, simply supported plate subjected to a uniform distributed transverse load.

The quasi-isotropic sublaminate [0/45/-45/90] presents low weight saving with respect to other sublaminates, the maximum value being 18% for a square plate.

For thin plates, the optimum laminate thickness can be calculated by means of the following expression:

$$t = 2 k a (P/X)^{1/2} \quad [8.1]$$

where a is the length of the plate, P is the load applied, X is the uniaxial tensile strength of a ply along the x -axis, and k is a non-dimensional coefficient that is a function of x and y . We can see the values of k along the x -axis and the diagonal in Fig. 8.7-8.10.



$$1 \leq \frac{b}{a} < 1.75$$

OPTIMUM SUBLAMINATE
[45/-45]

$$t = 2 k a \sqrt{\frac{P}{X}}$$

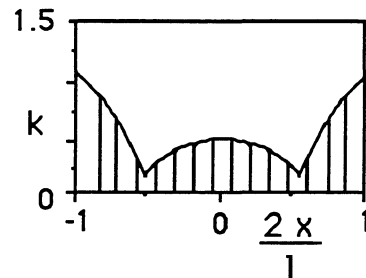
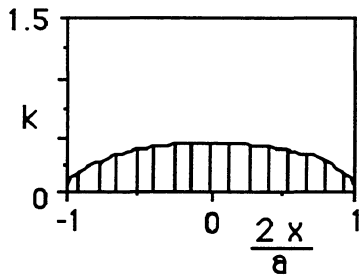
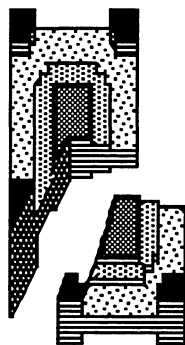
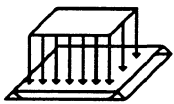


Figure 8.7 Representation of an optimal thin, simply supported plate subjected to a uniform distributed transverse load for aspect ratios between 1 and 1.75.



$$1.75 \leq \frac{b}{a} < 2.25$$

OPTIMUM SUBLAMINATE
[0/45/-45]

$$t = 2 k a \sqrt{\frac{P}{X}}$$

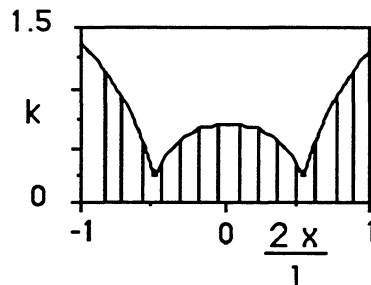
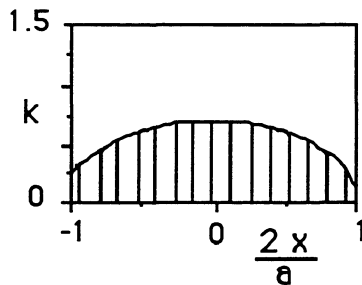
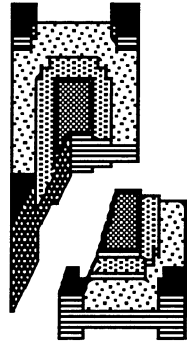
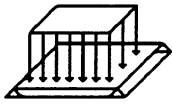


Figure 8.8 Representation of an optimal thin, simply supported plate subjected to a uniform distributed transverse load for aspect ratios between 1.75 and 2.25.



$$2.25 \leq \frac{b}{a} < 3.5$$

OPTIMUM SUBLAMINATE
[0₅/45/-45]

$$t = 2 k a \sqrt{\frac{P}{X}}$$

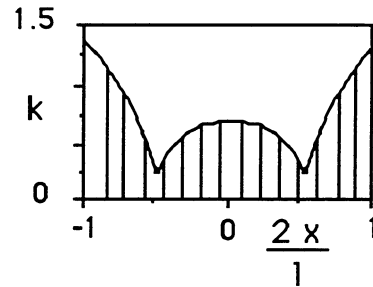
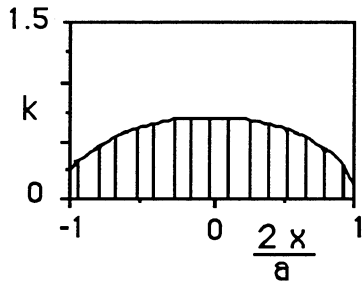
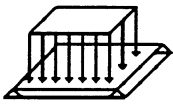


Figure 8.9 Representation of an optimal thin, simply supported plate subjected to a uniform distributed transverse load for aspect ratios between 2.25 and 3.5.



$$3.5 \leq \frac{b}{a}$$

OPTIMUM SUBLAMINATE
[0]

$$t = 2 k a \sqrt{\frac{P}{X}}$$

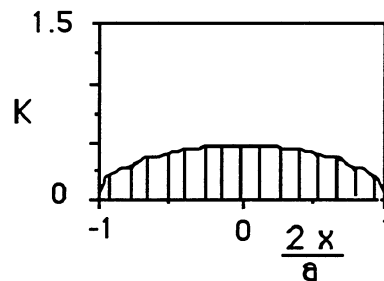


Figure 8.10 Representation of an optimal thin, simply supported plate subjected to a uniform distributed transverse load for aspect ratios higher than 3.5.

8.4.2 Thin, clamped plates subjected to a uniform load

Results for thin, clamped, uniform loaded plates are represented in Fig. 8.12. The weight saving with respect to the constant thickness plate is a function of the aspect ratio, the maximum value being 48% for $b/a=2$. The optimum sublaminar also varies as a function of the aspect ratio:

- $[0/90]$ for b/a between 1 and 1.5.
- $[0_5/90_2]$ for b/a between 1.5 and 4.4
- $[0]$ for b/a higher than 4.4

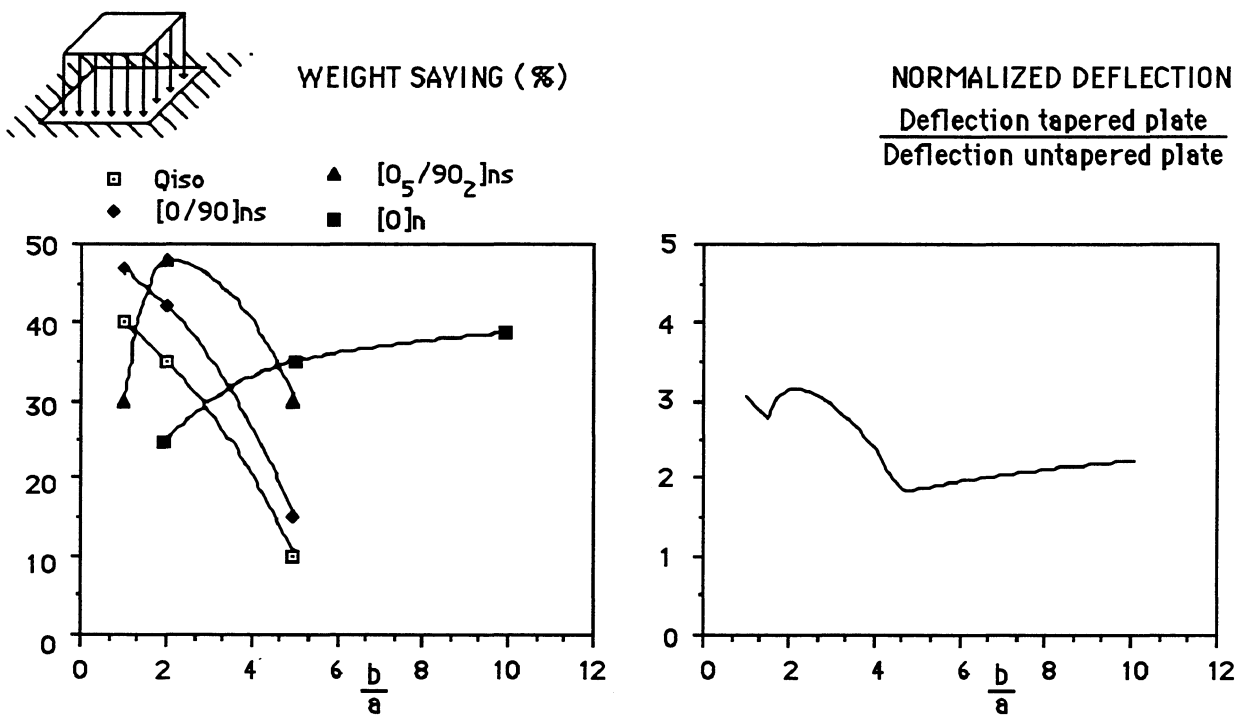
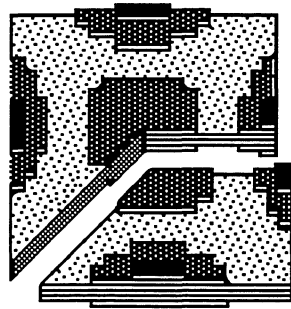
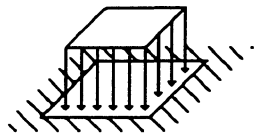


Figure 8.11 Weight saving and normalised deflection for a thin, clamped plate subjected to a uniform distributed transverse load.

The values of the non-dimensional parameter k along the x-axis and the diagonal are shown in Fig. 8.12-8.14.



$$1 \leq \frac{b}{a} < 1.5$$

OPTIMUM SUBLAMINATE
[0/90]

$$t = 2 k a \sqrt{\frac{P}{X}}$$

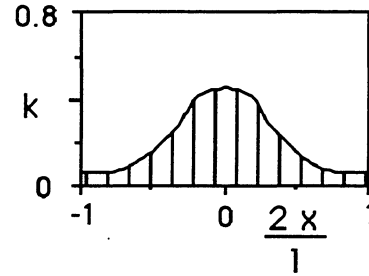
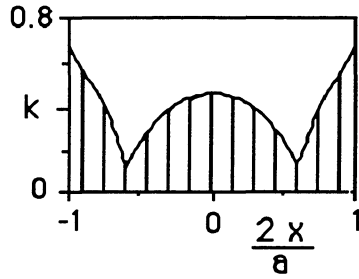
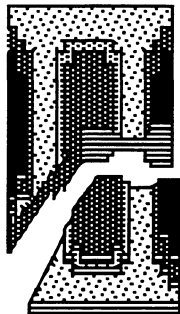
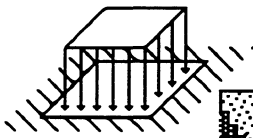


Figure 8.12 Representation of an optimal thin, clamped plate subjected to a uniform distributed transverse load for aspect ratios between 1 and 1.5.



$$1.5 \leq \frac{b}{a} < 4.4$$

OPTIMUM SUBLAMINATE
[0₅/90₂]

$$t = 2 k a \sqrt{\frac{P}{X}}$$

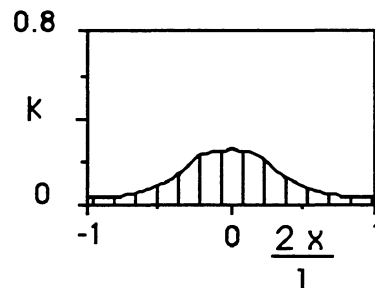
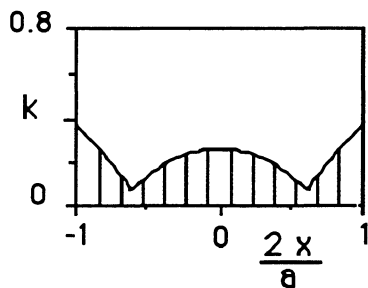
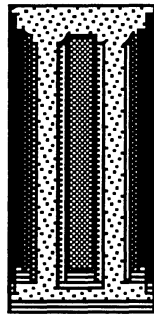
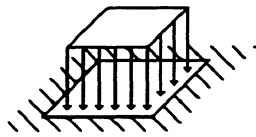


Figure 8.13 Representation of an optimal thin, clamped plate subjected to a uniform distributed transverse load for aspect ratios between 1.5 and 4.4.



$$4.4 \leq \frac{b}{a}$$

OPTIMUM SUBLAMINATE
[0]

$$t = 2 k a \sqrt{\frac{P}{X}}$$

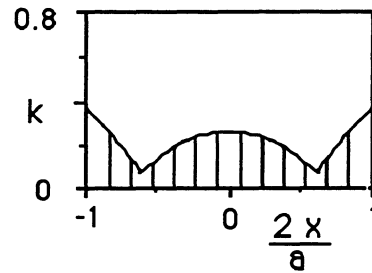
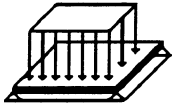


Figure 8.14 Representation of an optimal thin, clamped plate subjected to a uniform distributed transverse load for aspect ratios higher than 4.4.

8.4.3 Thick, simply supported plates subjected to a uniform load

Thick, simply supported, uniform loaded plates are analysed in Fig. 8.15. The maximum value of the weight saving with respect to the constant thickness plate is 46% for $b/a=10$. The optimum sublaminate also varies as a function of the aspect ratio:

- [45/-45] for b/a between 1 and 3.5.
- [0] for b/a higher than 3.5



WEIGHT SAYING (%)

- Qiso
- ◆ [45/-45]_{ns}
- ▲ [0]_n

NORMALIZED DEFLECTION

$\frac{\text{Deflection tapered plate}}{\text{Deflection untapered plate}}$

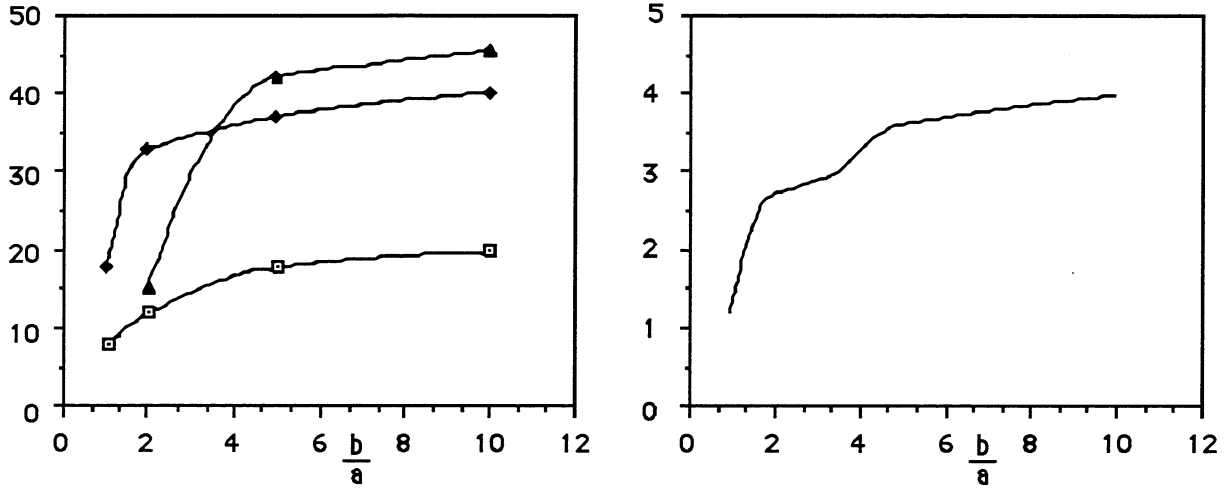


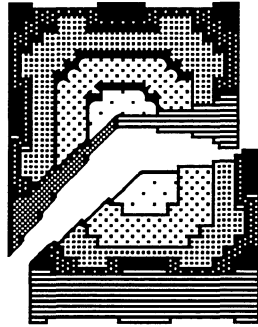
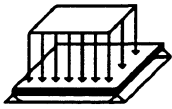
Figure 8.15 Weight saving and normalised deflection for a thick, simply supported plate subjected to a uniform distributed transverse load.

The quasi-isotropic sublaminate [0/45/-45/90] presents low weight saving with respect to other sublaminate, the maximum value being 20% for $b/a=10$.

For thick plates, the optimum laminate thickness can be calculated by means of the following expression:

$$t = 2 k a P/S \quad [8.2]$$

We can see the values of the non-dimensional parameter k along the x-axis and the diagonal in Fig. 8.16 to 8.17 .



$$1 \leq \frac{b}{a} < 3.5$$

OPTIMUM LAMINATE
[45/-45]_s

$$t = 2 k a \frac{P}{S}$$

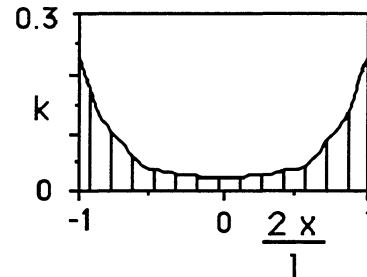
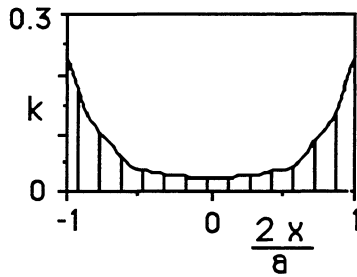
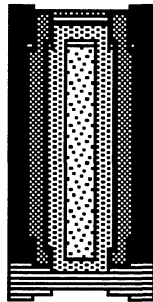
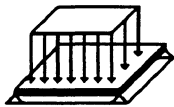


Figure 8.16 Representation of an optimal thick, simply supported plate subjected to a uniform distributed transverse load for aspect ratios between 1 and 3.5.



$$3.5 \leq \frac{b}{a}$$

OPTIMUM SUBLAMINATE
[0]

$$t = 2 k a \frac{P}{S}$$

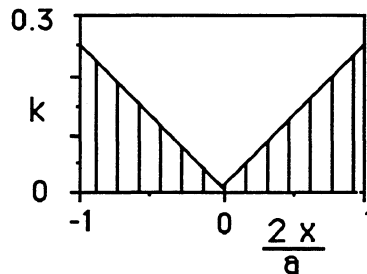


Figure 8.17 Representation of an optimal thick, simply supported plate subjected to a uniform distributed transverse load for aspect ratios higher than 3.5.

8.4.4 Thick, clamped plates subjected to a uniform load

Weight saving and normalised deflection for thick, clamped, uniform loaded plates are shown in Fig. 8.18. As we can see, the weight saving is a function of the aspect ratio, the maximum value being 46% for $b/a=10$. The optimum sublaminates also varies as a function of the aspect ratio:

- [45/-45] for b/a between 1 and 3.5.
- [0] for b/a higher than 3.5

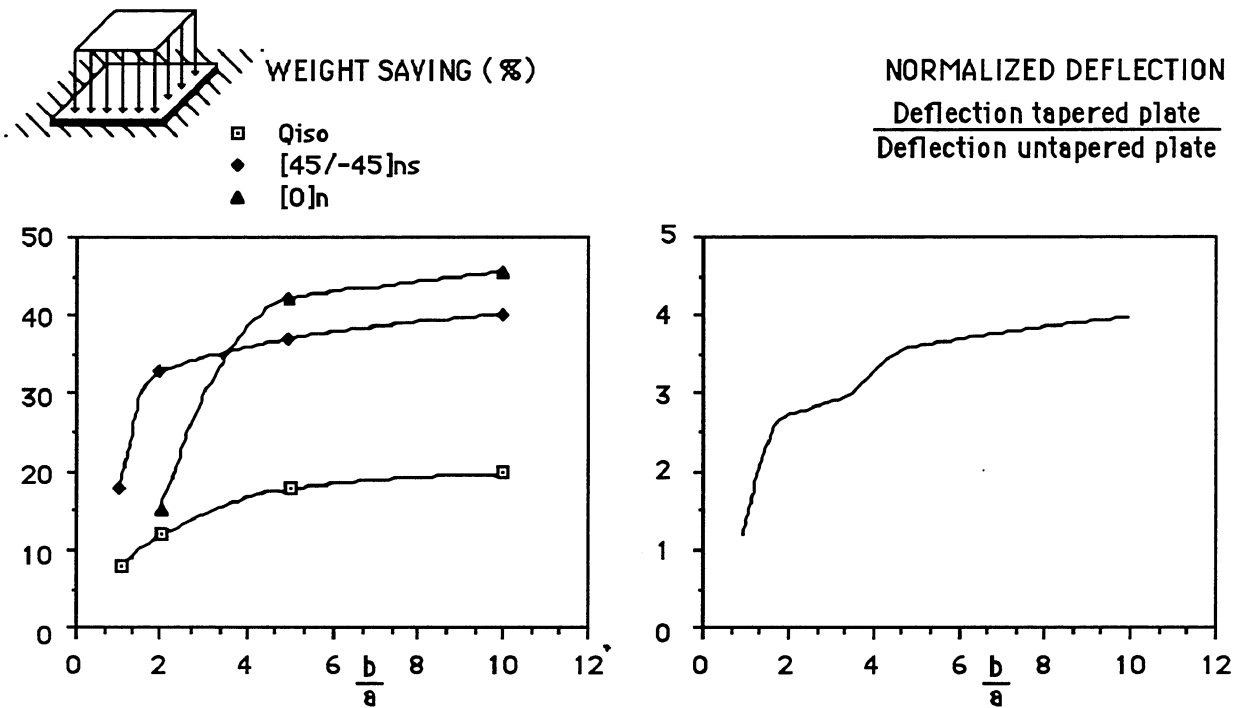
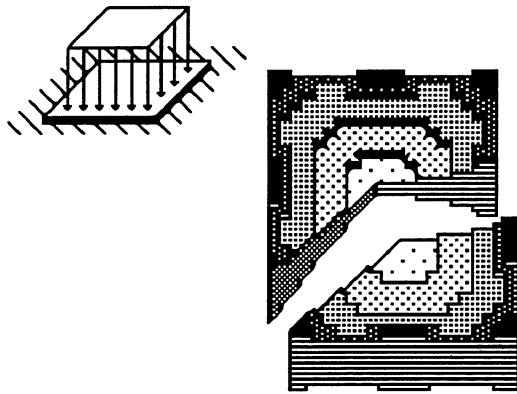


Figure 8.18 Weight saving and normalised deflection for a thick, clamped plate subjected to a uniform distributed transverse load.

We can see the values of the non-dimensional parameter k along the x-axis and the diagonal in Fig. 8.20 to 8.21.



$$1 \leq \frac{b}{a} < 3.5$$

OPTIMUM LAMINATE
[45/-45]_s

$$t = 2 k a \frac{P}{S}$$

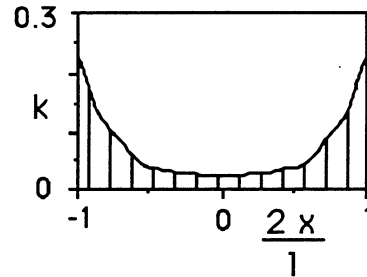
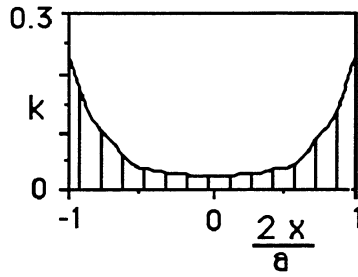
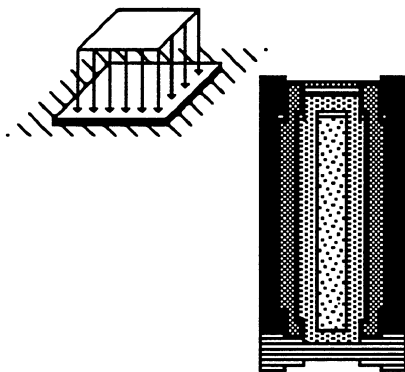


Figure 8.19 Representation of an optimal thick, clamped plate subjected to a uniform distributed transverse load for aspect ratios between 1 and 3.5.



$$3.5 \leq \frac{b}{a}$$

OPTIMUM SUBLAMINATE
[0]

$$t = 2 k a \frac{P}{S}$$

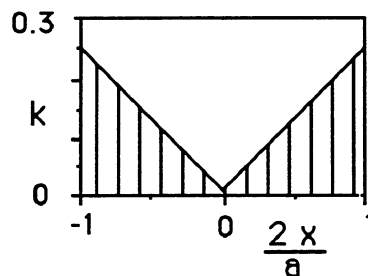


Figure 8.20 Representation of an optimal thick, clamped plate subjected to a uniform distributed transverse load for aspect ratios higher than 3.5.

8.4.5 Thin, simply supported plates subjected to a point load

Thin, simply supported plates subjected to a point load are analysed in Fig. 8.21. The weight saving is a function of the aspect ratio, the maximum value being 76% for $b/a=2$. The optimum sublaminates are $[0]_n$ for all plate aspect ratios analysed.

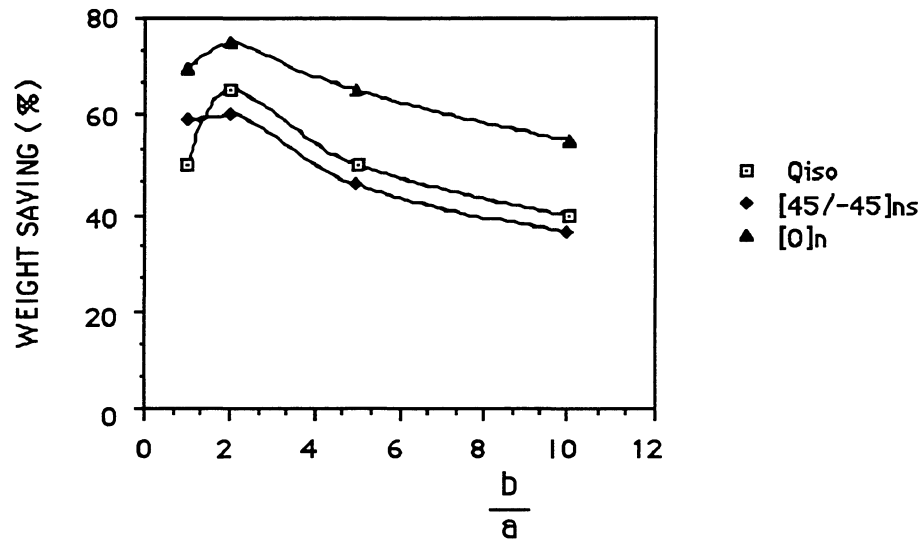
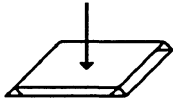


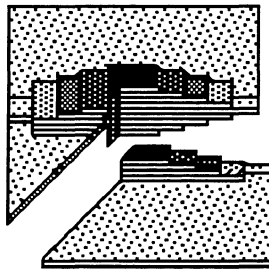
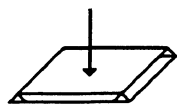
Figure 8.22. Weight saving for a thin, simply supported plate subjected to a point transverse load.

The quasi-isotropic sublaminates $[0/45/-45/90]_n$ presents low weight saving with respect to the optimum sublaminates, the maximum value being 63% for $b/a=2$.

Since no general formula for expressing the optimum laminate thickness has been found, the following particular case has been calculated:

- $a=7.87$ in (0.2 m)
- $P=1.125 \text{ E}4$ lb (5 E4 N)

In Fig. 8.22-8.24, we can see the values of the thickness in metres along the x-axis and the diagonal.



$$1 \leq \frac{b}{a} < 2$$

OPTIMUM LAMINATE
[0]

$$a = 0.2 \text{ m}$$

$$P = 5.0 \text{ E4 N}$$

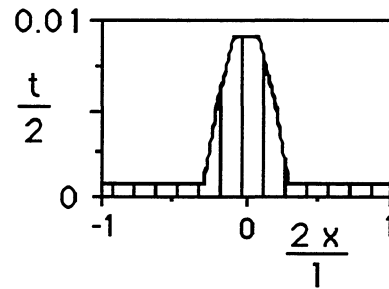
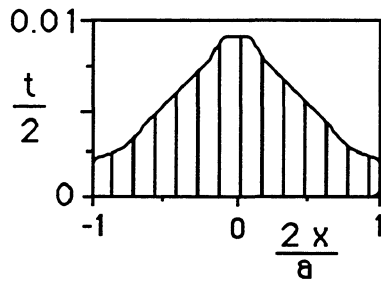
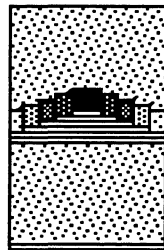
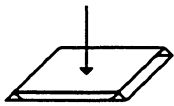


Figure 8.22 Representation of an optimal thin, simply supported plate subjected to a point transverse load for aspect ratios between 1 and 2.



$$2 \leq \frac{b}{a} < 5$$

OPTIMUM LAMINATE
[0]

$$a = 0.2 \text{ m}$$

$$P = 5.0 \text{ E4 N}$$

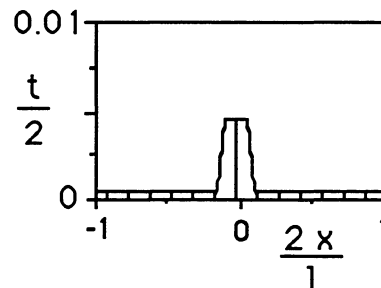
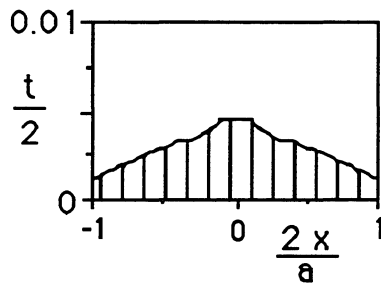
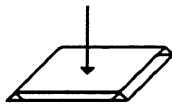


Figure 8.23 Representation of an optimal thin, simply supported plate subjected to a point transverse load for aspect ratios between 2 and 5.



$$5 \leq \frac{b}{a}$$

OPTIMUM LAMINATE
[0]

$$a = 0.2 \text{ m}$$

$$P = 5.0 \text{ E4 N}$$

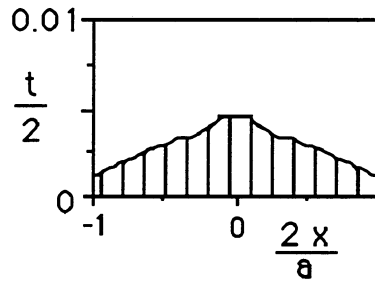


Figure 8.24 Representation of an optimal thin, simply supported plate subjected to a point transverse load for aspect ratios higher than 5.

8.4.6 Thin, clamped plates subjected to a point load

Weight saving for thin, clamped plates subjected to a point load is shown in Fig. 8.25. As we can see, the weight saving is a function of the aspect ratio, the maximum value being 83% for $b/a=10$. The optimum sublaminates also varies in function of the aspect ratio:

- [45/-45] for b/a between 1 and 1.5.
- [0] for b/a higher than 1.5.

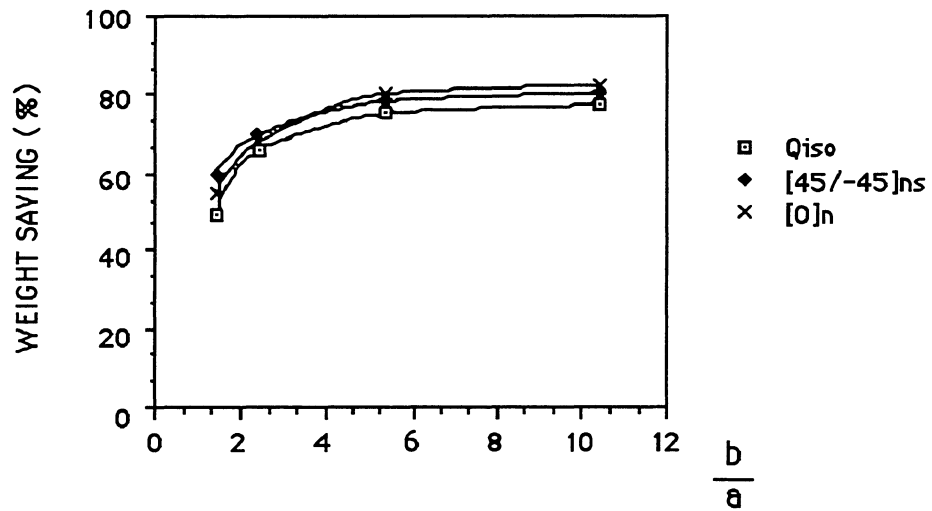
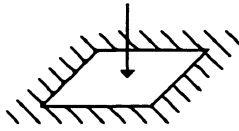


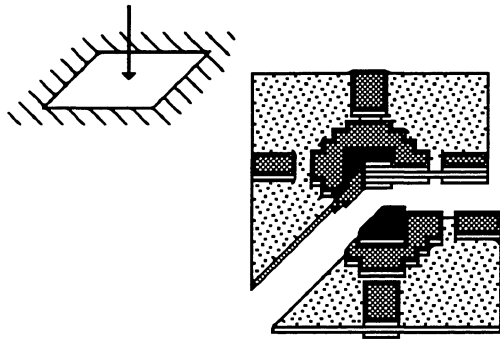
Figure 8.25 Weight saving for a thin, clamped plate subjected to a point transverse load.

The quasi-isotropic sublaminates [0/45/-45/90] presents low weight saving with respect to the optimum sublaminates, the maximum value being 80% for $b/a=10$.

Since no general formula for expressing the optimum laminate thickness has been found, the following particular case has been calculated:

- $a=7.87$ in (0.2 m)
- $P=1.125 \text{ E}4$ lb (5 E4 N)

In Fig. 8.26-8.28, we can see the values of the thickness in metres along the x-axis and the diagonal.



$$1 \leq \frac{b}{a} < 1.5$$

OPTIMUM LAMINATE
[45/-45]

$$a = 0.2 \text{ m}$$

$$P = 5.0 \text{ E}4 \text{ N}$$

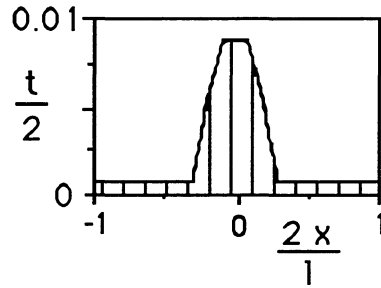
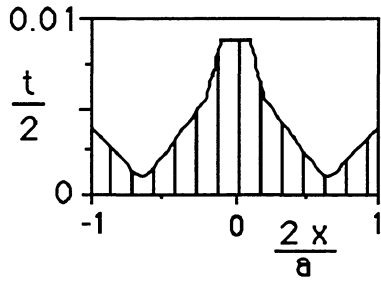
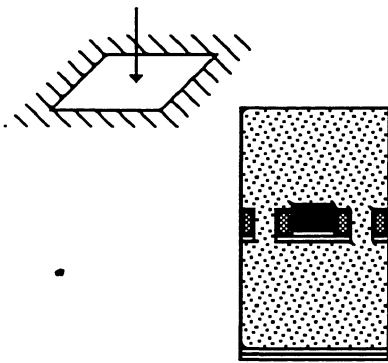


Figure 8.26 Representation of an optimal thin, clamped plate subjected to a point transverse load for aspect ratios between 1 and 1.5.



$$1.5 \leq \frac{b}{a} < 5$$

OPTIMUM LAMINATE
[0]

$$a = 0.2 \text{ m}$$

$$P = 5.0 \text{ E}4 \text{ N}$$

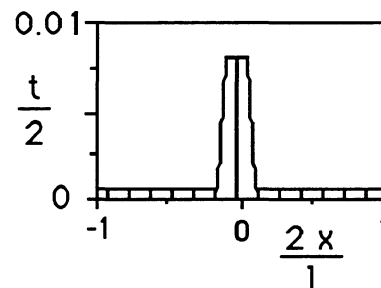
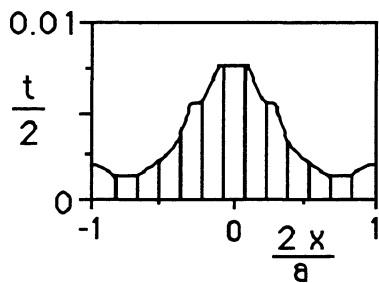


Figure 8.27 Representation of an optimal thin, clamped plate subjected to a point transverse load for aspect ratios between 1.5 and 5.

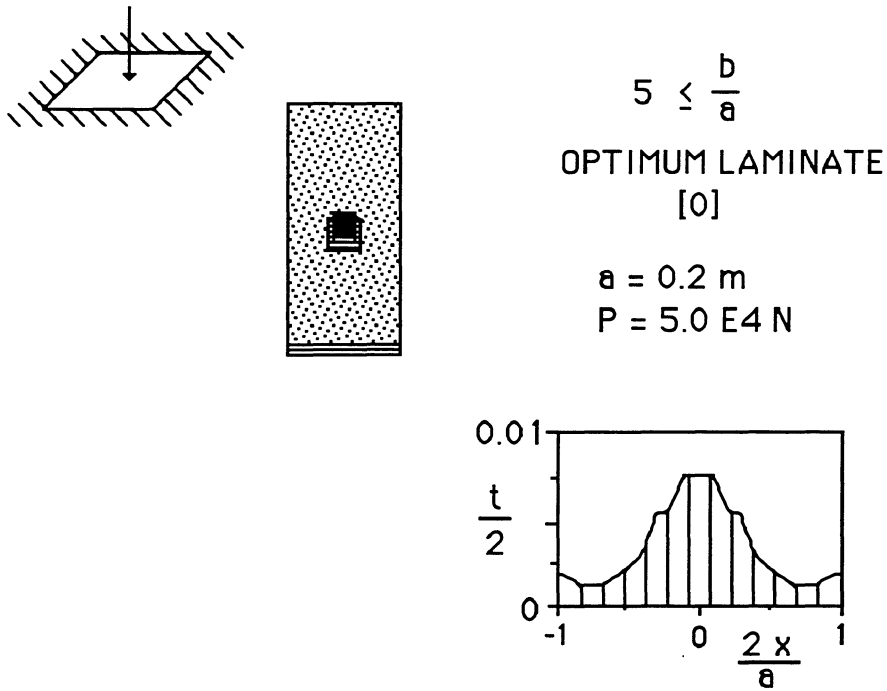


Figure 8.28 Representation of an optimal thin, clamped plate subjected to a point transverse load for aspect ratios higher than 5.

8.4.7 Thick, simply supported plates subjected to a point load

Thick, simply supported plates subjected to a point load are analysed in Fig. 8.29. The weight saving is a function of the aspect ratio, the maximum value being 82% for $b/a=2$. The optimum sublaminates also varies as a function of the aspect ratio:

- [45/-45] for b/a between 1 and 2.25.
- [0] for b/a higher than 2.25.

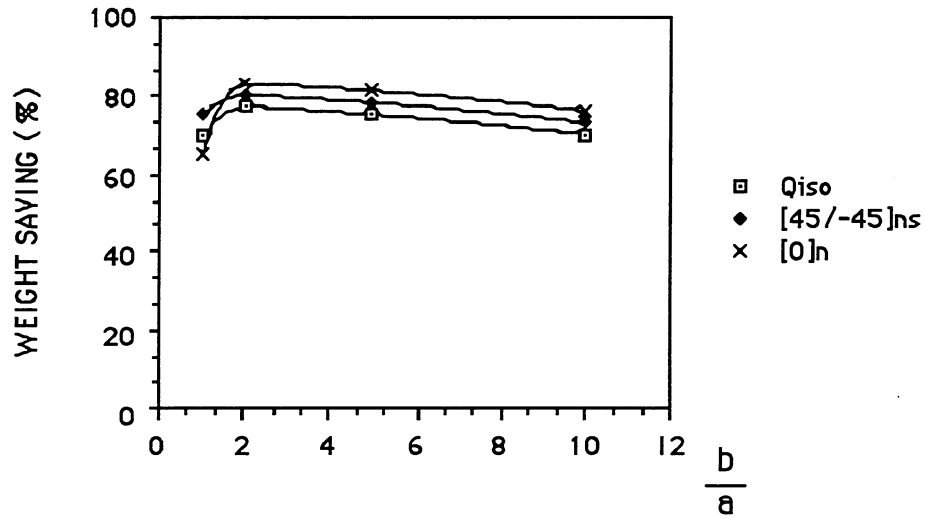
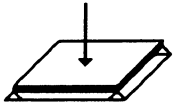


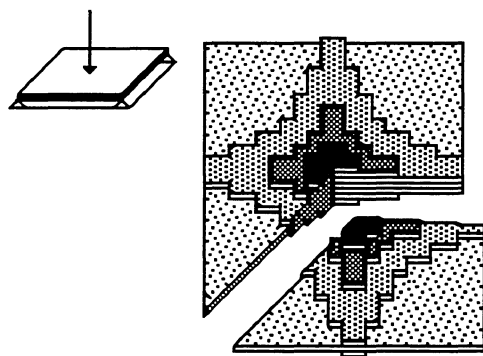
Figure 8.29 Weight saving for a thick, simply supported plate subjected to a point transverse load.

The quasi-isotropic sublaminate [0/45/-45/90] presents low weight saving with respect to the optimum sublaminate, the maximum value being 78% for $b/a=2$.

Since no general formula for expressing the optimum laminate thickness has been found, the following particular case has been calculated:

- $a=7.87$ in (0.2 m)
- $P=1.125$ E4 lb (5 E4 N)

In Fig. 8.30 and 8.31, we can see the values of the thickness in metres along the x-axis and the diagonal.



$$1 \leq \frac{b}{a} < 2.25$$

OPTIMUM LAMINATE
[45/-45]

$$a = 0.2 \text{ m}$$

$$P = 5.0 \text{ E4 N}$$

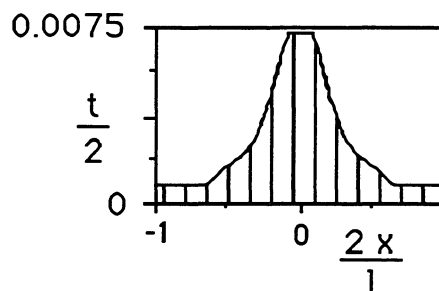
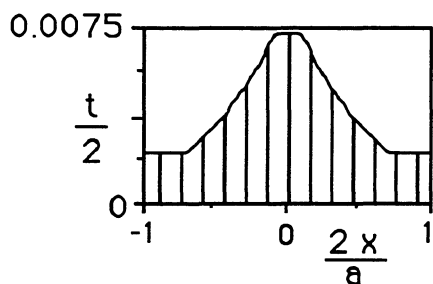
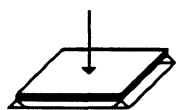


Figure 8.30 Representation of an optimal thick, simply supported plate subjected to a point transverse load for aspect ratios between 1 and 2.25.



$$2.25 \leq \frac{b}{a}$$

OPTIMUM LAMINATE
[0]

$$a = 0.2 \text{ m}$$

$$P = 5.0 \text{ E4 N}$$

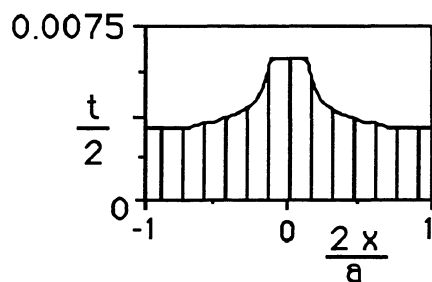
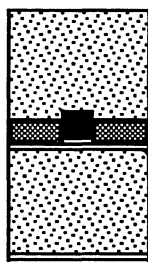


Figure 8.31 Representation of an optimal thick, simply supported plate subjected to a point transverse load for aspect ratios higher than 2.25.

8.4.8 Thick, clamped plates subjected to a point load

Weight saving for thick, clamped plates subjected to a point load, is shown in Fig. 8.32. As we can see, the weight saving is a function of the aspect ratio, the maximum value being 82% for $b/a=10$. The optimum sublaminates also varies as a function of the aspect ratio:

- [45/-45] for b/a between 1 and 2.5.
- [0] for b/a higher than 2.5.

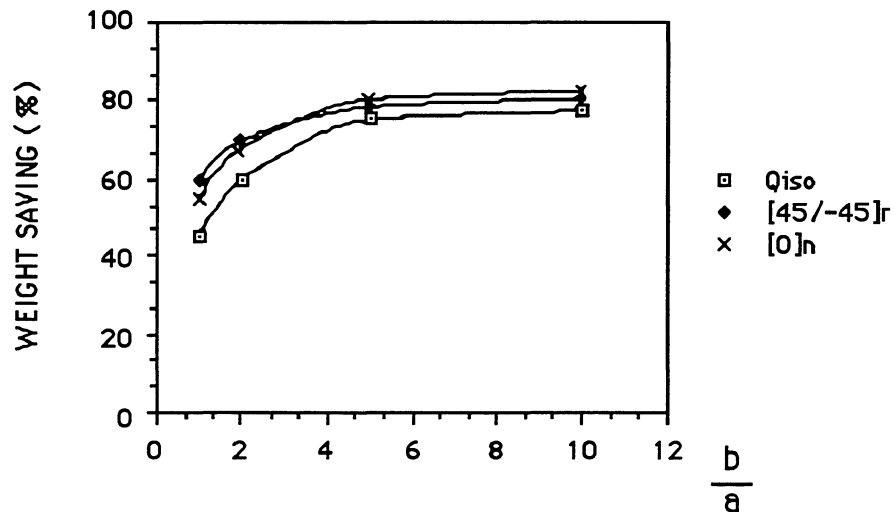
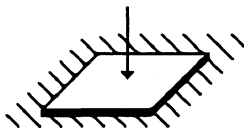


Figure 8.32 Weight saving for a thick, clamped plate subjected to a point transverse load.

The quasi-isotropic sublaminates [0/45/-45/90] presents low weight saving with respect to the optimum sublaminates, the maximum value being 78% for $b/a=10$.

Since no general formula for expressing the optimum laminate thickness has been found, the following particular case has been calculated:

- $a=7.87$ in (0.2 m)
- $P=1.125 \text{ E4 lb}$ (5 E4 N)

In Fig. 8.33-8.35, we can see the values of the thickness in metres along the x-axis and the diagonal.

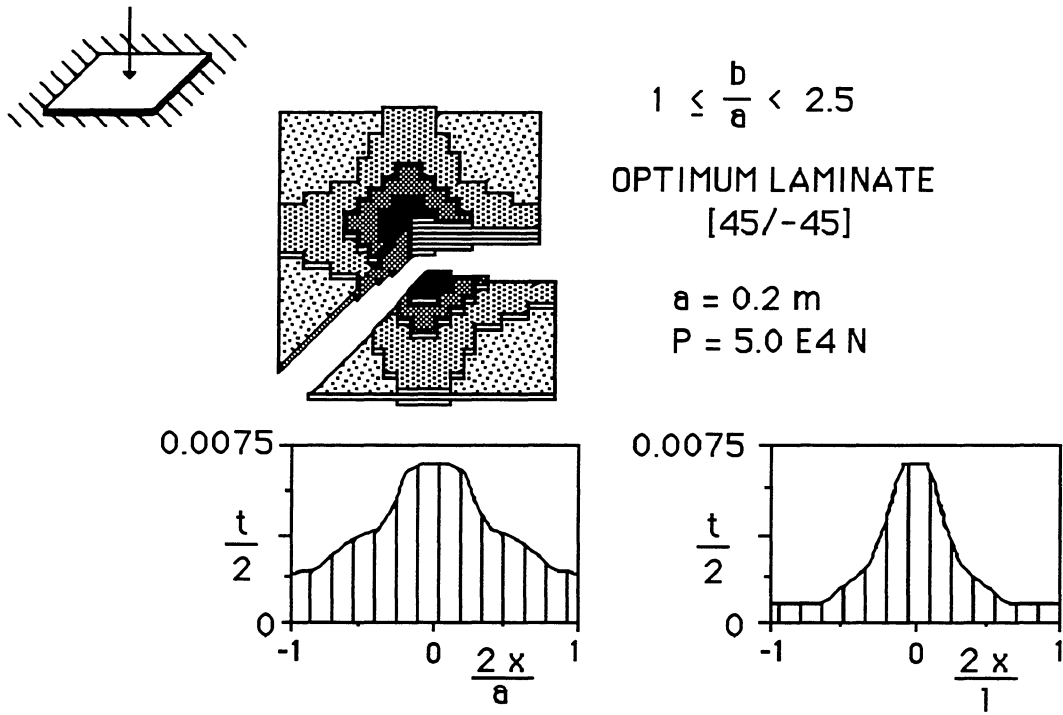


Figure 8.33 Representation of an optimal thick, clamped plate subjected to a point transverse load for aspect ratios between 1 and 2.5.

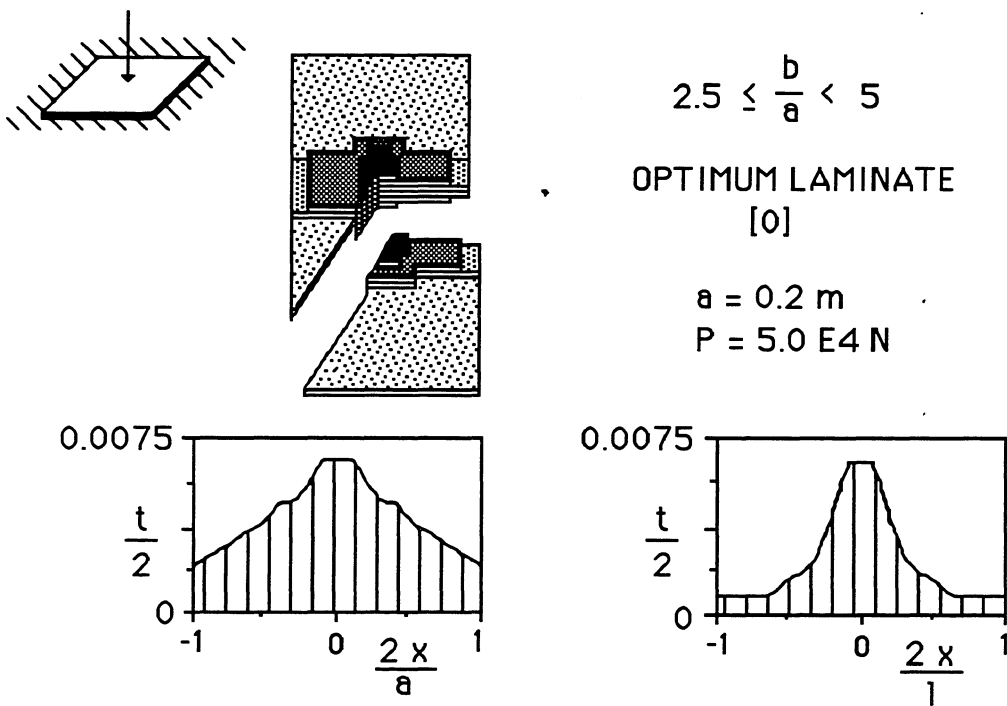


Figure 8.34 Representation of an optimal thick, clamped plate subjected to a point transverse load for aspect ratios between 2.5 and 5.

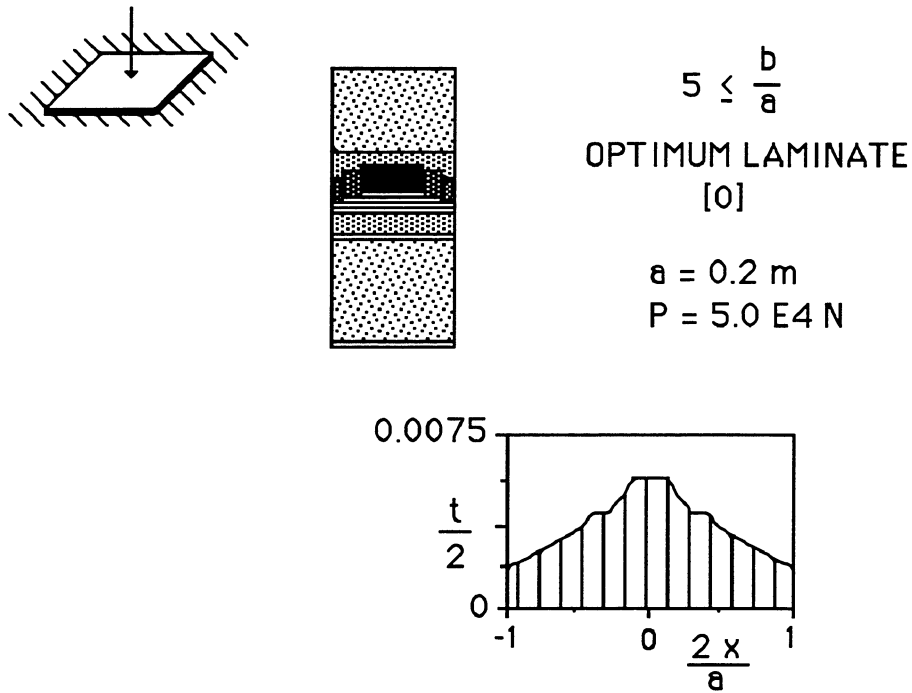


Figure 8.35 Representation of an optimal thick, clamped plate subjected to a point transverse load for aspect ratios higher than 5.

8.5 Conclusions

A study on analysis and optimisation of variable thickness composite plates subjected to transverse loads has been presented.

In the first part of this chapter, a comparison study between a 2-D model and the shear deformation theory was carried out. Since results from both models were very close, it is proved that a shear deformation theory can be used for the analysis of a variable thickness composite plate.

Once the method of analysis is known, the different input data required for the calculation can be obtained. Elastic constants and strengths of the material are described and interlaminar normal and interlaminar shear moduli are obtained as a function of the stacking sequence.

In the second part of this chapter devoted to optimisation, the following conclusions can be drawn:

- For uniform loads, optimum sublaminates, normalised deflections and weight saving have been reported. Analytical solutions for the weight savings are also obtained. The weight savings for thin simply supported plates are a function of the aspect ratio, varying between 27% and 16%. Meanwhile for clamped plates, the range is 48% and 34%. For thick plates, the weight savings obtained range from 45% to 18% for both simply supported and clamped plates.
- For central loads, optimum sublaminates and weight saving have been reported. The weight savings for thin simply supported plates are a function of the aspect ratio, varying in the range between 76% and 55%, meanwhile for clamped plates, the range is 80%-60%. For thick plates, the weight savings obtained range

from 83% to 76% for both simply supported and between 80% and 60% for clamped plates.

Optimum sublaminates are very difficult to predict because there is a strong dependence with the aspect ratio, boundary conditions and the type of loading. Thus, a calculation method must be undertaken. The weight savings reported are very high, especially for central loads but they also depend substantially on these four aspects (boundary conditions, type of plate, aspect ratio and type of loading).

References

1. Miravete A, 'A simple finite element formulation for three-dimensional laminated composite plates', Proc.5th Conf. Comp. Struct., Paisley, Scotland, 1989.
2. Roy A K and Tsai S W, '3-D effective moduli of laminated orthotropic plates', to appear in Journal of Applied Mechanics.
3. Reissner E and Stavsky Y, ASME J. Appl. Mech., 1961, 28,402.
4. Timoshenko S P and Woinowsky-Krieger S, Theory of Plates and Shells, McGraw- Hill, New York, 1959.
5. Cook R D, Concepts and applications of finite element analysis, John Wiley, New York, 1981.
6. Reissner E, 'The effect of transverse shear deformation on the bending of elastic plates', ASME. J. Appl. Mech. 1945, 12, A69-A77.
7. Mindlin R D, 'Influence of rotatory inertia and shear deformation on flexural motions of isotropic elastic plates', ASME. J. Appl. Mech., 1951, 18, 31.
8. Zienkiewicz O C, Taylor R L and Too J M, 'Reduced integration techniques in general analysis of plates and shells', Int. J. Num. Meth. Eng., 1971, 3, 275.
9. Pawsey S E and Clough R W, 'Improved numerical integration of thick shell finite elements', Int. J. Num. Meth. Eng., 1971, 3, 545.
10. Hughes T J R, Taylor R L and Kanoknukulchal W, 'A simple and efficient finite element for plate bending', Int. J. Num. Meth. Eng., 1977, 11, 1529.
11. Pugh E D L, Hinton E and Zienkiewicz O C, 'A study of quadrilateral plate bending with reduced integration', Int. J. Num. Meth. Eng., 1978, 12, 1059.
12. Lee S W and Pian T H, 'Improvement of plate and shell finite elements by mixed formulations', AIAA J., 1978, 16, 29.
13. Hughes T J R and Tezduyar T E, 'Finite elements based upon mindlin plate theory, with particular reference to the four-node bilinear isoparametric element', ASME. J. Appl. Mech., 1981, 48, 587.
14. Lo K H, Christensen R M and Wu E M, 'A high order theory of plate deformation part I: Homogeneous plates', ASME. J. Appl. Mech., 1977, 44, 663.
15. Lo K H, Christensen R M and Wu E M,, 'A high order theory of plate deformation part II: Laminated plates', ASME. J. Appl. Mech., 1977, 44, 669.
16. Reissner E, 'On transverse bending of plates, including the effects of transverse shear deformation', Int. J. Solids Struct., 1975, 11, 569.
17. Kant T, Owen D R J and Zienkiewicz O C, 'A refined higher order Co plate bending element', Comput. Struct., 1982, 15, 177.
18. Reddy J N, 'A simple higher order theory for laminated composite plates', ASME J. Appl. Mech., 1984, 51, 745.

19. Pandya B N and Kant T, 'A refined higher-order generally orthotropic Co plate bending element', Comput. Struct., 1988, 28, 119.
20. Lakshminarayana H V and Ramani T S, 'On improving the performance of a shear-flexible triangular laminated composite plate finite element' , Proc. Int. Conf. Com. Mat. and Struct., Madras, 1988.
21. Prathap G and Somashekar B R, 'A field-consistent 8-noded laminated anisotropic plate element', Proc. Int. Conf. Com. Mat. and Struct., Madras, 1988.
22. Tessler A, 'An improved higher-order theory for orthotropic plates', Proc. Rev.Mech. Comp, Bal Harbour, Florida, 1988.



9 VARIABLE THICKNESS SANDWICHES

9.1 Introduction

In the aerospace industry, shaped panels with variable thickness are widely used; components are frequently made as single integral sandwich panels. The shaping of the core can be done by complex machining (e. g. using a five-axis, 3-D profiler), by hot-forming in a mould (where the core is suitable) or by controlled crushing of honeycomb. Where expanded plastics are used, the density may be varied from point to point to suit the stress levels at different parts of the component. Clearly these processes can be expected to become even more complex and comprehensive as manufacturers gain experience, as tools become more controllable, and as materials become more versatile. The only problem is one of repair. Aircrafts sometimes suffer damage; repairs then become necessary. Repairs are difficult to carry out satisfactorily on a fully optimised component where the reasons for the variation in core density are not apparent. Perhaps the ultimate achievement in sandwich construction so far is the Starship project of the Beech Aircraft Corporation. This twin-engined aircraft has an unusual configuration. The wing span is 16.59 m. The fuselage is 14.06 m long and it consists of a single sandwich shell made of 19 mm NOMEX* core with graphite/epoxy faces. Hooper¹ mentioned that 8000 coupons, samples and components were tested before the aircraft became, on 14 June 1988, the first all-composite aircraft to be certified by the FAA.

The fabrication processes in ship- and boat-building are on a larger and heavier scale, with expanded plastics more common than honeycombs. The standard moulding techniques for fibre-reinforced plastics are too well known to be worth repeating here. However, the manufacture of the larger vessels (patrol boats, mine sweepers, etc.) requires a considerable amount of organisation to minimise the amount of effort in what is still basically a fairly labour-intensive process. Large jigs, hoists, rotating moulds, and automatic machinery for dispensing reinforcing fabrics and resins are all used in the bigger workshops to introduce a greater degree of automation. It is to be expected that the greatest advances in the future will come from improvements in this direction, rather than from dramatic changes in the materials used.

In boat construction there is a tendency to restrict sandwich construction to deck mouldings and possibly to the sides of the hull, and to retain single skin construction (with foam-filled stiffeners) for the bottom of the hull. Weston (2) gave a good description of this arrangement as applied to a 13 m fast patrol boat design. Sandwich construction has been used for complete hulls, especially in Scandinavia, but it has not been without problems; it would be interesting to hear more about this.

Perhaps the most massive form of sandwich construction so far is to be seen in the blades for wind-generators manufactured by MBB in the former West Germany. These blades are 24 m and 30 m long and proportionately broad and thick. Even the smallest blade is 2.4 m wide. They are made by forming GRP faces around a very large shaped block of expanded plastic material. Even larger blades, 40 m long, are planned.

Variable thickness rectangular sandwich panels with different types of transverse loading and boundary conditions are analysed and optimised throughout this chapter. One and two-dimensional sandwich panels are studied. Analytical solutions are obtained for one dimensional sandwich panels. Weight savings are reported for simply-supported and clamped panels. Further information about analysis and optimisation of sandwiches can be found in refs. 3-27.

9.2 One-dimensional laminated composite panels

The problem analysed here can be defined by the following points:

- The objective is to achieve a minimum weight structure by using strength as a design criterion.
- The laminate used is $[0]_n$ because it is the optimum for 1-D laminated composite plates subjected to transverse loads.
- Two sides tapered laminates have been considered.
- Boundary conditions are restricted to :
 - simply supported plates;
 - clamped plates;
 - cantilever plates.
- Two types of loading are applied:
 - uniform load;
 - point load, at the centre of the plate for simply supported and clamped plates, and at the free end of the plate for cantilever plates.
- The mesh is composed of 400 nodes.
- The material used is T300/N5208.

9.2.1 Sandwich panels subjected to a uniform load

Optimum 1-D uniform loaded sandwich panels are shown in Fig. 9.1. In this case, only the failure mode in the faces have been considered. The optimum laminate thickness can be calculated by means of the following expression:

$$t = 2 k (a^2 P/c X) \quad [9.1]$$

where c is the core thickness. Optimum sandwiches and the value of k as a function of x are presented for different boundary conditions. The weight saving is 31.2% for simply supported plates, 58.5% for clamped plates, and 56.9% for cantilever plates.

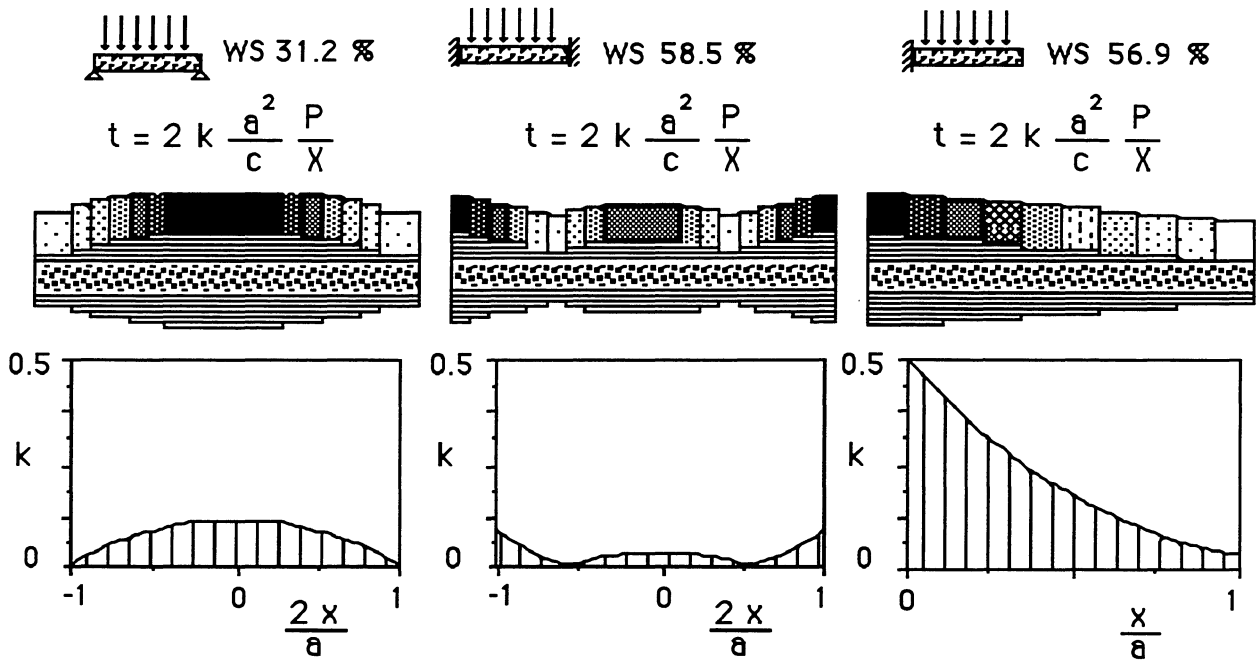


Figure 9.1 Representation of optimal one-dimensional sandwich panels subjected to a uniform distributed transverse load.

9.2.2 Sandwich panels subjected to a point load

Optimum 1-D sandwiches subjected to a point load, are shown in Fig. 9.2. In this case, only the failure mode in the faces have been considered. The optimum laminate thickness can be calculated by means of the following expression:

$$t = 2k \left(a \frac{P}{c X} \right) \quad [9.2]$$

Optimal sandwiches and the value of k as a function of x are presented for different boundary conditions. The weight saving is 45.7% for simply supported plates, 41.4% for clamped plates, and 45.7% for cantilever plates.

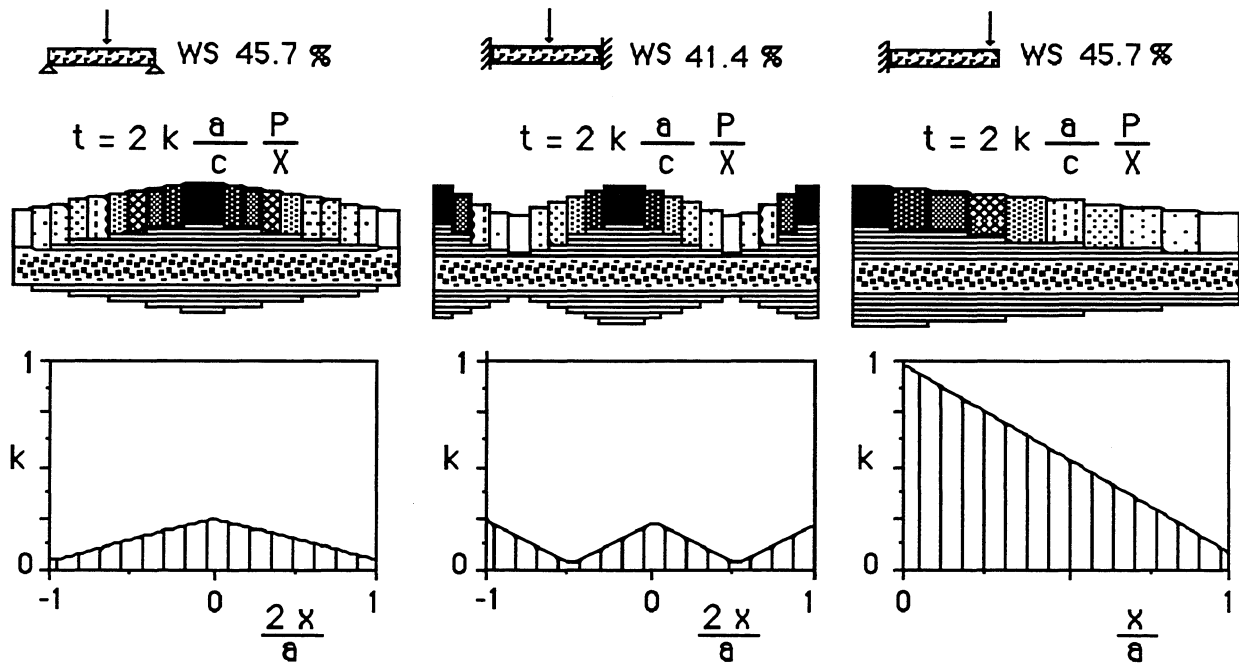


Figure 9.2 Representation of optimal one-dimensional sandwich panels subjected to a point transverse load.

9.3 Two-dimensional laminated composite panels

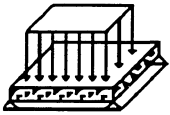
The problem analysed here can be defined by the following points:

- The objective is to achieve a minimum weight structure by using strength as a design criterion.
- The laminate used is $[0]_n$ because it is the optimum for 1-D laminated composite plates subjected to transverse loads.
- Two sides tapered laminates have been considered.
- Boundary conditions are restricted to :
 - simply supported plates along the four edges of the plate;
 - clamped plates along the four edges of the plate.
- Two types of loading are applied:
 - uniform load
 - point load, at the centre of the plate for simply supported and clamped plates, and at the free end of the plate for cantilever plates.
- The mesh is composed of 400 nodes.
- The material used is T300/N5208.

9.3.1 Simply supported sandwich panels subjected to a uniform load

Weight saving and normalised deflection for simply supported, uniform loaded sandwiches are shown in Fig. 9.3. As we can see, the weight saving is a function of the aspect ratio, the maximum value being 35% for $b/a=10$. The optimum sublaminates also varies as a function of the aspect ratio:

- $[45/-45]$ for b/a between 1 and 2.
- $[0]$ for b/a higher than 2.



WEIGHT SAVING (%)

□ [45/-45]_{ns}

■ [0]_n

NORMALIZED DEFLECTION

$\frac{\text{Deflection tapered plate}}{\text{Deflection untapered plate}}$

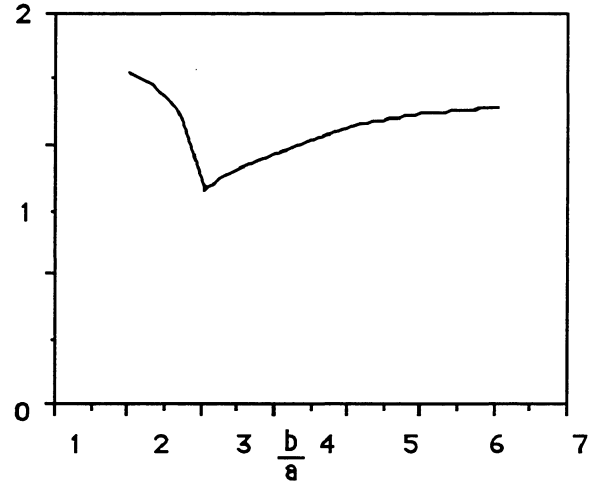
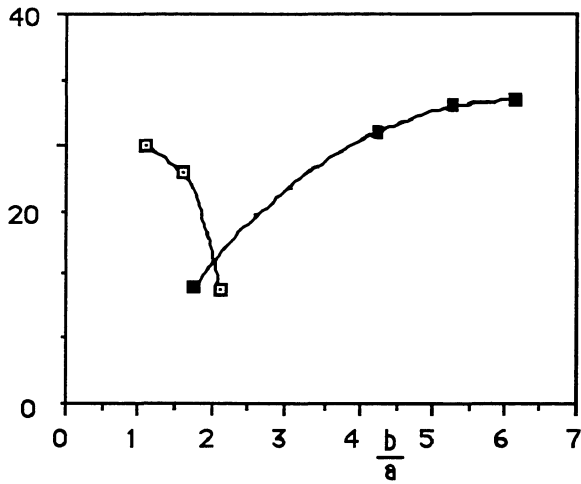
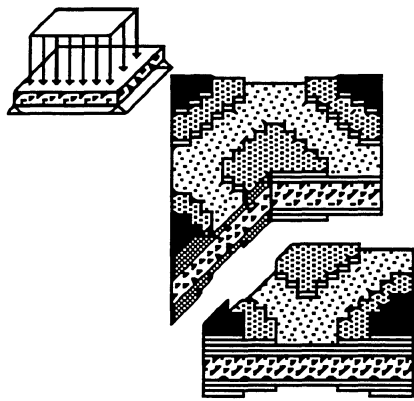


Figure 9.3 Weight saving and normalised deflection for a simply supported sandwich panel subjected to a uniform distributed transverse load.

The quasi-isotropic sublaminates [0/45/-45/90] presents low weight saving with respect to the rest of sublaminates, the maximum value being 20% for $b/a=10$. For uniformly loaded sandwich structures, the optimum laminate thickness can be calculated by means of the following expression:

$$t = 2 k (a^2 P/c X) \quad [9.3]$$

In Fig. 9.4 and 9.5, we can see the values of the non-dimensional parameter k along the x -axis and the diagonal.



$$1 \leq \frac{b}{a} < 1.5$$

OPTIMUM SUBLAMINATE
[45/-45]

$$t = 2 k \frac{a^2}{c} \frac{P}{X}$$

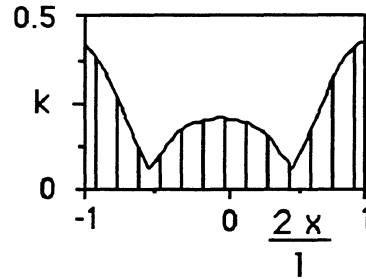
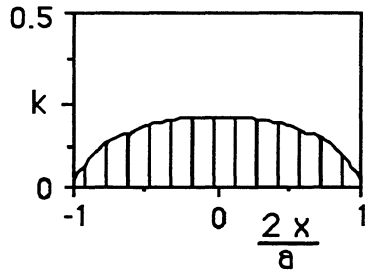
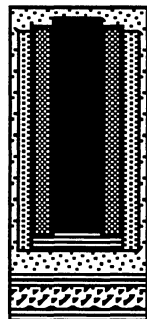
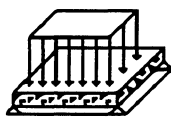


Figure 9.4 Representation of an optimal simply supported sandwich panel subjected to a uniform distributed transverse load for aspect ratios between 1 and 1.5.



$$1.5 \leq \frac{b}{a}$$

OPTIMUM SUBLAMINATE
[0]

$$t = 2 k \frac{a^2}{c} \frac{P}{X}$$

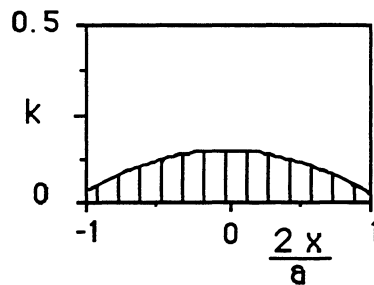


Figure 9.5 Representation of an optimal simply supported sandwich panel subjected to a uniform distributed transverse load for aspect ratios higher than 1.5.

9.3.2 Clamped, sandwich panels subjected to a uniform load

Clamped, uniform loaded sandwiches are analysed in Fig. 9.6. The weight saving is a function of the aspect ratio, the maximum value being 60% for $b/a=2$. The optimum sublaminates also varies as a function of the aspect ratio:

- $[0/90]$ for b/a between 1 and 1.5.
- $[0_5/90_2]$ for b/a between 1.5 and 2.5.
- $[0]$ for b/a higher than 2.5.

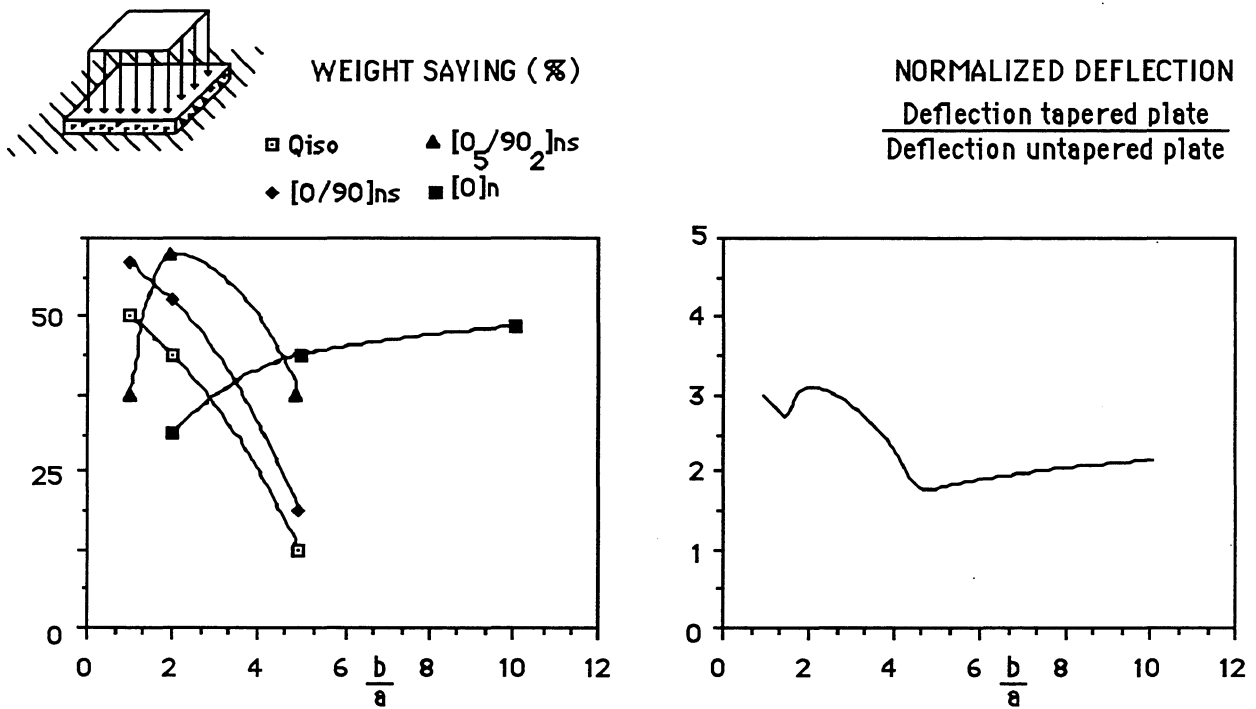


Figure 9.6 Weight saving and normalised deflection for a clamped sandwich panel subjected to a uniform distributed transverse load

The values of the non-dimensional parameter k along the x-axis and the diagonal are represented in Fig. 9.7-9.9.

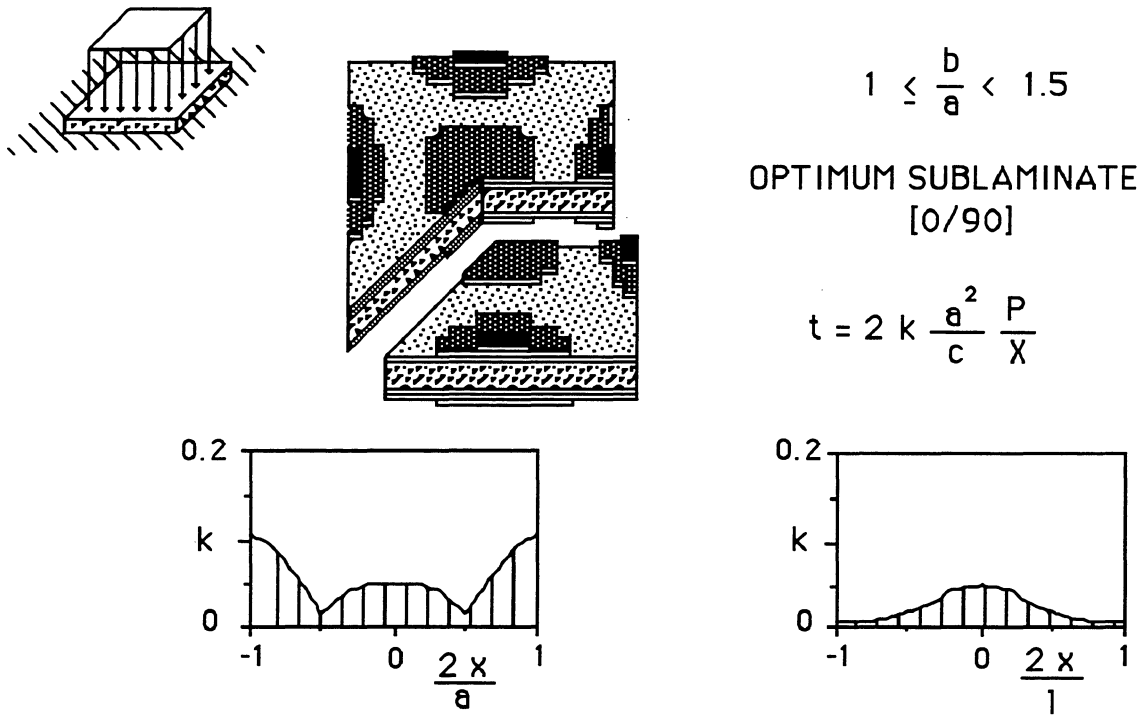


Figure 9.7 Representation of an optimal clamped sandwich panel subjected to a uniform distributed transverse load for aspect ratios between 1 and 1.5.

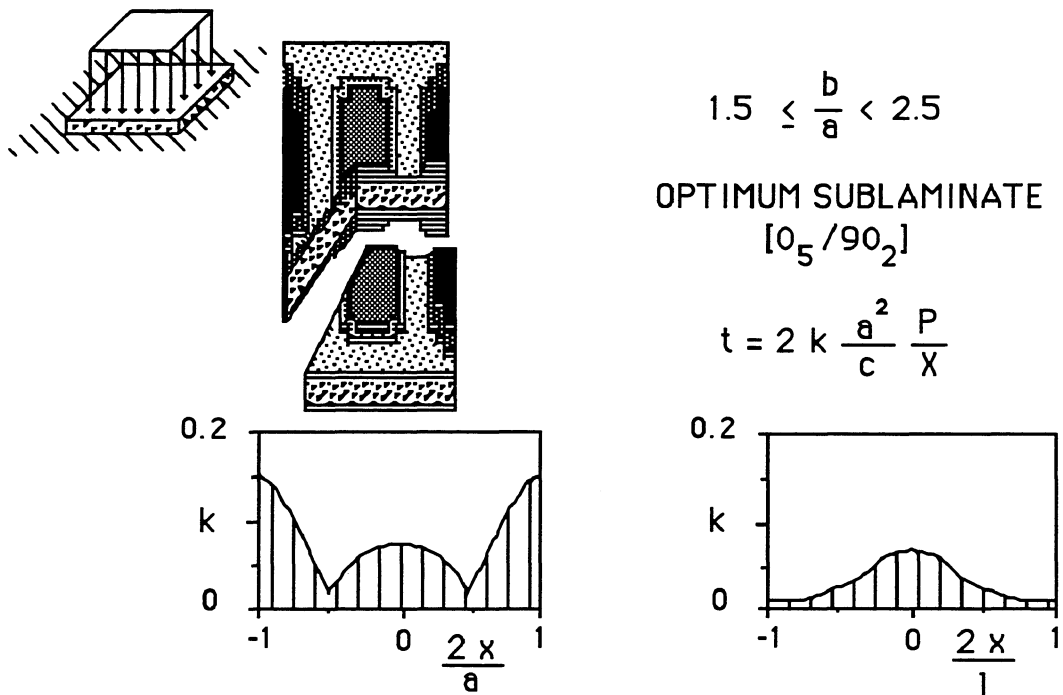


Figure 9.8 Representation of an optimal clamped sandwich panel subjected to a uniform distributed transverse load for aspect ratios between 1.5 and 2.5.

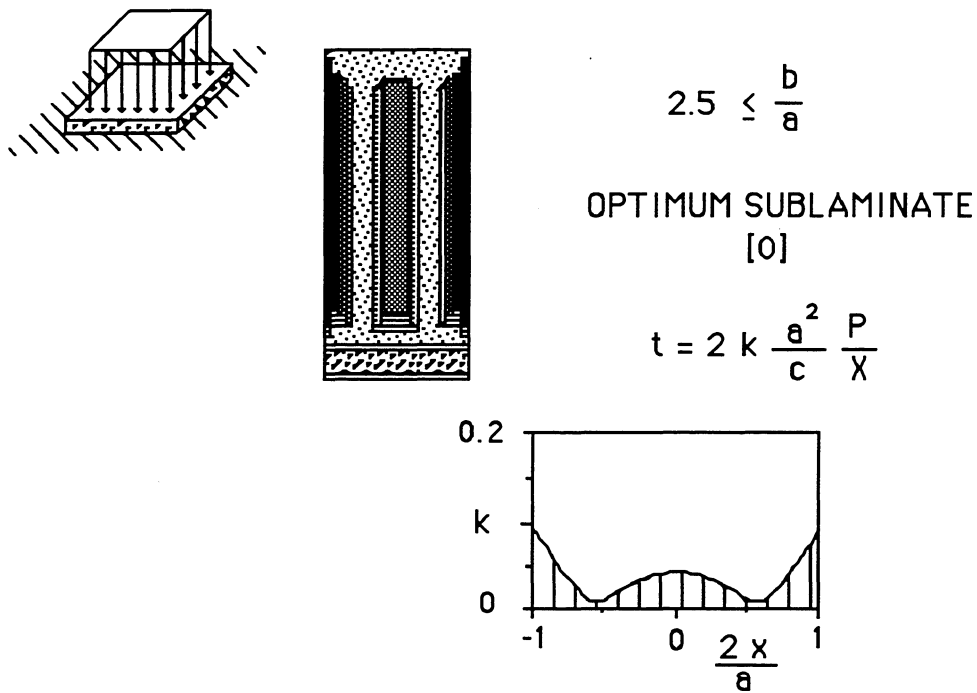


Figure 9.9 Representation of an optimal clamped sandwich panel subjected to a uniform distributed transverse load for aspect ratios higher than 2.5.

9.3.3 Simply supported sandwich panels subjected to a point load

The weight saving for simply supported sandwiches subjected to a point load, is shown in Fig. 9.10. As we can see, the weight saving is a function of the aspect ratio, the maximum value being 94% for $b/a=2$. The optimum sublaminate is [0] for all the plate aspect ratios analysed.

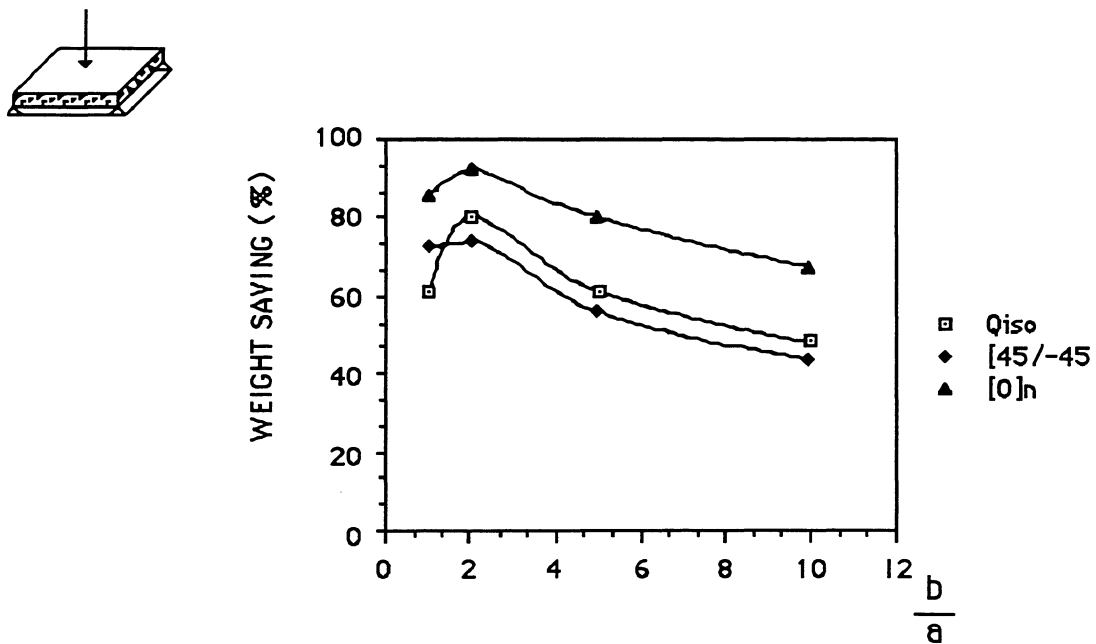


Figure 9.10 Weight saving for a simply supported sandwich panel subjected to a point transverse load.

The quasi-isotropic sublaminate [0/45/-45/90] presents low weight saving as compared to the optimum sublaminate, maximum value being 80% for $b/a=2$. Since no general formula for expressing the optimum laminate thickness has been found, the following particular case has been calculated:

- $a=7.87$ in (0.2 m)
- $P=1.125 E4$ lb (5 E4 N)

In Figure 9.11 to 9.13, we can see the values of the thickness in metres along the x-axis and the diagonal.

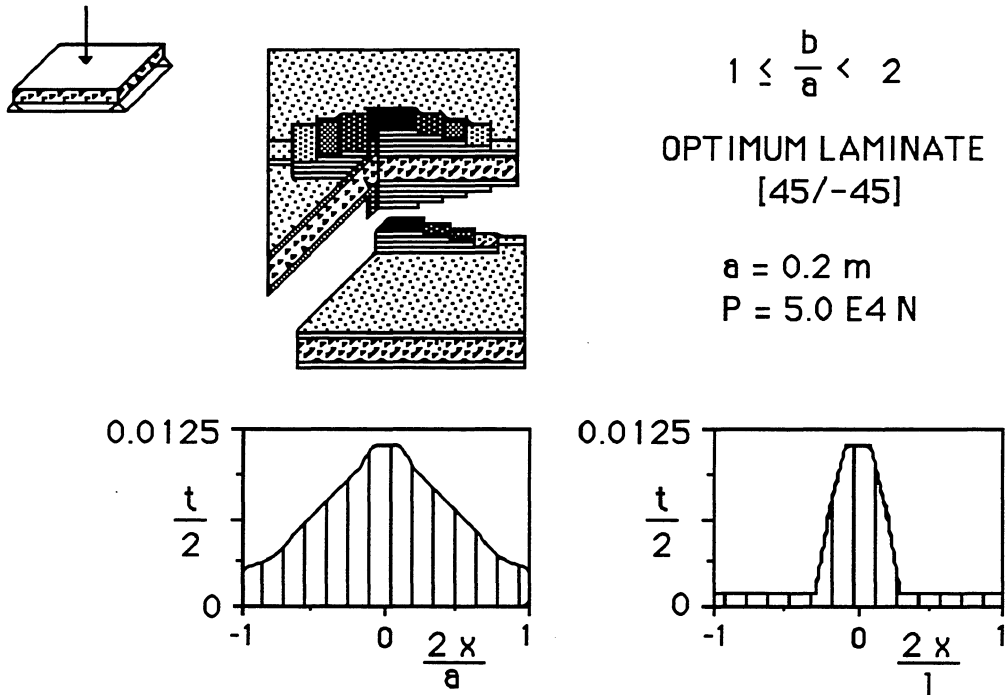


Figure 9.11 Representation of an optimal simply supported sandwich panel subjected to a point transverse load for aspect ratios between 1 and 2.

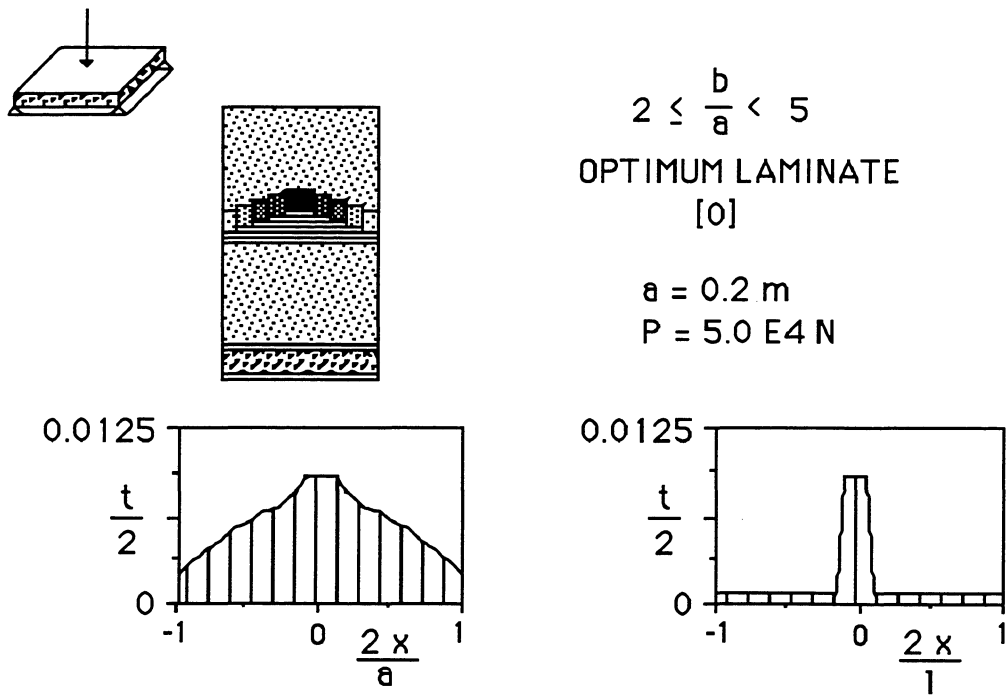


Figure 9.12 Representation of an optimal simply supported sandwich panel subjected to a point transverse load for aspect ratios between 2 and 5.

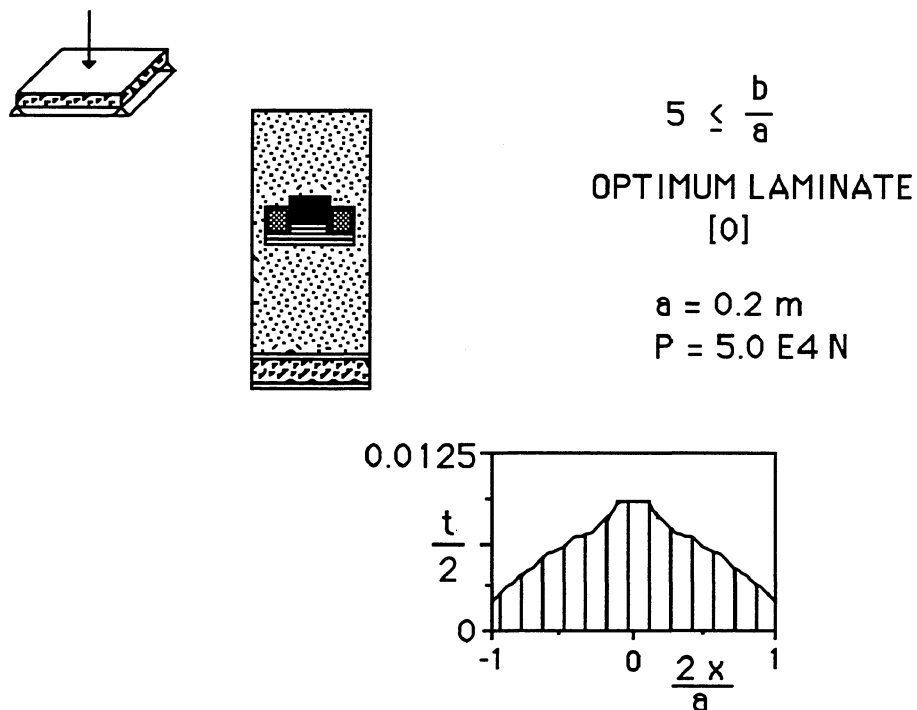


Figure 9.13 Representation of an optimal simply supported sandwich panel subjected to a point transverse load for aspect ratios higher than 5.

9.3.4 Clamped sandwich panels subjected to a point load

Clamped sandwiches subjected to a point load are studied in Fig. 9.14. The maximum value of the weight saving is 96% for $b/a=10$. The optimum sublaminates also varies as a function of the aspect ratio:

- [0/90] for b/a between 1 and 1.5.
- [0₅/90₂] for b/a between 1.5 and 5.
- [0] for b/a higher than 5.

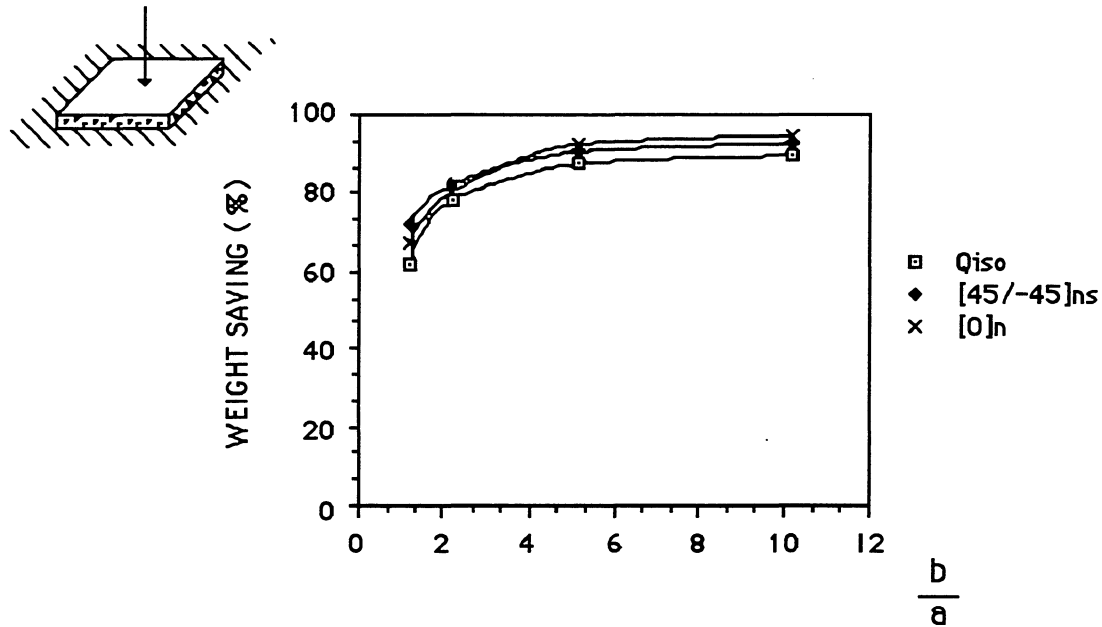


Figure 9.14 Weight saving for a clamped sandwich panel subjected to a point transverse load.

Since no general formula for expressing the optimum laminate thickness has been found, the following particular case has been calculated:

- $a=7.87$ in (0.2 m)
- $P=1.125 E4$ lb (5 E4 N)

The values of the thickness in metres along the x-axis and the diagonal are represented in Fig. 9.15-9.17.

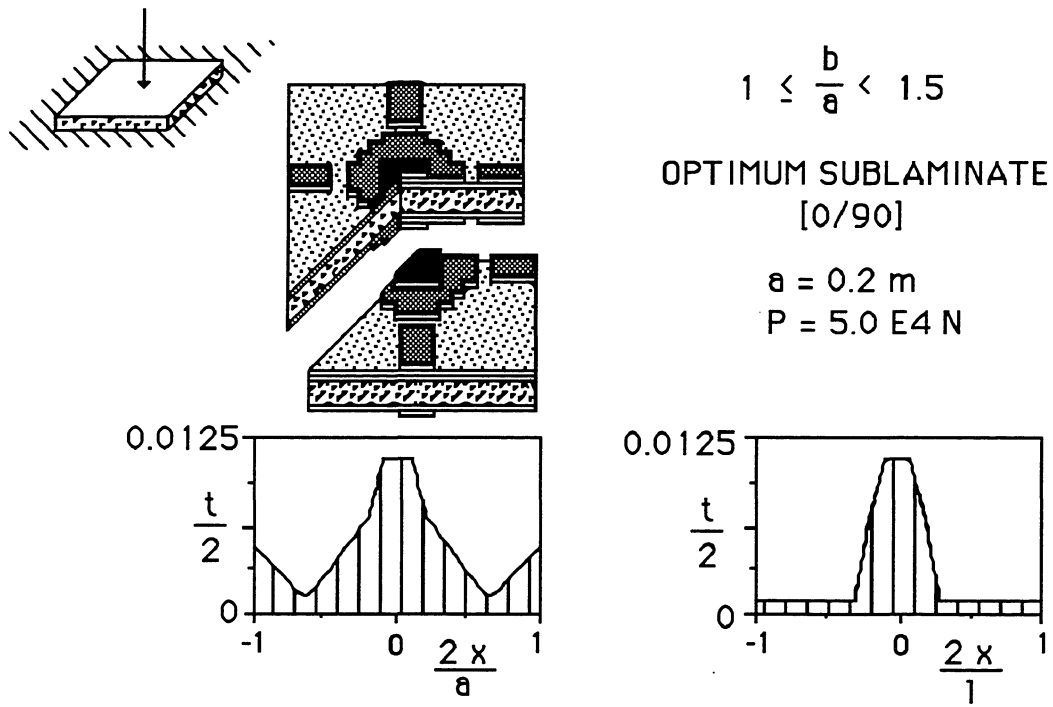


Figure 9.15 Representation of an optimal clamped sandwich panel subjected to a point transverse load for aspect ratios between 1 and 1.5.

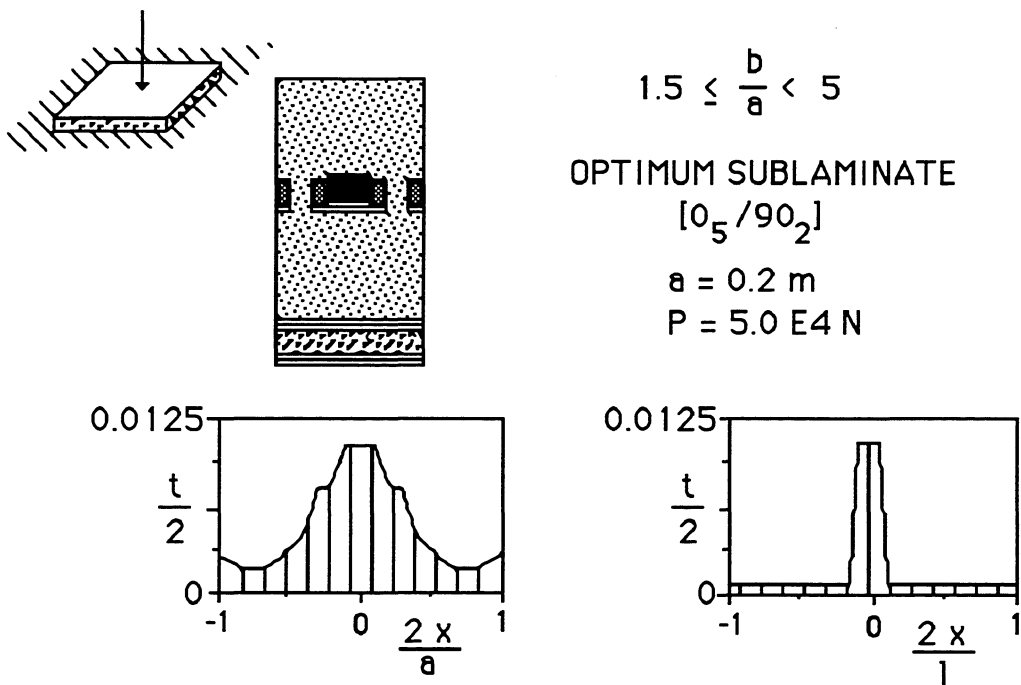


Figure 9.16 Representation of an optimal clamped sandwich panel subjected to a point transverse load for aspect ratios between 1.5 and 5.

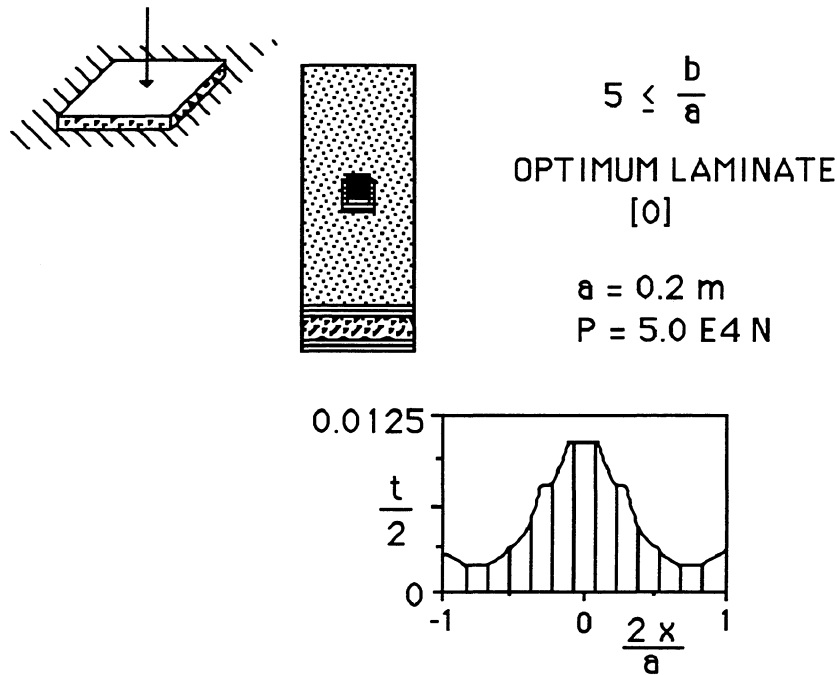


Figure 9.17 Representation of an optimal clamped sandwich panel subjected to a point transverse load for aspect ratios higher than 5.

9.4 Conclusions

Variable thickness rectangular sandwich panels with different types of transverse loading and boundary conditions have been analysed and optimised in this chapter.

First, 1-D sandwich panels have been studied and analytical solutions have been obtained. Weight saving and optimum sublaminates are reported for simply-supported and clamped panels. For uniform loads, the weight savings vary between 58.5% and 31.2%, depending on the boundary conditions. For point loads, the weight savings vary between 45.7% and 41.4%, also depending on the boundary conditions.

Second, 2-D sandwich panels have been analysed. Weight savings, normalised deflections and optimum sublaminates are reported for simply-supported and clamped panels. The weight saving is a function of the aspect ratio. Analytical solutions for uniform loaded panels are obtained. For uniform loaded and simply supported panels, the weight saving ranges from 10% to 35%. For uniform loaded and clamped panels, the weight savings range from 60% to 42%. For a central load and simply supported panels, the weight savings range from 95% to 70% and finally for a central load and clamped panels, the weight savings range from 97% to 72%.

Optimum sublaminates are very difficult to predict because there is a strong dependence on the boundary conditions and the type of loading. Thus, a calculation method must be carried out. The weight savings reported are very high but they also depend substantially on these two aspects (boundary conditions and type of loading).

References

1. Hooper E, "Starship: A Model for Future Design", "The First Core Conference" DuPont, Zürich, 20-21 Oct. 1988.
2. Weston C, "Fast Patrol Boat Design Concept", "The Core Material in Boat Building Sandwich Constructions", Pelf/Polimex, Padova, 27-28 April, 1989.
3. Hirano Y, 'Optimum design of laminated plates under axial compression', J. AIAA, 1979, 17, 1017.
4. Bert C W, 'Optimal design of a composite material plate to maximize its fundamental frequency', J. Sound & Vibration, 1977, 50, 229.
5. Bert C W 'Design of clamped composite material plates to maximize fundamental frequency', J. of Mech. Des. ASME, 1978, 100, 274.
6. Adali S 'Design of shear-deformable antisymmetric angle-ply laminates to maximize the fundamental frequency and frequency separation', Comp. Struct., 1984, 2, 349.
7. Pedersen P, "On Sensitivity Analysis and Optimal Design of Specially Orthotropic laminates", Proc. ASI CAD, Troia, Portugal, pp. 170, 1986.
8. Pedersen P, 'On sensitivity analysis and optimal design for laminates', in Mechanical Behavior of Composites and Laminates (eds. Green and Micunovic), Elsevier, pp. 274, 1987.
9. Joshi S P and Iyengar N G R 'Studies on optimization of laminated composite plates', Proc. 13 ICAS Cong., AIAA Sys. Conf, pp. 607, 1982.
10. Soni P J and Iyengar N G R 'Optimal design of clamped laminated plates', J. Fibre Sci. & Tech., 1983, 19, 281.
11. Joshi S.P., Iyengar N.G.R. 'Optimal Design of Laminated Composite Plates under Axial Compression', Trans. Can. Soc. Mech. Eng., Vol.9, pp. 45, 1986.
12. Khot N S, 'Computer Program (OPTCOMP) for Optimization of Composite Structures for Minimum Weight Design', AFFDL TR-76-149, Wright-Patterson Air Force Base, Dayton, OH, 1977.
13. McKeown J J, 'Optimal composite structures by deflection-variable programming' Comput. Meths. Appl. Mech. Eng., 1977, 12, 155.
14. Starnes J H and Haftka R T, "Preliminary Design of Composite Wings", AIAA, ASME Structures, Structural Dynamics and Material Conference, Bethesda, MD, 1978.
15. Schmit L A and Mehrinfar M, 'Multilevel optimum design of structures with fiber-composite stiffened-panel components', J. AIAA, 1980, 16,5.
16. Sobieszczanski-Sovieski J, An Integrated Computer Procedure for Sizing Composite Airframe Structures, NASA TP 1300, NASA Langley Research Center, Hampton, VA, 1979.
17. Park J W, An Optimal Design of Simple Symmetric Laminates Under the First Ply Failure Criteria, AFWAL-TR-81-4175, Air Force Materials Laboratory, 1982.
18. Donaldson S, 'Simplified weight saving techniques for composite panels', J. Reinf. Plastics Composites, 1983.
19. Wurzel D P, On the Optimal Design of Bidirectional Composites, AFWAL-TR-83-4060, Air Force Materials Laboratory, 1983.
20. Massard T N, 'Computer sizing of composite laminates for strength', J. Reinf. Plastics composites, 1984, 300, 1984.

21. Maksimovic S, 'Optimum design of composite structures', Proc. 3rd Conf. Comp. Struct, Paisley, pp. 148, 1985.
22. Tsai S W, "Composites design", (eds. Tsai, S. W., Massard, T. N., Susuki, I.), 1985.
23. Watkins R I, Morris A J, 'A multicriteria objective function optimization scheme for laminated composites for use in multilevel structural optimization schemes', Comp. Meth. Eng., 1987,60, 233.
24. Iyengar N G R, 'Optimal design of fiber reinforced composite plates', Proc. Advances in Aerospace structures, Madras, pp. 71, 1988.
25. Pedersen P, 'On Optimal orientation of Orthotropic Materials', to appear.
26. Leissa A W, Buckling of Laminated Composite Plates and Shell Panels, AFWAL-TR-85-3069, Air Force Materials Laboratory, 1985.
27. Muc A, 'Optimal fibre orientation for simply-supported, angle-ply plates under biaxial compression', Comp. Struct. 1988, 9,161.